The effect of forward flushing, with permeate, on gypsum scale formation during reverse osmosis treatment of $CaSO_4$-rich water in the absence of anti-scalant

by

Dietmar Norman Otto

Thesis presented in partial fulfilment
of the requirements for the Degree

of

MASTER OF ENGINEERING
(CHEMICAL ENGINEERING)

in the Faculty of Engineering
at Stellenbosch University

Supervisor

Prof AJ Burger

December 2014

Declaration

By submitting this thesis electronically, I declare that the entirety of the work contained therein is my own, original work, that I am the sole author thereof (save to the extent explicitly otherwise stated), that reproduction and publication thereof by Stellenbosch University will not infringe any third party rights and that I have not previously in its entirety or in part submitted it for obtaining any qualification.

Date: 21 November 2014

Abstract

When desalinating brackish water by reverse osmosis (RO) or other techniques, high overall water recoveries are essential to minimize brine production and the associated disposal costs thereof. As the overall water recovery increases, concentrations of sparingly soluble salts (e.g. barium sulphate, calcium sulphate) reach levels above saturation, especially near the membrane surface, drastically increasing the scaling propensity. Antiscalants are typically dosed into the feed water to prevent such scaling during RO desalination. However, the carry-over of antiscalant into the concentrate stream can complicate subsequent salt precipitation processes that may be used to increase overall water recovery. These precipitation techniques are sometimes used to reduce the levels of super-saturation in the RO concentrate prior to a subsequent RO desalination step.

The purpose of this study was to assess the feasibility of reducing calcium sulphate scaling on RO membranes, by using periodic permeate flushing when feeding a lab-scale RO unit with a supersaturated calcium sulphate solution *in the absence of anti-scalant*. The overall water recovery was increased by recycling the concentrate, after an intermediate de-supersaturation step. This simulated a multiple-stage RO system, typical of processes used in high-recovery acid mine drainage (AMD) treatment plants. De-supersaturation of the concentrate intermediate was achieved with direct seeded gypsum precipitation, in the absence of any antiscalant. On the membrane surface inside the membrane unit, calcium sulphate concentrations greatly exceeded saturation levels – a combined consequence of the normal concentration process and the well-known surface-based concentration polarisation phenomenon. Therefore, periodic forward-flushing of the supersaturated solution from the membrane unit was performed with permeate. In theory, the periodic flushing removes the highly concentrated layer at the membrane surface during every flush, before scaling can occur. Various flushing regimes were evaluated to assess the effectiveness of the process.

A lab-scale desalination unit with a 0.106 m^2 flat sheet polyamide RO membrane was designed and constructed. The unit could operate at a feed rate of 12-14 L/h and at permeate fluxes of 12-24 LMH. Super-saturated feed solutions were prepared by mixing sodium sulphate and calcium chloride dihydrate salts with demineralised water, with an initial salinity of ± 5300 mg/L TDS, corresponding to a gypsum saturation index (SI_g) of 1.2 for most experiments. The total production time, net permeate production and flux decline were used to compare the flushing efficiency in different experimental runs.

Initial tests showed that scaling could be prevented (when operating the unit in full recycle mode, i.e. where both concentrate and permeate were recycled to feed), at flushing frequencies between 12 and 2.4 h^{-1}, when the membrane feed and concentrate were slightly under-saturated (SI_g = 0.9) and slightly super-saturated (SI_g = 1.1) respectively. However, when switching the same system to non-flushing mode after 24 hours of operation, membrane scaling occurred within 2-3 hours, as indicated by a strong decline in flux.

However, when operating the system in concentrate recycle mode (i.e. permeate is withdrawn) with super-saturated feed solutions (e.g. SI_g = 1.2), and thus a notably more super-saturated solution in the membrane concentrate, scaling could not be prevented (albeit delayed for some time) with intermittent permeate flushing. A fractional 2^{5-1} factorial design was used to determine which factors had the most significant effect on total production time and permeate production rate, testing five factors: 1) flushing frequency, 2) flushing volume, 3) permeate soak time, 4) permeate flux and 5) instantaneous recovery. The ANOVA analysis showed that total production times were, not surprisingly, primarily affected by the permeate flux, where operation at 24 LMH resulted in a lower net permeate production between 3.0 - 4.2 L, compared to 7.6 - 9.7 L at 12 LMH. Higher permeate fluxes clearly resulted in higher levels of concentration polarisation at the membrane surface, thus increasing the propensity for membrane scaling. Flushing frequency and instantaneous recovery also affected the net permeate production, where 6 h^{-1} and 10 % were the optimal values respectively within the range of test conditions. The lowest permeate production rate resulted in the highest net permeate volume production (i.e. also longest total production time), confirmed by a least squares regression.

In summary: This study showed that periodic permeate flushing could delay the membrane scaling process. However, it failed to prevent membrane scaling completely when operating the system with supersaturated calcium sulphate solutions in the absence of antiscalants. The flushing technique effectively delayed the onset of precipitation, but scaling eventually occurred if the lab-scale RO system was operated in concentrate recycle mode with oversaturated feed solutions (SI_g = 1.2). Additional experiments at different cross-flow velocities during permeate flushing, while using an optimised RO test cell flow channel design, are recommended for future studies.

Uittreksel

Gedurende die ontsouting van brakwater deur tegnieke soos tru-osmose (TO), is ’n maksimum herwinning van water noodsaaklik om die produksie, en die gepaardgaande kostes van verwydering, van die sout/brak neweproduk te minimeer. Soos die herwinning van water verhoog, so ook verhoog die konsentrasie van moeilik-oplosbare soute (soos bariumsulfaat, kalsiumsulfaat) in die sout konsentraat stroom, totdat die soute uiteindelik superversadiging bereik. Hierdie superversadiging gebeur veral naby die membraanoppervlak, waar dit lei tot ’n verhoogde kans van presipitasie en skaalvorming. Om dit te voorkom word die voerwater na ’n TO stelsel tipies gedoseer met antiskaalmiddels. Hierdie antiskaalmiddels verlaat die stelsel saam met die konsentraat, waar hulle gevolglike die presipitasie van soute bemoeilik. Presipitasie van soute uit die konsentraat kan tipies gebruik word om die vlak van superversadiging in die konsentraat te verlaag, waarna verdere TO behandeling gebruik word om selfs ’n hoër algehele waterherwinning te bewerkstellig.

Die doel van hierdie studie was om die vatbaarheid van die vermindering van kalsiumsulfaat (gips) skaalvorming in die afwesigheid van antiskaalmiddels op TO membrane te toets. Dit is bewerkstellig deur ’n laboratoriumskaal TO eenheid te voer met ’n superversadigde kalsiumsulfaat oplossing en die membraan periodies met skoon produkwater (permeaat) te was. Die algehele waterherwinning is verhoog deur met ’n tussenstap die versadigingsvlak van gips in die konsentraat te verlaag, waarna dit hersirkuleer is na die voertenk. Sodoende is ’n multi-stadium TO stelsel nageboots, soos dit tipies in hoë herwinningsaanlegte, soos met die herwinning van suur mynwater (E: acid mine drainage, AMD), gebruik word. ’n Verlaging in superversadiging van die konsentraat in die tussenstap is behaal deur die konsentraat direk aan gipskristalle bloot te stel om presipitasie te bewerkstellig in die afwesigheid van enige antiskaalmiddels. Gedurende eksperimente het die soutkonsentrasie op die membraanoppervlak in die TO eenheid superversadigingsvlakke vêr oorskry, as gevolg van die natuurlike konsentrasie proses en die bekende konsentrasie polarisasie oppervlaksverskynsel. Om hierdie superversadiging teen te werk is periodiese saamstroom spoeling van die membraan met skoon produkwater uitgevoer. In teorie het die periodiese spoeling die hoogs gekonsentreerde oplossing van die membraan oppervlak verwyder voor skaalvorming kan plaasvind. Verskillende spoelpatrone is ondersoek om die doeltreffendheid van die spoeling te bepaal.

Om die eksperimente uit te voer is ’n laboratoriumskaal ontsoutingsaanleg met ’n maklik verwyderbare 0.106 m^2 plat-vel poli-amied TO membraan ontwerp en gebou. Die aanleg kan vloeistof voertempo’s tussen 12-24 L/h hanteer en skoon produkwater teen 12-24 LHM lewer. Die superversadigde voer oplossings, soos gebruik in die meerderheid van die eksperimentes is

voorberei deur natriumsulfaat en kalsiumchloried-dihidraat soute te meng in gedemineraliseerde water, tot ’n soutgehalte van ± 5300 mg/L TDS bereik is. Hierdie soutgehalte stem ooreen met ’n gips versadigingsindeks (E: gypsum saturation index, SI_g) van 1.2. Die skoon produkwater totale produksietyd en netto produksie, asook die membraan vloed afname, is gebruik as veranderlikes om die spoel doeltreffendheid tussen eksperimentele lopies te vergelyk.

Aanvanklike toetse het getoon dat skalering voorkom is by effens onderversadigde (SI_g = 0.9) en effens superversadigde (SI_g = 1.1) voer oplossings met die onderskeie spoel frekwensies van 12 en 2.4 h^{-1}, (terwyl die aanleg in algehele hersirkulasie bedryf is, m.a.w. wanneer beide die konsentraat en produkwater gedurig na die voertenk hersirkuleer word). ’n Effens-superversadigde eksperiment is ook sonder spoeling uitgevoer vir 24 uur. In hierdie geval het skaalvorming binne twee tot drie uur gebeur, soos bevestig deur ’n skerp afname in die membraan vloed.

Skaalvorming kon nie verhoed word terwyl die aanleg bedryf word met superversadigde (SI_g = 1.2) voeroplossings en slegs konsentraat hersirkulasie nie (m.a.w. skoon produkwater word opgevang), alhoewel skaalvorming vertraag kon word. Hierdie operasie het tot beduidend meer gekonsentreerde oplossings in die membraan gelei. Om te bepaal watter faktore die grootste invloed op totale produksietyd en netto produksie van skoon produkwater het, is ’n fraksionele faktoriaalontwerp van 2^{5-1} uitgelê wat vyf faktore toets, naamlik: 1) spoel frekwensie, 2) spoel volume, 3) skoon produkwater weektyd, 4) membraanvloed en 5) oombliklike herwinning. ’n AVOVA analise het getoon dat totale produksietyd hoofsaaklik deur membraanvloed beïnvloed is, soos verwag kan word. Dit word gestaaf deurdat die aanleg, bedryf teen 24 LMH, slegs 3 - 4.2 L netto produkwater gelewer het, teenoor 7.6 - 9.7 L by 12 LMH. Hoër membraan vloedtempo’s het tot hoër vlakke van konsentrasie polarisasie op die membraanoppervlak gelei, wat ’n groter neiging tot skaalvorming tot gevolg gehad het. Spoelfrekwensie en oombliklike herwinning het ’n invloed op die netto produksie van skoon produkwater gehad, met 6 h^{-1} en 10 % as die onderskeie optimale waardes. ’n Kleinstekwadraat regressie het aangedui dat die laagste produksietempo van skoon produkwater die hoogste netto produksie van skoon produkwater gelewer het, (asook die langste produksietyd).

In opsomming: Hierdie studie het getoon dat gereelde spoeling met skoon produkwater die membraan skaalproses kan vertraag. Gedurende bedryf met superversadigde kalsiumsulfaat oplossings sonder enige antiskaalmiddels is daar gevind dat skaalvorming nie geheel en al vermy kon word nie. Die spoeltegniek, soos gebruik in hierdie studie, het die aanvang van skaalvorming in die laboratorium skaal TO eenheid vertraag, maar bedryf met konsentraat hersirkulasie en

superversadigde oplossings (SI_g = 1.2) het steeds skaal gevorm. Bykomende eksperimente teen verskeie kruisvloei snelhede gedurende die spoel stap word aanbeveel vir toekomstige studies.

Acknowledgements

Foremost, I want to express my sincere gratitude to my supervisor Prof AJ Burger for the continuous support, patience and motivation throughout my study. His immense theoretical knowledge and many years of work experience in the water industry guided me through the study. I appreciate the fact that he always reminded me how real RO desalination plants operate in industry, ensuring that I also learned about the "bigger picture" of the water industry.

Without the financial support from my DAAD (German Academic Exchange Service) scholarship, via TUCSIN Namibia, and the Department of Chemical Engineering this study would not have been possible. Further, I want to thank Aqua Services and Engineering (Windhoek, Namibia) for giving me the opportunity to complete my postgraduate studies and funding my undergraduate studies. Furthermore, I would to thank Dr Günter Lempert who was/is an excellent mentor, always encouraging me to work hard and to be a successful chemical engineer in the future.

I would like to thank the Department of Process Engineering and all the staff members that helped me throughout my studies, especially the workshop staff: Oom Jannie, Oom Anton, Alvin, Vincent, Ollie; the administrative staff: Juliana, Nadine, Francis, Lynette and the analytical laboratory staff: Mrs Botha, Levine.

Last but not least, I want to thank all my friends and family for their continuous support and understanding throughout my studies, especially my parents Klaus and Brigitte Otto for encouraging me to study Chemical Engineering in the first place and for their continuous financial support.

Table of Contents

List of Abbreviations

AAS	atomic absorption spectroscopy
APS	accelerated precipitation softening
AS	antiscalant
CESP	chemically enhanced seeded precipitation
EMP	effective membrane permeability
HiPRO	Hi Recovery Precipitation Reverse Osmosis
ICD	intermediate chemical demineralisation
LMH	litre per meter squared of RO membrane per hour ($L/(m^2.h)$)
RO	reverse osmosis
PRO	primary reverse osmosis stage
PPR	permeate production rate
PPI	permeate production index
TDS	total dissolved solids
TMP	trans membrane pressure
SI	gypsum saturation index
SRO	secondary reverse osmosis stage
SPARRO	seeded precipitation and recycle RO

List of Symbols

Symbol	Description	Unit
α_i	activity of species i	-
$\alpha_{i,eq}$	activity of species i at equilibrium	-
ΔP	pressure difference across the membrane	bar
$\Delta \pi$	osmotic pressure difference across the membrane	bar
ΔG	change in Gibbs free energy	J
ε	dielectric constant for water	-
Ω	supersaturation ratio with respect to gypsum	-
ω_P	permeate production efficiency	-
Υ_i	activity coefficient of species I	-
A_m	effective membrane area	m^2
CF	concentration factor	-
C_F	feed solute concentration	mg/L
C_P	permeate solute concentration	mg/L
C_M	solute concentration at membrane surface	mg/L
J	permeate flux	$L/(m^2.h)$
J_S	solute flux through RO membrane	$g/(m^2.h)$
J_W	solvent flux through RO membrane	$L/(m^2.h)$
k'	kinetic growth constant	1/(M.min)
K_{SP}	solubility product	mol^x/L^x
L_P	effective membrane permeability	$L/(m^2.h.bar)$
$L_{P,25}$	effective membrane permeability normalised at 25 °C	$L/(m^2.h.bar)$
PPR	permeate production rate	L/h
PPI	permeate production index	-
Q_F	RO feed flow rate	L/h
Q_P	RO permeate flow rate	L/h
Q_C	RO concentrate flow rate	L/h
R	overall recovery	%
R_I	instantaneous recovery	%
R_U	universal gas constant	J/(mol.K)
s	solubility	g/L
SI_F	RO feed gypsum saturation index	-

SI_{OV}	precipitation overflow gypsum saturation index	-
SI_g	gypsum saturation index	-
SR	salt rejection	%
t_{ind}	induction time	min
t_O	operating time	min or h
t_P	production time	min or h
T	temperature	K or °C
V_F	RO feed volume	L
V_{flush}	permeate flushing volume	L/h
V_P	RO permeate volume	L
$[i]$	concentration of species i	mol/L
$[i]_{eq}$	equilibrium concentration of species i	mol/L

Glossary

Total operating time	The total operating time is the actual duration the lab scale RO unit was operated during one specific experimental run, from the start of the experiment until the experimental run was complete.
Total production time	The total production time only refers to the time at which permeate was produced during an experimental run. In a non-flushing experiment the total operating time was equal to the total production time. Conversely, in any flushing experiment the total production time was less than the total operating time, due to the periodic flushing. The magnitude of this difference was determined by the flushing frequency, flushing volume and soaking time. Therefore, the production time was used throughout this study to compare flushing and non-flushing experimental runs, since it was not possible to compare runs in terms of operating times.
Net permeate production	The net permeate production is defined by the total volume of permeate (in L), that was recovered during an experimental run. In flushing experiments a certain percentage of permeate is recycled to the RO unit, hence not all produced permeate is recovered.
Permeate Production Rate	The permeate production rate (PPR) is defined as the actual permeate flow rate in L/h and subtracting the volume of permeate used for flushing per hour.
Permeate Production Index	The permeate production (PPI) is calculated by dividing the permeate production rate by the actual permeate flow rate. Different experimental runs can be evaluated by comparing the dimensionless PPI.

List of Figures

List of Tables

Chapter 1 - Introduction

1.1. Background

1.1.1. Marginal water resources

Currently 780 million people do not have access to safe drinking water, 37 % of those are living in sub-Saharan Africa (WHO/UNICEF, 2012). Southern Africa is an arid region, hence it is essential to employ management strategies to use the available water resources effectively.

There is an ever increasing demand for more fresh water; therefore new technologies should be employed to treat marginal waters, previously not considered due to the adequate availability of fresh water resources. The declining quantities or quality of available fresh sources make marginal waters an excellent source, however modern technologies are required to treat the water. Marginal water includes brackish waters and mining wastewaters, which often contain high concentrations of sparingly soluble salts such as calcium sulphate or calcium carbonate. In South Africa the mining industry generates vast amounts of high-salinity effluent, which offers great potential for water recycling and reuse.

The reclamation of high-salinity brackish water sources has become more important, especially in semi-arid regions of the world, providing a source of potable and irrigation water (Glueckstern, 1986; Robinson et al., 1992; Watson et al., 1994). Currently, desalination by reverse osmosis (RO) is a viable option to treat mineral waters with a high scaling propensity.

1.1.2. High recovery brackish water RO desalination

RO is a cost-effective method for brackish desalination due to the emergence of low-pressure membranes, providing high salt rejections (>95%) and permeate fluxes (Rahardianto et al., 2006; Uchymiak et al., 2008). However, concentrate volumes should be minimized by operating at high levels of overall water recovery, thus reducing the brine disposal costs to make the process economically viable (Ahmed et al., 2000; Glater and Cohen, 2003; Glueckstern and Priel, 1997). Operating at recoveries above 90 % greatly increases the risk of membrane scaling by sparingly soluble salts, potentially leading to membrane scaling, ultimately resulting in flux declines and shortened membrane life (Pomerantz et al., 2006; Rahardianto et al., 2006; Shih et al., 2005; Uchymiak et al., 2008).

Higher overall water recoveries result in significant concentration of the concentrate stream, often forming supersaturated solutions where the solubility of sparingly soluble salts are exceeded (Borden et al., 1987; Gabelich et al., 2007). At the membrane surface the concentrations are even higher than in the bulk fluid, due to concentration polarisation, significantly increasing the risk of membrane scaling via surface crystallisation (Oh et al., 2009; van de Lisdonk et al., 2001).

Different strategies can be employed to mitigate the impact of mineral scaling on reverse osmosis membranes. They include pH adjustments, the use of antiscalants and operation below critical recoveries without triggering mineral scaling (Rahardianto et al., 2006; Shih et al., 2005). Typically, pH adjustments are used to control calcium carbonate scaling on RO membranes, however this process is ineffective to reduce calcium sulphate or barium sulphate scaling due to the weak pH dependence (Rahardianto et al., 2006).

Various studies have shown that antiscalant dosing in supersaturated solutions of sparingly soluble salts (e.g. calcium sulphate and barium sulphate), effectively delay scale nucleation and subsequent crystal growth (Amjad, 1985; Hasson et al., 2001; Le Gouellec and Elimelech, 2002; Oner et al., 1998; Shih et al., 2004). More specifically, antiscalants prolong induction times (i.e. time until precipitation occurs once the solution becomes supersaturated) or alter the crystal behaviour, preventing the scale from adhering to the membrane (Pomerantz et al., 2006).

Overall permeate recovery is significantly improved by using multiple RO stages. However intermediate concentrate treatment to remove the scaling ions is essential (Gabelich et al., 2011; McCool et al., 2013; Rahardianto et al., 2010; Shih et al., 2005). Previous studies have shown that intermediate chemical demineralisation (ICD) is an effective, yet chemically intensive, method allowing further desalination of desupersaturated concentrate in subsequent RO stages (Gabelich et al., 2007; Rahardianto et al., 2010, 2007). Another viable option is intermediate concentrate demineralisation via seeded homogenous precipitation of sparingly soluble salts (e.g. calcium sulphate or barium sulphate) (Bremere et al., 1998; Gabelich et al., 2007; Juby, 1994; McCool et al., 2013).

The presence of antiscalants in primary RO concentrate has an adverse effect on seeded precipitation, since antiscalants continue to inhibit crystal growth and thus lowering the rate of desupersaturation (Yang et al., 2008). Antiscalant action can be neutralised, for instance by alkaline-induced calcium carbonate precipitation, overriding the inhibitory effect of the antiscalants (McCool et al., 2013; Rahardianto et al., 2010).

Some aspects of brackish water desalination are summarised below:

- RO desalination of brackish water sources is a viable option; however the solubility of sparingly soluble salts often limits the maximum overall recovery. Careful plant designs are essential to prevent membrane scaling, which ultimately results in permeate flux declines and shortened membrane life. High recoveries (>90%) are essential, making brackish desalination economically viable, also minimising the brine disposal costs.
- Antiscalants are typically used to reduce membrane scaling, however the presence of antiscalants in the RO concentrate makes intermediate concentrate demineralisation complicated, due to antiscalant carryover inhibiting nucleation. Antiscalant scavenging is possible, for instance, by adding caustic soda to RO concentrate resulting in antiscalant scavenging via alkaline induced calcium carbonate precipitation.
- Intermediate concentrate demineralisation is essential to increase the overall water recovery when treating brackish water with high scaling propensities. The scaling potential of the primary RO concentrate is typically reduced by seeded precipitation, permitting higher overall recoveries by using subsequent RO stages.

1.2. Problem statement

Brackish water RO desalination is often only viable when operating at high overall recoveries, i.e. when minimising the brine production and the associated disposal costs. Brackish waters or mining effluent typically become supersaturated with respect to sparingly soluble salts as the overall recovery increases. Therefore, it is essential to use intermediate concentrate demineralisation techniques to reduce the scaling propensity of the primary RO concentrate, thus permitting higher water overall recoveries with subsequent RO stages. Antiscalants are commonly dosed to allow RO plant operation above salt solubility limits. However, antiscalant carryover in the concentrate stream complicates any further demineralisation via seeded precipitation and the accumulation of anti-scalant in the sludge ponds may even complicate further processing.

1.3. Motivation for permeate flushing technique

Membrane scaling is a direct consequence of concentration polarisation at the membrane surface, leading to surface crystallisation when the solubility of sparingly soluble salts is exceeded (van de Lisdonk et al., 2001). Further, concentration polarisation is considered to be a reversible process (Sablani et al., 2001). Therefore, reducing the level of concentration polarisation lowers the scaling

risk. Consequently, the effect of flushing was investigated in this study, exploiting this concept, where periodic flushing theoretically lowers the degree of concentration polarisation.

Precipitation generally occurs in two steps: nucleation and growth. In a supersaturated solution the nucleation process is initiated by the formation of structured aggregates, until a certain size is exceeded, leading to the formation of stable nuclei and spontaneous crystal growth (Söhnel and Garside, 1992). The induction time is defined as elapsed time from reaching supersaturation, until the first physical changes are observed and precipitation occurs. The formation of nuclei takes place within the induction time, a prerequisite for precipitation.

In theory, if a supersaturated solution adjacent to the RO membrane is periodically replaced with an undersaturated solution (i.e. permeate), at a time less than the induction time, any developed nuclei are flushed away. After permeate flushing, a complete induction time is necessary for the nuclei to redevelop and a concentration polarisation layer to build up again. If this is repeated every time before any precipitation occurs, in theory, no scaling should occur because complete nucleation and crystal growth is never allowed to occur. The obvious disadvantage of this technique is the loss of productivity during the flushing operation and the lower overall recovery since permeate is recycled after the flushing. Pomerantz et al. (2006) used a flow reversal technique, periodically switching the flow from membrane feed to membrane exit and vice versa. This periodic replacement of oversaturated solution at the membrane surface, increased the overall recovery from 75 % to 85 % and no scaling occurred, demonstrating the success of this concept.

The obvious disadvantage of permeate flushing is the reduction in overall permeate production rate (i.e. lower productivity), since only a certain portion of permeate is recycled back to the feed tank during the flushing. In other words, the actual permeate production rate will be lower than the permeate flow rate. This results in longer total operation times to produce a certain volume of permeate, compared to the non-flushing case where the permeate flow rate is equal to the permeate production rate.

1.4. Research objectives and key questions

- The key research question in this study was the following: To what extent was it possible to prevent calcium sulphate membrane scaling by periodically flushing the RO membrane with permeate, using an oversaturated calcium sulphate solution as feed without the use of antiscalants? More specifically, the research objectives were as follows: Determine the

effects that flushing frequency, flushing volume, permeate flux and instantaneous recovery have on calcium sulphate membrane scaling and RO system operation times until scaling occurs.

- Evaluate the permeate flushing technique to determine if the technique was effective to prevent calcium sulphate membrane scaling without the use of antiscalants using supersaturated calcium sulphate feed solutions.

1.5. Limitations

Due to the vastness of this field of study, it was only possible to choose a narrow range of operating conditions and factors for all the experiments, hence posing the following limitations on the project:

- Only calcium sulphate dihydrate or gypsum ($CaSO_4.H_2O$) was considered as model scalant. Gypsum has a greater difficulty in mitigating scaling, compared to the more common calcium carbonate scalant. The synthetic feed water was prepared by mixing pure reagent grade salts with demineralised water, hence the feed solution only contains Ca^{2+}, Na^{+}, SO_4^{2+} and Cl^{-} ions, isolating the effect of calcium sulphate scaling during the study.
- In actual multi-stage desalination plants, treated concentrate is typically not recycled and is rather fed to a subsequent RO stage to increase the overall recovery. In this study the lab-scale unit was operated in concentrate recycle mode (i.e. permeate was constantly withdrawn) to simulate a typical primary RO – intermediate concentrate demineralisation – secondary RO desalination plants.
- In actual RO plants, spiral wound RO membranes are typically used, whereas a flat sheet RO membrane test cell was used in this lab-scale study.

1.6. Methodology

A lab-scale RO desalination system was designed and constructed. The unit produced between 1.0 - 2.5 L/h of permeate, operating at maximum instantaneous recoveries of 30 %. Automatic periodic permeate flushing with permeate from an elevated permeate tank was achieved by installing multiple solenoid valves, controlled by relay timers. A seeded gypsum precipitation reactor was used for the intermediate concentrate demineralisation, which was designed according to results from initial batch gypsum crystallisation experiments. The lab-scale system was operated in concentrate recycle mode (i.e. constantly withdrawing permeate and recycling concentrate) to simulate multiple RO stages as typically encountered in actual RO plants. The membrane scaling process was evaluated

by physical inspection of scaled RO membranes using SEM and XRD analysis, after operating the lab-scale RO unit with oversaturated calcium sulphate solutions. A factorial design experiment was used to test the effect of various factors have on calcium sulphate scaling, indicating if the flushing technique was effective to prevent scaling.

Chapter 2 - Literature Review

2.1. Reverse osmosis: Basic terms and definitions

2.1.1. Introduction

Reverse osmosis is a membrane filtration technique that effectively separates molecules and ions from solutions, by forcing the solution through a semi-permeable membrane using an externally applied pressure. Solvent molecules can easily pass the membrane, while most of the dissolved solids (i.e. ions) are retained on the pressurised side of the membrane. However, the rate at which solvent molecules pass the membrane greatly exceeds the rate at which solute molecules pass through the membrane. Although RO separation is similar to other membrane technology applications, a key difference is present between the operating mechanisms. Filtration is based on the size-exclusion or straining principle, thus theoretically allowing perfect filtration, regardless of influent parameters such as inlet pressure and concentration. In contrast, RO separation entails a diffusive mechanism, thus the degree of separation is a function of solute concentration, flux rate and pressure (Crittenden et al., 2005).

Osmosis is the natural process whereby water flows through a semipermeable membrane, from a less concentrated solution to a concentrated solution of dissolved solids, to establish a chemical equilibrium between the two solutions (Baker, 2004). This process is illustrated in Figure 2-1, showing a container with two compartments separated by a semi-permeable membrane. The one compartment initially contains a high solute concentration while the adjacent compartment contains a low solute concentration. Osmosis takes place when the water moves through the semipermeable membrane, from the low dissolved solids concentration to the high dissolved solids concentration. This continues until the dissolved solids concentration is equal in both compartments and the chemical equilibrium is established. At equilibrium, the one compartment initially containing the high solute concentration has a higher water level. This height difference represents the osmotic pressure, and is related to the dissolved solids concentration of the solution (Kucera, 2010).

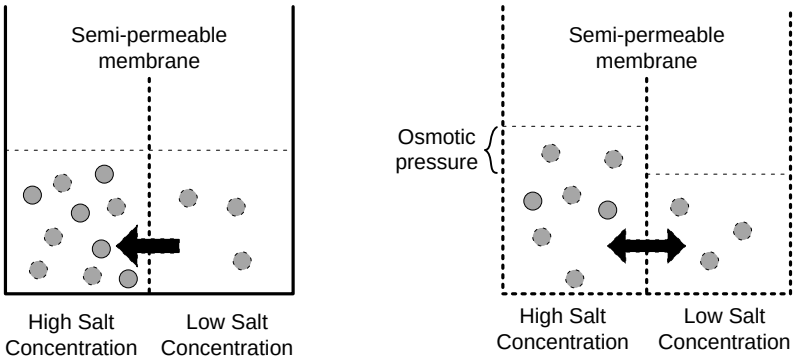

Figure 2-1 *Principle of osmosis. Water moves from low solute concentration to a high solute concentration, thereby creating a height difference corresponding to the osmotic pressure of the specific solution (redrawn from Kucera (2010)).*

The net flow of solvent can be reversed by applying an external pressure to the compartment with a high concentration, as shown in Figure 2-2. Water will then flow from the compartment with the high dissolved solids concentration, to the compartment with the low dissolved solids concentration. Therefore, the dissolved solids in the one compartment are concentrated up, since there is a net solvent flow through the membrane to the other compartment. The semipermeable membrane adds resistance, thus the applied pressure must be significantly greater than the osmotic pressure of the specific solution (Kucera, 2010).

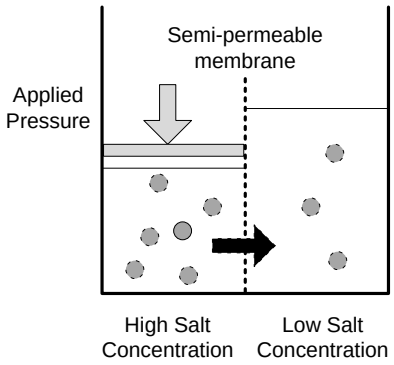

Figure 2-2 *Principle of reverse osmosis. Pressure, exceeding the osmotic pressure, is applied to the compartment with high dissolved solids concentration, thereby causing a net solvent flow through the membrane (redrawn from Kucera (2010)).*

Two different modes of filtration are employed in reverse osmosis separations: dead-end filtration and cross flow filtration. Dead-end filtration is primarily used for batch processes, where water is fed perpendicularly to the membrane surface, shown in Figure 2-3. This mode is rarely used in continuously operated RO plants, due to the high fouling and scaling tendency, requiring frequent cleaning (Baker, 2004; Seader and Henley, 2006).

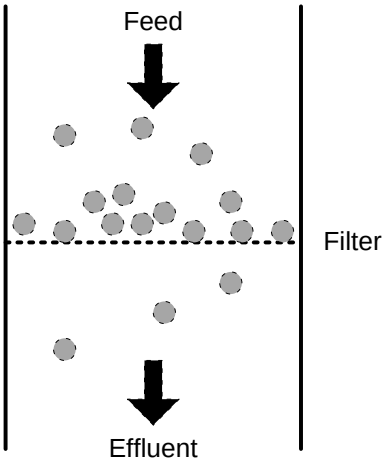

Figure 2-3 *Simplified block diagrams showing dead-end filtration (redrawn from Kucera (2010)).*

Cross-flow filtration is more suitable for large-scale, continuous RO plants, where feed water flows tangentially across the membrane surface (Baker, 2004; Seader and Henley, 2006). One influent stream will split in two effluent streams, as shown in Figure 2-4. The solution passing through the membrane is called permeate or product stream, containing a relatively low concentration of dissolved solids. The solution containing the majority of the dissolved salts is called the concentrate, retentate, brine, reject or waste stream. RO separation only occurs if the applied pressure is greater than the osmotic pressure of the solution (Kucera, 2010). A pressure regulating valve is typically installed in the concentrate stream after the RO membrane to regulate the operating pressure in the vessel.

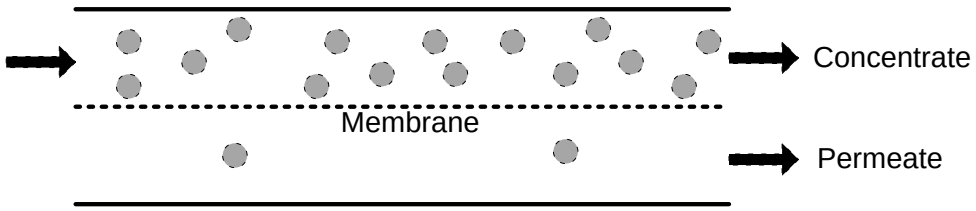

Figure 2-4 *Simplified block diagrams showing cross-flow filtration (redrawn from Kucera (2010)).*

Continuous operation of the cross flow membrane theoretically prevents fouling, by the scouring action along the membrane (Kucera, 2010). However, in practice scouring is typically not sufficient to prevent scaling and fouling completely. Therefore, periodic membrane cleaning is essential to ensure long membrane lifetimes.

2.1.2. Rejection

In RO applications, *rejection* refers to the percentage of a influent species retained by a specific membrane (Kucera, 2010). For instance, if the salt rejection of a specific membrane is 98%, only 2% of the dissolved salts will pass through the membrane and end up in the permeate stream. Salt rejection is typically given be the following equation:

$$SR = \frac{C_f - C_p}{C_f} \qquad \textbf{Equation 2-1}$$

where C_f and C_p are the components influent and permeate concentrations respectively (Kucera, 2010). Rejection varies with each specific feed water component and type of membrane used. In general the following characteristics affect the rejection of a particular species(Kucera, 2010):

- **Valency of ion:** rejection of multivalent ions is generally better than monovalent ions
- **Degree of dissociation:** the greater the degree of dissociation the greater the rejection
- **Molecular weight:** the rejection is increased as the molecular weight is increased
- **Polarity:** the greater the polarity, the lower the rejection
- **Degree of hydration:** the greater the degree of hydration, the greater the rejection
- **Molecular branching:** more branching will result in greater rejection

2.1.3. Recovery

In RO applications *recovery* generally refers to the volume percentage of influent water that is recovered as permeate (Kucera, 2010), however there is a difference between overall and instantaneous recovery. Overall recovery is the ratio between final collected permeate volume to initial feed volume, whereas instantaneous recovery is the ratio between the permeate flow rate to feed flow rate of a given membrane stage:

$$R_I = \frac{Q_P}{Q_F} \qquad \textbf{Equation 2-2}$$

$$R = \frac{V_P}{V_F} \qquad \textbf{Equation 2-3}$$

Where R_I is the instantaneous recovery per pass, Q_F the feed flow rate Q_P the permeate flow rate, R the overall recovery, V_F the initial feed volume and V_P final permeate volume. The concentration of dissolved salts in the brine stream increases as the overall recovery increases. For instance, when

operating at a recovery of 75%, the volume of the brine stream will be one quarter of the influent stream. The reject stream still contains all the dissolved salts (assuming hundred percent membrane rejection), therefore the reject stream is concentrated by a factor of 4. In reality the rejection is never 100 %, thus the concentration factor (CF) is calculated by (Baker, 2004):

$$CF = \frac{1+R.SR-R}{1-R} \qquad \textbf{Equation 2-4}$$

where ***CF*** is the overall concentration factor and ***SR*** is salt rejection. Further, this equation can be used to calculate the instantaneous concentration factor if the instantaneous recovery is used instead. The relationship between recovery and concentration factor is shown in Figure 2-5**.** For instance, scaling will be less severe or non-existent in plants operating at low recoveries below 50 % since the CF is less than 2. However, some plants are designed to operate at >90% recoveries, hence scaling becomes significant as the CF significantly increases (Baker, 2004).

In RO plants, higher recoveries result in lower concentrate volumes, however at the same time also resulting in lower purity permeate (Kucera, 2010). The recovery of any RO system is not a property of the membrane. Instead the designer should consider the trade-off between higher permeate recovery (and lower volumes of brine to dispose), but then also resulting in higher dissolved solids concentrations in the permeate (Kucera, 2010).

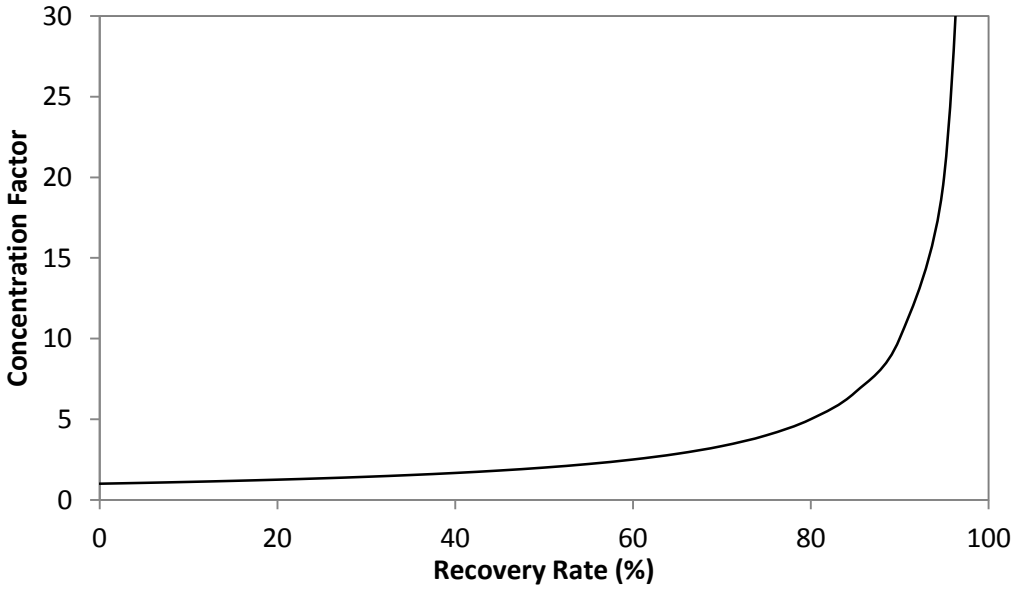

Figure 2-5 *The relationship between recovery rate and concentration factor at 100 % rejection*

2.1.4. Flux

In membrane applications flux refers to the volumetric flow rate through a certain area, and is typically expressed in L/(m^2.h), which is often abbreviated as LMH (Kucera, 2010). In RO systems flux is directly proportional to the applied pressure, hence an increase in applied pressure will also result in a higher flux. Flux is not a directly a property of the membrane, instead the operating flux is determined by the RO plant design, based on the influent water quality. In general, the lower the quality of the influent water, the lower the water flux at which the RO membrane should be operated.

Water flux can be calculated using the following equation (Baker, 2004):

$$\boldsymbol{J = K(\Delta P - \Delta \pi)} \qquad \textbf{Equation 2-5}$$

where:

J = water flux
K = water transport coefficient (unique for every membrane, temperature dependant)
ΔP = pressure difference across the membrane
Δπ = osmotic pressure difference across the membrane

2.1.5. Fouling

Fouling is defined as the accumulation of unwanted suspended solids, organics or microbes on the membrane surface, typically on the influent/feed side. Membrane fouling is a major cause of permanent flux decline and reduction in product water quality (Potts et al., 1981). Fouling mostly occurs in the initial stages of a multistage RO process; however with adequate pre-treatment and regular cleaning membrane fouling can be limited (Baker, 2004). Common fouling species are listed below (Kucera, 2010):

- Colloids that are suspended in the solvent
- Organic material, providing nutrients for microorganisms
- Micro organisms
- Colour, causing irreversible membrane fouling through absorption
- Metals, precipitating upon oxidation at the membrane surface
- Mineral scaling through precipitation of sparingly soluble salts

Membrane fouling is aggravated by operating at high membrane fluxes and low cross flow velocities, therefore also increasing the degree of concentration polarisation (Kucera, 2010). A high operating flux transports water faster through the membrane, and if the residence time is sufficient in the boundary layer, material rapidly deposits on the membrane surface. Further, a low cross flow velocity results in thicker boundary layer. This results in greater accumulation of solids at the membrane surface since the particles spend more time in the thicker boundary layer; hence the fouling action is accelerated.

The performance of RO membranes is adversely affected by membrane fouling, resulting in higher operating pressures and higher than normal pressure drops across the membrane (Potts et al., 1981). Through the deposition of material, an additional layer of resistance is created, thus the applied pressure should be greater to produce the same flux achieved prior to fouling.

2.1.6. Scaling

Membrane Scaling occurs when saturated salts precipitate in the bulk solution, leading to membrane scale deposition, or by direct surface precipitation (Le Gouellec and Elimelech, 2002; Shih et al., 2005; Uchymiak et al., 2008). Typical scalants include various calcium compounds (e.g. calcium carbonate, calcium sulphate, calcium fluoride and calcium phosphate) and sulphate-based scales of trace metals (e.g. barium sulphate and strontium sulphate) (Baker, 2004). Scaling is more severe in the later stages of a multi-stage RO process, since the modules are exposed to the most concentrated feed water (Kucera, 2010).

Scale formation, is aggravated by high membrane flux and low cross-flow velocities (Kucera, 2010). Operation at high fluxes leads to solute build up in the concentration boundary layer since more water permeates the membrane, thus increasing the propensity of scale formation. In addition, low cross flow velocities will result in thicker boundary layers, hence increasing the residence time the solute spends in the boundary layer. In both cases, the saturation index near the membrane increases, hence also the probability of precipitation.

Scale formation has many negative effects on the operation of RO membranes. Scale formation on RO membranes causes the following three performance issues: 1) higher than predicted operating pressures, 2) higher pressure drop across the membrane and 3) higher salt passage (i.e. lower salt rejection) (Kucera, 2010). Brusilovsky and Borden (1992) have shown that permeate salt

concentration increases with a decrease in permeate flux due to the higher apparent salt concentration near the membrane surface.

This study focuses on calcium sulphate scaling; refer to section 2.3 for a more detailed discussion of the scaling mechanism and the kinetics.

2.1.7. Membrane materials

Membrane selection is a very important aspect in any RO design since the performance of the system is directly proportional to the membrane. The type of polymer and the structure of the membrane will determine the salt rejection of the specific membrane. An ideal membrane offers excellent salt rejection and a high permeate flux, at the same time being rigid and durable. In reality both goals cannot be achieved, since a trade-off between salt rejection and flux exists. Extensive research over the past years have produced membranes with high flux rates without sacrificing salt rejection (Kucera, 2010).

RO membranes are classified according to their polymer backbone, where the two most common types are cellulose acetate and polyamide membranes. Each type of membrane has specific properties, making it suitable for certain applications. The main properties of the two membrane types are summarised the Table 2-1. Cellulose acetate membranes are often used in brackish RO applications, despite their few drawbacks: the slender operating pH range (4-6), tendency for biological fouling, low temperature limits (up to 35˚C) and mechanical compaction resulting in reduced water flux. On the other hand, polyamide membranes typically have higher fluxes and salt rejections, however the main disadvantage is the lower chlorine tolerance (Baker, 2004; Kucera, 2010).

Table 2-1 *Characteristics of cellulose acetate and polyamide RO membranes (Kucera, 2010)*

Property	Cellulose Acetate	Polyamide
Membrane Type	Homogenous asymmetric	Thin film composite
Salt Rejection (%)	≈ 95	≈ 98
pH Range	4-6	2-12
Feed Pressure (brackish water)	15-30 bar	10-30 bar
Temperature Tolerance	Up to 30˚C	Up to 45˚C
Surface Charge	Neutral	Negative (anionic)
Chlorine Tolerance	Up to 1 ppm continuously	<0.02 ppm
Fouling Tolerance	Good	Fair
Surface Roughness	Smooth	Rough

2.1.8. Solution-diffusion transport model

Transport models mathematically relate solvent and solute flux through the membrane to certain operating parameters, typically pressure and concentration (Dickson, 1998). The transport models are used to predict membrane behaviour under certain operating conditions; hence they are useful in the design of RO systems.

Many models have been developed over the years describing mass transport through membranes, based on different assumptions and with varying complexities. Lonsdale et al. (1965) proposed the solution-diffusion model, describing the performance of defect free membranes. The model is considered to be one of the leading theories in membrane transport literature (Baker, 2004), hence other models are not considered in this study.

The solution-diffusion model assumes a perfect nonporous membrane, without any imperfections. In the model, solute and solute molecules are assumed to dissolve into the membrane then subsequently pass through the membrane through diffusion (Lonsdale et al., 1965). This model is especially applicable for dense membranes, such as RO membranes, without any actual pores. In the model, the mass transport through the membrane is independent for the solvent and solute, given in Equation 2.6 and 2.7 respectively. The solvent flux through the membrane is linearly proportional to the pressure difference across the membrane (Wijmans and Baker, 1995), as given in Equation 2-5 (Kucera, 2010).

$$J_w = A(\Delta P - \Delta \pi) \qquad \textbf{Equation 2-6}$$

where:

J_w = solvent flux
A = water permeability constant (a function of water diffusivity through the membrane)
ΔP = applied pressure driving force (function of the feed, concentrate and permeate pressure)
$\Delta \pi$ = osmotic pressure of solution (a function of feed, concentrate and permeate concentration)

The mass transport flux of the solute is a function of concentration, and is proportional to the effective concentration difference across the membrane (Wijmans and Baker, 1995), given in Equation 2-6 (Kucera, 2010).

$$J_s = K(C_m - C_P) \qquad \textbf{Equation 2-7}$$

where:

J_s = solute flux

K = salt permeability constant (function of salt diffusivity through the membrane)

C_m = concentration of solute at boundary layer

C_P = concentration of solute in permeate

The solution diffusion transport model describes the salt and water passage through the membrane. Water flux is essentially zero until the applied pressure exceeds the osmotic pressure of the specific solution (Wijmans and Baker, 1995). As the applied pressure exceeds the osmotic pressure, the water flux increases linearly with increasing feed pressure (i.e. the driving force). Water passage increases with increasing applied pressure, hence more water passes through the membrane relative to the salt (Kucera, 2010). The salt flux differs significantly from the water flux, staying constant as the applied pressure increases as predicted by Equation 2.7. Therefore, the salt rejection should approach 100% as the applied pressure increases, since permeate solute concentration decreases.

2.1.9. Brine disposal methods

One of the key problems with desalination plants is the generation of brine and associated disposal thereof. Effective brine disposal management is critical to protect the environment (Arnal et al., 2005). Brine disposal in seawater desalination plants is relatively uncomplicated, since the brine is typically discharged into the ocean. Cost effective brine disposal in brackish water RO desalination plants is critical to make the process economically viable (Ahmed et al., 2001b, 2000; Glater and Cohen, 2003; Glueckstern and Priel, 1997).

The cost of brine disposal depends on: 1) the chemical brine composition, 2) the type of brine treatment prior to disposal, 3) the method of disposal, 4) the volume of brine and 5) the type of environment where the brine is disposed (Ahmed et al., 2001b). Glater and Cohen (2003) identified the three main disposal methods for brackish RO desalination plants: 1) evaporation ponds, 2) deep well injection and 3) solar ponds, amongst other less common methods such as irrigation of salt tolerant plants, discharge into municipal sewers and discharge into surface water.

Currently, evaporation ponds are the most widespread brine disposal method in brackish desalination (Glater and Cohen, 2003). Evaporation ponds are very useful to dispose brine, however, they require large surface areas, since the water evaporates naturally. Therefore, evaporation ponds are most suitable for relatively warm and dry climates with high evaporation rates, low precipitation

rates and low land costs (Ahmed et al., 2001b). Brackish RO plants are often at locations where adjacent land is available at a low cost, favouring this method of brine disposal. The sealing of the pond is essential to reduce the risk of groundwater contamination. Further, evaporation ponds produce salt as a by-product which can be sold as a raw product to many industries (Ahmed et al., 2000).

Deep well injection is also a common brine disposal method, where the brine is injected underground between layers of impermeable rock, thus preventing salination of ground water aquifers. Generally, brine disposal via deep well injection is more cost effective than other land based brine disposal methods (Glater and Cohen, 2003), especially if existing deep wells are used. The main disadvantages of the technique include: 1) difficulty in selecting a suitable well site, 2) the costs of treating the brine before it can be disposed, 3) underground seismic activity can damage the well resulting in contamination of underground water aquifers and 4) corrosion of well pipeline causing leakage in the well casing (Glater and Cohen, 2003).

Solar ponds are an emerging brine disposal method, where the salt gradient in the solar ponds is used as a renewable energy source (Glater and Cohen, 2003). In solar ponds the three different layers forming a salinity gradient, where the most dense layer (i.e. most salty) is at the bottom of the pond, an intermediate insulating layer in the middle and top layer with a low salt content. Solar energy heats up the bottom layer, essentially passing through the top layers, due to the density gradient that prevents mixing through convection. Currently, this method of brine disposal is limited to small scale desalination units (Ahmed et al., 2001a)

2.2. Calcium sulphate properties

2.2.1. Saturation concentration

Calcium sulphate, one of the most troublesome compounds in RO desalination plants, typically causing scale formation on RO membranes (Power, 1964). This study focuses on calcium sulphate scaling on RO membranes, although other mineral salts commonly occur in natural waters. The phase transformation in the calcium-sulphate-water system has a severe effect on the scaling, where crystallisation and precipitation cause mineral scaling on the membrane. Studies over the years have established that calcium sulphate can crystallise in three different molecular forms: $CaSO_4.2H_2O$ (gypsum), $CaSO_4$ (anhydrate) and $CaSO_4.½H_2O$ (hemihydrate) (Alimi and Elfil, 2003; Ben Ahmed et al., 2008; Helalizadeh et al., 2000; Power, 1964).

The solubility of calcium sulphate as a function of operating temperature, as given in Figure 2-6**,** showing the solubility curves for each of the three solid calcium sulphate molecules. At temperatures above approximately 40°C the solubility decreases for all three phases, effectively favouring precipitation at higher temperatures even at low calcium sulphate concentrations. The gypsum solubility stabilises around 40°C, before decreasing slightly as the temperature is lowered. Further, the solubility of calcium sulphate is also affected by the presence of other ions in the solution. The solubility increase as the concentration of other ions in the solution increases (Helalizadeh et al., 2000).

In this study model solutions will be at temperatures lower than 40°C, hence only calcium sulphate dihydrate is considered. Studies showed that calcium sulphate dihydrate is the only stable hydrate below 40°C (Klepetsanis and Koutsoukos, 1991; Lui and Nancolass, 1970).

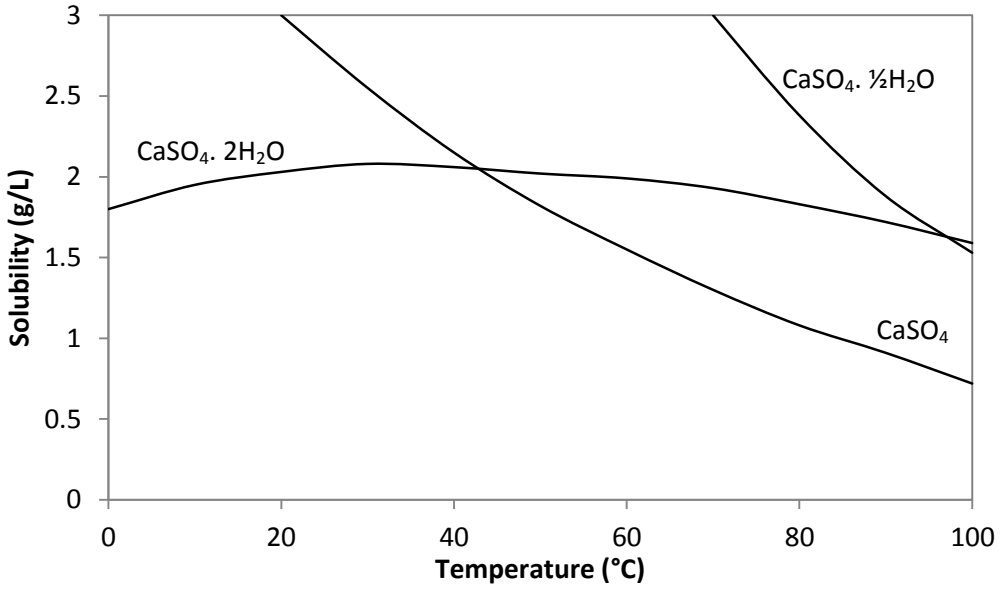

Figure 2-6 *Solubility of calcium sulphate as a function of temperature (redrawn from Helalizadeh & Mu (2000) and Power (1964)).*

2.2.2. Thermodynamics

The gypsum precipitation reaction, from an aqueous solution of calcium and sulphate ions is given as:

$$Ca^{2+}{}_{(aq)} + SO_4^{2-}{}_{(aq)} \leftrightarrow CaSO_4.2H_2O_{(solid)}$$

The forward reaction occurs from a supersaturated state, until the thermodynamic equilibrium is established. The change in Gibbs free energy is the thermodynamic driving force in the calcium sulphate precipitation reaction (Ben Ahmed et al., 2008), given as:

$$\Delta G = -\frac{R_u T}{2} ln\, \Omega \qquad \textbf{Equation 2-8}$$

Where: R_U is the universal gas constant, T the absolute solution temperature in Kelvin and Ω the supersaturation ratio with respect to gypsum. The supersaturation ratio (Ω) is calculated considering the liquid solid equilibrium between Ca^{2+}, SO_4^{2-} and $CaSO_4$ (Ben Ahmed et al., 2008).

$$\Omega = \frac{(\alpha_{Ca^{2+}})(\alpha_{SO_4^{2-}})}{K_{SP}} \qquad \textbf{Equation 2-9}$$

where α_i is the ionic activity of species i and K_{SP} the solubility product based on:

$$K_{SP} = \gamma_{Ca^{2+}}[Ca^{2+}]_{eq} \cdot \gamma_{SO_4^{2-}}[SO_4^{2-}]_{eq} \qquad \textbf{Equation 2-10}$$

where γ_i is the activity coefficient of species i. The equilibrium concentrations, $[i]_{eq}$, of the calcium and sulphate ions are calculated from the solubility, **s**, given by (Seidell, 1958):

$$s = 2.091 + 0.0031 \cdot T - 8.19310^{-5} \cdot T^2 \ (T\ in\ ℃) \qquad \textbf{Equation 2-11}$$

Alternatively, the K_{SP} is equated using an empirical correlation from previous studies (Marshall and Slusher, 1966), where the solubility of the calcium sulphate dihydrate water system was extensively studied over between 0-110°C:

$$\ln(K_{SP}) = 390.9619 - 152.6246\, log(T) - \frac{12\,545.62}{T} + 0.0818493(T) \qquad \textbf{Equation 2-12}$$

The activity coefficients can be calculated by using the modified Debye-Hückel equation for electrolyte solutions (Davies, 1962), given as:

$$\log(\gamma_i) = -A.z_i^2\left(\frac{\sqrt{I}}{1+\sqrt{I}} - 0.3I\right) \qquad \textbf{Equation 2-13}$$

and

$$A = 1.82 \times 10^6 (\varepsilon.T)^{-\frac{2}{3}} \qquad \textbf{Equation 2-14}$$

$$I = 0.5 \sum c_i z_i^2 \qquad \textbf{Equation 2-15}$$

where: ε is the dielectric constant for water, T the temperature in Kelvin, c_i the molar concentration of species i and z_i the charge of the ion.

2.2.3. Precipitation and kinetics

Precipitation and crystallisation are the processes whereby a solid phase forms from an aqueous solution. The primary difference between the two processes is the solid end product. Precipitation generally occurs much faster than crystallisation, forming amorphous solids while crystallisation forms highly ordered crystalline solids (Söhnel and Garside, 1992). Generally, a crystal solid will form if the desupersaturation process occurs slowly in a controlled way, while precipitation occurs when a rapid desupersaturation occurs. Further, precipitation occurs at a constant temperature and does not depend on cooling to produce a supersaturated solution (Söhnel and Garside, 1992).

The precipitation process occurs in two different stages, namely: nucleation and growth. In a supersaturated solution the process is initiated by the formation of structured aggregates, until the aggregates exceed a certain size i.e. the critical nucleus size. This leads to the formation of a stable nucleus spontaneously growing in size (Söhnel and Garside, 1992). The kinetics of the calcium sulphate dehydrate precipitation is described in more detail in the following sections.

2.3.3.1 Nucleation

The mechanism of nucleation takes place in several steps, as shown in Figure 2-7. In primary nucleation the formation of the new solid phase is not influenced by the presence of the same solid phase being formed (Söhnel and Garside, 1992). Secondary nucleation on the other hand only takes place in the presence of the same solid phase that is being formed. This concept was very important in this study, since gypsum seeding is used to initiate secondary nucleation to desupersaturate the RO concentrate. Further, primary nucleation takes place in two distinct mechanisms: homogenous and heterogeneous nucleation. Homogenous nucleation is not influenced by the presence of any other solid particles, whereas heterogeneous nucleation is favoured by the presence of any foreign solid phase. In essence, homogenous nucleation rarely takes place since the solution always makes contact with some solid surface and often contains solid particles as impurities.

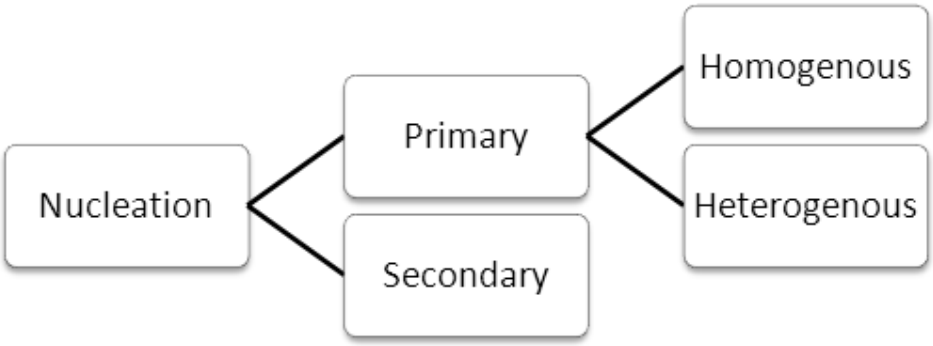

Figure 2-7 *Schematic of the different nucleation mechanisms (redrawn from (Gerber 2011)).*

If a solution becomes supersaturated, precipitation does not occur immediately, since crystal nuclei must develop prior to precipitation. The elapsed time from reaching supersaturation until the first physical changes are observed is defined as the induction time, as shown in Figure 2-8**.** Initially the supersaturated solution exhibits meta stable behaviour, until the primary nucleation is initiated, followed by a solid particle growth. The onset of precipitation has been intensively studied, using various analytical techniques including to observe physical changes in: concentration (Le Gouellec and Elimelech, 2002; Rahardianto et al., 2010; Shih et al., 2004), conductivity (Rahardianto et al., 2006; Shih et al., 2004) and turbidity (McCartney and Alexander, 1958; Pomerantz et al., 2006), indicating the start of the actual solid growth phase. Further, Alimi and Elfi (2003) determined that the induction period also depends on the cation to anion ratio.

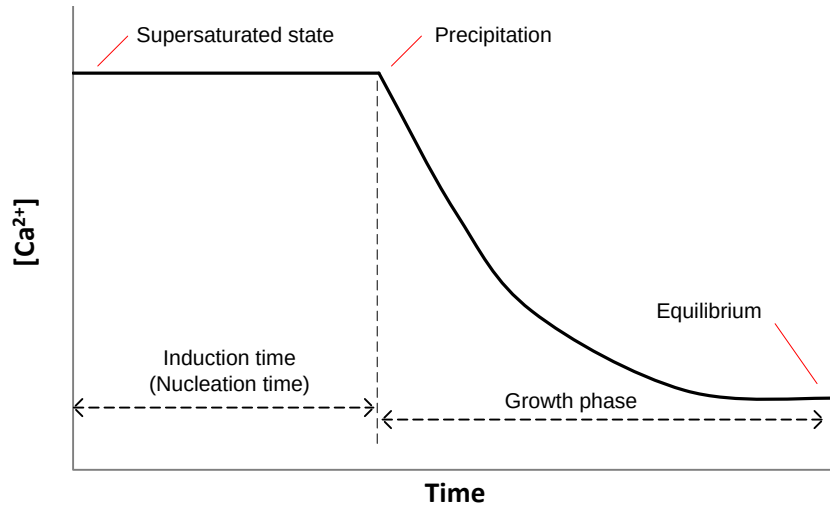

Figure 2-8 *Theoretical growth curve of gypsum precipitation (redrawn from Gerber (2011))*

Growth

Calcium sulphate crystal growth is initiated upon precipitation, hence crystal growth occurs between the onset of precipitation and chemical equilibrium, as shown in Figure 2-8. In previous studies there have been uncertainties about the calcium sulphate growth kinetics. Liu and Nancolass (1970) proposed that growth follows a second order in supersaturation, where the rate constant is a function of active growth sites in the system. Further, results showed that, under high supersaturation or low seed concentrations the growth period is preceded by an induction period. The growth model (Liu & Nancolass, 1970), is mathematically described by:

$$-\frac{dm}{dt} = k' S_n (m - m_{eq})^2 \qquad \textbf{Equation 2-16}$$

where: m is the calcium ion concentration ([Ca^{2+}], for equimolar solutions [Ca^{2+}]=[SO_4^{2-}]), k' is the kinetic growth constant expressed in 1/M min, S_n a constant related to the number of growth sites in the solution (e.g. seeding) and m_{eq} is the equilibrium concentration for the specific solution depending on temperature and ionic strength (Lui and Nancolass, 1970).

Alternatively, Brusilovsky and Borden (1992) proposed a diffusion-based first order gypsum crystal growth model. The model describes the growth of a single gypsum crystal, assuming the development of gypsum hemispheres on the membrane surface. The kinetic growth model is given as:

$$\frac{dM}{dt} = k_c A_s (C - C_S) \qquad \textbf{Equation 2-17}$$

where: M is the crystal mass, A_s the surface area of a single crystal in contact with the solution, C the bulk solution concentration and C_s the saturation concentration as the crystal surface (Brusilovsky and Borden, 1992).

2.3. Factors influencing gypsum crystallisation

In RO desalination applications, the feed stream becomes more concentrated while flowing axially across the membrane, as more solvent passes through the membrane. This can cause the solution to become supersaturated; however this does not necessarily result in mineral scaling through precipitation. The following factors, amongst others, are known to significantly influence gypsum scaling. Each of the factors is described in more detail in the subsequent subsections.

- Temperature
- Degree of supersaturation
- Seeding

In addition to the above mentioned factors, admixtures also influence nucleation. Admixtures are of ionic nature, often in the form of metal cations, absorbing onto the surface of the precipitating solid phase, forming complexes with the nucleating solids (Söhnel and Garside, 1992). Generally, the effect of admixtures on precipitation will depend on the admixture concentration. The investigation of the effect of admixtures on gypsum scaling is beyond the scope of this project, thus admixtures will not be considered further.

2.3.1. Temperature

The effect of temperature on induction time

In various studies it was shown that the increase in temperature shortens the induction period for calcium sulphate dihydrate precipitation (Amjad and Hooley, 1986; Amjad, 1985; Klepetsanis and Koutsoukos, 1991; Klepetsanis et al., 1999; Lui and Nancolass, 1970). This logarithmic relationship is explained by classical nucleation theory, whereby a 10°C increase in solution temperature reduces the induction time by approximately a factor of 2, for a given set of fixed operating conditions.

The temperature – induction time relationship is shown in Figure 2-9, where the inverse trend can be observed. In the experiments anti-scalants were dosed as follows: TENTMP at 1.89×10^{-6} M with 1930 mg/L seed (Lui and Nancolass, 1970), P-AA at 0.25 mg/L with 2000 mg/L seed (Amjad, 1985) and PAA at 0.2 mg/L with 2000 mg/L seed. However, in this study no antiscalants are used and alternatively the use of intermediate chemical desupersaturation to prevent gypsum scaling on the RO membranes was assessed. Although antiscalants were used for the experiments, the results show the reduction in induction time with a temperature increase. However, the antiscalants prolonged the induction times in these specific experiments, thus the induction times without antiscalants would be even lower.

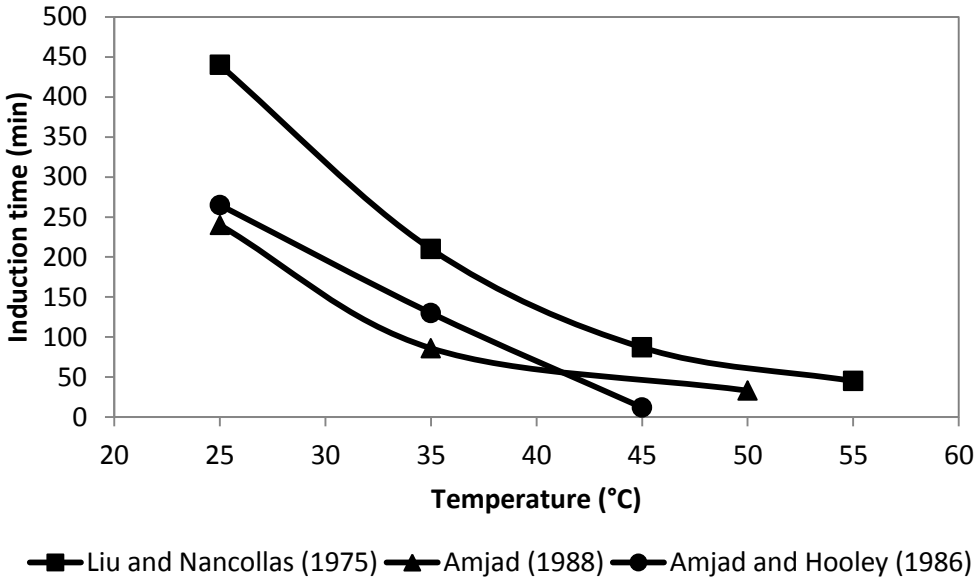

Figure 2-9 *The temperature - induction time relationship for gypsum precipitation, under the presence of anti-scalants.*

The effect of temperature on growth rate

Various studies have shown that the gypsum crystal growth rate, expressed in terms of the growth rate constant (k'), increased as the temperature is raised (Amjad and Hooley, 1986; Ben Ahmed et al., 2008; Klepetsanis and Koutsoukos, 1991; Klepetsanis et al., 1999; Lui and Nancolass, 1970). This trend follows the general Arrhenius relationship, where an exponential increase in growth rate was observed with increasing temperature. This relationship is shown in Figure 2-10 where the kinetics of calcium sulphate dihydrate precipitation were studied, showing the natural logarithm of the growth rate as an inverse function of absolute temperature.

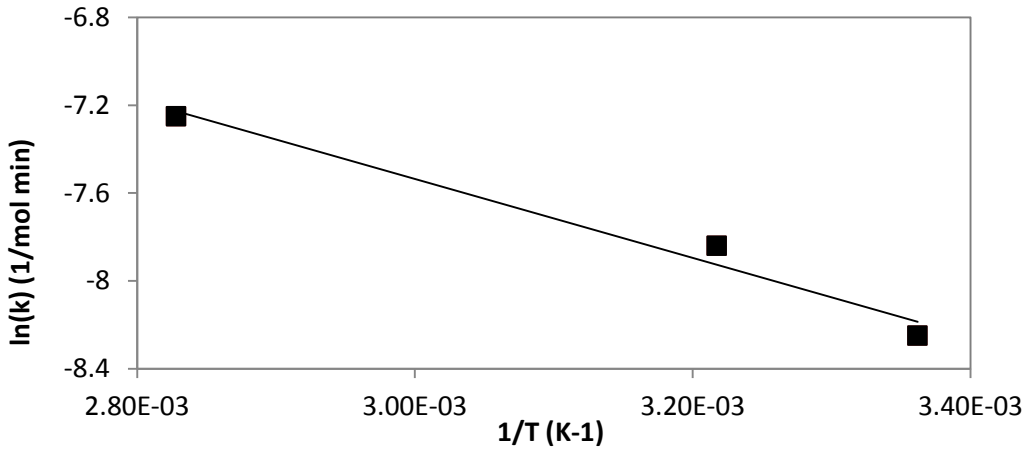

Figure 2-10 *Arrhenius plot of gypsum precipitation rate constant over the temperature range between 25-80°C (redrawn from Klepetsanis (1999)).*

2.3.2. Supersaturation

The supersaturation ratio is mathematically defined as the degree of saturation above or below the equilibrium concentration for a given temperature as given in Equation 2.8. The degree of saturation is an essential factor, directly influencing precipitation, by indicating the amount of available molecules available for precipitation near the nuclei surface at a given time (Gerber, 2011; Söhnel and Garside, 1992).

The effect of supersaturation on induction time

Söhnel and Mullin (1987), proposed the classical nucleation theory for homogenous precipitation, given in the following equation:

$$\log(t_{ind}) = B + \frac{C}{T^3(log\Omega)^2} \qquad \textbf{Equation 2-18}$$

$$C = \frac{\alpha N_A \sigma^3 V_M^2 f(\theta)}{(2.3R_u)^3} \qquad \textbf{Equation 2-19}$$

where: B is an empirical constant, α is geometric shape factor equal to 16π/3 of the spherical nucleus, N_A the Avogardos number (1/mol), σ is interfacial tension (empirically determined from the slope C), V_M the molar volume (74.69 cm^3/mol for calcium sulphate dihydrate), $f(\vartheta)$ a correction factor (equal to 1 for purely homogenous and 0.01 for purely heterogeneous nucleation) and R_U is the universal gas constant (Söhnel and Mullin, 1987).

The logarithm of the induction time was inversely proportional to the square of the logarithm of the supersaturation ratio (Ben Ahmed et al., 2008; Klepetsanis and Koutsoukos, 1991; Söhnel and Mullin, 1987). Typical experimental data are shown in Figure 2-11 where the inverse relationship between supersaturation ratio and induction time was evident. Increasing the temperature will further lower the induction times for gypsum precipitation.

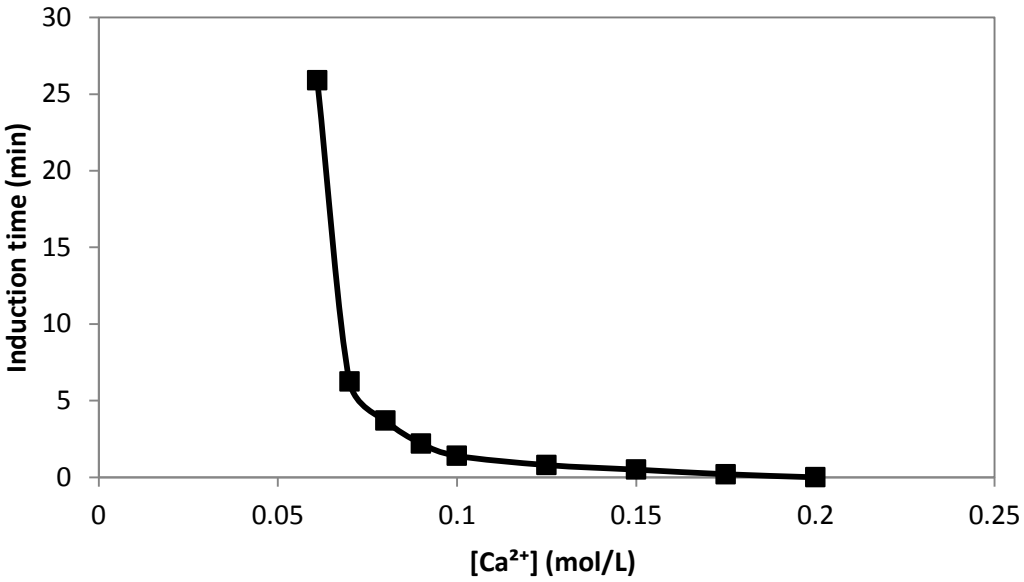

Figure 2-11 *Calcium concentration against induction time plot, at 25°C (redrawn from Liu and Nancollas (1973)).*

The effect of supersaturation on growth rate

Previous studies investigated the relationship between the supersaturation ratio and gypsum crystal growth rate, however the results from different studies varied significantly. However, all studies showed an increase in growth rate as the level of gypsum saturation increases (Ben Ahmed et al., 2008; Klepetsanis and Koutsoukos, 1991; Klepetsanis et al., 1999; Lui and Nancolass, 1970).

Liu and Nancollas (1973) proposed a second order relation between supersaturation level and gypsum crystal growth rate, using 0.028-0.0424 mol/L [Ca^{2+}] at 25°C. This second order relationship was caused by the 2-dimensional surface nucleation and is independent of surface area but depends on the amount of active growth sites available or introduced into the system.

Klepetsanis and Koutsoukos (1991) conducted experiments using equimolar calcium and sulphate solutions, and found that the gypsum crystal growth rates are directly proportional to degree of supersaturation. A semi empirical rate equation suggested an apparent order of 5, after interpreting the experimental data. Further, a polynuclear mechanism was suggested, indicating a surface-controlled mechanism.

Klepetsanis (1999) suggested a linear relationship between the growth rate and the solution supersaturation. Further a mechanism was suggested, integrating the growth units into the active sites of the supercritical nuclei through surface diffusion.

2.3.3. Seeding

In aqueous solutions of gypsum, precipitation is generally not favourable if the level of supersaturation is too low. Precipitation can be accelerated or induced by seeding the solution with solid particles. The rate of precipitation greatly depends on the type, concentration and morphology of the seed species. Each of the three factors is discussed in more detail in the subsequent sections.

Seed type

Two distinct types of seeded growth can occur in the aqueous solutions: homogenous seeded growth and heterogeneous seeded growth (Söhnel and Garside, 1992). Homogenous seeded growth takes place if the seed species have the same chemical structure as the nucleating phase, whereas in heterogeneous seeded growth the seed species have a different chemical structure compared the nucleating phase.

Gill and Nancollas (1979) conducted seeded gypsum crystallisation experiments using gypsum, barite (dendritic and rhombic) and calcite as seed material. The experiments showed immediate gypsum precipitation upon feeding gypsum seed to the metastable solution, whereas the precipitation was delayed by an induction period in the barite and calcite seeded experiments. However, once the precipitation was initiated in the calcite and barite seeded experiments, the crystal growth rate was much faster compared to the gypsum seeded experiments. Scanning electron micrographs showed that surface nucleation of calcium sulphate occurred on the calcite an barite seed crystal during the induction period. Therefore, the faster growth rate for the calcite and barite seeds is explained by the higher number of active growth sites formed during the nucleation phase.

Yang et al. (2008) performed similar gypsum precipitation experiments using various different inorganic seed crystals, namely: calcium sulphate dihydrate, kaolin, aluminium oxide, dolomite, magnesium oxide and diatomite. Gypsum seeding caused immediate gypsum precipitation, agreeing with the results from Gill and Nancollas (1979). In most heterogeneous seeding experiments, nearly immediate precipitation occurred, observing only a very short nucleation/induction period. Further, the precipitation rate with the heterogeneous seeding resulted in lower growth rates, compared to the homogenous case, contrasting the results from Gill and Nancollas (1979). However, Yang et al. (2008) used much higher seed concentrations compared to Gill and Nancollas (1979), for the heterogeneous seeding, thus explaining these results (Gerber, 2011).

Seed Concentration

The induction period and rate of gypsum precipitation for a specific aqueous system depends on the quantity of detectable growth sites the specific solution (Söhnel and Garside, 1992). In various studies it was shown that the gypsum crystal growth rate was directly proportional to the initial seed concentration, due to the higher number of available growth sites (Amjad and Hooley, 1986; Amjad, 1988, 1985; Lui and Nancolass, 1970). The data for the respective experiments is given in Table 2-2, where an increase in growth rate with increasing seed concentration was observed.

Table 2-2 *Comparison of gypsum seed concentration versus gypsum crystal growth for various studies*

Gyspum Seed Conc. (mg/L)	Induction Period (min)	Rate constant k (1/mole min)	Temperature	Source
1990	0	8.66	25°C	Amjad (1995)
2860	0	12.9		
790	80	15.1		
880	0	2.57	25°C	Amjad (1988)
440	67	1.37		
2487	0	1.2	35°C	Liu and Nancollas (1970)
1327	0	0.61		
1213	0	0.58		
247	50	0.55		

For lower gypsum seed concentrations, crystal growth was preceded by an induction time (Amjad, 1988, 1985; Lui and Nancolass, 1970). Microscopic analysis showed that surface nucleation took place on the seed crystals, most likely also accompanied by bulk crystallisation.

Further, Amjad (1985) and Amjad (1988) reported larger growth constants after the induction period, compared to the growth constants at higher seed concentrations, shown in Table 2-2. Liu and Nancollas (1979) did not observe the same results for the experiments without antiscalants, however in the experiments with antiscalants the same trend were observed. This phenomenon can be explained by the larger number of active growth sites, formed during the induction period . Therefore, the gypsum crystallisation rate was higher compared to the cases without the induction period.

Seed Morphology

In the literature it is reported that gypsum crystal growth primarily takes place in two distinct forms: needle and platelet structures (Klepetsanis et al., 1999; Lui and Nancolass, 1970; Najibi et al., 1997; Oner et al., 1998; Seewoo et al., 2004), varying in size, shape and surface area as shown in Figure 2-12. Needle-like crystals are generally thinner and elongated, while plate like crystals are shorter, thicker, more robust and have a greater surface area.

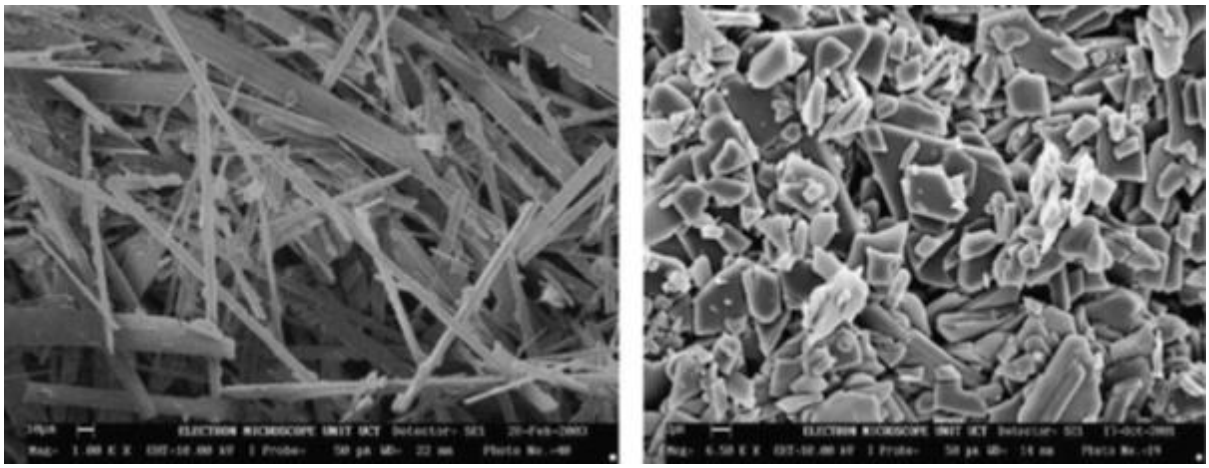

Figure 2-12 *Needle-like morphology in gypsum crystals (left), scale bar 10 µm. Plate type structures in gypsum crystals (right), scale bar 2 µm. (reprinted with permission from Seewoo et al. (2004)).*

Liu and Nancollas (1970) added gypsum seed crystals to metastable supersaturated gypsum solutions, thereby forming 80-120 µm needle-like crystals from 0.1M solutions and 20-50 µm long plate-like crystals from 0.6 M solution. Christofferson et al. (1982) obtained similar results, where 0.3 M gypsum solutions favoured needle-like crystal growth and higher concentrations around 0.725M produced smoother surfaces. Therefore, lower gypsum concentrations generally favour needle-like crystallisation and higher gypsum concentrations favour plate-like crystallisation (Alimi and Elfil, 2003; Christoffersen et al., 1982; Lui and Nancolass, 1970; Seewoo et al., 2004).

During seeded gypsum crystallisation experiments, it was established that the addition of plate-like seeds to a meta-stable supersaturated solution resulted in higher growth rates, compared to the addition of needle-like crystal seeds (Liu and Nancollas, 1973; Lui and Nancolass, 1970; Seewoo et al., 2004). Therefore, it is desirable to add plate-like crystal feeds to rapidly desupersaturate a metastable supersaturated solution. Seewoo et al. (2004) suggested that this phenomenon was caused by an increase in specific surface area. Plate-like crystal structures generally have a higher surface area, thus more growth sites are available.

2.4. Calcium sulphate scaling in RO membranes

2.4.1. Concentration Polarisation

Concentration polarisation is a membrane surface phenomena where dissolved ions accumulate at the membrane surface, thus the local concentration at the membrane surface is higher than in the bulk solution (van de Lisdonk et al., 2001). This membrane phenomenon is associated with the permselectivity of the membrane and the presence of a stagnant film, inherent in all cross flow filtration regimes (Matthiasson and Sivik, 1980). Considering the flow across the membrane, a velocity boundary layer will form at the membrane surface, as shown in Figure 2-13, where the velocity approaches zero when moving closer to the membrane surface. A convective permeate flow transports solvent from the bulk fluid to the membrane surface and a diffusive back-transport moves the solutes away from the membrane (Kucera, 2010). Within this stagnant film, a concentration boundary layer forms, where the thickness depends on the diffusive back transport and convective permeate flow. Solutes are rejected by the membrane and diffusive transport is much slower than convective permeate transport, hence the solutes tend to build up at the membrane surface.

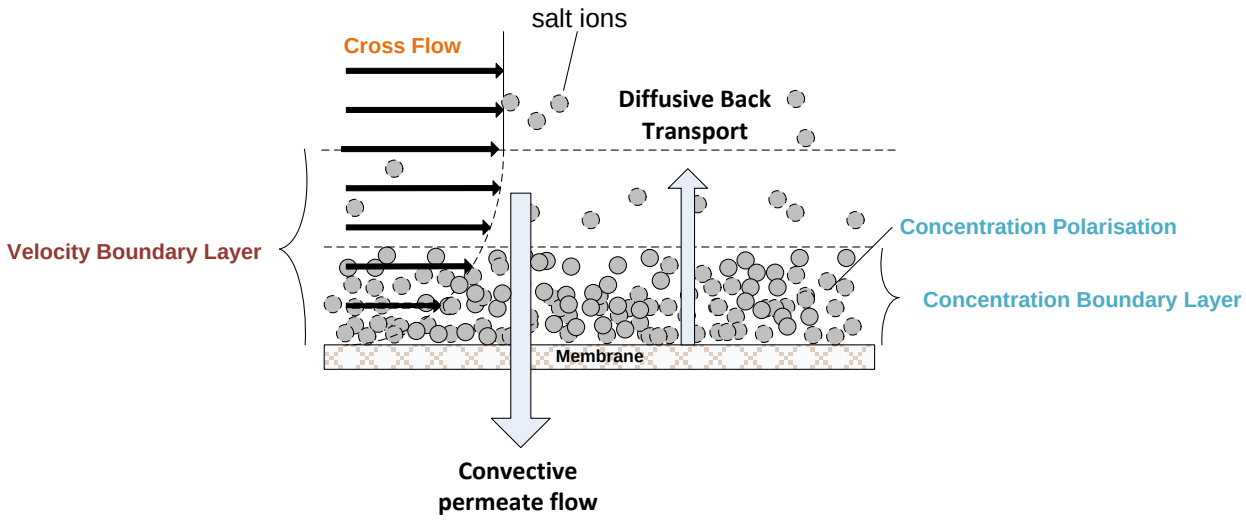

Figure 2-13 *Mass transport phenomena near the membrane surface where the grey dots are salt ions near the membrane surface and in the bulk fluid (redrawn from (Hamann, 2010))*

Concentration polarisation can have serious consequences in brackish RO desalination, directly leading to surface crystallisation on the membrane if the solubility of sparingly soluble salts is exceeded (van de Lisdonk et al., 2001). In bulk crystallisation the driving force for the crystallisation is the difference between bulk and saturation concentration, whereas in surface crystallisation it is

the difference in membrane and saturation concentration, implicating that concentration polarisation is only associated with surface crystallisation (Oh et al., 2009).

The level of concentration polarisation is primary affected by the permeate flux and cross flow velocity along the membrane surface. Higher permeate fluxes result in higher levels of concentration polarisation at the membrane surface, thereby increasing the propensity for membrane scaling (Bartman et al., 2011; Gabelich et al., 2007; Oh et al., 2009; Pomerantz et al., 2006; Shih et al., 2004). Increasing the cross flow velocity reduces the membrane scaling propensity, due to the thinner boundary layer at the membrane surface (Kucera, 2010). Reducing the boundary layer thickness decreases the level of concentration polarisation at the membrane surface, thus reducing the risk of membrane scaling (Oh et al., 2009; Sablani et al., 2001; Uchymiak et al., 2008).

Additionally, concentration polarisation has three negative effects in RO operations (Kucera, 2010), reducing the permeability if the specific membrane as follows:

- The concentration polarisation layer acts as hydraulic resistance to the water.
- The osmotic pressure of the solution is increased within the boundary layer due to the build-up of solutes, resulting in a flux decline if the applied pressure is not increased accordingly.
- Concentration polarisation leads to higher salt passage through the membrane, since the concentration of solutes at the surface is higher compared to the bulk solute concentration. The actual rejection of the membrane does not change, however the apparent rejection will be lower. Membranes reject solutes based on the concentration closest to the membrane.

2.4.2. Scaling mechanism

It is generally accepted that RO membrane scaling takes place by direct surface crystallisation and/or deposition of bulk solution formed crystals (Brusilovsky and Borden, 1992; Shih et al., 2005). This conceptual scaling mechanism is shown in Figure 2-14. In aqueous salt solutions, containing ions A^+ and B^-, crystallisation takes to from precipitate P. This reaction can occur in the bulk fluid, or alternately directly on the membrane. In typical desalination plants, the convective residence time in the RO membranes is relatively short, hence scale formation is likely to occur via surface crystallisation (Shih et al., 2005).

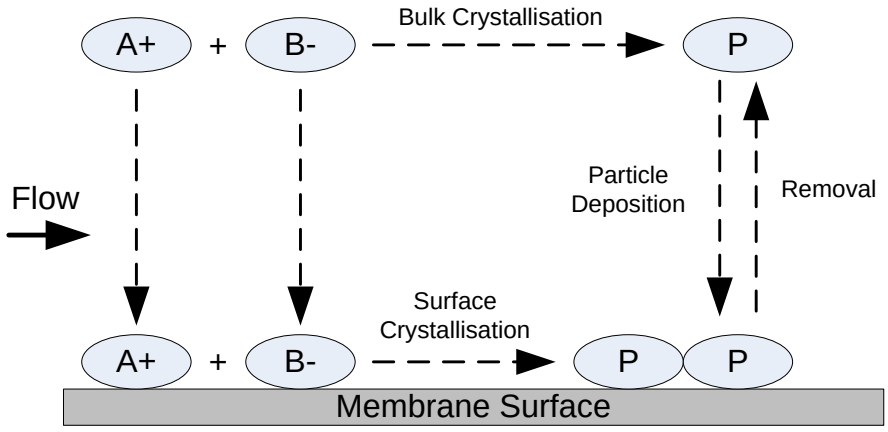

Figure 2-14 *Schematic diagram showing the conceptual membrane scaling mechanism (redrawn from Shih et al. (2005)).*

Experiments have shown that the bulk induction time is much longer, compared to the induction time in RO modules, indicating that surface crystallisation is the primary mechanism of RO membrane scaling (Rahardianto et al., 2006; Shih et al., 2005; Uchymiak et al., 2008).

2.4.3. Scale development in cross flow configurations

Currently most RO osmosis plants use spiral-wound membrane, due to the high packing densities, compared to plate and frame or tubular modules (Kucera, 2010). These spiral wound membranes are suitable for large industrial desalination operations. However, flat sheet membranes are preferred for laboratory scale experiments. Analysis of gypsum scaling on flat sheet membranes is less complex, compared to spiral-wound membranes.

Rahardianto et al. (2006) investigated the mineral scale development on RO membranes and the impact of gypsum scale on permeate flux decline. An optical surface analysis was used to determine the fraction of scaled membrane, where actual photographs are shown in Figure 2-15. The optical images showed that the extent of surface scaling increases with axial position, corresponding to increasing degree of supersaturation along the axial position. A more uniform flow field in the central region resulted in more uniform scale coverage in the traverse direction. Scale formation was more significant near the channel exit and edges, due to the concentration variations in the more complex flow field.

In similar experiments, Shih et al. (2005) investigated the axial development of gypsum surface crystallisation on RO membranes. A correlation between surface crystal size and axial position was observed, increasing towards the flat sheet membrane exit. These findings are consistent with the

corresponding increase in level of concentration polarisation along the membrane surface in cross flow RO membranes (Kim and Hoek, 2005; Matthiasson and Sivik, 1980; Srinivasan and Chi, 1970). Therefore, the surface mass density was higher towards the end of the exit region (Shih et al., 2005).

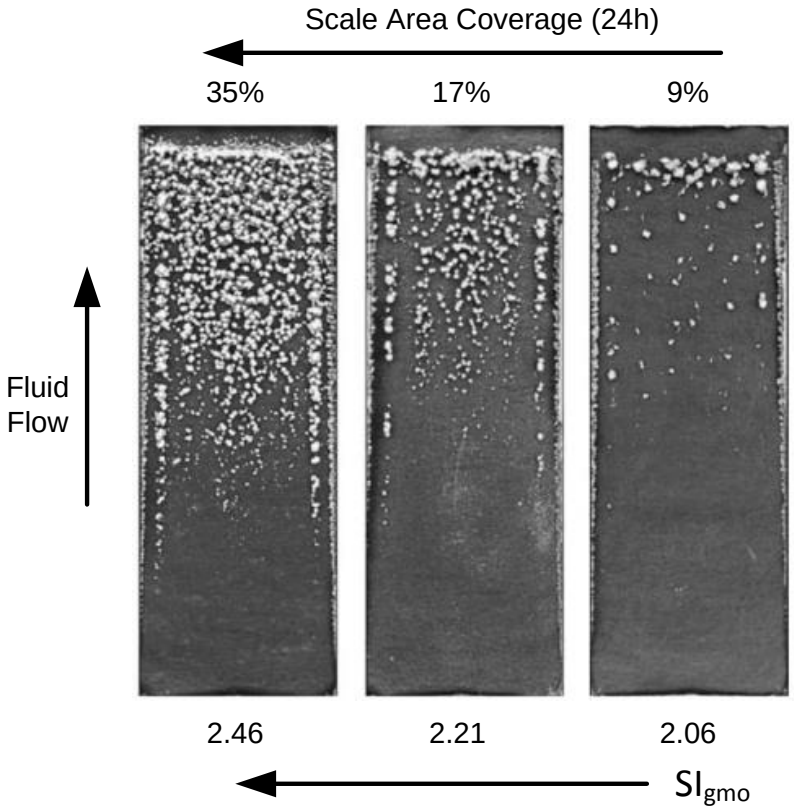

Figure 2-15 *Photographs of gypsum scaled LFC1 membranes at varying initial gypsum saturation indexes (at the membrane surface), showing the scale development after 24 hours of operation in the absence of antiscalants (reprinted with permission from Rahardianto et al (2006)).*

Gypsum scale morphology studies on actual RO membranes showed that surface crystals form partial or complete rosettes, depending on the position of the membrane (Rahardianto et al., 2006; Shih et al., 2005). Shih et al. (2005) showed that crystal morphologies change along axial position in an RO membrane, due to the changing degree of supersaturation. It was found that the crystal structures progressed from needle-like to plate-like to partial rosette and eventually to complete rosettes, when moving axially along the membrane.

Uchymiak et al. (2005) determined that the nucleation rate of new surface crystals depends on the amount of scale free membrane area available. With increasing surface scale coverage, the progressive growth of new gypsum crystals declines and ultimately results in diffusion controlled growth of existing crystals.

2.4.4. Flux decline

In any RO membrane operation permeate flux decline is, amongst other, the direct consequence of surface crystallisation and deposition of bulk crystallised mineral scales onto the membrane surface (Borden et al., 1987; Gilron and Hasson, 1987; Shih et al., 2005). The surface crystallisation is initiated by the difference between the supersaturated solution concentration and the equilibrium concentration thereof (Borden et al., 1987; Brusilovsky and Borden, 1992). The convective residence time in RO modules commonly used in RO desalination plants is short, hence the scale formation mostly occurs via surface crystallisation. Therefore, the permeate flux decline is often correlated with the solution saturation index at the membrane surface. Furthermore, bio-growth and organic adhesion can also cause flux decline.

Rahardianto et al. (2005) studied the effects of concentration polarization on permeate flux decline. Increasing the initial membrane saturation level from 1.96 to 2.46 resulted in a flux decline from 4 % to 27 %, as shown in Figure 2-16, using a LFC1 membrane without any antiscalants. This suggested an exponential rise in fractional permeate flux decline with the initial gypsum saturation level at the membrane surface. Furthermore, the scaling propensity depended on the type of membrane, even under identical operating conditions (Shih et al., 2005).

Further, the rate of permeate flux decline depends on the rate of surface crystallisation which is a function of available precipitation area and level of solution supersaturation (Borden et al., 1987). Through the precipitation on the membrane surface, the supersaturated solution is relieved and the degree of concentration polarization is diminished. This is also in agreement with another study, where it was found that the fraction of total surface area covered by scale correlates linearly to the fractional flux decline (Rahardianto et al., 2006).

Brusilovsky and Borden (1992) found that the salinity of the permeate increases as the permeate flux increases. It was suggested that pockets of stagnant solution develop around the previously formed surface scale, thus the salt concentration builds up and increasing the salt passage of the membrane.

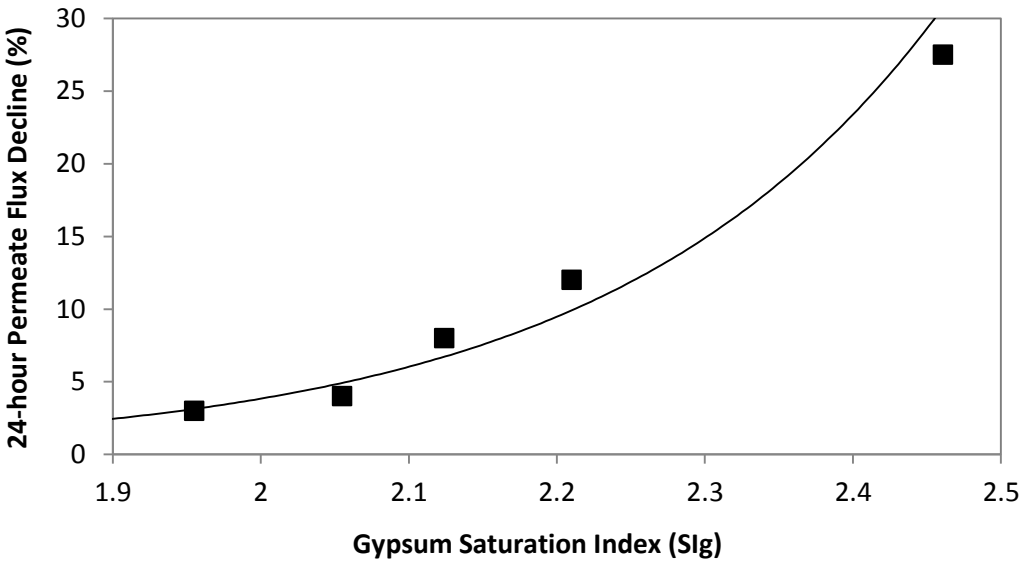

Figure 2-16 *Permeate flux decline over 24-hours for a LFC1 RO membrane as a function of initial gypsum saturation index at the membrane surface in the absence of antiscalants (redrawn from Rahardianto et al. (2006)).*

2.5. Scaling prevention in brackish RO desalination

The overall recovery in any brackish water desalination operation is limited by the scaling potential of the feed water, since oversaturation of sparingly soluble salts can cause membrane scaling (Sanciolo et al., 2012; Shih et al., 2005; Uchymiak et al., 2008). Therefore, it is important to design brackish RO plants carefully, to ensure operation below saturation concentrations or to employ a method to prevent scaling. To date, there are several methods to prevent membrane scaling of sparingly soluble salts in brackish RO desalination. Each method is briefly discussed individually and then the methods were compared.

2.5.1. Antiscalants

Currently, antiscalants are the most commonly used strategy to prevent membrane scaling in brackish RO desalination. Antiscalant additives affect the gypsum crystal nucleation rate, growth rate, precipitated variety and the crystal habit (Ben Ahmed et al., 2008), thus effectively preventing precipitation. The effect of antiscalants on gypsum scaling is a very well-studied field. Although antiscalants are not used in this study, a brief overview of antiscalant behaviour on gypsum scaling in RO membranes is given below.

The antiscale additives are usually polyelectrolytes, for instance polycarboxylates, polyacrylates, polyphosphonates and polyphosphates (Amjad and Hooley, 1986; Amjad, 1985; Ben Ahmed et al., 2008; Oner et al., 1998). It has been suggested that antiscalants inhibit mineral salt crystallisation through the adsorption onto the formed crystals or onto the developing nuclei (Oner et al., 1998). The addition of antiscalants to supersaturated solutions of sparingly soluble salts, results in a delay in crystal nucleation and subsequent growth (Shih et al., 2004).Typically, antiscalants can prevent precipitation in calcium sulphate solutions below and up to a supersaturation index of 3, however precipitation is likely to occur at supersaturation levels higher than 3 (Pomerantz et al., 2006). Even if antiscalants are used, there is a limit at what supersaturation ratios the RO plant can be operated, thus also limiting the maximum overall recovery. Further, the effectiveness of antiscalants differs depending on the specific membrane type (Rahardianto et al., 2006).

2.5.2. Permeate recycling

Al Bastaki et al. (2003) performed process simulations on lab scale brackish RO desalination plant, operating with mildly saline (3000 mg/L TDS) feed. The aim of the computer simulation was the investigation of permeate recycling into the RO feed, to improve the overall permeate quality and maintain a constant feed quality. The results showed that permeate recycling and mixing it with the RO feed water was beneficial in reducing the concentration polarisation on the membrane surface, thus ultimately reducing the scaling risk and improving membrane life times. Further, the quality of the RO permeate was also improved due to the constant salt passage at the membrane surface. The main disadvantage of this was the reduction in permeate production rate, where a recycle ratio of 25% caused a 22% reduction in permeate production rate.

2.5.3. Flow Reversal

Pomerantz et al. (2006) investigated alternative methods to prevent mineral scaling in RO plants. Firstly, switch experiments were performed with a small 34 cm^2 flat sheet RO test cell, where the RO feed was periodically switched from an oversaturated calcium sulphate solution to a undersaturated feed solution. The principle behind this technique: by switching the RO feed from oversaturated to undersaturated calcium sulphate solution, in less than a complete induction time, prevents mineral scaling. This removes the supersaturated solution from near the membrane, periodically replacing it with an undersaturated solution, before the heterogeneous induction time is reached. Further, all developed crystal nuclei would be swept away hence crystal growth, at least theoretically, will not occur.

Secondly, Pomerantz et al. (2006) investigated a flow reversal technique, whereby feed flow reversal was used to periodically switch between the entrance and exit of the RO modules. A three-stage RO plant (in series) was used to for these experiments, with two 2.5" spirals in each pressure vessel per stage. The disadvantage of the first method from the study was overcome by this flow reversal technique. The pressure must not be lowered to allow fast flushing with undersaturated solution, instead the feed was reversed, hence the production does not stop during the flow reversal. Membrane scaling typically occurred in the latter stages where the concentration polarisation was most severe. For this technique to work, the induction time of the specific system must be long enough so that the switching frequency is relatively low. In highly supersaturated solutions, this required antiscalant dosing, to further extend the induction period.

In the laboratory scale experiments, a baseline run at 10 bar, using a 30 mM calcium sulphate (SI = 1.7 - 2.5) resulted in an induction time of 170min, after which a flux decline was observed. Under the same experimental conditions, the flow was switched to the undersaturated solution (SI = 0.4 - 0.7) for 10 min each hour. No flux decline was observed, and the membrane could be operated scale free for 480 min until the end of the experimental run. However, the experiment did not show if scaling, indicated by a flux decline, would eventually occur after prolonged operation exceeding 480 min. This flow switching with undersaturated solution, basically zeroed the induction clock every time a switch was made, thus prevented membrane scaling.

Experimental runs with a pilot RO system showed that without flow reversal a flux decline occurred after 0.5-1 hours, operating with supersaturated feed solution (SI = 1.7 - 2.5). By reversing the flow every 0.5 hours, the pilot plant could be operated without any flux decline for 22 hours. The calcium concentration in the feed and concentrate remained stable over the entire length of the experiment, further suggesting that no scale formation occurred. In general, this method of scaling prevention allowed the overall recovery to increase from 75 to 85 %. However, it must be stressed that this was not demonstrated for periods longer than 22 hours.

2.5.4. Intermediate concentrate precipitation techniques

In brackish RO desalination, the reduction in scaling ions in the RO concentrate is crucial for the operation at high permeate recovery levels (Gabelich et al., 2007). Typically the primary RO stage is followed by a demineralisation step before feeding the desupersaturated concentrate to a subsequent RO stage, to prevent scaling, thus allowing higher overall water recoveries. Several studies have shown that high product water recoveries can be achieved, using various intermediate

precipitation techniques (Bremere et al., 1999; Gabelich et al., 2007; Juby and Schutte, 2000; Rahardianto et al., 2007; Seewoo et al., 2004), where the relevant studies are discussed in the following sections.

Accelerated precipitation softening (APS)

Rahardianto et al. (2007) studied the accelerated precipitation softening (APS) process on a lab-scale pilot plant using model solutions as a feed (SI_g = 1.1). In the APS process sodium hydroxide is dosed to RO concentrate, followed by calcite seeding to desupersaturate the RO concentrate. Next, acid dosing and microfiltration ensures that no calcite scaling occurred in the secondary RO desalination step. Essentially the APS process was used to desupersaturate the primary RO concentrate, in order to feed with low scaling propensity to the subsequent RO stage.

The APS process proved to be effective, significantly reducing calcium (>90%), barium (>95%) and strontium (~78%) concentrations, whereas moderate reduction was achieved for magnesium and silica (10-20%). With traditional membrane scaling control strategies (i.e. antiscalants), recoveries of up to 90% were attained with actual field water, having a feed gypsum SI of 0.07. Experiments with model solutions and field samples showed that recoveries of up to 98% could be achieved, by combining primary RO with the subsequent APS, followed by secondary RO desalination with antiscalant make up. This showed that high recovery desalination using the Primary RO – APS – Secondary RO method was possible, and precipitation kinetics were favourable even with antiscalant carryover.

Chemically enhanced seeded precipitation (CESP)

Rahardianto et al. (2010) demonstrated the two-step chemically enhanced seeded precipitation (CESP) process, to treat RO concentrate of high scaling propensity. In the first step lime was added to the RO concentrate in order to elevate the pH, thus raising the saturation index of calcite, with the aim to induce rapid nucleation and growth of $CaCO_3$ crystals. This leads to antiscalant scavenging by $CaCO_3$ particles, which was critical for the next step. In the second CESP step, gypsum seed crystals were dosed to induce calcium sulphate precipitation under minimal or no retardation by antiscalants.

Initial laboratory jar tests were completed by Rahardianto et al. (2010) to evaluate if the CESP was suitable for high recovery brackish desalination. The experiments were carried out with a solution that mimics the concentrate from typical agricultural drainage RO desalination, supersaturated with

respect to gypsum (SI ~2.5) and calcium carbonate (SI ~ 20). The alkaline pre-treatment using hydrated lime (1.35-3.37 mM) increased the pH of the solution to around 9.5, to ensure favourable precipitation conditions for the gypsum seeding process. Batch experiments showed that lime precipitated calcite effectively scavenges antiscalants, hence enabling unhindered growth of calcium sulphate onto the gypsum seed crystals. Further, solids recycling in batch experiments proved to be effective, thus suggesting that continuous CESP is viable.

McCool et al. (2013) completed field tests with a pilot CESP plant, using real agricultural drainage water having a feed gypsum saturation index of about 0.85-0.97 (6700 - 14 400 mg/L TDS). The CESP step proved to be effective, removing calcium (32-34%) and phosphate ions (44%) via precipitation and other minor ions such as strontium (19%), magnesium (6-7%) and silica (1-3%). The gypsum saturation index was reduced from 1.7 to 1.1 in the primary RO concentrate and CESP effluent respectively. This water with a low scaling propensity was further desalted in the secondary RO stage, ultimately increasing the recovery up to 93 % if the concentrate was partially recycled. The maximum recovery in the secondary RO step was achieved up to the limit posed by the antiscalants. Actual plants using the CESP technique would require vigorous process control to account for temporary feed water variations and continuous removal of solids from the solids contact reactor, to ensure operation at high recoveries.

Intermediate chemical demineralisation (ICD)

Gabelich et al. (2007) proposed a pilot plant to evaluate an intermediate chemical demineralisation technique by using feed water from the Colorado river with a low gypsum saturation index of 0.08. The study was based on previous experimental work (Rahardianto et al., 2007), suggesting that about 60-65 % Ca^{2+} removal was necessary in the ICD step, to achieve an overall recovery of 95% by dosing antiscalants and operating a secondary RO membrane. In the ICD step NaOH was dosed to the primary RO concentrate, followed by the alkaline-induced precipitation in a solids contact reactor operated at pH 10 or above. This resulted in the removal of Ca^{2+}, Ba^{2+}, Sr^{2+} and silica (the main scaling precursors) via the ICD step at levels of 94 %, 97 %, 88 % and 67 % respectively. The prolonged operation of the pilot plant demonstrated that 95 % recovery desalination is viable via the Primary RO – ICD – Secondary RO approach, regardless of the fluctuating feed conditions. A large scale implementation of the process requires strict real time pH control strategies to maintain a pH above 10 in the solids contact reactor.

Further ICD testing was done by Gabelich et al. (2011), by operating the pilot plant with Colorado river water having SI_g of 0.08. Microfiltration and dual media filtration was evaluated as the filtration step in the secondary RO desalination. The study showed that reactor influent Ca^{2+} and total carbonate concentrations, as well as reactor effluent pH are the key operating variables controlling ICD performance, (i.e. the removal efficiency of Ca^{2+}, Ba^{2+}, Sr^{2+} and silica). Microfiltration was more suitable as a pre-treatment to the secondary RO step for this specific feed water. Continuous operation for over 550 hours at 95 % overall recovery without any scale formation on the spiral membranes, demonstrated the effectiveness of the Primary RO – ICD – Secondary RO desalination method.

Slurry precipitation and recycle reverse osmosis (SPARRO)

Juby (1994) proposed a novel seeded slurry precipitation technique to increase the overall recovery in extensive lab and pilot plant work using pre-treated water. In the process, the feed stream to the tubular cellulose acetate membranes consists of pre-treated mine water, mixed with a recycle slurry stream containing about 20 g/L calcium sulphate crystals. As the solubility of calcium salts is exceeded in the tubular membranes, the seed crystals act as growth sites, thus preventing surface crystallisation on the membrane surface. This process is only applicable to membranes systems that will not clog up quickly (for instance spiral membranes), since slurry is circulated within the membrane, therefore the tubular cellulose acetate membranes were used. The concentrated slurry was pumped to a hydro cyclone, where the underflow contained the excess calcium sulphate and brine waste. The overflow was fed to a stirred reaction tank with 1 hour hydraulic residence time, before it was mixed with the pre-treated mine water and fed to the RO membranes.

The pilot plant was operated over a period of 5 years, operated in various modes and varying degrees of pre-treatment in the raw mine water, where new membranes were installed for different phases. Generally, an overall recovery of over 90 % was achieved (up to 98 % in Phase 4), while the instantaneous recovery ranged between 27 and 50 %. The overall salt rejection for the tubular membranes was steady or decreasing for different phases, while no trend for permeate flux was observed since it increased or decreased during different phases. In general, all membranes ultimately fouled prematurely and an average membrane life expectancy of 1 year was observed. Membrane autopsies suggested that no membrane damage occurred from the abrasion of the seed crystals.

Hi Recovery Precipitation Reverse Osmosis (HiPRO)

In South Africa the state of the art eMalahleni Water Reclamation Plant was commissioned in 2007, to recover acid mine drainage from several mines in the eMalahleni (Witbank) area. The plant currently produces over 25 ML/day, while running at recoveries above 99%, often reaching monthly values in the order of 99.5% (Hutton et al., 2009). These high recoveries are achieved by using multiple stages of membrane filtration, while operating with low chemical and energy input.

The entire process occurs in three stages. In stage one the raw acid mine drainage water is neutralised, before ultrafiltration is used to reduce the SDI below 3. In the first RO stage a low salinity permeate below 200 mg/L TDS is produced while operating at overall recoveries of about 65%. In the second stage the supersaturated RO concentrate is demineralised via seeded gypsum precipitation in continuous operated reactors. The reactor effluent is fed to clarifiers and hydro cyclones to remove solid particles from the seeding. Again, ultrafiltration is employed to reduce the SDI below 3, before the secondary RO stage. A low salinity effluent below 200 mg/L is produced while operating at recoveries of 65 % in the secondary RO stage. The third stage is very similar to the second stage, only producing a slightly more saline permeate of about 400 mg/L while the overall recovery is slightly lower at 60%. This combined permeate from all three stages complies with SANS 0241 Class 1 2005 drinking water specifications (SANS 241, 2011), well below a TDS of 450 mg/L.

Currently, the plant produces about 100 m^3 of concentrated brine and 100 tons of gypsum-rich solid waste every day (Bhagwan, 2012). The brine is further concentrated in large plastic lined evaporation ponds, while the solid waste has great potential to be reused in the construction industry.

Operating a plant with this complexity requires skilled operators, since optimum performance and membrane health are vital for the process to be successful. Furthermore, another HiPRO plant is currently in operation at Optimum Coal Holdings in the Middleburg area.

2.5.5. Comparison of techniques

In the previous sections various methods of calcium sulphate scaling prevention were discussed for typical brackish RO desalination, where the main results for each technique are given in Table 2-3. It is difficult to compare the methods directly, since the feed gypsum saturation index ranged from 0.07 to 2.7. In all methods antiscalants were dosed, except for the SPARRO process where antiscalants would inhibit precipitation onto seed crystals.

The APS and ICD process is suitable for waters with a low gypsum scaling propensity, achieving overall recoveries of 98 % and 95 % for the specific ASP and ICD processes respectively. In both processes lime dosing ensures antiscalant scavenging, before desupersaturation occurs via precipitation onto calcite crystals. In the APS method calcite seed crystals are dosed, while calcite is precipitated in the reactor in the ICD process to provide nucleation sites for the desupersaturation. The feed water has an average calcite SI of 1.1 (0.6 min., 2.6 max.), thus making this method unsuitable for waters with a low calcite scaling index, where the increase in pH will not result in $CaCO_3$ supersaturation (Gabelich et al., 2007).

Table 2-3 *Comparison of various methods to achieve high recoveries in brackish water desalination. Note: The seed type for the ICD method is shown in brackets, since calcite is alkaline-precipitated in the reactor and not actually dosed.*

Method	Reference	RO Feed SI_{gypsum}	Seed Type	Overall Recovery (%)	AS Dosing	Plant Type	Comments
Flow Reversal	Pomerantz et al. (2006)	1.7 - 2.5	NA	85	Yes	Lab-scale & Pilot	- Flat sheet membrane switching to SI < 1 feed - Flow reversal - Spiral RO
Accelerated Precipitation Softening (APS)	Rahardianto et al. (2007)	0.07	Calcite	98	Yes	Lab - scale	- PRO - APS - SRO method - Flat sheet membrane - pH adjustment with NaOH
Chemically Enhanced Seeded Precipitation (CESP)	Rahardianto et al. (2010)	0.96	Gypsum	NA	Yes	NA	- Lab scale beaker tests - NaOH for AS scavening
	McCool et al. (2013)	0.8 - 1.0	Gypsum	93	Yes	Pilot	- PRO - CESP - SRO - Field testing - NaOH for AS scavening
Intermediate Chemical Demineralisation (ICD)	Gabelich et al. (2007)	0.08	(Calcite)	91 - 95	Yes	Pilot	- PRO - ICD - SRO method - Field testing - NaOH dosed
	Gabelich et al. (2011)	0.08	(Calcite)	95	Yes	Pilot	- PRO - ICD - SRO method - Field testing - NaOH and $NaHCO_3$ dosed
Seeded Prec. and Recycle RO (SPARRO)	Juby (1994)	0.98	Gyspum	> 90%	No	Pilot	- Tubular CA membranes - Field testing with mine water
Hi Recovery Precipitation RO (HiPRO)	Hutton et al. (2009) Bhagwan (2012)	no info.	Gypsum	99.5	Yes	Real Plant	- 25 ML/day plant - 3 RO stages - Gypsum Precipitation

The flow reversal technique effectively increased the recovery from 75 - 85 %. This was with a feed solution having a gypsum SI of 1.86, corresponding to an induction time of 1 hour, therefore

reversing the flow once every 30 minutes. Flow measurements showed that the permeate flux in the last spiral element (also the first element after switching) was stabilized, even when operating with extremely supersaturated feed solutions above the manufacturers recommended limits (Pomerantz et al., 2006). However, it was also reported that "almost" no calcium sulphate dihydrate precipitated on the membrane, surely implicating that minor scaling occurred on the RO membranes. Therefore, it is questionable if the technique was effective to prevent scaling during an operation longer than 22 hours (the maximum duration tested) even with the use of antiscalants, because of the high supersaturation levels in the solution. It would be useful to combine the flow reversal technique and an intermediate concentrate desupersaturation method, to possibly achieve recoveries higher than 85%.

The CESP and SPARRO process seem to be the most suitable processes for high recovery brackish desalination, with high initial gypsum saturation indexes, where recoveries of 93 % and up to 98 %. The SPARRO process was effective to treat high scaling mine water without the use of antiscalants, however a constant flux of 550 L/m^2 day could not be maintained due to premature membrane fouling, probably caused by suspended silicate particles (Bowell, 2000). Further, the mine water in the SPARRO process contained high concentrations of metal ions such as Fe, Zn, Mn, Ba, Ni and Al, whereas the feed water in the CESP process did not contain heavy metal ions, thus increasing the fouling potential of the mining feed water. In general the CESP process was the most suitable out of the compared methods, for feed waters with moderate gypsum scaling propensity (SI_g = 0.85-0.97), achieving recoveries up to 93% and no membrane scaling was observed (McCool et al., 2013).

However, it must be mentioned that the 25 ML/day eMalahleni Water Reclamation Plant near Witbank currently is the most advanced and existing large scale plant of its kind in the world. This shows that the intermediate concentrate demineralisation process is viable and can be applied to large scale processes while anti-scalants are dosed. All the other studies demonstrated similar intermediate concentrate demineralisation techniques, however only on the pilot plant or small-scale laboratory level.

2.6. Literature review summary

The most important finding from the literature study are summarised below:

- **Brackish water desalination:**

  Cost effective brine disposal in brackish water RO desalination plants is critical to make the process economically viable and currently evaporation ponds are the most widespread brine disposal method in brackish desalination. Evaporation ponds are effective for brine disposal, however, they require large surface areas, since the water evaporates naturally. Therefore, large scale brackish water RO desalination is only viable when brine disposal costs are minimized by operation at high recoveries.

- **Calcium sulphate precipitation:**
  - In calcium sulphate precipitation/crystallisation the driving force is the difference in solution and saturation concentration, at a specific temperature. The calcium sulphate scaling potential is defined by the gypsum saturation index. An undersaturated solution has a SI < 1, while supersaturated solution has a SI > 1 and equilibrium is reached when the SI = 1.
  - Gypsum (calcium sulphate dihydrate) precipitation occurs in two steps: nucleation and growth. If a solution becomes supersaturated, precipitation does not occur immediately, since crystal nuclei must form prior to precipitation. The elapsed time from reaching supersaturation until the first physical changes are observed, is defined as the induction time.

- **Factors influencing gypsum precipitation:**
  - ***Temperature:*** An increase in temperature shortens the induction period (a 10°C increase reducing induction time by roughly half). However, an exponential increase in growth rate is observed with increasing temperature
  - ***Supersaturation ratio:*** Induction time is inversely proportional to level of supersaturation and growth rate increases directly with supersaturation.
  - ***Seed:*** Addition of improves nucleation kinetics and eliminates the induction period.

- **Scale formation on membranes**
  - ***Concentration polarisation:*** can have serious consequences in brackish desalination, directly leading to surface crystallisation on the membrane if the solubility of

sparingly soluble salts is exceeded. The level of concentration polarisation is primary affected by the permeate flux and cross flow velocity along the membrane surface.

- ***Mechanism:*** It is generally accepted that RO membrane scaling takes place by direct surface crystallisation and deposition of bulk solution formed crystals, predominantly by surface crystallisation due to the short convective residence time in the RO modules.
- ***Scale Development:*** Membrane scaling increases with axial position along the membrane, corresponding to degree of supersaturation, towards the membrane exit.
- ***Flux Decline:*** A permeate flux decline is caused by increased hydraulic resistance from a scaling layer that causes flow reduction.

- **Prevention of scale formation on RO membranes:** several methods are discussed in literature.
  - ***Antiscalants:*** They are commonly used to prevent membrane scaling in brackish RO desalination, inhibiting mineral salt crystallisation.
  - ***Permeate recycling:*** Permeate recycling to reduce the feed water salinity, thus reducing concentration polarisation and improving feed water quality.
  - ***Flow reversal:*** The periodic switching of feed flow between entrance and exit of the RO module, thereby reducing concentration polarisation by replacing the oversaturated solution at the membrane surface with an undersaturated solution at a time less than the induction time, thus preventing scaling.
  - ***Intermediate concentrate precipitation techniques:*** High recoveries (>90%) are achieved by reducing the scaling propensity of primary RO concentrate by chemical desupersaturation via alkaline-induced or seeded precipitation, followed by subsequent RO desalination stage(s).

In this chapter a thorough review of the relevant literature was given, laying the theoretical foundation for the remainder of the thesis. Calcium sulphate scaling on RO membranes and the prevention thereof is a well-studied field, and multiple prevention techniques have been tested and optimised in the past. However, no information was found on any previous permeate flushing techniques without the use of antiscalants for RO membrane scaling prevention. It seems that the use of antiscalants is inevitable to prevent calcium sulphate scaling, when operating RO units with solutions with a high scaling potential. In theory, periodic permeate flushing should prevent calcium sulphate membrane scaling, even without the use of antiscalants although this strongly depends on

the operating conditions. In this study periodic membrane flushing was investigated, to determine to what extent and under which operating conditions calcium sulphate membrane scaling can be prevented or reduced. The findings from the literature review were used to design the experimental apparatus and methods, which are explained in the subsequent chapter, in order to answer the key research questions.

Chapter 3 - Materials and Methods

In this chapter the materials and methods are described in detail, explaining the experimental equipment used and experimental procedures followed to answer the research questions.

3.1. Experimental approach

In order to achieve the research objectives, an experimental approach was developed: testing if regular permeate flushing and intermediate concentrate desupersaturation via gypsum seeding was effective to prevent gypsum scaling on RO membranes.

Calcium sulphate precipitation/scaling was the focus of the study, thus it was vital to choose process monitoring techniques to qualitatively investigate the crystallisation process. The literature review revealed that both synthetic and actual field solutions are commonly used to study calcium sulphate scaling. In this study it was decided to prepare synthetic scaling solutions, to maintain constant scaling conditions throughout the experiments.

Initially a batch crystallisation technique was used to gain a better understanding of the calcium sulphate scaling reaction, investigating the effect of temperature, seed concentration and initial supersaturation level. The batch experiments were useful to show if trends from literature could be repeated. Investigation of membrane scaling was only possible with a RO desalination plant, thus a lab-scale unit with a flat sheet RO membrane was carefully designed and constructed to test the research objectives. A larger plant using spiral wound membranes was unsuitable in this study, since flat sheet tests made regular replacement of the membranes possible (i.e after fouling). The data from the batch experiments were useful to optimize the design and operation of the gypsum precipitation reactors in the lab-scale unit.

3.2. Analytical methods

In this study it was essential to monitor the process conditions during any experiment, as indicated by the extent and onset of the calcium sulphate precipitation. Common methods to monitor the gypsum precipitation process include:

- ***Atomic absorption spectroscopy (AAS)*** (Christoffersen et al., 1982; Klepetsanis et al., 1999; Sanciolo et al., 2012, 2008)

Atomic absorption is commonly used to analyse the liquid samples for calcium ion concentration. The method is simple, rather time consuming, but very accurate.

- ***Turbidity*** (Pomerantz et al., 2006; Rahardianto et al., 2007; Shih et al., 2004)
  Turbidity measurements are effective to determine if bulk precipitation occurs, however surface crystallisation is the primary contributor to membrane scaling (Uchymiak et al., 2008), hence the method was less adequate for this study.
- ***Conductivity*** (Gabelich et al., 2011; Rahardianto et al., 2007; Seewoo et al., 2004; Uchymiak et al., 2008)
  Conductivity measurements offer real-time accurate measurements of the dissolved salts contained in the sample. However, exact concentration measurements are not possible.
- ***Titration methods using EDTA*** (Amjad and Hooley, 1986; Liu and Nancollas, 1973)
  Titration with ETDA is an accurate but time consuming method to determine the calcium concentration.
- ***Ion selective electrode (ISE)*** (Gerber, 2011; McCool et al., 2012; Rahardianto et al., 2007; Sanciolo et al., 2012)
  Calcium selective electrode measurements are fast, simple, fairly accurate and easily reproducible. However, sample preparation and calibration are critical for accurate results (Rahardianto et al., 2010).
- ***Permeate flux decline*** (Borden et al., 1987; Brusilovsky and Borden, 1992; Gilron and Hasson, 1987; Hasson et al., 2001)
  Permeate flux decline measurements are a real time indicator for membrane scaling, indicating the extent of surface blockage on the RO membrane.

The following three methods were chosen to monitor the calcium sulphate scaling process. It should be noted, measuring the permeate flux decline was only applicable for the lab-scale system experiments, whereas conductivity and AAS measurement were used for both batch and lab-scale unit experiments. The methods described are the main process monitoring tools, however other parameters such as pressure (lab-scale system only), temperature (batch and lab-scale unit) and flow rates (lab-scale unit only) were also monitored throughout all experiments.

3.2.1. Conductivity

A handheld conductivity meter (*YSI, Model 63)* was used to measure the specific conductance of the liquid. Specific conductance is the temperature compensated conductivity, where the reading is automatically adjusted to a chosen reference temperature. Based on average readings throughout

the study, 25˚C was chosen as the reference temperature for all the experiments. Only specific conductivity was measured in this study, hence from now onwards "conductivity" always refers to "specific conductivity".

The conductivity probe was carefully washed with demineralised water before taking any reading. This was repeated after each reading, to ensure accurate readings. Calibration of the meter was performed with standard 1413 µS/cm and 5000 µS/cm potassium chloride solutions *(Spraytech, South Africa)*. The calibration was performed at 25˚C, as recommended by the manufacturer of the conductivity calibration solution.

The measured conductivity was used to estimate the total dissolved solids by multiplying the conductivity (in µS/cm) by 0.63 to give a TDS value in mg/L. This empirical conversion is generally acceptable for brackish waters with salinities ranging from 2 000 to 20 000 mg/L TDS (Walton, 1989).

3.2.2. Atomic absorption spectrometry

A *Varian SpectrAA 250 plus* atomic absorption spectrometer (AAS) was used to analyse the samples for calcium ion concentration. To overcome the common interferences in the air-acetylene flame, which depress the calcium absorbance, a releasing agent such as Strontium (5000 mg/L) or Lanthanum (10000 mg/L) was introduced (Varian, 1979).

Calibration of the AAS performed with 1.000 g/L Ca^{+2} standard calcium chloride solution (*21049-500mL, Sigma-Aldrich*) mixed with 10000 mg/L Lanthanum solution prepared from lanthanum chloride heptahydrate (*Merck, ACS Reagent*). Standards were prepared by mixing the solutions accordingly, thus obtaining 1,2,3,5 and 10 mg/L calcium standards. The addition of the releasing agent requires matching of samples and standard solutions, to obviate the combined interference effects (Varian, 1979).

The upper limit of detection of *Varian*AAS was 10mg/L Ca^{+2}, however samples were typically in the range of 750-1250 mg/L Ca^{+2}. Therefore, samples were diluted with the prepared 10000 mg/L Lanthanum solution to remain below the detection limit of the AAS. Samples were filtered with a 0.45 µm cellulose acetate syringe filter to remove any possible gypsum seed crystals present in the sample.

A pipette was used to transfer 180 µL of the sample, to 25 mL of 10000 mg/L Lanthanum solution, resulting in 140 times dilution. This also ensures that no bulk precipitation occurred in the container,

after the sample was added to the 25 mL Lanthanum solution. The collected samples were oversaturated with respect to calcium sulphate; hence it is critical to dilute them, since the AAS analysis was not done immediately after each experiment. Dilution prevented any calcium sulphate precipitation in the sample container, which would result in a lower calcium reading in the AAS.

3.2.3. Permeate flux decline

A permeate flux decline in RO membrane operation is caused by two different phenomena: the increase in osmotic pressure of the concentrating brine causes a reduction in net pressure (i.e. the driving force), and/or increased hydraulic resistance from the scale layer causes a flow reduction (Hasson et al., 2001). Membrane scaling by sparingly soluble salts causes an increased hydraulic resistance at the membrane surface; hence permeate flux declines can be used to monitor membrane scaling. In order to isolate this effect from the other causes of permeate flux decline, the feed pressure was adjusted to account for the increasing osmotic pressure in the feed due to the recycling of concentrate, thereby operating at a constant flux. Typically, the permeate flux is not affected by membrane compaction in modern brackish composite polyamide RO membranes, if operated below recommended maximum pressure (Fritzmann et al., 2007; Kucera, 2010; Potts et al., 1981). Therefore, monitoring the permeate flux decline was used in this study to determine the onset of calcium sulphate membrane scaling.

In order to compare different experimental runs at varying feed pressures and stream temperatures, the effective membrane permeability was calculated to compare experimental runs to determine the onset of the membrane scaling. The effective membrane permeability was calculated by Equation 3-1 (Hasson et al., 2001; Pomerantz et al., 2006).

$$L_P = \frac{Q_p/A_m}{\Delta P - \Delta \pi} \qquad \textbf{Equation 3-1}$$

where Q_p/A_m was the permeate flux in LMH, i.e. L/(m^2.h) , ΔP the difference in feed and permeate pressure in bar, and Δπ the difference in feed and permeate osmotic pressure. In this study the temperature was kept constant at 15 ± 2 °C, however the specific permeate flux was normalised to the standard value of 25°C to compensate for these slight temperature variations using Equation 3-2 (Pomerantz et al., 2006).

$$L_{P,25} = L_{P,T} 1.035^{(25-T)} \qquad \textbf{Equation 3-2}$$

where ***T*** is the water temperature in °C.

3.3. Scaling solutions and gypsum saturation index

In this study model scaling solutions were prepared according to a certain gypsum saturation index, given in the equation below (Gabelich et al., 2007; McCool et al., 2013; Rahardianto et al., 2010; Sanciolo et al., 2012; Shih et al., 2005; Uchymiak et al., 2008) :

$$SI_g = \frac{(\alpha_{Ca^{2+}})(\alpha_{SO_4^{2-}})}{K_{sp}} \qquad \textbf{Equation 3-3}$$

The activities of the calcium and sulphate ions are dependent on temperature, pressure and composition of the mixture. In this study, the pressure was kept constant at atmospheric pressure since all tanks/reactors were open to the atmosphere, thus the activity (i.e. SI_g) was only influenced by temperature and mixture composition.

If the saturation index was larger than one ($SI_g > 1$), there was a thermodynamic tendency for solid gypsum crystals to form and the solution was oversaturated. Conversely, the crystallisation was not thermodynamically favoured when the saturation index was less than one ($SI_g < 1$), forming an undersaturated solution (OLI Systems, 2011).

Thermodynamic calculations were performed with the *OLI Analyser ScaleChem 9.0* software, to determine the exact amounts of calcium chloride and sodium sulphate salts required, in order to form a solution with a specific gypsum saturation index. The software allows the user to determine the exact gypsum saturation index, by entering the concentrations of all the ions present in the solution. *OLI Analyser ScaleChem 9.0* uses the *OLI Aqueous Model* (AQ Model) to predictively model the speciation of an extensive range of chemicals in water, thus accurately predicting reactions between chemicals, solid formation, pH and ionic composition (OLI Systems, 2011). The true speciation AQ thermodynamic model uses the predictive Helgeson equation of state, an activity coefficient model and convergence heuristics. Further, the model covers over 80 elements of the periodic table and was based upon published experimental data, using data regression and/or extrapolation to generate accurate electrolytic water data (OLI Systems, 2011). The AQ Model is valid for temperatures from -50 to 300 ˚C, pressures from 0 to 1500 bar and ionic strengths from 0 to 30 M, making the model suitable for the process conditions in this study.

In previous calcium sulphate precipitation studies, the model scaling solution was typically made from calcium chloride and sodium sulphate anhydrous/hydrous salts, amongst other salts such as magnesium sulphate (Rahardianto et al., 2010, 2006; Shih et al., 2004; Uchymiak et al., 2008). In this study other ions were excluded from the model solution, thus isolating the gypsum crystallisation during the experiments. The model scaling solution was prepared with equimolar amounts of calcium chloride (*Merck, ACS Reagent*) and sodium sulphate dihydrate (*Merck, ACS Reagent*). The correct mass of each salt was dissolved in demineralised water, where the exact masses are shown in Table 3-1. This resulted in a model solution with a scaling potential with regards to gypsum only and no other salts, since the sodium chloride has no scaling potential within the range of concentrations used in this study. Sodium and chloride ions were also present in the solution, thus contributing to the overall osmotic pressure of the solution.

Table 3-1 *Initial gypsum saturation index at various temperatures with corresponding ion concentrations and conductivities as obtained from OLI Analyser ScaleChem 9.0. The table also shows the calculated stoichiometric amounts of calcium chloride dihydrate and sodium sulphate salts required to make up a scaling solution according to a certain* SI_g.

Concentration (g/L)		Cations (mg/L)		Anions (mg/L)		Saturation Index		
Na_2SO_4	$CaCl_2.H_2O$	Na^+	Ca^{+2}	Cl^-	SO_4^{-2}	25°C	20°C	15°C
5.00	5.17	1619	1411	2496	3381	1.99	2.06	2.15
4.75	4.92	1538	1340	2371	3212	1.88	1.95	2.04
4.50	4.66	1457	1270	2246	3043	1.77	1.83	1.92
4.25	4.40	1376	1199	2121	2874	1.67	1.72	1.80
4.00	4.14	1295	1129	1997	2705	1.56	1.61	1.69
3.75	3.88	1214	1058	1872	2536	1.45	1.50	1.57
3.50	3.62	1133	988	1747	2367	1.34	1.39	1.45
3.25	3.36	1052	917	1622	2198	1.23	1.28	1.33
3.00	3.10	971	847	1498	2029	1.13	1.16	1.22
2.75	2.85	890	776	1373	1860	1.02	1.05	1.10
2.50	2.59	809	705	1248	1691	0.91	0.94	0.98
2.25	2.33	728	635	1123	1522	0.80	0.83	0.87
2.00	2.07	647	564	998	1353	0.70	0.72	0.75
1.75	1.81	567	494	874	1183	0.59	0.61	0.64
1.50	1.55	486	423	749	1014	0.49	0.50	0.53

The temperature dependence of the SI_g is graphically illustrated in Figure 3-1, comparing the SI_g at 15, 20 and 25 °C respectively, linearly increasing with increasing calcium concentration. As the temperature increases from 15 to 20 to 25 °C, the equilibrium solubility of Ca^{2+} and SO_4^{2+} increases (Helalizadeh et al., 2000). Considering Equation 3-3, the equilibrium activities decrease with increasing temperature in the range from 15-25 °C, thus the SI_g is lower at 25°C compared to 15°C.

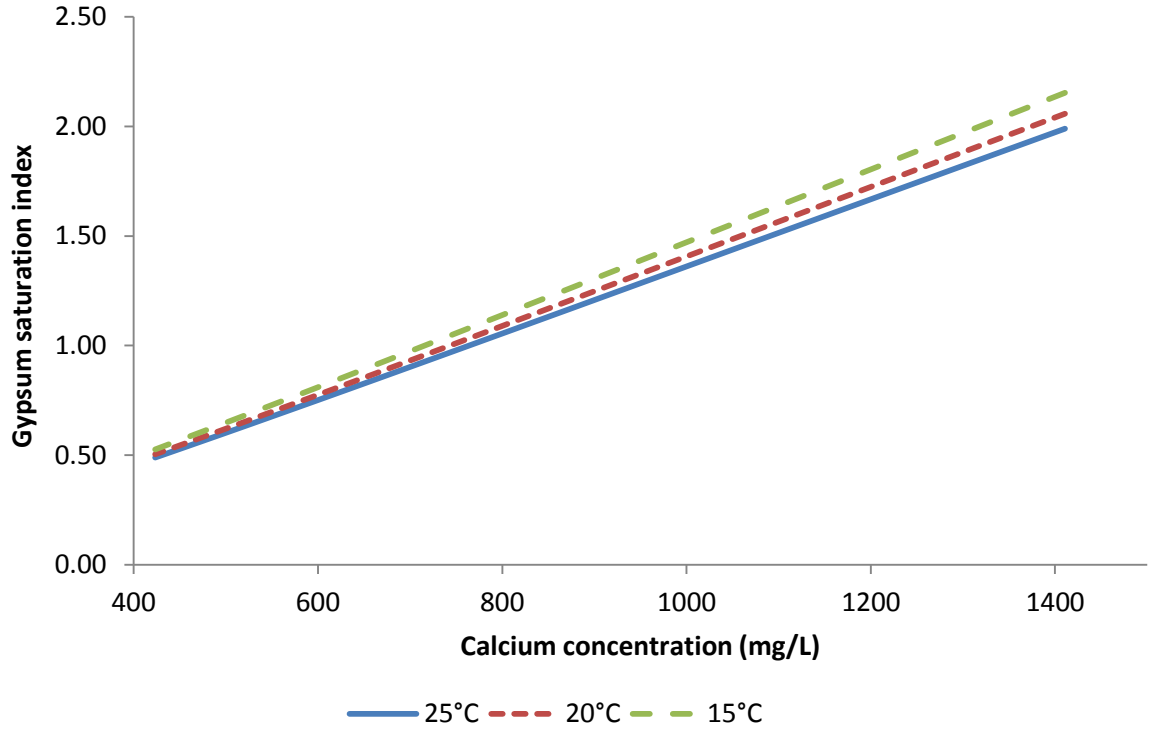

Figure 3-1 *Initial gypsum saturation index at various temperatures, based on thermodynamic calculations from the OLI Analyser ScaleChem 9.0 software, for a solution with equimolar amounts of* $CaCl_2$ *and* $NaSO_4$.

3.4. Batch crystallisation experiments

3.4.1. Experimental setup

The experimental setup for the batch experiments is depicted in Figure 3-2. A 2000 mL glass beaker reaction vessel, filled with 1800 mL of calcium sulphate solution in each experiment, was placed on the heated plate on the *RET basic safety control IKAMAG (LCD)* magnetic stirrer. A 30x8 mm Teflon coated stirrer bar ensured a well-mixed and homogenous solution, in terms of temperature and concentration. The stirrer speed was accurately controlled by the *IKAMAG* stirrer, where the speed was constant at 300 rpm for all batch experiments. Temperature inside the reactor was measured by a PT100 temperature probe, connected to the *IKAMAG* unit to automatically maintain a constant temperature. The temperature was set manually turning the knob on the *IKAMAG* unit, where the temperature was constant within ± 0.5 ˚C.

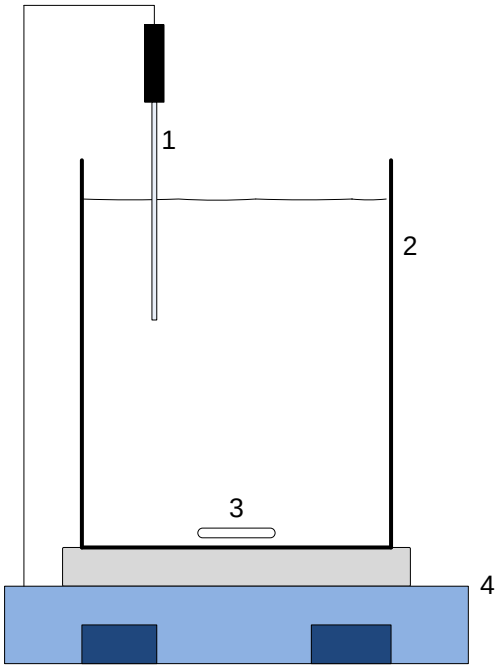

1 – PT 100 temperature probe
2 – Glass reactor vessel (2L)
3 – Magnetic stirrer bar
4 – IKAMAG magnetic stirrer/temperature controller

Figure 3-2 *Simple schematic of equipment used in batch experiments*

3.4.2. Experimental preparation

Equipment

The glass reactor vessel was thoroughly cleaned before each run, by cleaning the inside with a sponge. This was essential to remove any gypsum solids or any calcium residues from the previous experiments. After this, the glass reactor was thoroughly washed with demineralised water and allowed to dry.

Scaling solution

The scaling solution was prepared on the day before the actual experiment, by making separate calcium chloride and sodium sulphate solutions. This ensured that all of the salt was completely dissolved and homogenous solution was prepared, only forming a saturated solution once they are mixed together just before the experiment. Each solution contained half the volume of the total scaling solution volume, in order to achieve the desired final concentration once the solutions were mixed together. A total of 1.8 L of model solution was prepared for each experiment, thus two clean glass beakers were each filled with 900mL demineralised water, before adding the required amount

of $CaCl_2.H_2O$ and $NaSO_4$ salt respectively (refer to Table 3-1). After stirring each beaker carefully, the solutions were left overnight to allow the dissolution to complete.

3.4.3. Experimental procedure

Before commencing with any experiment, the calcium chloride and sodium sulphate solutions were heated to the desired temperature by using the *IKAMAG* stirrer/heater. This allowed each solution to reach thermal equilibrium before they were added together, by pouring the contents into the 2000 mL glass reactor vessel and placing it on the *IKAMAG* unit. After the solutions was agitated for 2min, the solution was assumed to be completely homogenous and supersaturated with regards to gypsum. The conductivity was measured and an AAS sample was taken, before a certain amount of gypsum seed crystals was added (if applicable in the specific experiment).

The samples and measurements were taken after 5, 15, 30 and 60 minutes after gypsum seed addition *(Kimix Chemical, ACS Reagent)* addition, and then every 60 minutes thereafter. Seed addition resulted in a very short or no induction times (Gerber, 2011), hence it made sense to take most samples within the first hour of the experiment since the drop in calcium concentration will be the greatest. For batch experiments without seed addition, the measurements and samples were taken at evenly spaced intervals of 30 minutes, since the exact onset of precipitation cannot be predicted prior to the experiment.

3.4.4. Experimental plan

Seeded batch precipitation has been well studied, hence the batch experiments were used to confirm findings of certain literature and for optimisation of the precipitation reactor in the lab-scale RO system. Previous studies showed that gypsum precipitation was strongly affected by temperature, seed concentration and level of supersaturation (Klepetsanis and Koutsoukos, 1991; Klepetsanis et al., 1999; Liu, 1975), thus the three parameters were investigated.

The batch experiments were used to study gypsum crystallisation reaction, simulating the operation of the precipitation reactors of the lab-scale RO unit. Under the studied conditions, the RO concentrate was expected to have a saturation index of 1.57, based on a 30 % instantaneous recovery and feed saturation index of 1.2. The ambient temperature at the lab-scale unit was typically close to 15°C, thus it was important to study the reaction at this temperature. Previous seeded batch experiments showed almost complete elimination of the induction time if the seeding dose was high enough, generally dosing gypsum above 1.5 g/L, under similar conditions to this study

(Amjad, 1988, 1985; Lui and Nancolass, 1970). In the gypsum precipitation reactor it was desirable to minimise the induction time, thus only seeding above 2 g/L was considered.

The experimental conditions are summarised in Table 3-2. In the first set of experiments (1-4), the effect of seed dose was investigated while feed concentration and temperature remained constant. In the second set of experiments (5-7), the effect of temperature was studied while feed concentration and seeding dose remained constant. Finally the effect of supersaturation level was investigated in experiments 8-10, while temperature and seeding dose stayed constant. The gypsum seed concentration was constant at 2 mg/L for experiments 5-10, based on the results from experiments 1-4.

Table 3-2 *Experimental plan for batch experiments*

Experiment	SI_o	Initial Ca^{2+} (mg/L)	Temperature (°C)	Gypsum Seed (g/L)
1	1.57	1058	25	0
2	1.57	1058	25	2
3	1.57	1058	25	4
4	1.57	1058	25	6
5	1.57	1058	15	2
6	1.57	1058	20	2
7	1.57	1058	25	2
8	1.57	1058	15	2
9	2.15	1411	15	2
10	2.73	1764	15	2

3.5. Lab-scale RO unit experiments

3.5.1. Experimental setup

In this section only a brief description of the lab-scale system is presented, whereas the complete design and construction details are given in Appendix A. A schematic diagram of the lab-scale unit is given in Figure 3-3, followed by a description of each part of the equipment.

The synthetically prepared scaling solution was poured into a 15 L stainless steel tank T-101. The tank was fitted with a 6mm stainless steel heating/cooling coil connected to a water bath cooler *(Haake, Typ 000-3959)* and heater element *(Haake, Typ 000-3350)* to maintain a constant temperature at 15 ± 2 °C. Feed solution was fed to the pump through a 10" filter housing *(Atlas Filtri, SKU WCU006),* fitted with a melt blown polypropylene 1 micron filter cartridge *(Sun Central,*

CPPM60-001-10). The filter trapped any potential crystals that may have formed in the bulk fluid, preventing them from fouling the membrane via surface deposition. The filter is essential to prevent seed crystal from entering the RO membrane unit. The filter was a precaution since bulk induction times are usually much longer than convective residence times in the RO module, hence membrane scaling primarily occurred via surface crystallisation (Rahardianto et al., 2006; Shih et al., 2005), and to a lesser extent in the bulk fluid.

A 0.55 kW diaphragm positive displacement pump *(Hydra-cell, Model F20)* was used to feed between 12 and 14 L/h of scaling solution to the membrane. The recycle stream around the pump was essential to regulate the flow rate to the membrane and during permeate flushing operation, allowing the oversaturated solution to be recycled back to the feed tank T-101.

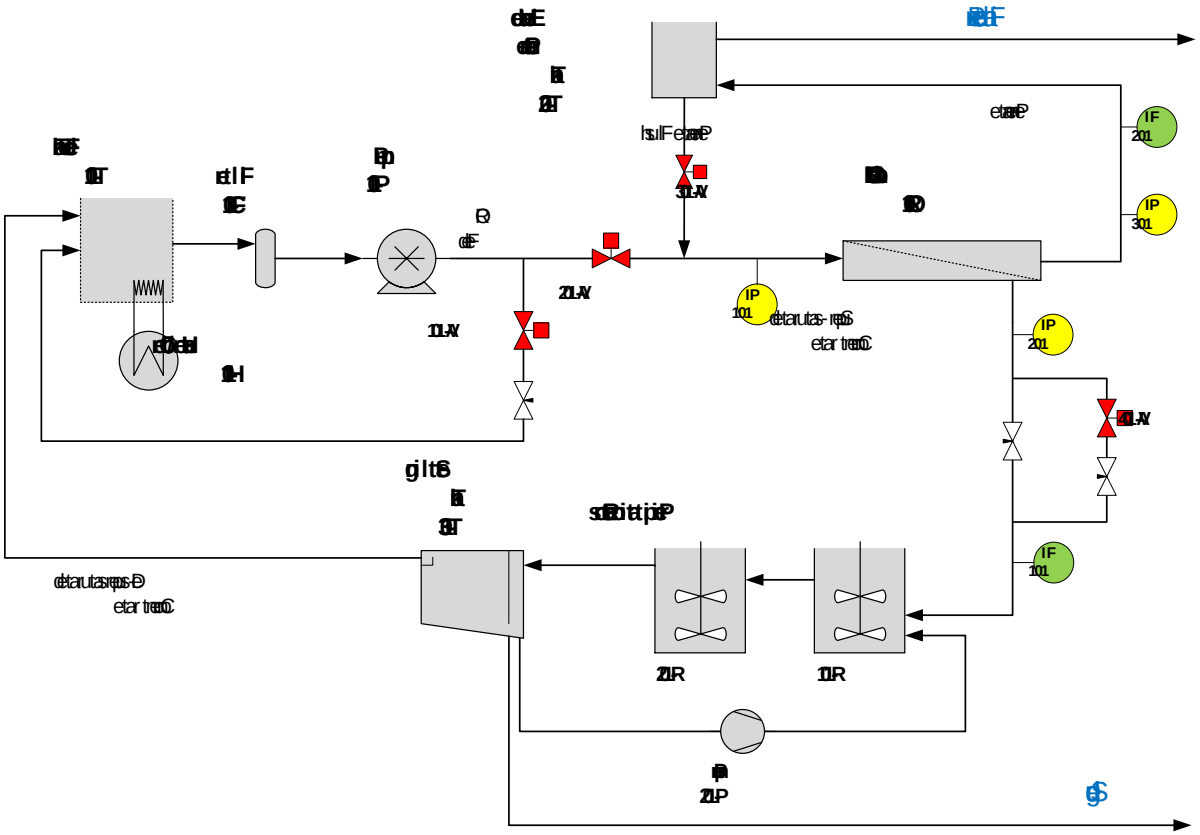

Figure 3-3 *Schematic diagram of lab-scale unit used for the experiments*

A schematic of the membrane test cell is given in Figure 3-4 and a photo is shown in Figure 3-5. The feed side PVC membrane block had a tortuous flow path with a depth of 1mm, with a total flow path length of 1.8 m. The six adjacent connected flow channels, each approximately 300mm long, were decreasing from 50 to 40 mm in width to maintain the same cross flow velocity while the flow rate decreases due to the permeation. The cross flow velocities were between 0.02 and 0.14 m/s,

corresponding to 30 % and 10 % instantaneous recovery respectively, also influenced by the permeate flux. A stainless steel perforated plate with 0.4 mm holes at 1.5mm triangular pitch was used as permeate spacer. The flat sheet RO membrane *(DOW Flimtec, XLE-2540)* with a total active area of 0.106 m^2, was placed between the two PVC blocks. Two 5 mm orings provided the necessary seal, ensuring that no fluid leaks out of the membrane test cell and no membrane bypassing occured. 3 mm orings ensured that no bypassing occurred between individual flow channels. 20mm steel plates were placed on either side of the membrane test cell to provide a rigid support. The entire membrane test cell was bolted together with 22 M8 high tensile galvanised iron bolts. A high operating pressure resulted in large forces acting on the entire block, hence additional 75mm channel irons were used to provide additional support by pressing the two blocks firmly together.

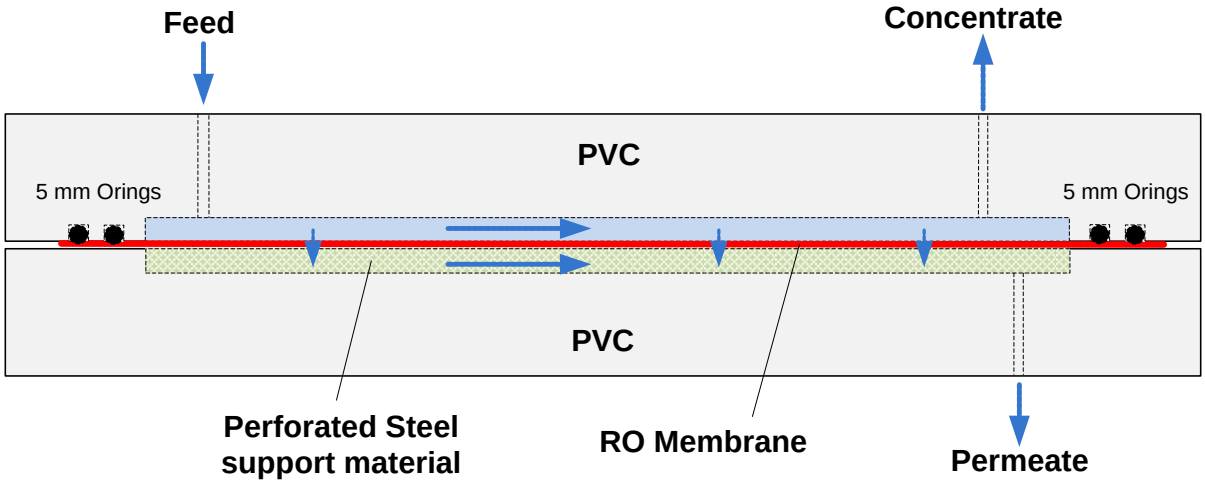

Figure 3-4 *Schematic cross section of RO membrane test cell*

Figure 3-5 *Photographs of RO membrane test cell. Left: the entire membrane cell showing how the membrane block is bolted together. Right: The flow channel from feed entry to brine exit, showing the outer 5mm o-rings and 3mm o-rings separating the individual flow channels.*

RO permeate was collected in a small 0.35 L PVC permeate tank T-102, storing enough permeate for the flushing operations. The tank was positioned 11m above the membrane unit, in order to generate approximately 1 bar for the permeate flushing operation. The overflow from this permeate tank was collected in a measuring beaker in order to measure the net amount of recovered permeate. The flushing velocity ranged from 0.08 to 0.10 m/s from flow channel entry to exit respectively, constant during all flushing experiments throughout the study.

The RO concentrate was fed to the Perspex precipitation reactors, each having a volume of 13 L with a total residence time of 130 min. The results from the batch experiments showed that a minimum of 120 min was required to reduce the gypsum saturation index from 1.5 to 1.1, while seeding 2g/L gypsum powder at a constant temperature of 15 °C. Only gypsum was considered as a seed crystal, since it was reported that gypsum was highly effective as a seed crystal (McCool et al., 2013; Rahardianto et al., 2010, 2007). Based on those results, the reactors were sized accordingly. Each reactor was fitted with two horizontal baffles, in order to create stirred plug flow reaction kinetics, dividing the reactor into three equal zones. Each reactor was agitated with a stirrer *(Camlab, R50D and VelpScientifica, F20100151),* where two 4 blade (25x80 mm) stainless steel impellers were fitted to the 6mm stainless steel shaft to create axial flow.

The slurry overflow from the reactor R-102 flowed into the rectangular Perspex settling tank with a total volume of 2.7 L, with a sloped bottom plate. In order to reduce the settling time, eight inclined plates were installed at an angle of 60° to the water horizontal water level, thus increasing the overall settling area and reducing the settling distance. Settling tank overflow was fed back to the feed tank T-101. The clarifier underflow was recycled back to reactor R-101 with a peristaltic pump *(Watson Marlow, 504U)* at 1-2 L/h to reuse the gypsum solids for the seeded precipitation. Rahardianto et al. (2010) showed that gypsum crystal recycling was feasible to reduce the fresh seed addition.

Three 63 mm stainless steel pressure gauges *(WIKA Instruments)* measured the feed, permeate and concentrate pressures respectively. The permeate and concentrate flow was measured by two stainless steel rotameters *(Tecfluid flowmeters, 2150N-0010 and 2150N-0005).* The permeate flushing sequence was controlled by four solenoid valves *(Burkert, Model 0255)* and initiated by a PLC *(Phoenix Contact, Nanoline).* The PLC controlled the opening/closing of each valve, by settling the timers for each valve. Various other needle valves were installed in the lab-scale RO systen to control/adjust pressures and flow rates.

3.5.2. Operation of complete lab-scale RO system

The lab-scale RO unit could be operated in two modes: concentrate recycle or full recycle mode. In concentrate recycle mode only the RO concentrate was recycled to the feed tank, whereas both RO permeate and concentrate were recycled in full recycle operation. For most experiments the lab-scale RO system was operated in concentrate recycle mode, together with periodic permeate flushing.

A total cycle consisted of three individual steps: 1. Production time, 2. Flushing time and 3. Soak time, as shown in Figure 3-6. Permeate was only produced during production time when operating in concentrate recycle mode. Directly after permeate flushing, the elevated permeate tank was again filled up with permeate, since the tank level dropped during the previous permeate flushing. This occurred until the maximum level was reached and the overflow permeate was collected. Theoretically, the soak time enhanced the mass transfer of ions from the membrane surface into the bulk fluid, thus effectively reducing the scaling potential.

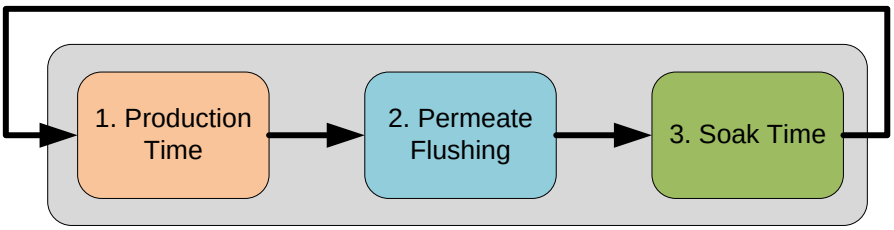

Figure 3-6 *Total cycle consisting of production time, flushing time and soak time*

During concentrate recycle operation, water from the feed tank was pumped to the membrane and only valve VA-102 was open, as shown in Figure 3-7. The concentrate stream was recycled, via the reactors and the settling tank, back to the feed tank while permeate was collected in the elevated permeate tank. The overflow from the permeate tank was collected in a measuring beaker to determine the net recovery by measuring the produced permeate.

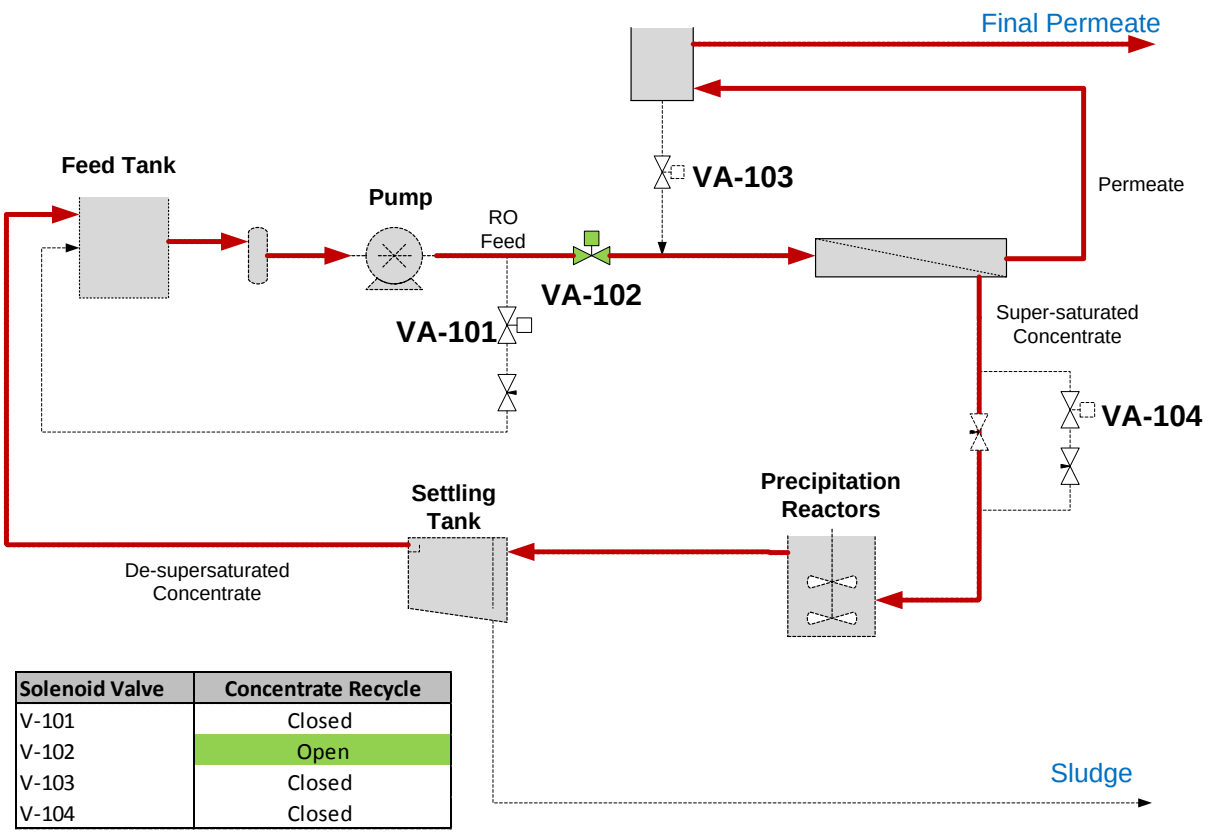

Solenoid Valve	Concentrate Recycle
V-101	Closed
V-102	Open
V-103	Closed
V-104	Closed

Figure 3-7 *Simplified flow diagram during concentrate recycle operation, where the red arrows show the normal path of the water*

The flushing sequence was initiated by the *Phoenix Nanoline* PLC, using a simple ladder logic program to open/close the valves in a specific sequence. The sequence to switch from concentrate recycle operation to flushing operation was as follows (summarised in Table 3-3):

- During concentrate recycle operation only valve VA-102 was open
- Valve VA-101 was activated, allowing all the feed to solution to be recycled back to the feed tank.
- Valve VA-102 was closed to block any flow to the membrane. At the same time valve VA-104 was opened to reduce the fluid pressure in the block. This was vital since the permeate flushing was gravity driven, and any excess pressure would create an upward flow to the permeate tank.
- The actual permeate flushing was initiated by opening valve VA-103, while valve VA-101 and VA-104 remain open.
- Exactly the same procedure was followed in the reverse order to switch back to concentrate recycle operation where only valve VA-102 was open.

Table 3-3 *Solenoid valve sequence to change from operating concentrate recycle mode to flushing operation, the timers are set on the PLC thus controlling the exact flushing frequency and permeate volume. The green highlighted blocks indicate an open valve.*

Timer	Solenoid Valves				Operation
TC00	V-101	V-102	V-103	V-104	Concentrate Recycle
TC01	V-101	V-102	V-103	V-104	Valve switching time
TC02	V-101	V-102	V-103	V-104	
TC03	V-101	V-102	V-103	V-104	
TC04	V-101	V-102	V-103	V-104	Flushing
TC05	V-101	V-102	V-103	V-104	Valve switching time
TC06	V-101	V-102	V-103	V-104	
TC07	V-101	V-102	V-103	V-104	

During flushing operation the solution from the feed tank was recycled back to the feed tank, since valve VA-102 blocks the feed to the membrane. During the gravity driven flushing, permeate flowed to the membrane through valve VA-103 and eventually back to the feed tank via the reactors and settling tank, as shown in Figure 3-8.

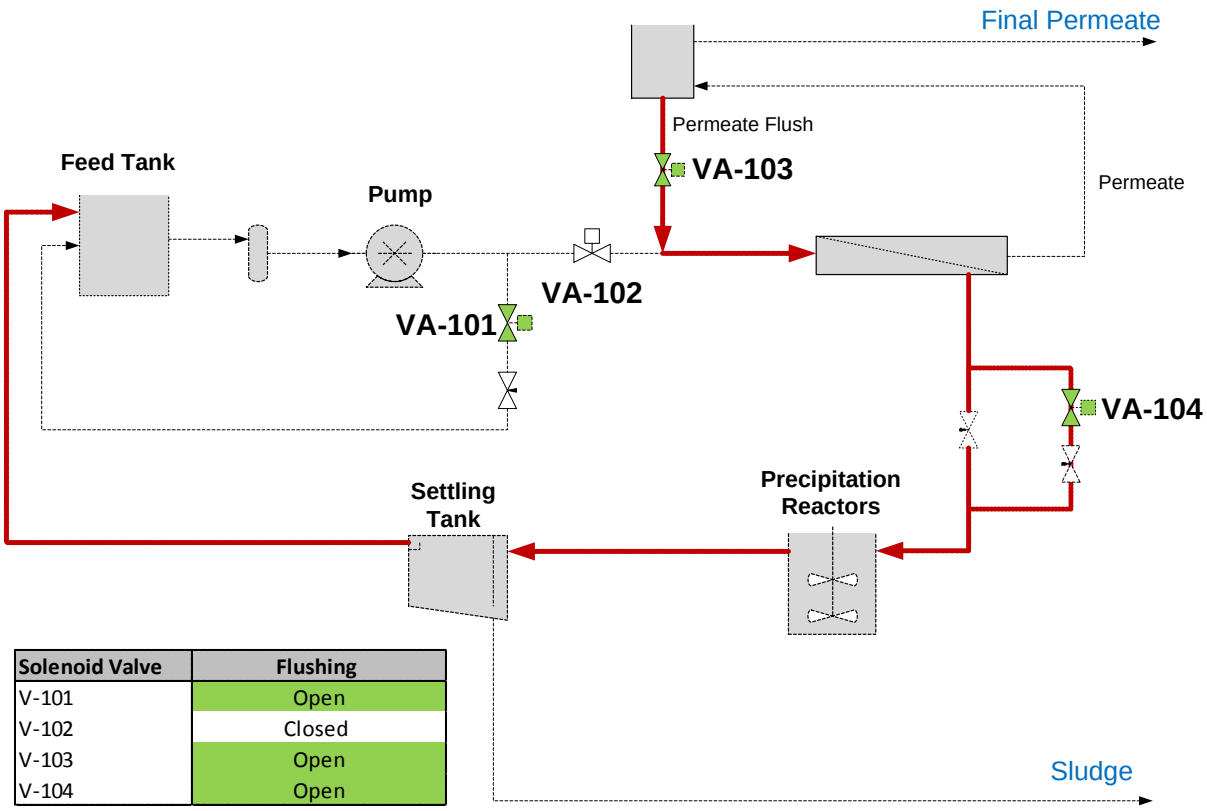

Figure 3-8 *Simplified flow diagram during permeate flushing, where the red arrows only show the path of the permeate from the elevated permeate tank. The solution from the feed tank was recycled back to the feed tank.*

3.5.3. Experimental preparation

RO membrane conditioning

A new membrane sheet *(DOW Flimtec, XLE-2540)* was installed after every experimental run, thus ensuring the same scale-free initial conditions for every run. A wet membrane reaches a stable performance faster than a dry membrane (DOW Filmtec, 2011), hence the new membrane was soaked in demineralised water for 24h before installation. Membrane conditioning was subsequently performed with standard 2500 mg/L NaCl solution in full recycle mode, operating at 7 bar TMP and a flux of 12 LMH for 5-6 hours. It was important to gradually increase the feed pressure initially, since a sudden increase in pressure can cause cracks in the membrane or excessive membrane compaction (Kucera, 2010). After the membrane conditioning period, the system was rinsed with demineralised water, operating at 5 bar TMP and a flux of 12 LMH for 20-30 minutes.

Equipment

Prior to any experiment all the vessels, reactors, feed tank, permeate tank and settling tank, were thoroughly cleaned and rinsed with demineralised water. The 1 micron inline filter cartridge was manually back-flushed after every experimental run and replaced after every third experimental run. The filter was hydraulically over-designed to ensure that no particles could reach the RO membrane.

Scaling solution

The scaling solution was prepared on the day before the actual experiment, by making separate calcium chloride and sodium sulphate solutions. This ensured that all of the salt was completely dissolved and homogenous solution was prepared, only forming a saturated solution once they are mixed together just before the experiment. Each solution contained half the volume of the total scaling solution volume, in order to achieve the desired final concentration once the solutions were mixed together. A total of 40 L of model solution was prepared for each experiment, thus two clean plastic drums were each filled with 20 L demineralised water, before adding the required amount of $CaCl_2.H_2O$ and $NaSO_4$ salt respectively (refer to Table 3-1). After stirring each container carefully, the solutions were left overnight to allow the dissolution to complete.

3.5.4. Experimental method

Firstly, the prepared calcium chloride and sodium sulphate solutions were added together and thoroughly mixed. After mixing the solution for 5 minutes the scaling solution was assumed to be

completely homogenous and oversaturated with respect to gypsum (generally the feed SI_g was 1.2 for most experiments).

In each experiment the overall mass balance only considered the volume in the feed tank and the recovered permeate to determine the overall recovery. Consequently the two reactors, the settling tank and the permeate tank were filled with the synthetic scaling solution before an experiment. Before the actual experiment started, 2-3 L of scaling solution were placed in the feed tank and the RO unit was run in concentrate recycle mode, in order to produce permeate to fill the permeate tank completely. Further, this ensured that the entire liquid volume in the filter, pump, tubing and membrane block was replaced with the specific scaling solution. After this, the feed tank was filled up with the scaling solution, generally 10 L for most experiments.

The individual valve timers on the *Phoenix Contact Nanoline* operating panel were set to a specific flushing frequency and flushing volume, before the pump was switched on. The desired flux and instantaneous recovery were set by adjusting the respective needle valves and monitoring permeate and concentrate flow rate. Gypsum seed crystals were added in a semi continuous method (i.e. in evenly spaced intervals throughout the experiment) to the first reactor at a rate of 2 g/L of concentrate. The seed was added to the bottom of the reactor, where the concentrate entered the reactor. The upward solids flux caused the seed crystals to overflow into the second reactor and eventually into the settling tank.

During any experimental run it was essential to adjust the respective needle valve to maintain a constant flux and instantaneous recovery. With increasing overall recovery the osmotic pressure in the feed solution rose, thus the feed pressure was adjusted to maintain a constant permeate flux and instantaneous recovery.

The RO unit operation data were collected in evenly spaced intervals, the shorter the run the more frequent AAS samples were taken and measurements were recorded. The theoretical effective permeate production rate was calculated and used to estimate the duration of the experiment, taking the downtime during flushing and permeate flushing volume into account. Generally for low flux experiments this was every 90 min and every 60 min for higher flux experiments. The effective permeate production rate was higher, implicating a shorter overall duration compared to the low flux experimental run. The following parameters were recorded/samples taken:

- ***Conductivity (mS/cm):*** feed, concentrate and permeate

- ***Temperature (°C):*** feed, concentrate and permeate
- ***Flow rate (L/h):*** concentrate and permeate
- ***Pressure (bar):*** feed, concentrate and permeate
- ***Recovered permeate volume (mL)***
- ***AAS samples:*** feed, concentrate and settling tank overflow
- ***Gypsum seed mass (g)***

The RO system was run until a flux decline was observed and constant flux operation was not possible thereafter, even after increasing the feed pressure significantly by adjusting the respective valve. This indicated that the scaling layer increased the hydraulic resistance across the membrane substantially, thus preventing constant flux operation. The time at which this occurred was recorded, in order to work out the total production time for the specific experiment.

3.5.5. Experimental design

In this study it was critical to determine how individual factors affect gypsum scaling on RO membranes. More specifically, how long can the lab-scale unit be operated without a flux decline due to membrane scaling for a certain set of operating conditions? The literature review showed that calcium sulphate scaling on RO membranes is influenced by many factors, including supersaturation level, temperature, permeate flux, instantaneous recovery and permeate to concentrate cross flow ratio. In this study, the permeate flushing technique added more factors, for instance flushing frequency, flushing volume and soaking time after the flushing. Furthermore, the intermediate concentrate crystallisation process added more factors, including seed dose, seed type and dosing frequency.

A factorial experiment is often used to determine the effect of each factor on a certain response variable and the interactions between the factors on the response variable (Montgomery et al., 1998). In this study, a factorial design was considered to determine the combined effect of all the major factors on a certain response variable, in this case the total production time until a flux decline was observed. More specifically, a 2^k factorial design was chosen where each factor is tested on two levels.

The main focus of this study was the permeate flushing technique to reduce gypsum scaling on RO membranes, therefore it was critical to include flushing frequency, flushing volume and soak time in the factorial design. Further, preliminary tests showed that permeate flux and instantaneous

recovery have a significant effect on membrane scaling. This would add up to five factors total, and no additional factors were considered, as this was beyond the scope of this study.

The full factorial experimental design considered the main factor effects, low order interactions and higher order interactions (Montgomery et al., 1998), resulting in a total of 32 runs for a 2^5 factorial design. Due to time constraints the more economical half factorial 2^{5-1} design was used in this study. The complete 2^{5-1} design was generated with *Statistica 11* software, consisting of 16 experimental runs, as shown in Table 3-4. Further, a centre run was performed in triplicate in order to validate the statistical analysis. Each factor was tested at high and low values, where the specific factor values are given in Table 3-5.

Table 3-4 *Half factorial 2^{5-1} resolution V factorial design obtained from Statistica software, with centre runs performed in triplicate to validate the statistical model (Run 17-19)*

Run	Flushing Frequency (h^{-1})	Flushing Volume (mL/flush)	Soak Time (sec/flush)	Permeate Flux (LMH)	Inst. Recovery (%)
1	-	-	-	-	+
2	+	-	-	-	-
3	-	+	-	-	-
4	+	+	-	-	+
5	-	-	+	-	-
6	+	-	+	-	+
7	-	+	+	-	+
8	+	+	+	-	-
9	-	-	-	+	-
10	+	-	-	+	+
11	-	+	-	+	+
12	+	+	-	+	-
13	-	-	+	+	+
14	+	-	+	+	-
15	-	+	+	+	-
16	+	+	+	+	+
17	0	0	0	0	0
18	0	0	0	0	0
19	0	0	0	0	0

Table 3-5 *Factors considered in the factorial design with the actual values for the high (+), centre (0) and low (-) levels.*

Factor	High (+)	Centre (0)	Low (-)
Flushing Frequency (h^{-1})	6	3.4	2.4
Flushing Volume (mL/flush)	70	52.5	35
Soak Time (sec/flush)	90	55	20
Permeate Flux (LMH)	24	18	12
Instantaneous Recovery (%)	30	20	10

The high and low values for each factor were chosen as follows:

- *Flushing frequency, flushing volume and permeate soak time* – these three factors are directly linked to the permeate flushing technique and all have an effect on the PPR and PPI (the concept of the PPR and PPI was explained in detail in section 4.2). An increase in any one these three factors or a combination thereof reduces the permeate production index. The flushing operation has the obvious disadvantage of reduced productivity, hence it was decided to not operate the RO unit below an PPI of 0.5, even if it would be beneficial for scaling prevention. Operation below a PPI of 0.5 would be highly uneconomical, since production rates would be reduced drastically, hence it was not considered in this study.

  Therefore, the high and low values for the factors were chosen in such a way that the experimental run at the lowest PPR still results in a PPI above 0.5. This was the case for Run 7 in the factorial design (refer to Table 3-4), where the combination of the factors caused the maximum reduction in PPR, hence the PPI would also be the lowest. The factor low values were chosen in such a way that the PPI was just above 0.5, as shown in Figure 3-9 where the calculated PPI for Run 7 was 0.53. Further, preliminary experiments (refer to section 5.3) were used to determine the corresponding high values.
- *Permeate flux* – brackish RO membranes are typically operated at permeate fluxes between 15-25 LMH, sometimes up to 30 LMH (DOW Filmtec, 2013). Higher permeate fluxes result in higher fouling and scaling rates, thus it was critical to remain within the recommended flux specifications. The main aim of the study was to prevent scaling, hence it did not make sense to operate at fluxes above 25 LMH. The high value of 24 LMH was chosen, while a conservative 12 LMH was chosen as low value.
- *Instantaneous recovery* – the maximum instantaneous recovery per 4" DOW XLE-2540 RO element was 15 % (DOW Filmtec, 2011). The high value was chosen to be 30 %, which was well above the recommended 15 % to test the effects of high instantaneous recoveries on

membrane scaling. Conversely, a conservative 10% was chosen for the low level, to remain below the manufacturers maximum level, even though a flat sheet membrane was used and not a spiral membrane. Further, this ensured that the magnitude between the two values was large enough to make a significant difference in the experimental results.

Various other RO system parameters were kept constant during all factorial experiments, given in Table 3-6.

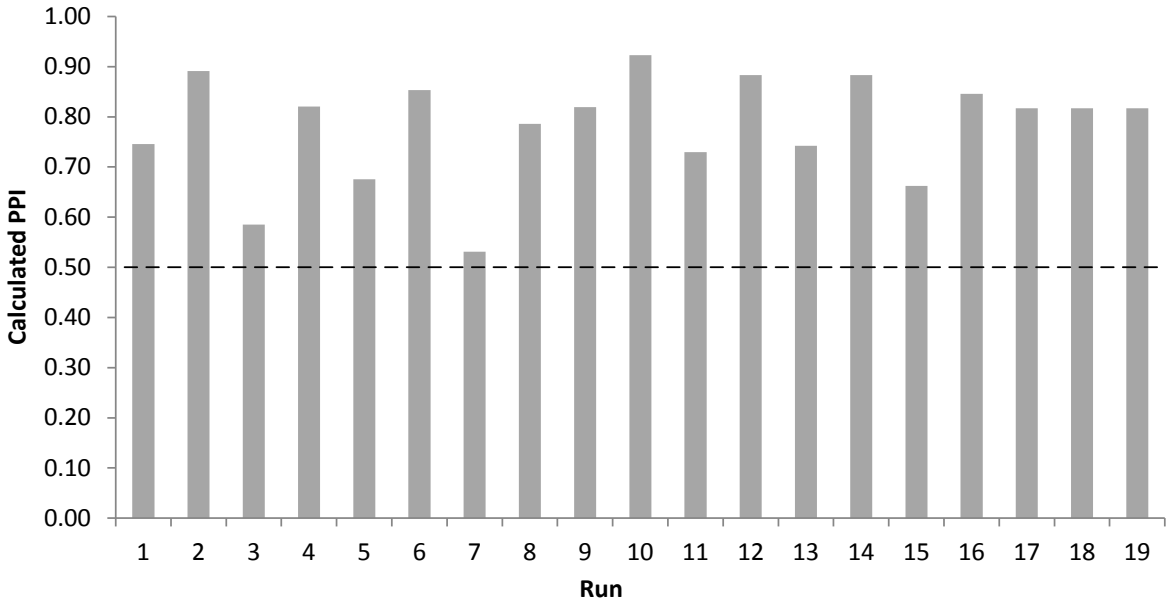

Figure 3-9 *Calculated permeate production index for each factorial run*

Table 3-6 *RO system parameters constant during all factorial design experiments*

Temperature	15°C ± 2°C
Feed volume	10L
Feed Solution	3.00 g/L Na_2SO_4 and 3.1 g/L $CaCl_2.H_2O$ in demineralised water
SI_0	1.22 @ 15°C (971 mg/L Na^+, 847 mg/L Ca^{2+}, 1498 mg/L Cl^-, 2029 mg/L SO_4^{2-})
Seed	Gypsum (calcium sulphate dihydrate)
Seed dosing	2 g/L concentrate (dosed hourly)
Solids recycle	1.5 L/h
Stirrer Speeds	50 rpm
Flushing Velocity	0.10 m/s @ 14 L/h permeate flushing

Chapter 4 - Permeate Flushing Calculations and Thermodynamic Predictions

Throughout this study the total production time was used to compare experimental runs under different operating conditions. This concept is explained in this chapter, discussing how permeate flushing affects the net recovery. Further, permeate flushing results in a lower net permeate production rates, compared to non-flushing operation. The effect of flushing frequency, flushing volume and soak time on the permeate production rate is explained in section 4.2. Further, the thermodynamic equilibrium calculations using the *OLI Analyser ScaleChem 9.0* software for RO unit operation are given in section 4.3.

4.1. Total production and total operating time

The obvious disadvantage of permeate flushing is the reduction in overall permeate production rate, since a certain portion of permeate is recycled back to the system during the flushing, hence the actual permeate production rate will be lower than the permeate flow rate. This results in a longer operation time to achieve a certain overall recovery, compared to the non-flushing case where the permeate flow rate is equal to the permeate production rate. Further, permeate flushing results in loss of productivity. A total cycle consists of "production time", "flushing time" and "soak time", as shown Figure 4-1.

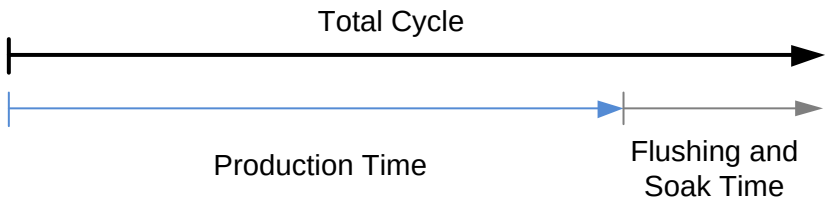

Figure 4-1 *Total cycle consisting of production time, flushing time and soak time*

The permeate production efficiency (ω_P) is strongly influenced by the flushing frequency and flushing volume. An increase in either of the two factors results in a lower production efficiency, calculated by the following equation:

$$\omega_P = \frac{production\ time\ (sec)}{total\ cycle\ duration\ (sec)} \qquad \textbf{Equation 4-1}$$

The operating time (t_O) is simply the time the unit operated, which includes any flushing and soaking times during flushing experiments, whereas permeate is only produced during production time (t_P). The production time is calculated by multiplying the permeate production efficiency and the operating time, as given in the equation below:

$$t_P = t_O \omega_P \qquad \textbf{Equation 4-2}$$

In this study the flushing technique was evaluated by comparing flushing and non-flushing experimental runs, however comparison by operating time was not possible due to the periodic downtimes during any flushing experiment. In a non-flushing experiment the total operating time (t_{OT}) was equal to the total production time (t_{TP}), as illustrated in Figure 4-2. Conversely, in any flushing experiment the total production time was less than the total operating time, due to the periodic flushing. The magnitude of this difference was determined by the flushing frequency, flushing volume and soaking time. Therefore, the production time was used throughout this study to compare flushing and non-flushing experimental runs, since it was not possible to compare runs in terms of operating times.

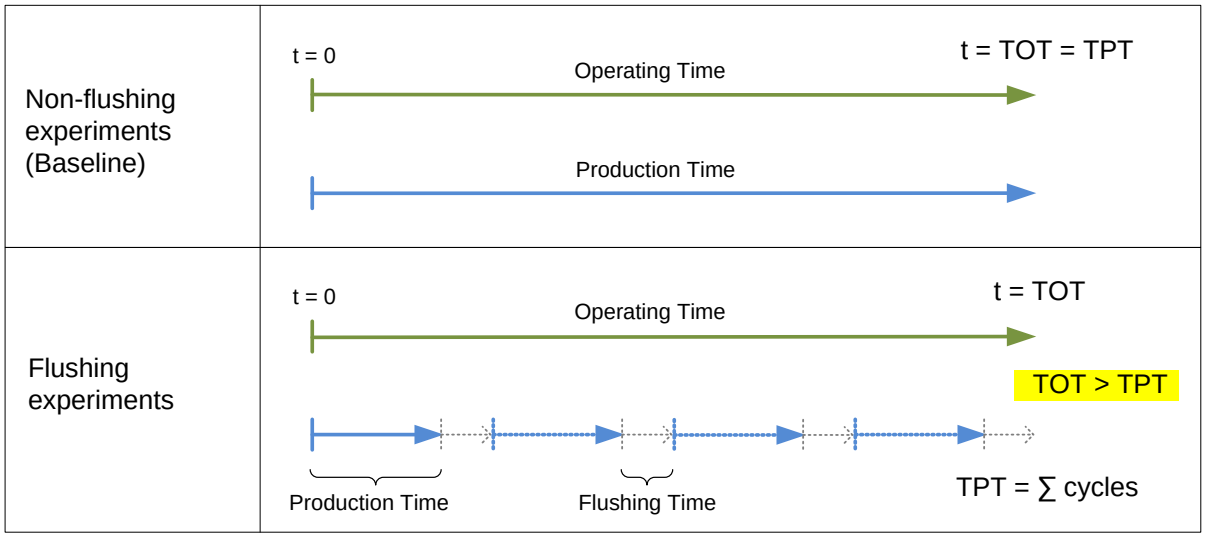

Legend:
TOT = Total Operating Time
TPT = Total Production Time

Figure 4-2 *Comparison of total production time for non-flushing and flushing experiments*

The total production time was determined from the last reading, before a flux decline was observed although the feed pressure was increased significantly. This indicated that the membrane was completely scaled and the unit could not be operated at a constant flux, indicating the upper scaling

limit. In other words, the longer the total production time, the longer the membrane was scale free, hence the more effective the membrane scaling prevention technique.

4.2. Permeate production rate (PPR) and index (PPI)

The periodic permeate flushing also lowered the permeate production rate. The theoretical permeate production rate, was calculated with

$$PPR = Q_P\omega_P - V_{flush} \qquad \textbf{Equation 4-3}$$

where ***PPR*** is the permeate production rate in L/h, Q_P is the permeate flow rate in L/h, and V_{flush} the volume of permeate used for flushing per hour (L/h).

In order to compare the permeate production rate under different experimental conditions, the dimensionless permeate production index was defined as:

$$PPI = \frac{PPR}{Q_P} \qquad \textbf{Equation 4-4}$$

where ***PPI*** is the permeate production index and Q_P the actual permeate flow rate (i.e. production rate) at a specific flux. The PPI has a value between 0 and 1, indicating how close the permeate production rate of a flushing case was to that of the non-flushing case.

The permeate production rate is affected by permeate flux, flushing frequency, flushing volume and soak time. Lowering the flushing frequency, as well as minimising the flushing volume and soak time will result in the highest possible permeate production rate. Each of these effects is further discussed in the following sections, except for permeate flux as it was obvious that a higher flux will result in a higher permeate production rate.

4.2.1. The effect of flushing volume on permeate production index

The flushing volume is the total volume used during one flushing cycle, effectively displacing the saline solution in the RO membrane test cell on the feed-brine side. An increase in flushing volume caused a linear decrease in permeate production index, as shown in Figure 4-3. As the flushing volume increases, the production index decreases since more water is recycled during a total cycle. This effect is more severe at lower fluxes, where the flushing volume makes up a greater volume of

the produced permeate per hour, hence the gradient of the line is steeper at 12 LMH compared to 18 or 24 LMH.

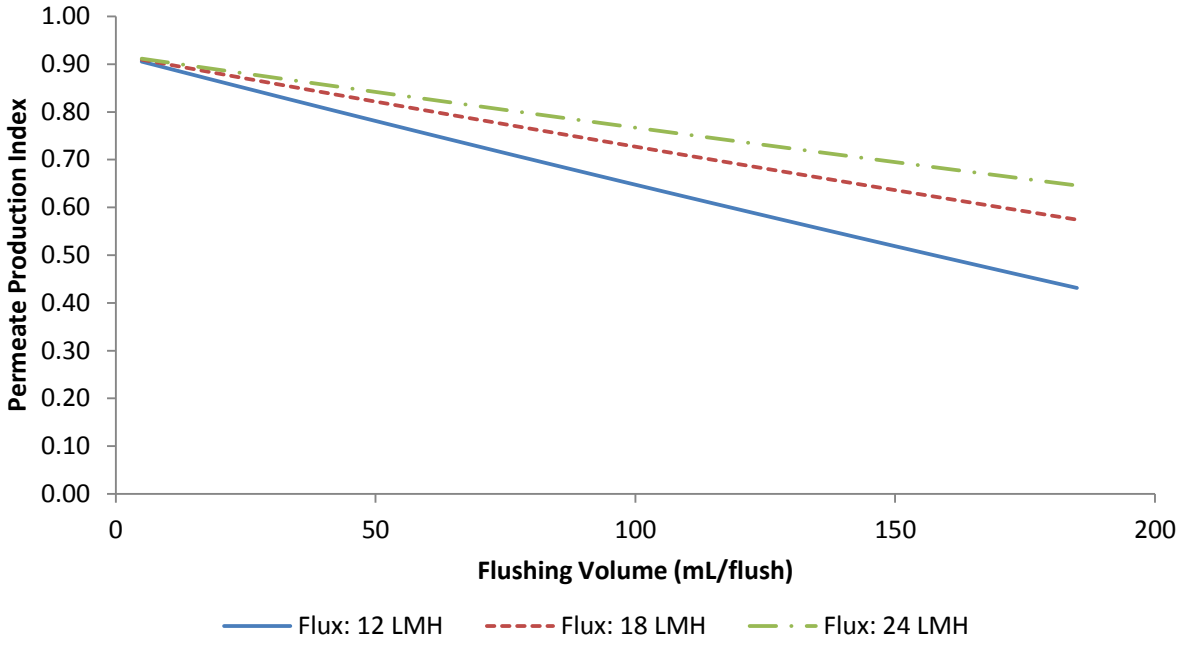

Figure 4-3 *The effect of flushing volume on permeate production rate at 12, 18 and 24 LMH flux. The soak time and flushing frequency are constant, at 55 seconds and 3.4 h^{-1} respectively.*

4.2.2. The effect of flushing frequency on permeate production index

Lower flushing frequencies results in higher overall permeate production indexes, as shown in Figure 4-4. As the flushing frequency (measured in h^{-1}) decreases, an increase in PPI is observed. Less frequent permeate flushing results in a higher production efficiency, hence the PPI will approach 1 if the flushing frequency decreases indefinitely, which means that the permeate production rate is equal to the permeate flow rate. For each specific permeate flux, there is a certain absolute minimum flushing frequency resulting in net permeate production of zero. In other words, all the produced permeate is recycled back to the feed tank during flushing and the net permeate production is zero. The critical values for 12, 18 and 24 LMH are 24, 36 and 48 h^{-1} respectively. Operating the unit at flushing frequencies higher than that is not possible; because the produced permeate volume would be less than the required volume for the permeate flushing.

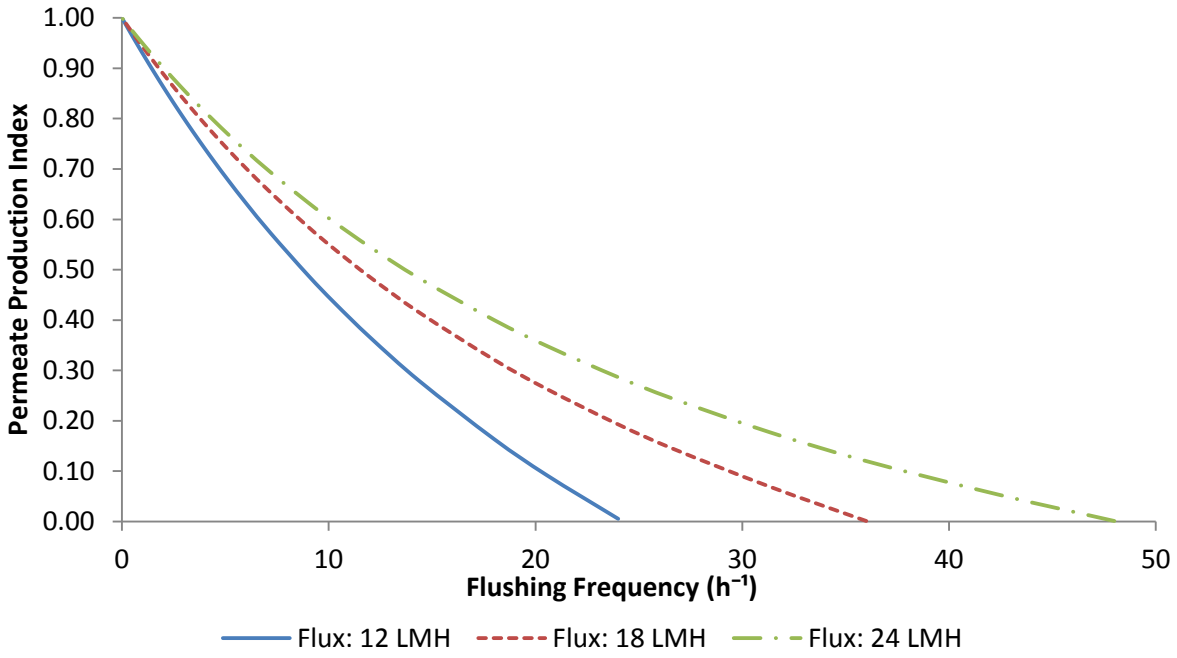

Figure 4-4 *The effect of flushing frequency on permeate production rate at 12, 18 and 24 LMH flux. The soak time and flushing volume are constant, at 55 seconds and 52.5 mL/flush respectively.*

4.2.3. The effect of soaking time on permeate production rate

The soak time is part of the flushing cycle, succeeding the permeate flushing, to enhance the mass transfer from the membrane surface to the bulk solution. Longer soak times decrease the production efficiency during a flushing cycle, hence also reducing the permeate production index, as shown in Figure 4-5. A negative linear trend is observed, as the soaking time increases the PPI decreases. The gradient for each line is the same, where the initial PPI at zero seconds soak time is determined by the magnitude of the permeate flux.

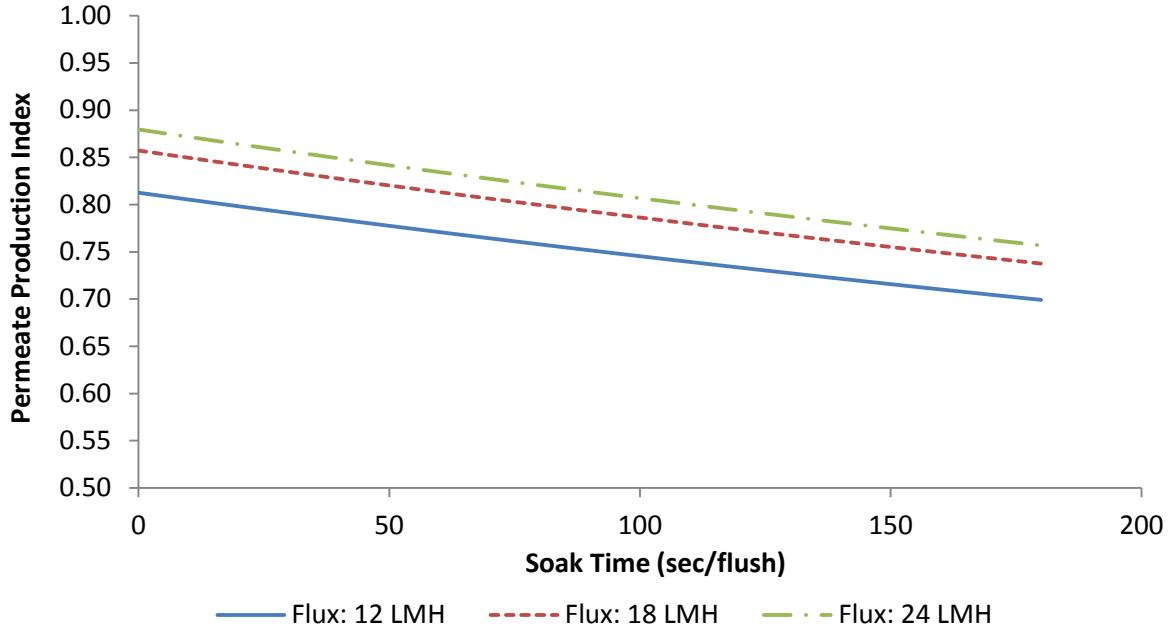

Figure 4-5 *The effect of soaking time on permeate production rate at 12, 18 and 24 LMH flux. The flushing frequency and flushing volume are constant, at 3.4 h^{-1} and 52.5 mL/flush respectively*

4.3. Thermodynamic predictions

OLI Analyser ScaleChem 9.0 was used to perform thermodynamic calculations, in order to predict the ion concentrations, gypsum saturation index, specific conductivities and osmotic pressures at various operation conditions. The data from this section were compared to real experimental data, in order to verify the experimental method used in this study. For the calculations the following assumptions were made:

- The calcium ion and sulphate ion concentrations were always in stoichiometric proportion. The initial feed solution was prepared with equimolar amounts of Ca^{+2} and SO_4^{-2}, hence this assumption was valid. One mole of calcium ions will react with one mole of sulphate ions in order to produce a one mole of solid calcium sulphate dihydrate, justifying this assumption.
- The sodium and chloride ion concentrations were not affected by the gypsum precipitation reaction and the increase thereof was determined by the concentration factor based on overall recovery.
- In the gypsum seeding scenario, the RO feed saturation index was constant at 1.2 and 1.1 in the precipitation reactor effluent overflow. McCool et al. (2013) studied RO concentrate demineralisation via gypsum seeding under similar feed conditions used in this study. The feed SI was reduced from 1.7 to 1.1 after gypsum seeding, resulting in a 29% reduction in

calcium concentration. Similar results were obtained by Rahardianto et al. (2010), where the gypsum saturation index was reduced to 1.1 after the gypsum seeding. Therefore, the thermodynamic calculations were completed by assuming constant saturation indexes: SI_f = 1.2 and SI_{ov} = 1.1.

Further, the temperature was kept constant at 15°C in all calculations, since that was the target temperature in all experimental runs. The initial feed solution has a saturation index of 1.2, corresponding to the experimental feed SI, with ion concentrations as given in Table 3-1. The generated data for both scenarios are given in Appendix C, and the results are discussed in the following sections.

Scenario 1: It was assumed that all ion species concentrations in the RO feed increase according to the overall recovery and absolutely no calcium sulphate scaling occurred, resulting in excessively large saturation indexes at higher recoveries. In reality it would not be possible to operate a plant under these conditions, since scaling will take place after certain production time, even with the use of antiscalants. The feed stream concentrations were determined by the overall concentration factor, while the RO concentrate concentrations were determined by the instantaneous concentration factor, based on salt rejection and instantaneous recovery.

Scenario 2: The RO feed sodium and chloride ion concentrations increase according to the overall concentration factor, while the calcium and sulphate ion concentrations correspond to a constant gypsum saturation index of 1.2. An iterative approach was followed, where the calcium and sulphate ion concentration were varied in *OLI Analyser ScaleChem 9.0* until the SI was equal to 1.2, while keeping the sodium and chloride concentrations fixed. The RO concentrate composition was determined by the instantaneous concentration factor, based on salt rejection and instantaneous recovery. The precipitation reactor overflow composition was calculated with the same iterative procedure used for the RO feed.

4.3.1. Theoretical non scaling vs. gypsum seeding scenario

The ion concentrations for two scenarios are given in Figure 4-6, showing the ion concentrations for the RO feed as the overall recovery increases. A clear exponential increase in concentration is observed for all ion species, representing Scenario 1. These trends are typical for any RO operation if the concentrate stream is directly recycled back into the feed, and all the ions are concentrated according to the overall concentration factor. The gypsum saturation index rises exponentially from

1.22 to 10.89, corresponding to 0 to 90% recovery respectively. It is important to notice that operation at a SI of 10.89, even with antiscalants would be impossible since membrane scaling would occur. With antiscalants, brackish RO membranes can typically be operated up to saturation indexes of 4 (Pomerantz et al., 2006), and an SI above 10 would be well above that.

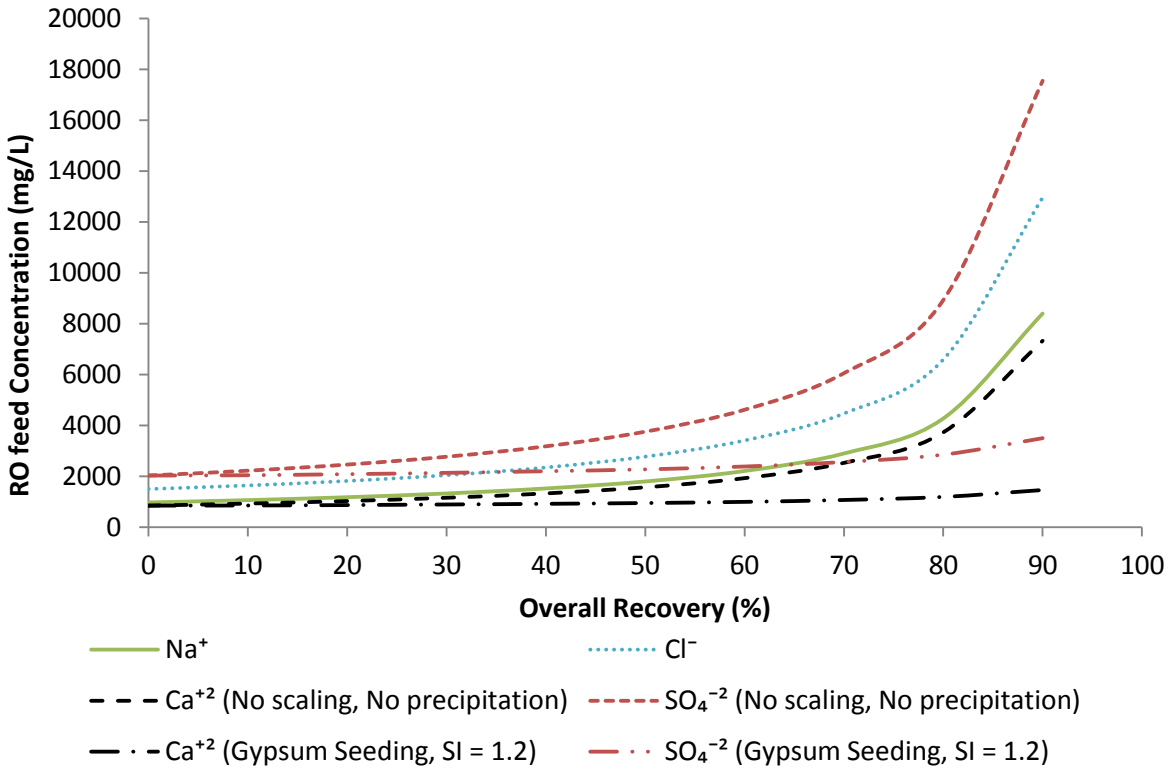

Figure 4-6 *RO feed concentrations for theoretical non-scaling/no precipitation scenario and seeded gypsum precipitation scenario.*

In the second scenario, inter-stage gypsum precipitation is assumed, thus the RO feed has a constant SI of 1.2. The operation of the gypsum precipitation reactor only affects the calcium and sulphate concentrations, as shown in Figure 4-6, whereas the sodium and chloride concentration remain unchanged. The Ca^{2+} and SO_4^{2-} concentrations increase from 847 to 1460 mg/L and 2029 to 3499 mg/L respectively, as the recovery increases from 0 to 90 %. The feed saturation index is constant at 1.2, thus one would assume that the Ca^{2+} and SO_4^{2-} concentrations would stay constant. However, the gradual rising trend in calcium and sulphate concentrations can be explained by the increasing solubility with an increasing concentration of other dissolved salts (i.e. NaCl) (Brandse et al., 1977; Hamdona and Al Hadad, 2007; Helalizadeh et al., 2000). In other words, the solubility product (K_{SP}) increases with increasing solution ionic strength (Pomerantz et al., 2006), hence the Ca^{2+} and SO_4^{2-} concentrations increases gently whilst the saturation index remains constant at 1.2.

4.3.2. The effect of instantaneous recovery on RO concentrate

The ion concentrations in the RO concentrate primarily depend on feed salinity and instantaneous recovery, where the effect of instantaneous recovery on gypsum saturation index is shown in Figure 4-7. The concentrations steadily increase from 927 to 1598 mg/L and 1156 to 1992 mg/L, at 10 and 30 % instantaneous recovery respectively. The gypsum saturation index at 10 and 30 % instantaneous recovery are 1.33 and 1.71 respectively, providing the RO feed had a constant SI of 1.2, since higher instantaneous recoveries resulted in higher concentrate salinities.

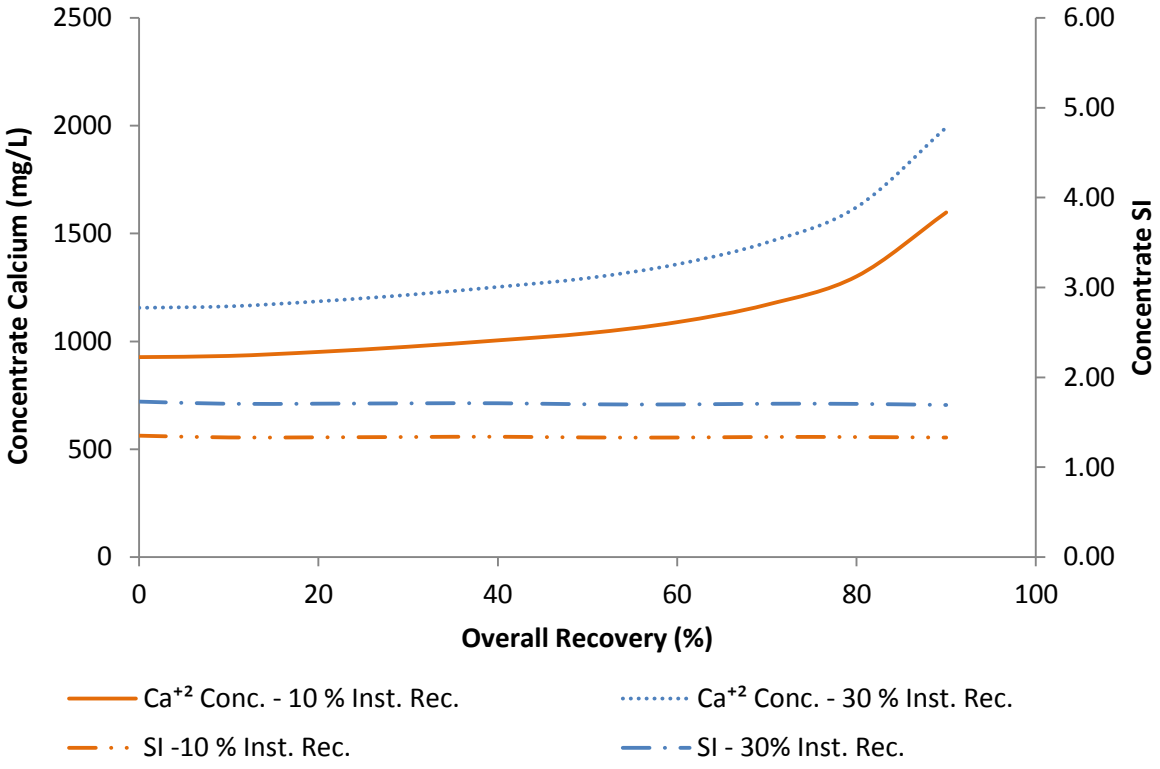

Figure 4-7 *The effect of instantaneous recovery on calcium concentration and gypsum saturation index during seeded gypsum precipitation RO system operation.*

4.3.3. Equilibrium calcium concentration

At equilibrium, the gypsum saturation index is equal to one and the solution is thermodynamically stable since the Gibbs free energy was minimized. The equilibrium calcium concentration for the equimolar Ca^{+2} and SO_4^{-2} system is shown in Figure 4-8. The Na^{+} and Cl^{-} concentrations correspond to the overall concentration factor based on the membrane salt rejection. The calcium concentrations for RO feed and concentrate are also shown, following the exact same trends as the saturation index increases. Again, the increasing calcium and sulphate concentration are explained by the higher

calcium sulphate solubility with increasing ionic strength of the solution, due to the presence of the Na^+ and Cl^- ions (Brandse et al., 1977; Hamdona and Al Hadad, 2007; Helalizadeh et al., 2000).

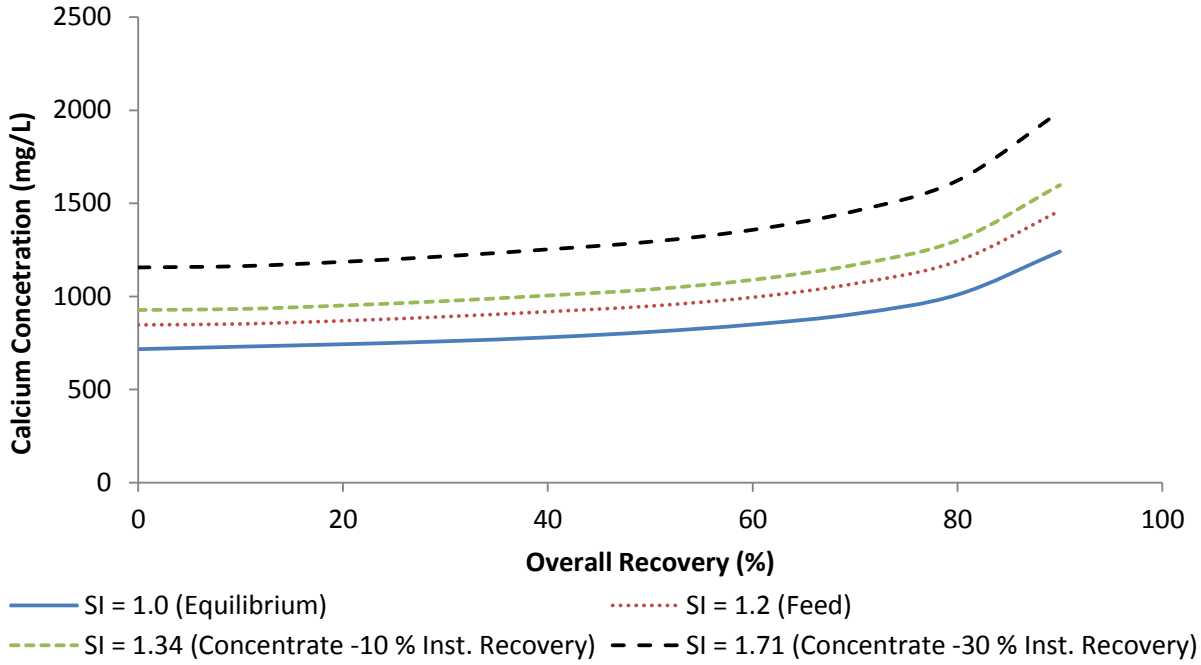

Figure 4-8 *Calcium concentration for various saturation indexes at 15°C, where sulphate ions are present in a stoichiometric amount. The sodium and chloride ion concentration are based on the overall concentration factor.*

4.4. Summary

In this chapter the permeate production rate (PPR) and permeate production index (PPI) were defined, as used for normalisation of experimental data to compare experimental runs performed under different experimental conditions. The PPI is affected by the periodic permeate flushing, more specifically by the following factors: permeate flux, flushing frequency, flushing volume and soak time. Further, the *OLI Analyser ScaleChem 9.0* software was used to predict the ion concentrations at certain saturation indexes, conductivities and osmotic pressures. These data were used as baseline data for the experimental runs, to verify the experimental technique by comparing the theoretical and actual data. In chapter 5 initial experimental results are provided, demonstrating that the experimental apparatus could produce reliable results.

Chapter 5 - Experimental Evaluation of Equipment, Repeatability and Scale Formation

In this section the experimental evaluation of the lab-scale RO system is presented, discussing the operation of the precipitation reactors and the flushing technique, confirming that repeatable results can be produced. A detailed physical membrane scale evaluation, by using analytical techniques was used to investigate scaling pattern on the flat sheet RO membranes. The baseline data were generated to determine the effectiveness of the flushing technique, by comparing flushing and non-flushing experimental runs. It should be noted: "*baseline*" experiments/runs refer to runs conducted with a scaling solution under concentrate recycle mode, without the operation of the precipitation reactors and permeate flushing. During all *"flushing and seeding"* experiments/runs the gypsum precipitation reactors were operated together with the permeate flushing technique.

5.1. Gypsum precipitation – batch experiments

The results from the batch tests were used to study the calcium sulphate crystallisation reaction and optimising the lab-scale RO system crystallisation reactor. Three important parameters were determined: the optimal seed dose, the residence time for the reactor and the kinetics of the reaction at ambient temperatures.

5.1.1. The effect of seed dose

Crystal growth will take place without a nucleation phase (i.e. induction time) if a sufficient amount of seed is added. If no seed or too little seed crystals are added, the crystallisation phase would only be initiated after the initial nucleation phase when the actual growth sites are formed. The batch experiments showed that an increase in the gypsum seed dose increased the crystal growth rate, as shown in Figure 5-1. In each experiment the initial calcium concentration was the same and the temperature was constant at 25°C. The induction time was eliminated by dosing 2 g/L or more gypsum seed crystals, compared to a 30 minute induction time for the non-seeding experiment. This showed that a seed dose of 2 g/L was adequate to remove the induction time completely, as previously confirmed by the literature (Amjad, 1985; Gerber, 2011; Lui and Nancolass, 1970).

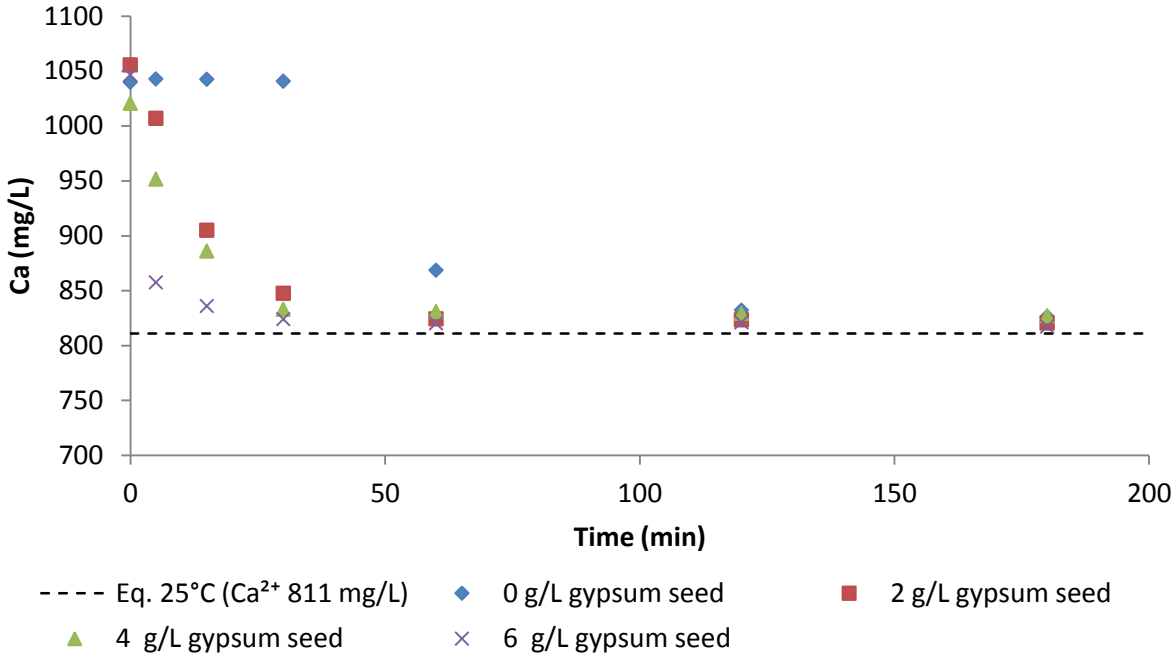

Figure 5-1 *The effect of gypsum seeding dose on growth rate and induction time. The dotted line represents the equilibrium calcium concentration at 25°C, obtained from OLI Analyser ScaleChem 9.0.*

Further, the growth rate increased with an increasing seed dose from 2 to 6 g/L, while using seed particles ranging between 10-40 µm in size. This increase in growth rate was attributed to larger number of available growth sites during the nucleation period, since the growth rate and induction time were directly related to the number of available growth sites (Amjad and Hooley, 1986; Amjad, 1985).

5.1.2. The effect of temperature

The batch experiments showed a proportional increase of growth rate with increasing temperature, as shown in Figure 5-2. As expected, the induction time was eliminated since gypsum seed was added at 2 g/L. The calcium equilibrium concentration increased with rising temperature, since the solubility of calcium sulphate increases in the range from 0 - 40°C (Helalizadeh et al., 2000; Power, 1964), shown by the dashed lines. The growth rate was the highest at 25°C where the equilibrium concentration was reached after approximately 35 minutes, whereas it took about 120 minutes at 15°C. This increase in growth rate with rising temperature can be explained by an Arrhenius type relationship, where an exponential increase in growth rate is observed (Amjad and Hooley, 1986; Amjad, 1988; Lui and Nancolass, 1970).

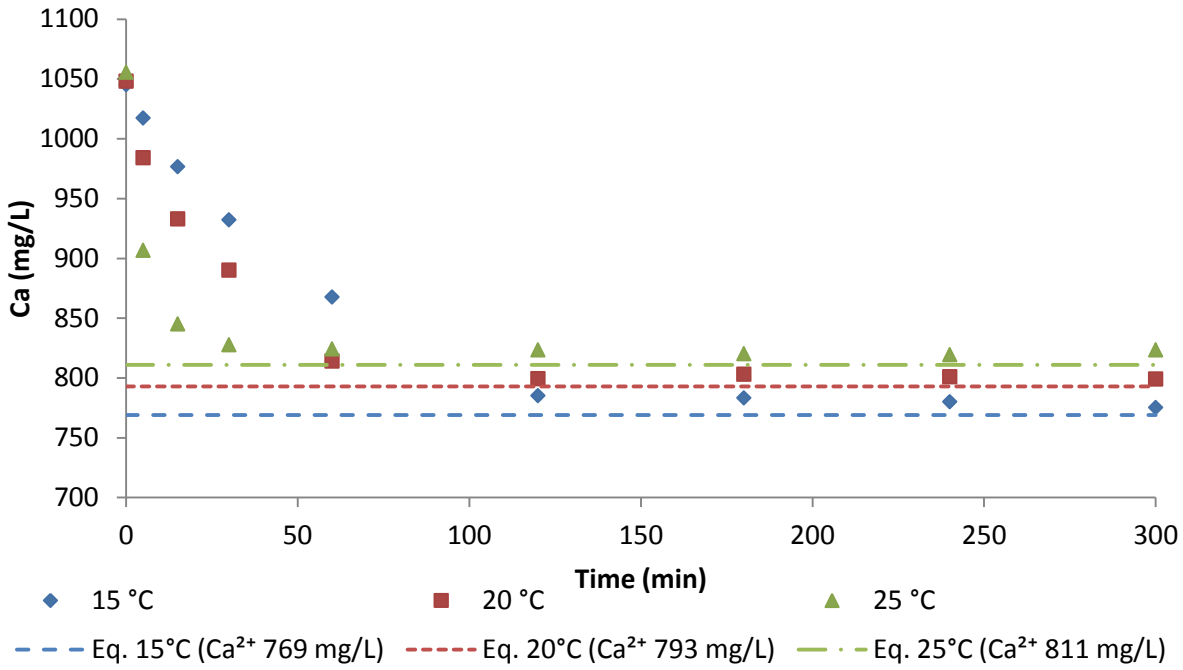

Figure 5-2 *The effect of temperature on growth rate and induction time, for experiments 5-7 (refer to Table 3-2). The dotted lines represent the equilibrium calcium concentration at 15, 20 and 25°C respectively, calculated by OLI Analyser ScaleChem 9.0.*

5.1.3. The effect of supersaturation

As expected, higher supersaturation levels resulted in a higher calcium sulphate growth rates, as it can be seen in Figure 5-3. The temperature remained constant at 15°C during each experiment. An increase of roughly 350 mg/L calcium caused the growth rate to increase approximately by a factor of two. For an initial SI_o of 2.73 the equilibrium was reached after roughly 33 minutes, while it was reached after 65 minutes for a SI_o of 2.15. The same trend was observed when comparing the growth rates where the SI_o was 2.15 and 1.57 respectively. This was in good agreement with the literature, where Gerber (2011) observed an increase in growth rate by a factor slightly more than 2 for an increase of 0.01 M (400 mg/L) in calcium concentration. Further, this also agreed with Klepetsanis (1999) where a linear relationship between growth rate and supersaturation level was proposed.

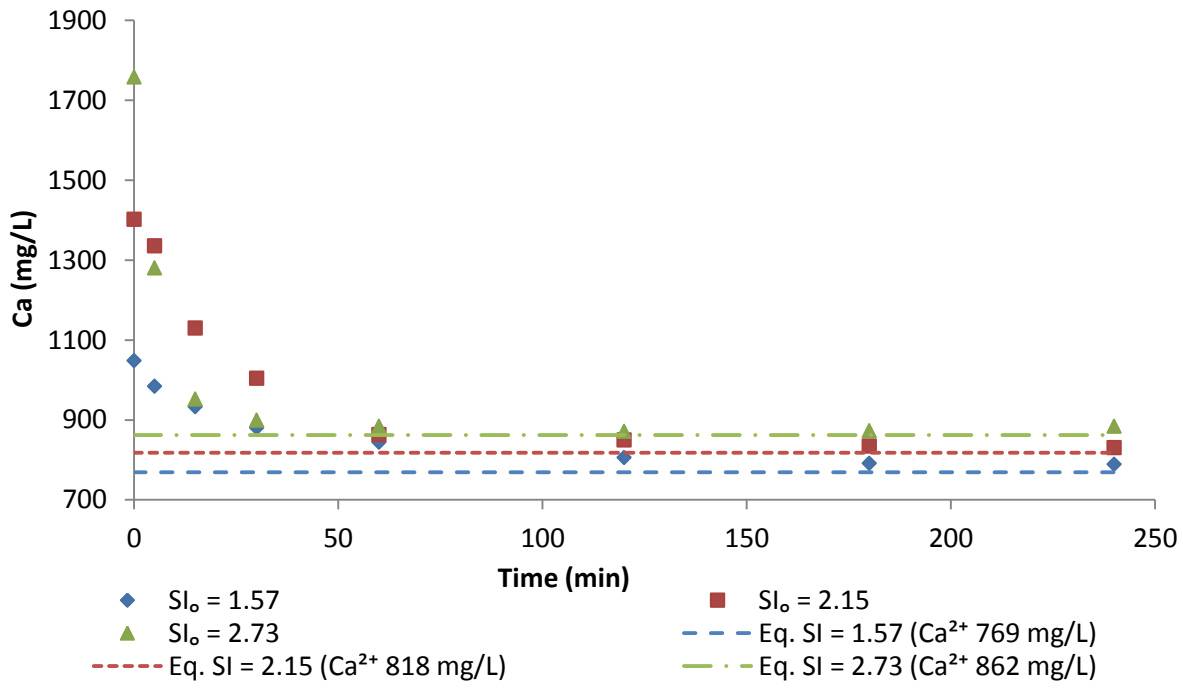

Figure 5-3 *The effect of supersaturation level on growth rate and induction time, experiments 8-10 (refer to Table 3-2) at 15°C. The dotted lines represent the equilibrium calcium concentration at each initial calcium concentration, calculated by OLI Analyser ScaleChem 9.0, also at 15°C.*

5.2. Baseline data – no flushing, no seeding

The baseline data was generated by operating the RO unit in concentrate recycle mode without permeate flushing and operating the precipitation reactors. This data indicated how long the membrane must be exposed to a scaling solution until membrane scaling occurred (under certain operating conditions). The data was useful to act as reference when determining if the flushing technique was effective. Experimental runs were performed using the same initial conditions as described in section 3.5.5, using the high and low values from the experimental design (only flux and instantaneous recovery). A total of 4 baseline runs were completed, at 12 and 24 LMH permeate flux, each at 10 and 30 % instantaneous recovery respectively. Further, the repeatability for one baseline run is discussed in section 5.5.1.

In each run the lab-scale RO unit was operated at constant permeate fluxes and instantaneous recoveries, by adjusting the RO feed and concentrate needle valve accordingly. This was essential since the recycling of the concentrate stream caused an increase in feed osmotic pressure, hence the net driving force (i.e. feed pressure) was adjusted accordingly. The experimental run was stopped once the permeate flux decline was observed. A permeate flux decline was caused by an increase in feed osmotic pressure or increased hydraulic resistance from a scaling layer that causes flow

reduction (Hasson et al., 2001), thus the flux decline was deduced to be caused by the scaling layer since the feed pressure was adjusted to compensate for the increased osmotic pressure (refer to section 5.6 for a detailed scaling evaluation discussion).

The effective membrane permeability for each run is shown in Figure 5-4, indicating how the RO membrane scales under certain operating conditions. It was observed that higher fluxes and instantaneous recoveries, caused faster membrane scaling. The drop in effective membrane permeability was most gradual at 10 LMH and 10 % instantaneous recovery. These results are in good agreement with previous studies (Al-Bastaki and Abbas, 2003; Rahardianto et al., 2006; Sablani et al., 2001; Shih et al., 2005). Instantaneous recovery is directly related to feed-brine cross flow velocity, where a lower cross flow velocity increases the risk of membrane scaling due to the higher levels of concentration polarization. Further, high permeate fluxes increased the degree of concentration polarization and supersaturation at the membrane surface thus increasing the risk of membrane scaling (Pomerantz et al., 2006; Uchymiak et al., 2008).

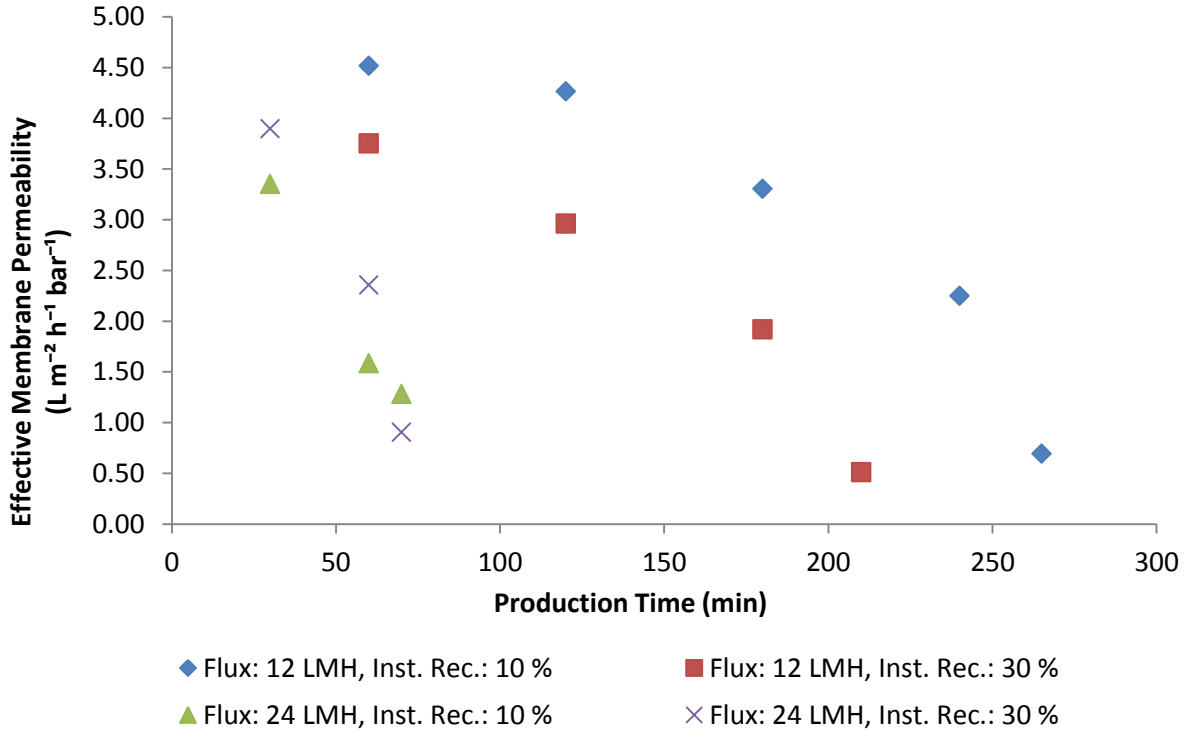

Figure 5-4 *Effective membrane permeability for the non-flushing and non-seeding experimental runs, at various permeate fluxes and instantaneous recoveries.*

In theory, the effective membrane permeability should stay constant, provided that no scaling occurs and the feed pressure was adjusted to compensate for the increase in osmotic pressure. However, the data in Figure 5-4 clearly show rapid (at 24 LMH flux) and gradual (at 12 LMH flux)

decrease in effective membrane permeability, indicating that scaling occurred early during each experiment. Initially the rate of scaling was low, however once enough nucleation sites had developed on the membrane, scaling was almost instantaneous (shown by the rapid drop in membrane permeability). To further study the rate of scaling, the concentrate conductivity and calcium concentrations were measured, shown in Figure 5-5 and Figure 5-6 respectively.

Figure 5-5 shows the gradual increase in conductivity with time, due to the increasing osmotic pressure of the feed solution. This upward trend was followed by a slight drop in conductivity after a certain time, deviating from the calculated values, where the details of the calculations are explained in section 4.3. This drop in concentrate conductivity was caused by gypsum precipitation on the membrane, since the concentration of calcium and sulphate ions decreased, thus decreasing the bulk solution conductivity slightly. The experiment was aborted once the permeate flux could not be maintained, indicating severe surface blockage due to the scaling layer.

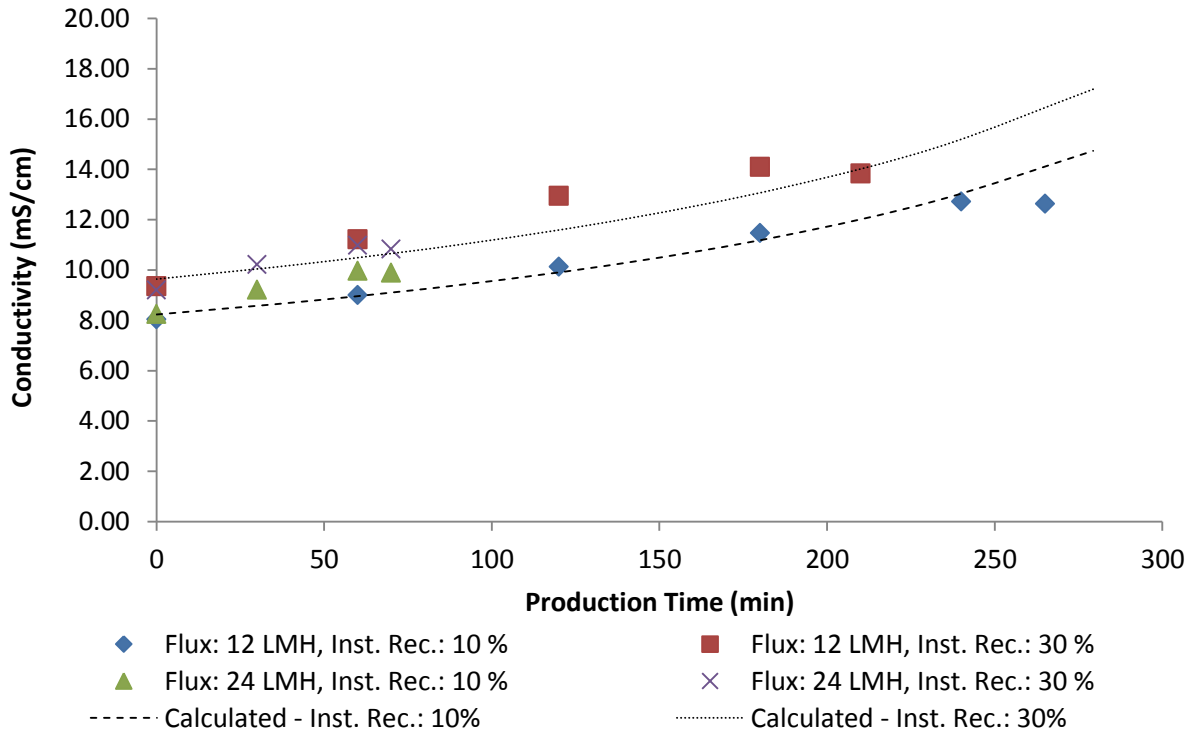

Figure 5-5 *RO concentrate conductivity for the non-flushing and non-seeding experimental runs, at various permeate fluxes and instantaneous recoveries.*

Similar trends were observed in the RO concentrate calcium concentrations, as shown in Figure 5-6, also agreeing to the trends in Figure 5-5. The calcium concentrations increased steadily, until it levelled out or decreased slightly, deviating from the calculated concentrations, where the details of the calculations are explained in section 4.3. The overlapping trends observed in conductivity and

calcium concentrations were useful to determine an approximate total production time for an experimental run under certain operating conditions. For instance, if one operates the lab-scale unit at 12 LMH flux and 30 % instantaneous recovery, the membrane will be completely scaled after about 220 minutes, as shown in Figure 5-5 and Figure 5-6.

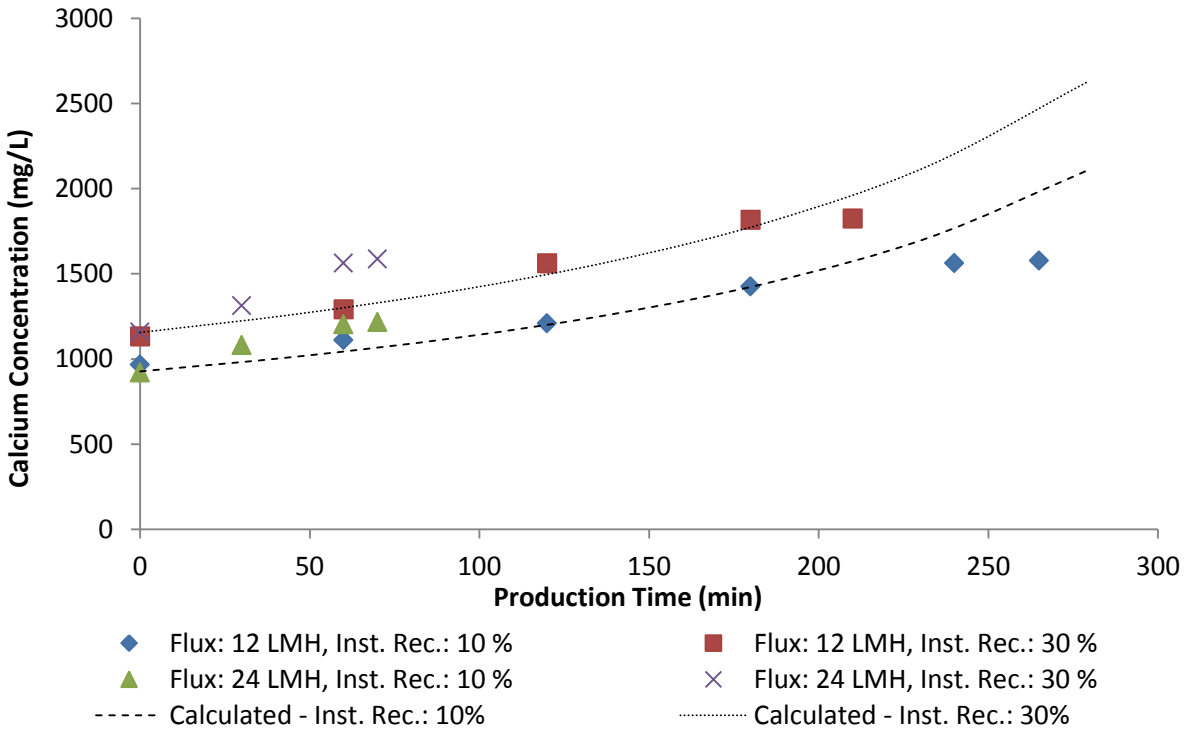

Figure 5-6 *RO concentrate calcium ion concentration for the non-flushing and non-seeding experimental runs, at various permeate fluxes and instantaneous recoveries.*

5.3. Initial evaluation of flushing technique

The flushing technique was evaluated by operating the lab-scale system in full recycle mode, where both permeate and concentrate were recycled back to the feed tank, thus the net overall recovery was zero. Initially 10 L of slightly undersaturated calcium sulphate solution with an SI_g of 0.9 was fed to the RO membrane, operating at 12 LMH permeate flux and 10 % instantaneous recovery, with an instantaneous concentration factor of roughly 1.1. Theoretically the concentrate would have an SI ≈ 1.0 (0.9 x 1.1), thus the bulk solution should be at saturation or slightly oversaturated. It should be noted that no seeded gypsum precipitation took place, in order to isolate the effect of permeate flushing.

In Figure 5-7 the membrane permeability for 3 different flushing frequencies is shown. After the initial 24 hour operation in permeate flushing mode, the RO unit was switched to non-flushing operation. For the initial 24 hours during flushing operation the effective membrane permeability was constant, since the flux, conductivities and feed pressures remained constant. However, once the operation was switched to non-flushing, a flux decline occurred. A steady decrease was observed, until the permeability levelled out. This indicated that the flushing technique effectively prevented scaling, since the effective membrane permeability was constant for 24 hours during the flushing operation. However, only if the initial feed solution was slightly undersaturated (SI_g = 0.9) and the RO system operated in full recycle mode. Further, no significant differences at different flushing frequencies was observed, indicating that even the lowest frequency of 2.4 h^{-1} was shorter than the induction time of under these specific operating conditions. In other words, the flushing technique was effective to remove any potential nucleation sites near the membrane surface thus preventing membrane scaling. With every flushing cycle the oversaturated solution at the membrane surface was replaced with an undersaturated solution. The results indicated that the flushing period (i.e. time between two consecutive flushes) must be lower than the induction time for the specific operating conditions, in order to prevent scaling. This fully agreed with Pomerantz et al. (2006), where a flow reversal technique was used to "zero" the induction time clock every time the feed and brine streams were switched, although antiscalants were used.

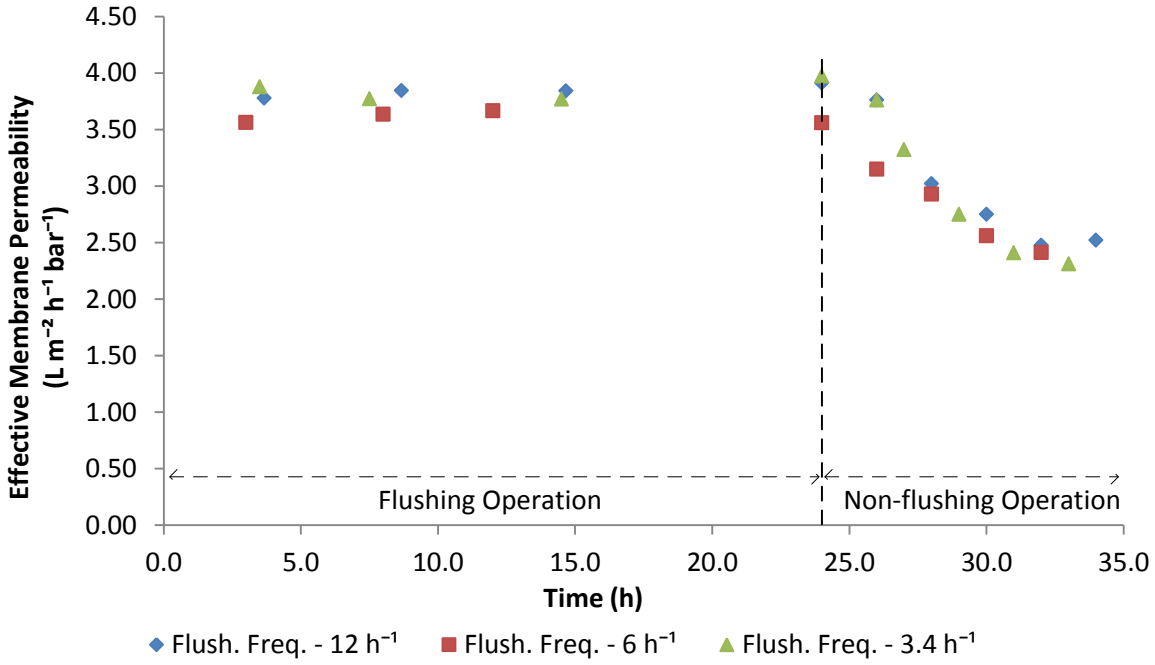

Figure 5-7 *Effective membrane permeability during full recycle RO unit operation. The unit was switched to non-flushing mode, after flushing for 24 hours at a certain flushing frequency.*

The measurements in concentrate conductivity also showed the same trend, as observed for the membrane permeability, depicted in Figure 5-8. For the first 24 hours the concentrate conductivity was constant, and only slight variations due to inevitable measurement error were observed. Once the RO system operation was switched to non-flushing, the conductivity of the concentrate slowly decreased, indicating that membrane scaling occurred. Again, no significant differences were observed for the different experimental runs at varying flushing frequencies.

The concentrate calcium concentrations remained constant for 24 hours before the concentration levelled out. This was shown in Figure 5-9 where an average calcium concentration drop of 60 mg/L was observed. Assuming that $Ca^{2+}$and SO_4^{2-} reacted in stoichiometric proportion, the equivalent drop in SO_4^{2-} concentration was 143 mg/L, thus the total drop was about 203 mg/L. This compares well to the drop in conductivity in Figure 5-7, where a total drop of about 400 µS/cm was equivalent to about 256 mg/L TDS (1000 µS/cm = 640 mg/L TDS, (Walton, 1989)). It should be noted, this is a generalised conductivity to TDS conversion for brackish waters, thus explaining the difference.

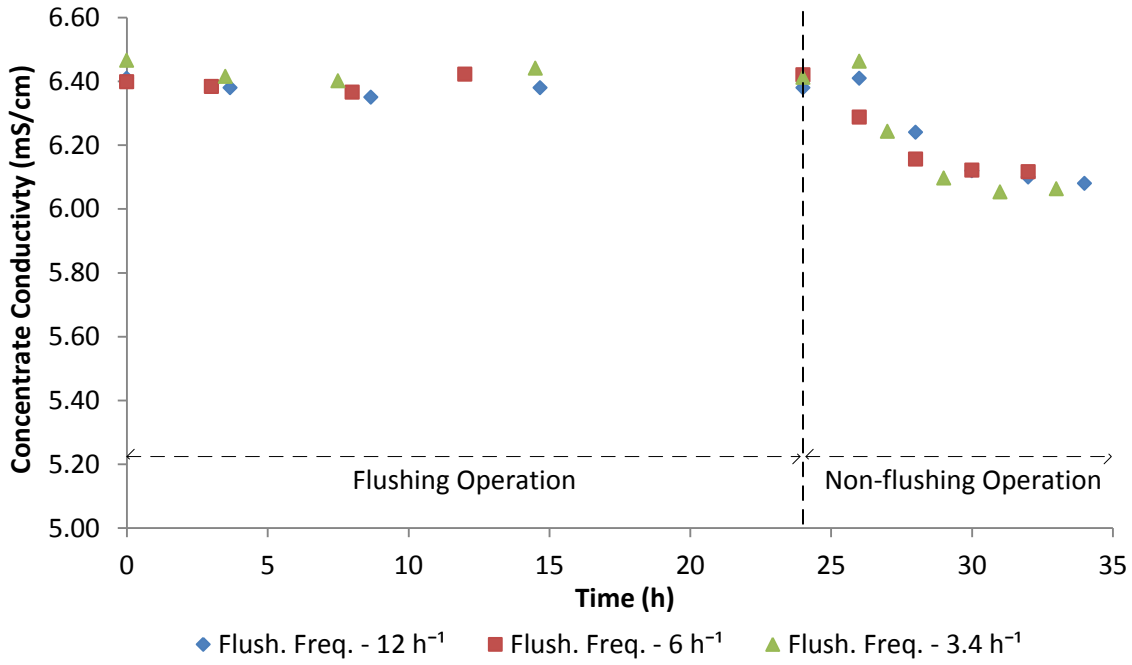

Figure 5-8 *Concentrate conductivity during full recycle RO unit operation. The unit was switched to non-flushing mode, after flushing for 24 hours at a certain flushing frequency.*

Figure 5-9 also shows the concentrate gypsum saturation index for each run at different flushing frequencies. For the first 24 hours, the gypsum saturation index in the bulk solution was constant at about 0.98, very close to the predicted value of 1.0. If the RO concentrate bulk saturation index was roughly 0.98, the apparent saturation index at the membrane surface was even higher than the bulk

saturation index due to concentration polarisation, estimated to be equal to 1.2. This finding agrees with results from previous studies (Pomerantz et al., 2006; Rahardianto et al., 2007, 2006; Uchymiak et al., 2008). After 24 hours a drop in gypsum saturation index in the RO concentrate was observed, levelling out at about 0.85.

The RO feed saturation index (not shown in Figure 5-9) was constant at about 0.89 for the first 24 hours, ultimately dropping to about 0.73 once the unit operated in non-flushing mode. This drop in feed SI was caused by the scale formation on the membrane, once the unit operated without permeate flushing. The saturation index in feed and concentrate remained at a constant level thereafter, indicating that the gypsum SI at the membrane surface is 1.0 or less. Theoretically, no further scaling will occur since the saturation index at the membrane surface is 1.0 or less. This was observed in the experiments, since stable concentrations after about 35 hours were observed, indicating unfavourable scaling thermodynamics. Scaling is likely to occur if a supersaturated solution is present at the membrane surface, since the thermodynamic driving force for any crystallisation reaction is the difference in oversaturated solution and equilibrium concentration (Ben Ahmed et al., 2008).

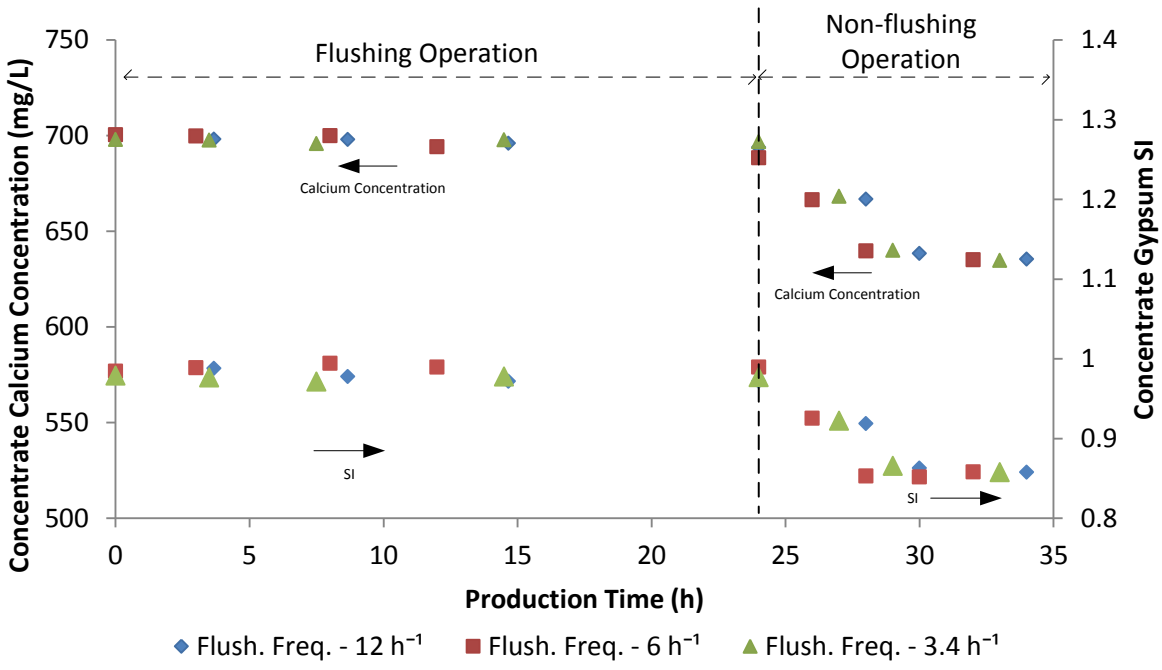

Figure 5-9 *Concentrate calcium concentrations during full recycle RO unit operation. The unit was switched to non-flushing mode, after flushing for 24 hours at a certain flushing frequency.*

5.4. Intermediate seeded gypsum precipitation

In this study it was critical that the gypsum precipitation reactor operated effectively, in order to demineralise the RO concentrate, to achieve higher overall water recoveries by recycling the concentrate with a lowered scaling propensity. The precipitation reactor performance of a typical permeate flushing and seeded precipitation run was discussed in this section, to demonstrate that the precipitation reactor works effectively. The measured calcium and sulphate concentrations for a typical concentrate recycle experiment run is given in Figure 5-10, operating at 12 LMH flux, 10 % instantaneous recovery and flushing 2.4 times per hour with 35 mL permeate. The calcium concentration was measured using an AAS (refer to section 3.2.2), whereas the sulphate concentrations were determined with a *Dionex 4500i Series* ion chromatograph. For calcium and sulphate clear trends were identified, showing a significant concentration drop from the RO concentrate to precipitation reactor overflow. On average the calcium and sulphate concentrations dropped by 104 ± 9 mg/L and 201 ± 27 mg/L respectively, which was in stoichiometric proportion indicating that only calcium sulphate precipitation occurred. In other words, the calcium and sulphate concentrations approximately dropped by 10 % and 8 % respectively. These results were consistent throughout the study, and only slight variations were observed.

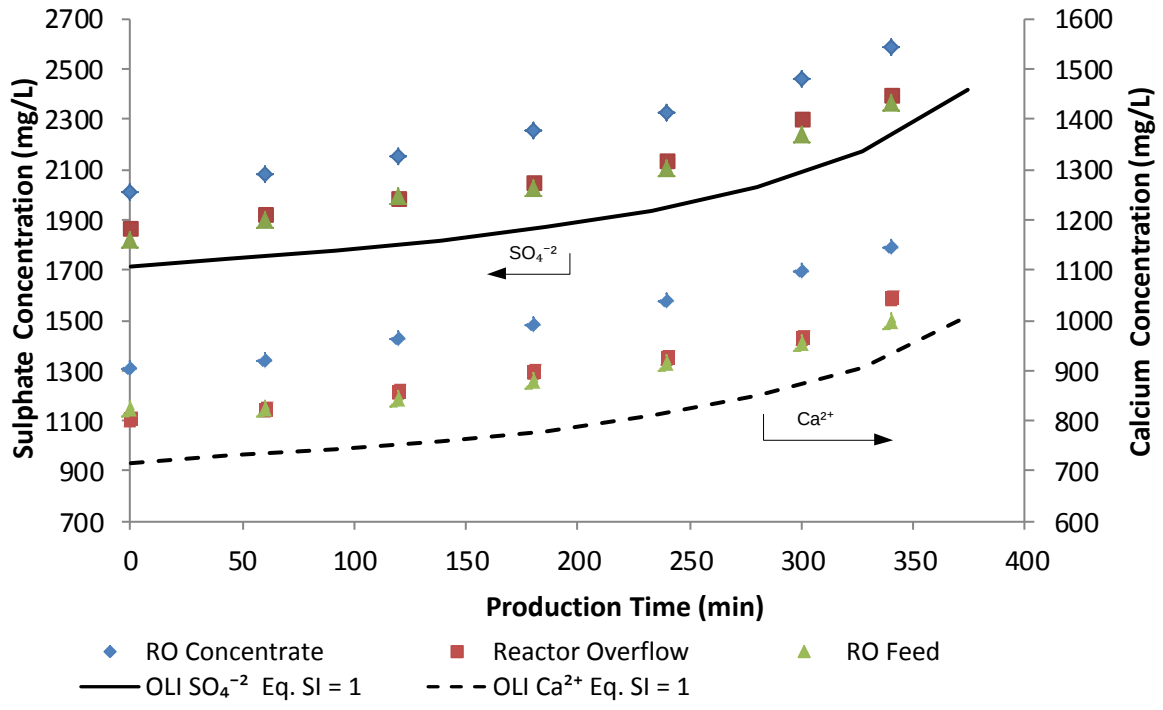

Figure 5-10 *Measured calcium and sulphate concentration showing that the seeded precipitation effectively reduced the scaling potential of the concentrate*

The concentrations in Figure 5-10 are increasing steadily, although the gypsum saturation index in each stream stays relatively constant as the production time increased, as shown in Figure 5-11. The calcium and sulphate concentration increased steadily in each stream, due to the increased solubility of calcium sulphate with increasing sodium and chloride concentrations (Brandse et al., 1977; Freyer and Voigt, 2003; Helalizadeh et al., 2000). On average the concentrate SI was approximately 10 % higher than the feed SI, which was expected due to the operation at 10 % instantaneous recovery. Other experiments at 30 % instantaneous recovery were consistent with these results, on average showing an increase from 1.1 to 1.4 SI, which approximately corresponded to a 30 % increase. On average the reactor effluent had an SI of 1.1, which agreed with previous studies. McCool et al. (2013) and Rahardianto et al. (2010) reported reactor effluent saturation indexes of 1.1 and 1.2 respectively, for gypsum seeded precipitation under similar conditions.

Conductivity measurements confirmed the drop in calcium and sulphate concentrations from RO concentrate to reactor effluent, as shown in Figure 5-11, where an average drop of approximately 623 µS/cm was observed. This corresponds to a drop of approximately 400 mg/L TDS, since 1000 µS/cm equals 640 mg/L TDS (Walton, 1989). This was in relatively good agreement with the actual drop in TDS, where an average drop of 304 mg/L TDS was observed (i.e. the sum of calcium and sulphate concentration drop). It should be noted that the conversion from conductivity to TDS was an estimate at best.

The literature review and the current experimental results both indicated that the reactor effluent had a gypsum saturation index between 1.1 and 1.2. This implied that the seeded precipitation reaction did not reach the thermodynamic equilibrium where the SI is equal to 1. In theory this could be achieved by significantly increasing the residence time in the reactors, thus allowing the reaction to go to completion. The main driving force for the precipitation was the calcium sulphate supersaturation level, thus the reaction kinetics to reduce the SI from 1.1 to 1.0 are very slow, hence this would not be viable, as the reactors volume would be excessively large.

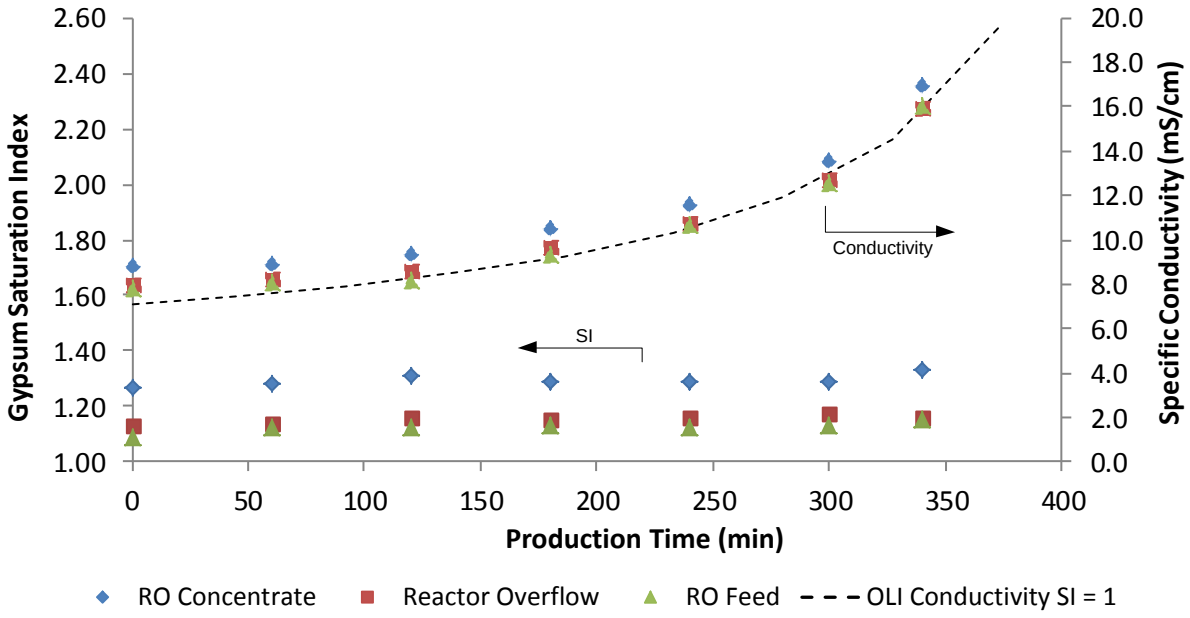

Figure 5-11 *Calculated gypsum saturation index and measured specific conductivity, indicating the effective operation of the precipitation reactor.*

5.5. Repeatability of experimental data

Repeatability of experiments shows the variation of data obtained using the same equipment and operating the lab-scale RO unit exactly at the same operating conditions. Repeating the experiments on different days will show if the data is reliable. The repeatability for one baseline experiment and the 3 centre runs of the factorial design experiments are discussed in the subsections below. The repeatability is validated by comparing the effective membrane permeability, concentrate conductivity and concentrate calcium concentration for experiments performed in triplicate.

5.5.1. Baseline runs – non flushing, non-seeding

The repeatability margins for the baseline experiment at 12 LMH permeate flux and 10 % instantaneous recovery is discussed in this section. The results are given in Figure 5-12 to Figure 5-14, showing the effective membrane permeability, concentrate conductivity and concentrate calcium concentration respectively. Each vertical error bar shows the range of measurement for three independent runs performed on three different days, taken at the same time during each experimental run.

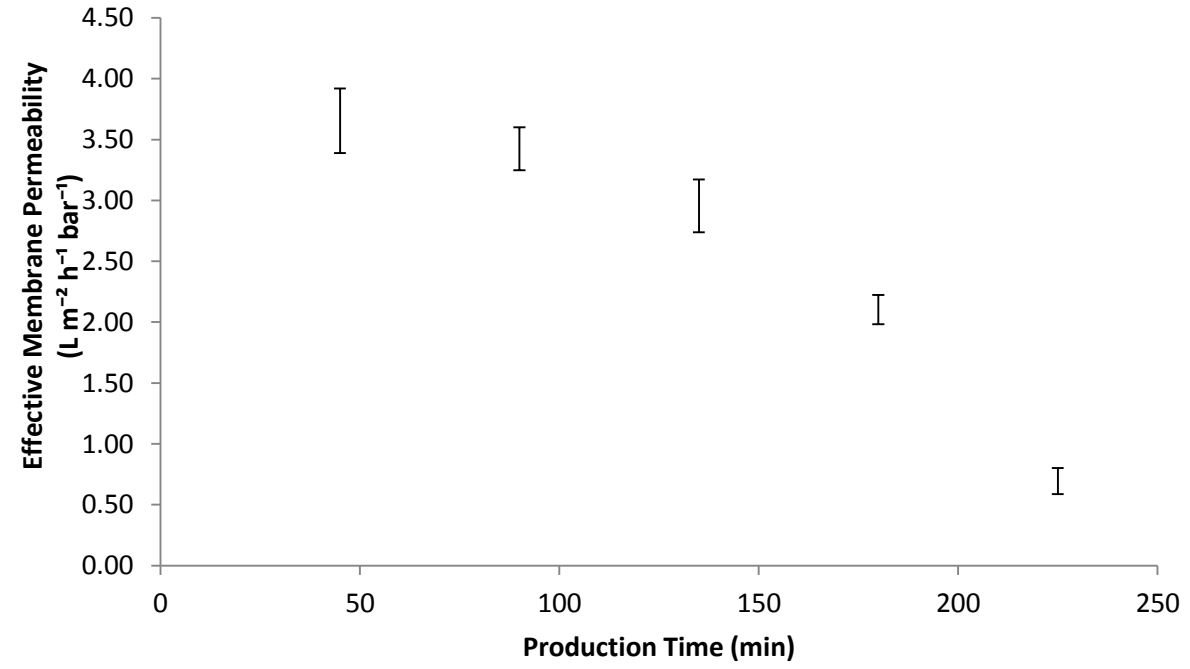

Figure 5-12 *Repeatability of effective membrane permeability measurement for a baseline run at 12 LMH flux and 10 % instantaneous recovery, showing the range of measurement between the three replicates.*

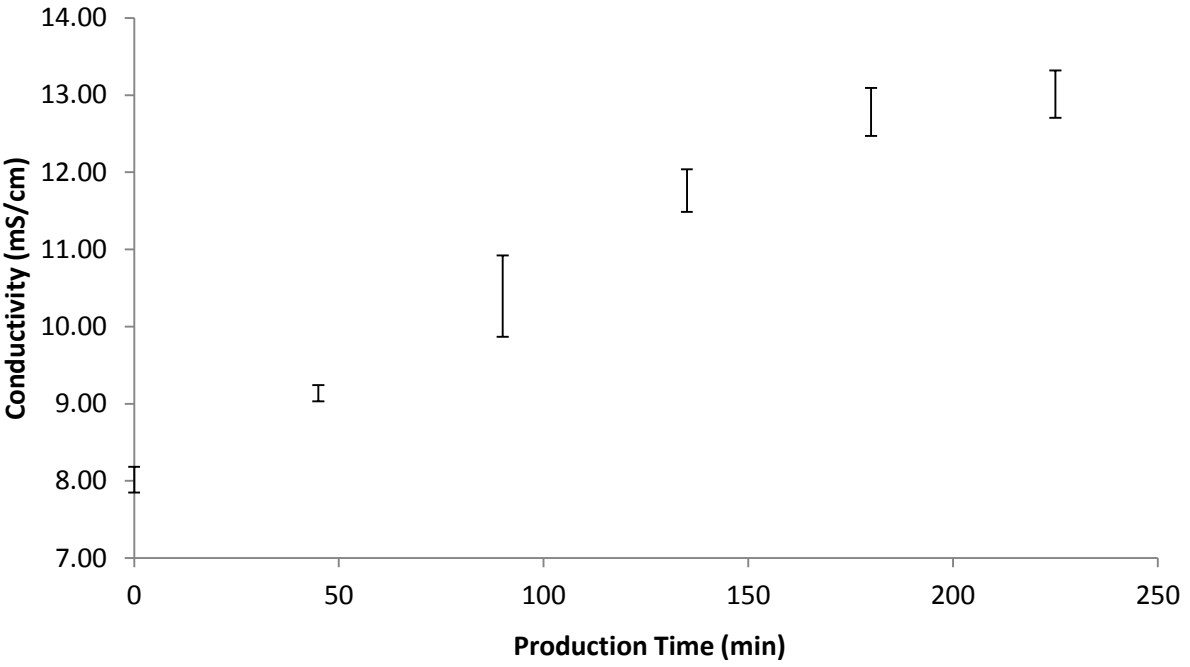

Figure 5-13 *Repeatability of concentrate conductivity measurement for a baseline run at 12 LMH flux and 10 % instantaneous recovery, showing the range of measurement between the three replicates.*

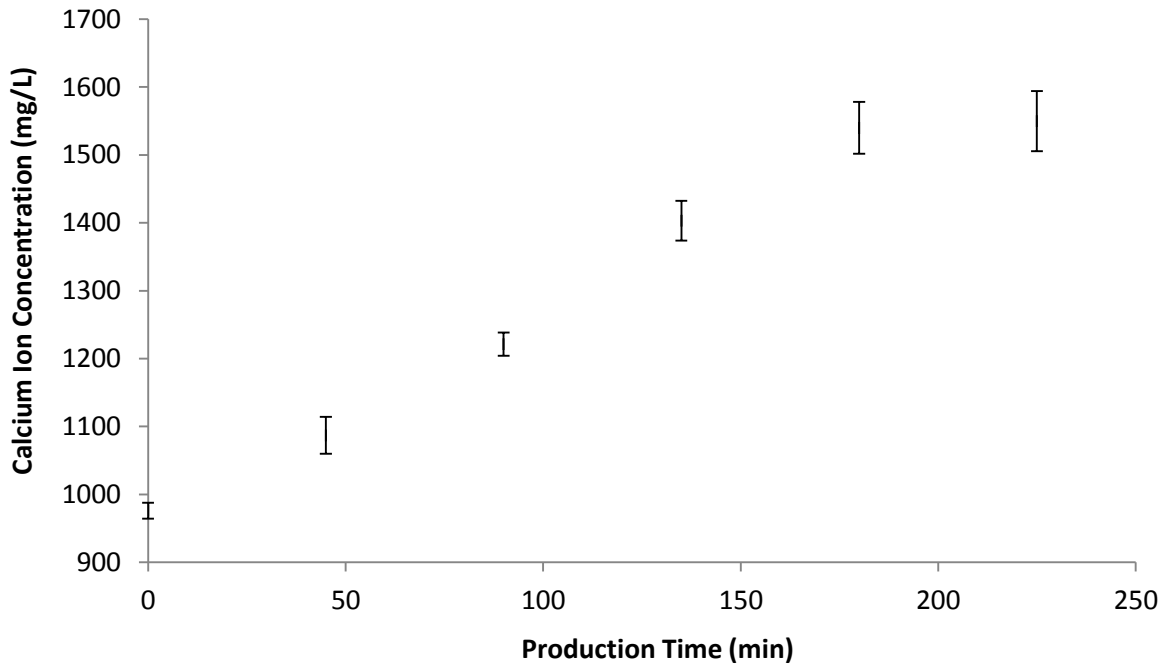

Figure 5-14 *Repeatability of concentrate calcium concentration measurement for a baseline run at 12 LMH flux and 10 % instantaneous recovery, showing the range of measurement between the three replicates.*

The average error margin was calculated for each measured parameter, based on three readings taken at the same time during each independent experimental run for the baseline experiments, as shown in Figure 5-12 to Figure 5-14 respectively. On average the error margin was 8.2 % for each effective membrane permeability reading, 2.6 % for each conductivity reading and 2.1 % for each calcium concentration reading. This was considered to be an acceptable variation.

The lab-scale system was operated at constant fluxes, by manually adjusting certain needle valves during an experimental run. This introduced human errors since it was never possible to maintain a perfectly constant flow rate, explaining the small variances in total production times for each independent run.

5.5.2. Factorial Runs - Flushing and seeding

The three centre runs of the factorial design experiment were used to test the repeatability of the experiments with permeate flushing and seeded precipitation. Each experiment was repeated under the same RO unit operating conditions on three different days. The average margin of error for the measurements was based on three readings taken at the same time during each independent experimental run for the replicate runs. The error bars are shown in Figure 5-15 to Figure 5-17 respectively. This corresponds to an average error margin of 7.7 % for each effective membrane

permeability reading, 1.2 % for each conductivity reading and 0.8 % for each calcium concentration reading, indicating that the experimental data was reliable.

In the factorial design experiments the total production times were used to compare the effectiveness of the flushing technique under different experimental conditions. The repeatability runs indicated that total production time measurements were reliable. The total production time for the three runs was 218, 227 and 231 minutes respectively, corresponding to a margin of error of 2.5 %.

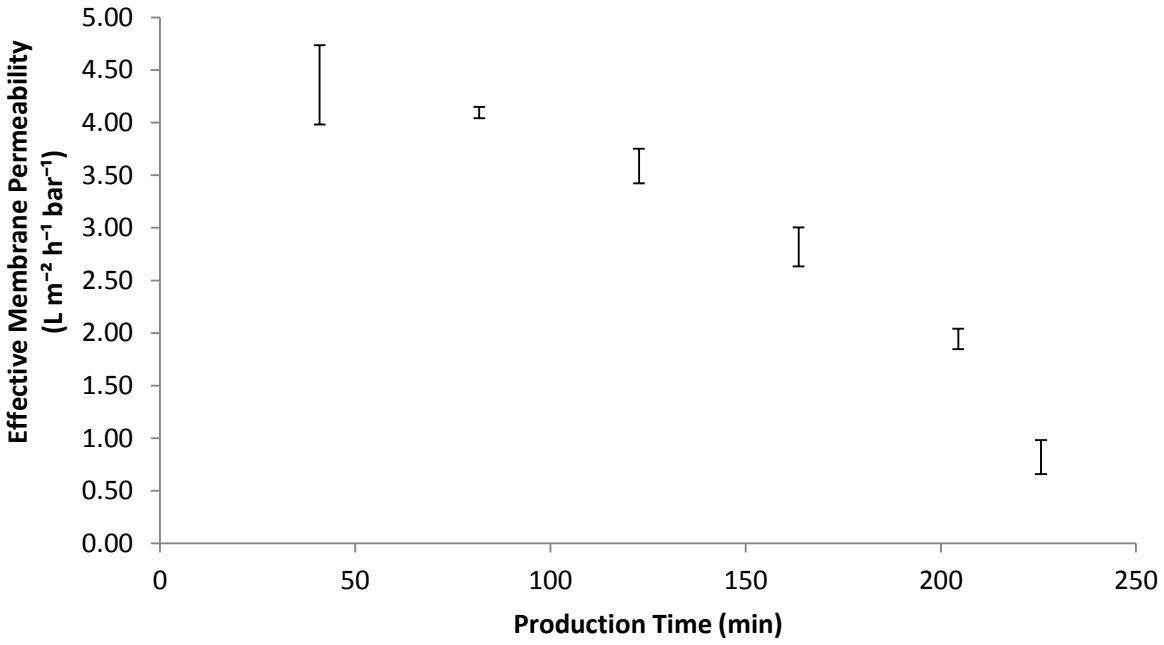

Figure 5-15 *Repeatability of effective membrane permeability measurement for Run 17-19 showing the range of measurement between the three replicates.*

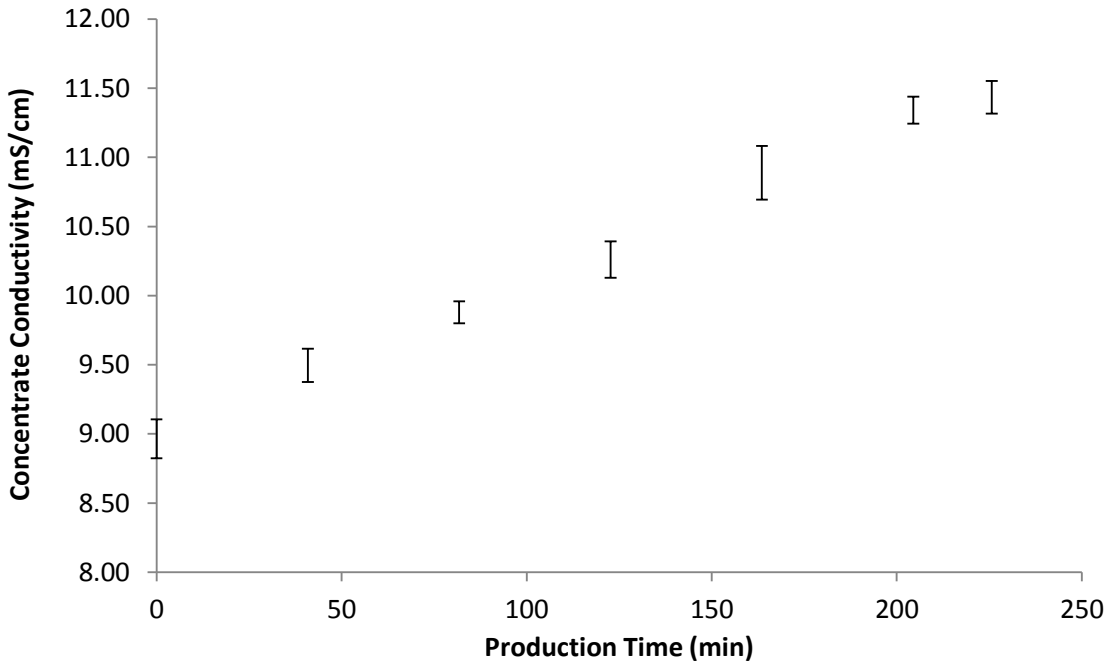

Figure 5-16 *Repeatability of concentrate conductivity measurement for Run 17-19 showing the range of measurement between the three replicates.*

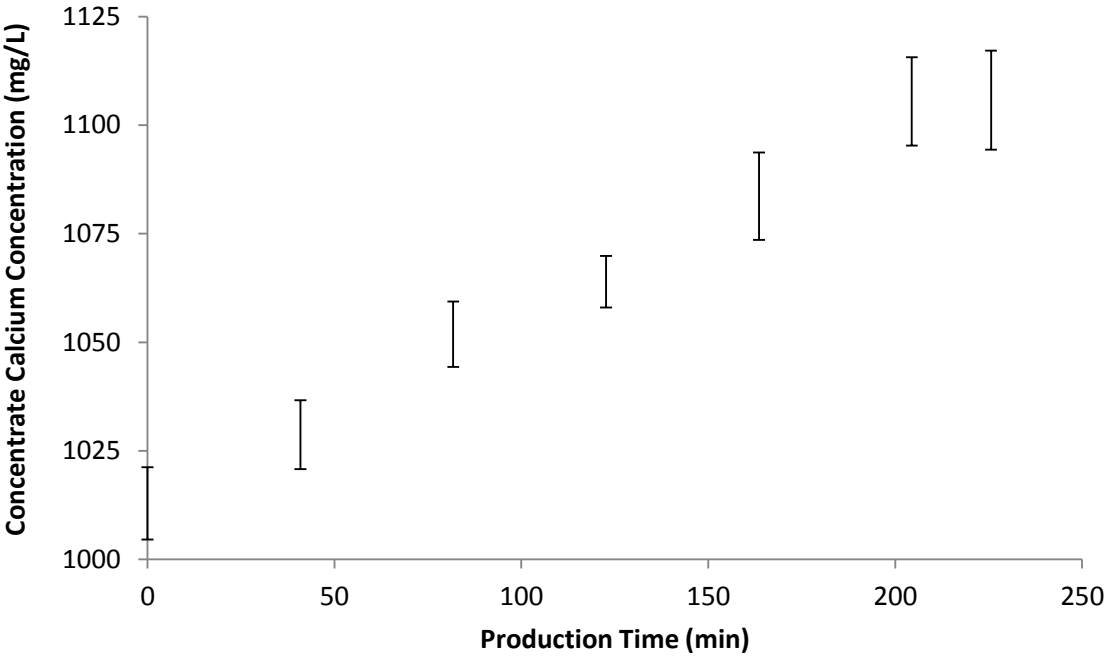

Figure 5-17 *Repeatability of concentrate calcium concentration measurement for Run 17-19 showing the range of measurement between the three replicates.*

5.6. Membrane scaling evaluation

5.6.1. Scale development along the flow channel

During an experiment, conductivity measurements and flux decline observations were the only real time monitoring tools used to determine the onset of membrane scaling. The pilot system was operated in concentrate recycle mode until a constant permeate flux was impossible to maintain, even after significantly increasing the feed pressure, marking the end of an experimental run. At this point the membrane was severely scaled, indicating that no or very few open scale-free areas were available to allow permeation.

A visual membrane inspection revealed that the membrane was often completely covered with scale crystals. A photograph from a baseline run without permeate flushing is shown in Figure 5-18. The image was modified by adjusting the contrast and inverting the colours, to make the crystals on the membrane more visible. The feed entered the flow path at channel 1, flowing along the tortuous path, until the brine exited after flowing through channel 6. Typically, scaling first occurred in the dead zones between the flow path and the outer 5 mm o-ring, indicated by the yellow dashed lines. Pockets of supersaturated water were stagnant in this area, increasing the scaling propensity. Scaling always occurred in this region, even if the rest of the membrane was completely scale free.

Visual inspection revealed that the extent of surface scale coverage was higher in the regions towards concentrate exit and the crystals appeared to be larger, compared to the entry region in channel 1. This is somewhat visible in Figure 5-18, where the individual crystals appear larger in channel 6 compared to channel 1. SEM images of individual crystals confirmed these findings, where the diameter of individual rosette crystals where larger in the exit region compared to the entry region. The size of the surface crystals increased with axial position from flow channel entry to exit, consistent with the corresponding with the higher level of supersaturation (i.e. concentration polarisation) at the membrane surface towards the channel exit. Rahardianto et al. (2006) and Shih et al. (2005) reported the same trends, where the extent of surface coverage and size of surface crystals increased with axial position along the rectangular membrane, corresponding with the degree of concentration polarisation at the membrane surface.

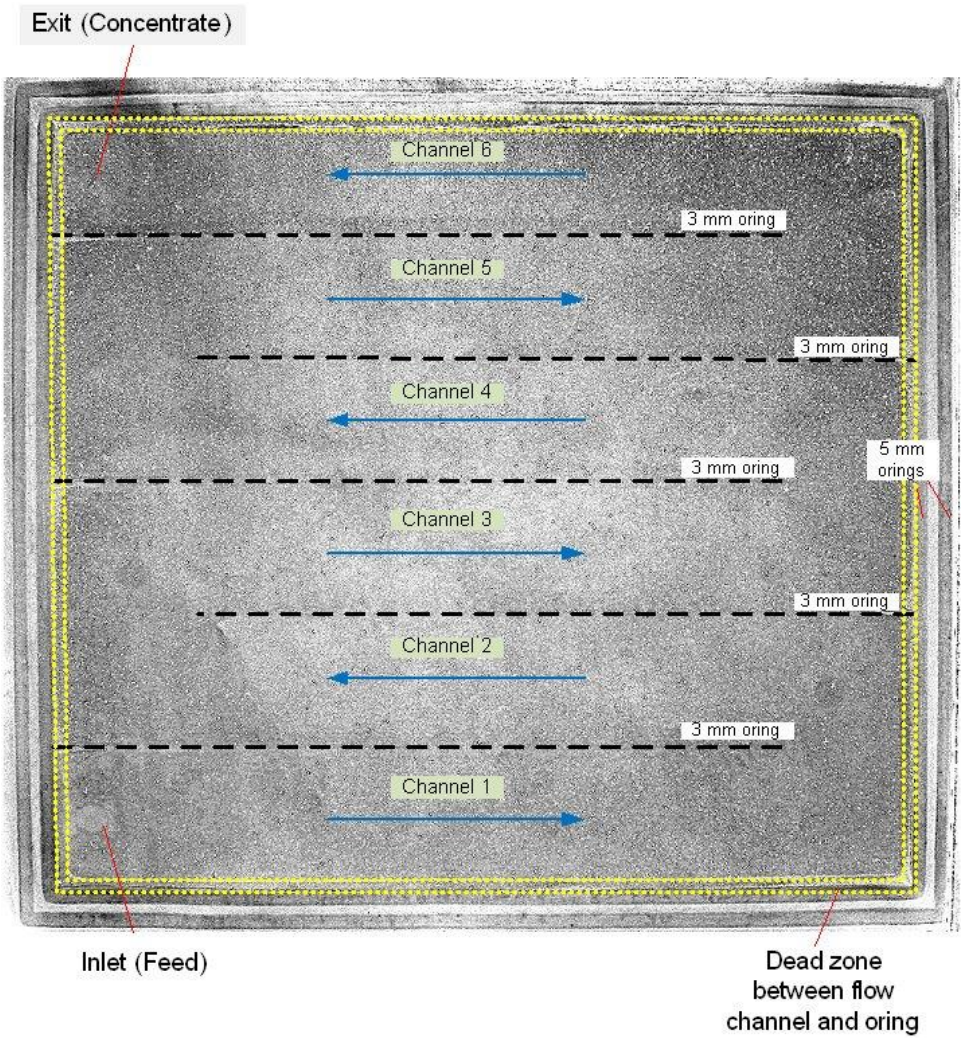

Figure 5-18 *Modified image showing surface scale coverage for a completely scaled membrane used in a baseline run, operating at 12 LMH permeate flux and 10 instantaneous recovery without permeate flushing.*

Visual inspection of scaled membranes indicated that the rate of surface scale formation increased from flow channel entrance towards the exit region, corresponding to the higher degree of supersaturation at the membrane surface. Generally, the membrane scaling would start in channel 6, migrating along each channel until scaling eventually occurred in channel 1. The 3 mm o-rings ensured that no bypassing occurred between the channels, resulting in a gradual increase in concentration. Subsequently, the level of concentration polarisation at the membrane surface as the exit region was approached increased, due to permeation through the membrane. This trend was also reported in various previous experimental studies, suggesting an increase in rate of surface crystal formation as the channel exit is approached in flat sheet cross flow membrane system (Bartman et al., 2011; Hoek et al., 2008; Matthiasson and Sivik, 1980; Rahardianto et al., 2006; Shih et al., 2005; Srinivasan and Chi, 1970). A partially scaled membrane is shown Figure 5-19, where

channel 3 was completely scaled, whereas channel 2 and 1 were essentially scale free, demonstrating that scaling first occurred in the channels closer towards the exit region. The experimental run was stopped before the membrane was completely scaled, investigating the scaling patterns on the actual membrane. Further operation of the lab-scale system in concentrate recycle mode would most certainly result in complete scaling in channel 2, eventually migrating to channel 1.

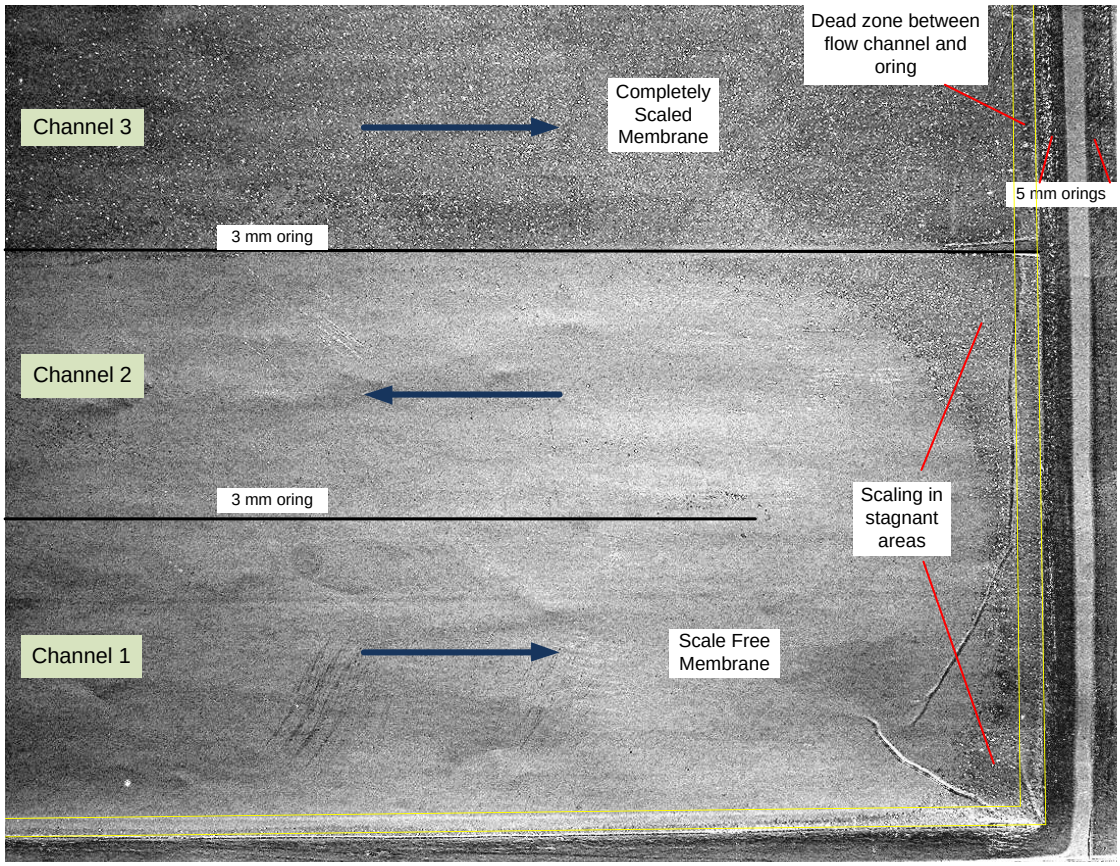

Figure 5-19 *Modified image showing how the flow profile affects the membrane scaling.*

Figure 5-19 also shows how the flow profile affected the membrane scaling, where stagnant areas had a high membrane scaling propensity. The flow path is clearly visible, flowing from channel 1 around the edge of the 3 mm o-ring towards channel 2, where cross flow velocity was high enough to prevent scaling for the certain operating conditions. Due to boundary effects, stagnant areas were present in the corners where the net flow velocity was low or zero, creating optimal conditions for crystal growth. Scale formation in the stagnant areas had a negative impact on the overall membrane scaling. Once nucleation sites are available spontaneous precipitation occurs (Klepetsanis and Koutsoukos, 1991; Liu and Nancollas, 1973).

The physical analysis showed that early membrane scaling occurred in the stagnant areas and dead zones. However, with the current scale monitoring tools it was not possible to detect this early scaling. The flux decline was detected by a drop in permeate flow rate, however operation in concentrate recycle mode caused an increase in feed osmotic pressure, thus also causing a drop in permeate flux as the feed salinity increases. This made it difficult to determine the exact onset of membrane scaling. Therefore, the total production time was used to compare different runs under varying operating conditions, comparing the total amount of time the membrane surface was exposed to a scaling solution. It is important to notice that minor scaling occurred in the dead zones and stagnant areas.

5.6.2. X-Ray Diffraction (XRD) analysis

The scaled membranes from certain experimental runs were analysed by XRD, to verify that if only calcium sulphate dihydrate scaling occurred. A random run was selected from different experiments: factorial runs (at 12, 18 and 24 LMH permeate respectively), a baseline run and one full recycle experiments with a feed SI of 0.9. The results from the XRD analysis showed that only calcium sulphate dihydrate membrane scaling occurred, as shown in Table 5-1, regardless of the operating conditions of the lab-scale system. It was expected that only calcium sulphate dihydrate scaling could occur, since it is the only stable form of calcium sulphate under 40 ˚C (Klepetsanis and Koutsoukos, 1991; Lui and Nancolass, 1970).

Table 5-1 *X-Ray Diffraction (XRD) results of surface crystals from scaled RO membranes.*

Sample		Weight Percentage (%)
Source	**Describtion**	**$CaSO_4.2H_2O$**
Scaled RO Membrane	Run 6	>99
Scaled RO Membrane	Run 13	>99
Scaled RO Membrane	Run 17	>99
Scaled RO Membrane	Baseline Run 12 LMH	>99
Scaled RO Membrane	Feed SI = 0.9	>99

5.6.3. Gypsum scale morphology

Visual inspection of the scaled membranes revealed that gypsum crystal size increased towards the flow channel exit, corresponding to the increasing concentration polarisation level (refer to Section 5.6.1). SEM imaging was used to inspect scaled membranes, to further investigate the surface scale

morphology. The image sequence in Figure 5-20 shows the progressive development of gypsum crystals from the flow channel entry to exit region, demonstrating how crystal surface coverage increases. Image ***a)*** shows the early rod-like structures that transformed into thin needles/platelets type structures shown in image ***b)***. Further scaling eventually caused formation of partial or complete rosettes as shown in image ***c)***. The scale free membrane area was progressively decreasing due to the growth of the rosette structures, until the completely developed rosettes overlap, covering the entire membrane surface as shown in image ***d)***. The images ***a), b), c)*** and ***d)*** correspond to positions in the centre of channel 1, 3, 5 and 6 respectively, approximately half ways the channel length in the flow direction, since the flow field is more uniform in the central region. These results compare well with previous studies where an increase in crystals size along the flow channel and the development of complete rosettes were reported (Gilron and Hasson, 1987; Rahardianto et al., 2006; Shih et al., 2005).

During an experimental run the lab-scale system was operated until constant permeate flux operation was not possible, even if the feed pressure was increased significantly. Previous studies have shown the direct linear correlation between percentage surface scale coverage and flux decline (Borden et al., 1987; Brusilovsky and Borden, 1992; Rahardianto et al., 2006; Shih et al., 2005). This suggested that most of the membrane was covered with crystals, mostly developed rosettes, since the scale free area did not allow sufficient permeation for constant flux operation. Once the flux decline occurred, the net permeate flow rate decreases drastically, however it never reached zero. Rahardianto et al. (2005) suggested that only the base of the crystal rosettes is in contact with the membrane surface, thus allowing a certain amount of permeation through the interstitial spaces between the rosette arms, even if the fully developed roses overlap. Further investigation on the effect surface crystal morphologies on permeate flux decline was beyond the scope of the present study.

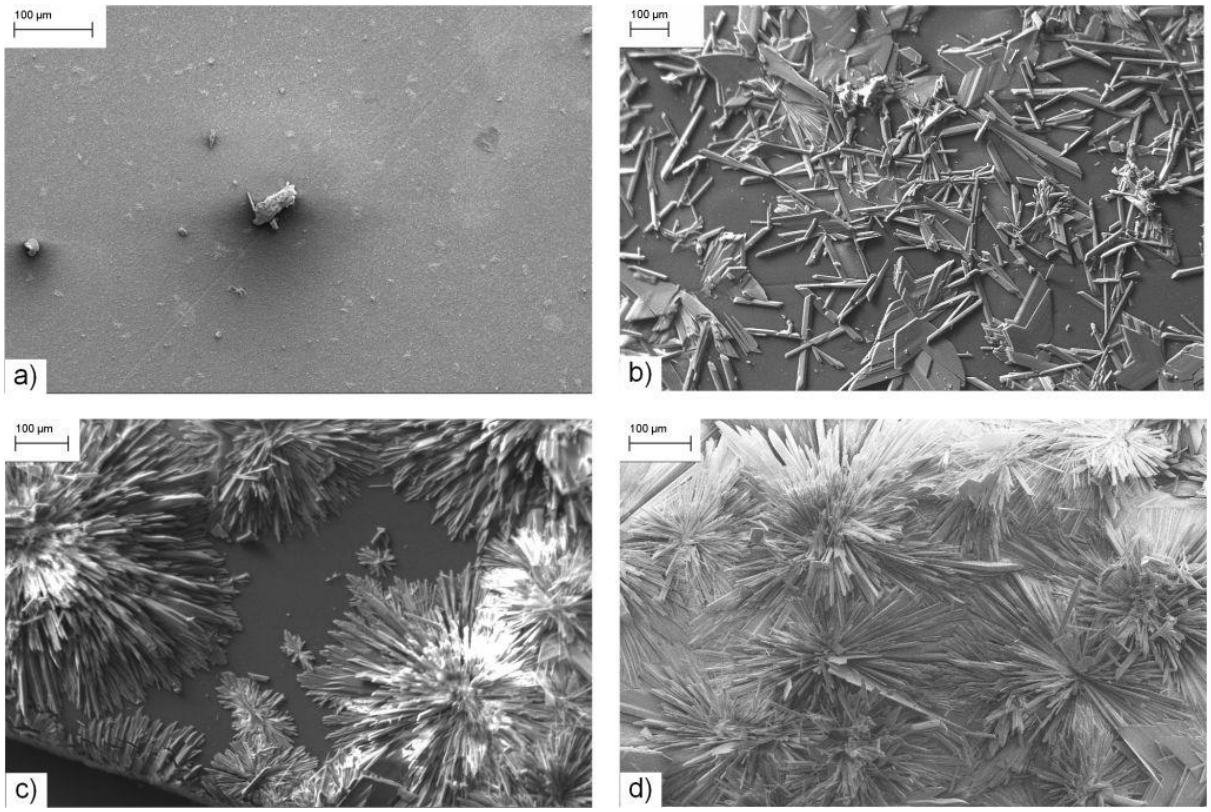

Figure 5-20 *SEM images of scaled RO membranes a) to d) showing the development of gypsum crystals along the tortuous flow path from channel entrance region towards the exit region.*

5.7. Summary

In this chapter the initial evaluation of the permeate flushing and intermediate concentrate precipitation showed the potential to operate the lab-scale system at higher overall recoveries. The initial results are summarised below:

- In the batch experiments it was established that a retention time of about 120 min was adequate to reduce the gypsum saturation index from about 1.6 to 1.1 at a temperature of 15 ° C and seeding gypsum at 2 g/L. These results were used to size the gypsum precipitation reactors in the lab-scale system, operating at the same gypsum seeding rate.
- The permeate flushing technique was effective to prevent membrane scaling for 24 hours. The lab-scale system was operated in full recycle mode for 24 hours with an feed SI equal to 0.9 at 12, 6 and 2.4 h^{-1} flushing frequencies respectively. In theory the unit should be able to operate for longer than 24 hours in full recycle mode where permeate and concentrate are recycled back to the feed tank. After the 24 hours, the RO unit was operated without flushing and a flux decline due to scaling occurred within 2-3 hours.

- The preliminary tests indicated that the gypsum precipitation reactor in the lab-scale system worked effectively, where the reactor overflow typically had a SI of 1.1 - 1.15. On average the calcium and sulphate concentrations dropped by 104 ± 9 mg/L and 201 ± 27 mg/L respectively, which was in stoichiometric proportion indicating that only calcium sulphate precipitation occurred.
- Measuring the permeate flux decline, specific conductivity and calcium concentration throughout an experimental run, proved to be effective to determine the total production time. From this point onwards, it was not possible to maintain constant permeate flux, even after a significant increase in feed pressure, indicating severely scaled membrane due to physical membrane blockage.
- The baseline experiments confirmed the strong effect of permeate flux and instantaneous recovery had on membrane scaling. Generally, the higher the flux and instantaneous recovery, the faster the rate of scaling. Lower cross flow velocities and higher degrees of concentration polarisation at the membrane surface increased the risk of membrane scaling.
- For all baseline (non-flushing, non-seeding) experimental replicates an average error margin of 8.2 % for effective membrane permeability, 2.6 % for conductivity and 2.1 % for calcium concentrations was obtained. Similarly, an average error margin of 7.7 % for effective membrane permeability, 1.2 % for conductivity and 0.8 % for calcium concentrations was obtained for all seeding and flushing experimental replicates. Theses margins of error were considered to be acceptable.

In this chapter the analytical methods and the experimental methods were verified showing that the lab-scale RO desalination unit can produce reliable and repeatable data. Initially the lab-scale system was commissioned, independently demonstrating that the flushing technique is effective to prevent membrane scaling with an undersaturated feed solution (SI = 0.9). This shows that the seeded gypsum precipitation in the reactors effectively reduced the scaling potential of the RO concentrate reducing the SI to 1.1-1.2. in the reactor effluent. Further, it was demonstrated that experiments were repeatable with low error margins between replicate. The main results and discussion are given in the following chapter.

Chapter 6 - Results and Discussion

In this chapter the results from the factorial design are presented and discussed, where the effect of each factor on effective permeation production time and permeate production index is presented. All experimental runs were performed in concentrate recycle mode.

6.1. Typical flushing and seeding experimental run

6.1.1. Raw and processed data

In this study numerous experimental runs were performed, testing the permeate flushing technique under various operating conditions, thus large amounts of data were collected. In this section, typical data from one randomly selected factorial experiment are discussed. After this section, only the main results will be discussed in this section, whereas all the raw and processed data are given in Appendix C.

The data for one factorial design experiment is given in Table 6-1, illustrating the type of data that was collected after every experiment. Pressure, specific conductivity, temperature and flow rates for the concentrate, permeate and feed streams were recorded throughout an experimental run. These were used to calculate the salt rejection, instantaneous recovery and permeate flux, based on the measured raw data. A theoretical correlation was used to calculate the TDS in mg/L based on the measured conductivity, where 1 mS/cm is approximately equal to 640 mg/L TDS (Walton, 1989), suitable for brackish water ranging between 2-20 mS/cm. The osmotic pressure for each stream was worked out using an empirical correlation, where a 1000 mg/L TDS is approximately equivalent to 0.76 bar osmotic pressure (El-Dessouky and Ettouney, 2002). The respective measured and osmotic pressures were used to calculate the effective membrane permeability according to Equation 3.2. Further, the overall recovery was worked out according to the cumulative permeate volume, collected from the elevated permeate tank overflow. Calcium concentrations were determined by AAS, as described in section 3.2.2. The last section in Table 6-1 gives the theoretical and experimental permeate production rate, where the theoretical values were calculated with Equation 4.3 and 4.4 respectively.

Table 6-1 *Typical set of raw and processed data recorded for a flushing and gypsum seeding run*

Run 13	Flush Freq (h^{-1})	Flush Vol (mL)	Soak time (sec)	Flux (LMH)	Inst. Rec. (%)
	2.4	35	90	24	30

Operating Time (min)		0	30	60	90	120	150	180
Production Time (min)		0	28	55	83	110	138	165
Gauge Pressure (bar)	Feed	11.5	11.5	11.6	11.8	12.3	14.5	21.4
	Concentrate	10.7	10.8	10.8	11.0	11.5	13.7	20.5
	Permeate	1.1	1.1	1.1	1.1	1.1	1.1	1.1
Spcific Conductivity (mS/cm)	Feed	7.58	8.47	8.87	9.06	9.54	10.27	10.23
	Concentrate	8.34	9.49	9.76	10.33	10.68	11.40	11.76
	Permeate	-	0.845	0.896	0.902	0.921	0.954	0.965
Temperature (˚C)	Feed	13.6	13.9	14.3	14.7	14.4	14.9	14.7
	Concentrate	14.4	14.9	15.2	15.2	15.6	15.8	16.0
	Permeate	-	14.3	14.5	14.8	14.9	14.9	14.8
Flow rate (L/h)	Concentrate	6.00	5.95	6.00	6.00	6.00	6.05	6.00
	Permeate	2.55	2.55	2.55	2.55	2.55	2.55	2.15
	Feed	8.55	8.50	8.55	8.55	8.55	8.60	8.15
Salt Rejection (%)		NA	90.0	89.9	90.0	90.3	90.7	90.6
Inst. Recovery (%)		29.8	30.0	29.8	29.8	29.8	29.7	26.4
Permeate Flux (LMH)		24.1	24.1	24.1	24.1	24.1	24.1	20.3
Osmotic Pressure (bar)	Feed	3.69	4.12	4.31	4.40	4.64	4.99	4.97
	Concentrate	4.05	4.61	4.74	5.02	5.19	5.54	5.72
	Permeate	-	0.41	0.44	0.44	0.45	0.46	0.47
TMP (bar)		-	6.69	6.62	6.73	7.01	8.87	15.80
Lp (L/m².h.bar)		-	3.59	3.63	3.57	3.43	2.71	1.28
Lp (25°C) (L/m².h.bar)		-	5.18	5.17	5.05	4.84	3.78	1.79
Permeate Recovered (mL)		-	990	910	870	860	880	520
Overall Recovery (%)		0	10	19	28	36	45	50
Concentration Factor		-	1.1	1.2	1.3	1.5	1.7	1.9
Ca+ Conc. (mg/L)	Concentrate	941	965	979	1008	1030	1043	1044
	Overflow Sed. Tank	857	877	888	902	911	943	969
	Feed	848	864	869	892	920	938	958

Pemeate Flushing	Total time	180	min
	Time / Flush Cycle	1636	sec
	Total Flushes	7	
	Flushing Time	9	sec
	Flushing Flowrate	14	L/h
	Total Flushing Volume	0.23	L
	Total Feed	10.0	L
	Total Permeate	5.0	L
PPR (L/h)	Calculated	1.85	L/h
	Measured	1.90	L/h
PPI	Calculated	0.73	
	Measured	0.75	

6.1.2. Total production time

Calcium sulphate membrane scaling was investigated by comparing the total production time of each specific run to determine which factors effectively prevent/reduce membrane scaling. In this section the method to determine the total production time for one factorial run is described, based on the experimental data given in Table 6-1. The theoretical background was discussed in section 4.1.

The lab-scale unit was operated at steady state conditions, maintaining a specific permeate flux and instantaneous recovery as shown in Figure 6-1. It was essential to adjust the feed and concentrate needle valves throughout an experiment, in order to maintain a constant driving force for the RO desalination due to the increasing osmotic pressure. A constant flux could not be maintained after roughly 120 minutes, where a flux decline was observed, even after the feed pressure was increased significantly. This indicated a severely scaled membrane due to the increased hydraulic resistance from the calcium sulphate dihydrate layer at the membrane surface (Borden et al., 1987). This trend is also reflected in the trans-membrane pressure, which increases steadily throughout the experiment, followed by a rapid increase which occurred due to the membrane scaling after roughly 120 minutes. Correspondingly, the instantaneous recovery also dropped slightly. The experiment was terminated at this point, since the constant flux could not be maintained, indicating a total production time for the specific run as 120 minutes.

Further, the salt rejection stayed constant at about 90 % throughout the experiment, evident in Figure 6-1. However, this was significantly lower than the *Dow Filmtec XLE 2540* spiral membrane specification, with a stabilised salt rejection of 99.0 % for a 500 ppm NaCl solution at 15% recovery (DOW Filmtec, 2011). The feed solution during for experimental runs was much higher than 500 ppm, typically >5000 mg/L TDS for most experiments. Therefore, one would expect much lower salt rejections for the flat sheet membrane system while operating with high scaling feed solutions.

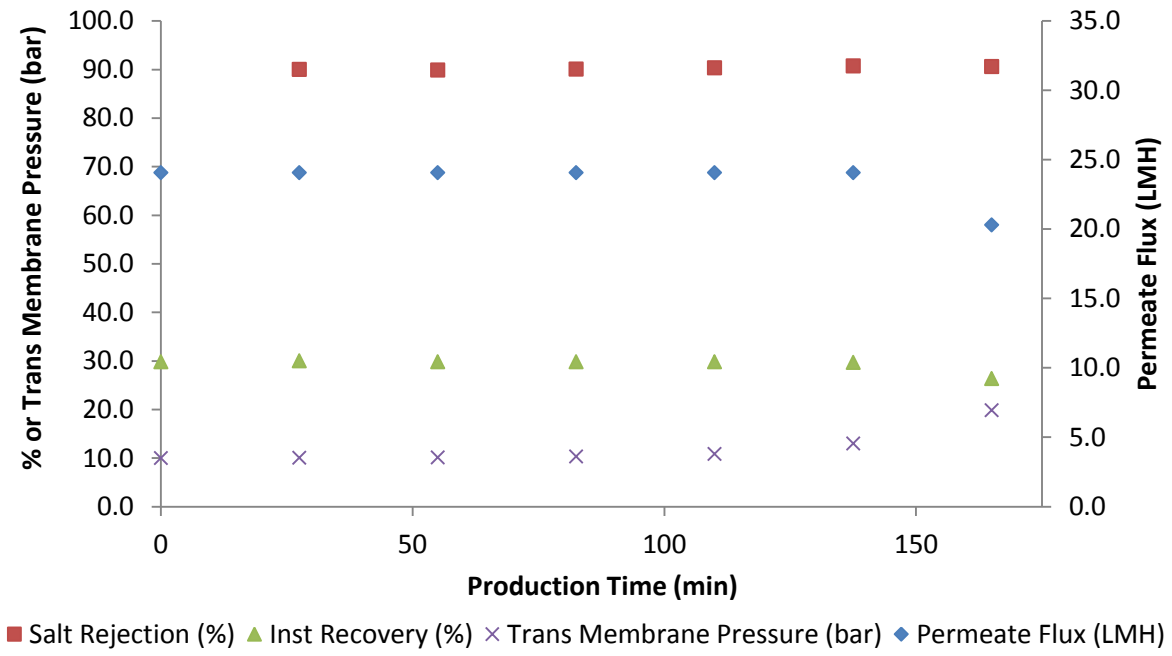

Figure 6-1 *Typical trends observed during permeate flushing and seeded gypsum precipitation experimental runs.*

A constant salt rejection resulted in constant permeate conductivities, as shown in Figure 6-2. A slight drop in permeate conductivity was observed, corresponding to the very gradual increase in salt rejection. The concentrate conductivity was 0.77-1.53 mS/cm higher than the feed conductivity, corresponding to a 500-980 mg/L TDS increase with an instantaneous concentration factor of about 1.1. Both feed and concentrate conductivity increased exponentially up to roughly 120 minutes, followed by a drop in conductivity to below values below the thermodynamically predicted conductivity. This levelling out/drop was caused by a reduction in calcium and sulphate concentration, indicating severe gypsum scaling via surface crystallisation.

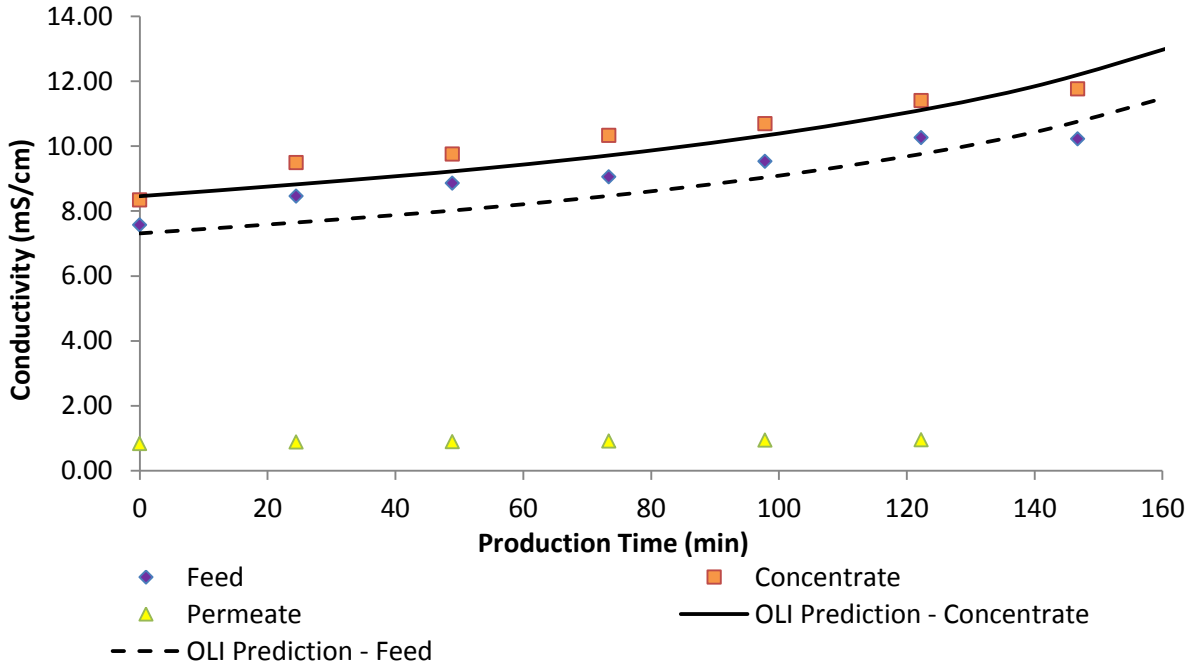

Figure 6-2 *Specific conductivity measurements for a typical permeate flushing and seeded gypsum precipitation experimental run.*

This trend was also observed by the drop in RO concentrate calcium concentrations, as seen in Figure 6-3, deviating from the thermodynamically predicted value after roughly 120 minutes and indicating severe membrane scaling. All concentrations increased steadily as the production time increased, although saturation indexes remained approximately constant, due to the higher solubility of calcium and sulphate ions with increasing ionic strength. As expected, the RO concentrate was supersaturated with a SI of ± 1.3, whereas the reactor overflow and feed were only slightly saturated with a SI of ± 1.1. These results compare well to Rahardianto et al. (2010) and McCool et al. (2013), where the concentrate saturation index was reduced to 1.1 and 1.15 respectively, after seeded gypsum precipitation for similar initial supersaturation levels.

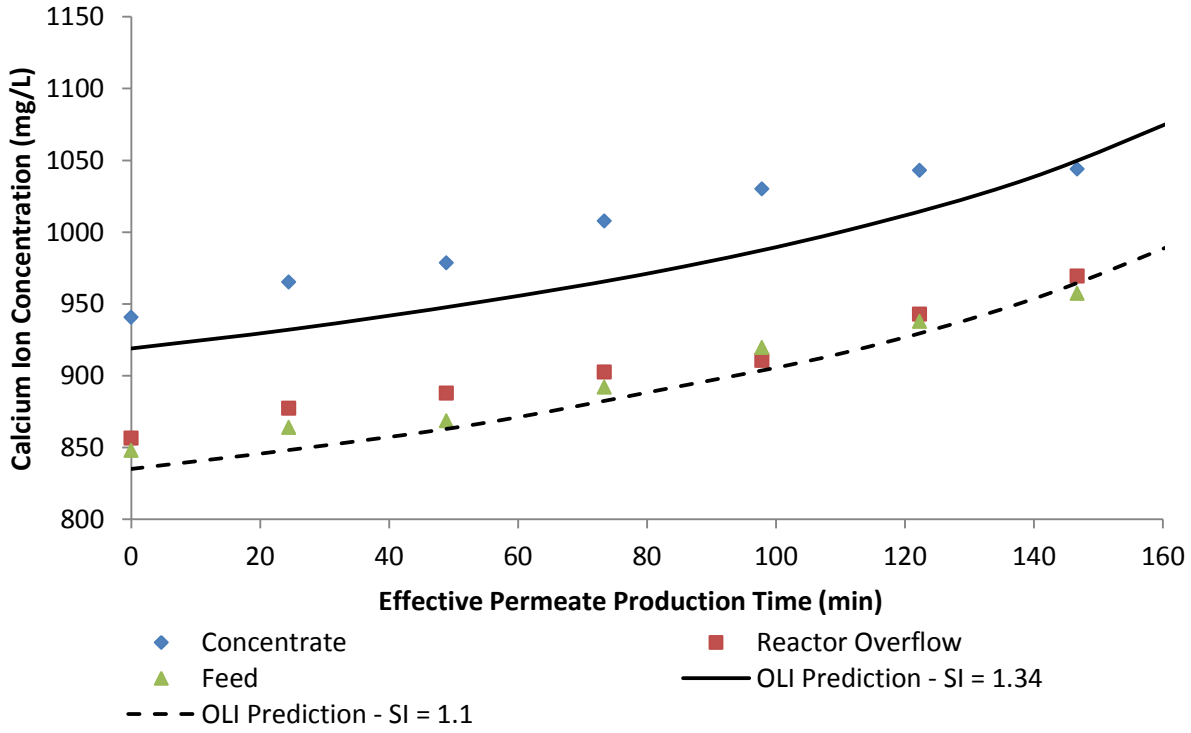

Figure 6-3 *Calcium concentrations for a typical permeate flushing and seeded gypsum precipitation experimental run, also showing the predicted equilibrium calcium concentration for the specific operation conditions.*

By comparing the permeate flux, conductivity and calcium concentration trends in Figure 6-1 to Figure 6-3 respectively, a clear trend can be identified. A drop in all three parameters occurred after roughly 120 minutes into the experimental run. Based on those observations, the total effective production time was about 125 minutes during which the membrane was exposed to a scaling solution. This value indicated the upper limit, where the membrane scaling became too severe, making it impossible to operate the unit under constant flux thereafter.

It is important to note that it was impossible to determine the total production time hundred percent accurately, since operating data were recorded manually in certain intervals. Surely more data points during each run would be beneficial to determine the total production time for each run; however an electronic data logging system was beyond scope of the project. Generally overlapping trends were observed in all three parameters and the value was determined graphically by comparing the respective graphs, as explained in this section. For the purpose of this study this accuracy was adequate to determine which operating conditions resulted in the highest total production time until a flux decline was observed.

6.2. Statistical analysis of factorial design experiments

All 16 experimental runs were successfully completed, testing the various factors at the high and low levels. The repeatability of the experimental technique was demonstrated (refer to section 5.5) by performing centre run in triplicate. In this section only the significant results for each run are presented and discussed, while all the experimental raw and processed data are given in Appendix B. It was crucial to determine the total production time and the permeate production rate for each run, as this would ultimately be used to determine the effectiveness of certain operating conditions for a specific run, as shown in Table 6-2.

Table 6-2 *Results summary for the 16 factorial experiments plus 3 centre runs, showing the total production time, permeate production rate (PPR) and permeate productivity index (PPI).*

Run	Flushing Frequency (h^{-1})	Flushing Volume (mL/flush)	Soak Time (sec/flush)	Permeate Flux (LMH)	Inst. Recovery (%)	Total Prod. Time (min)	Net Permeate Prod. (L)	PPR (L/h)	PPI
1	6.0	35	20	12	30	527	8.5	0.96	0.76
2	2.4	35	20	12	10	431	7.7	1.07	0.84
3	6.0	70	20	12	10	720	9.7	0.81	0.64
4	2.4	70	20	12	30	429	7.7	1.08	0.85
5	6.0	35	90	12	10	587	8.4	0.86	0.68
6	2.4	35	90	12	30	413	7.6	1.10	0.86
7	6.0	70	90	12	30	580	8.6	0.89	0.70
8	2.4	70	90	12	10	492	7.8	0.95	0.75
9	6.0	35	20	24	10	108	3.7	2.08	0.82
10	2.4	35	20	24	30	86	3.5	2.44	0.96
11	6.0	70	20	24	30	107	3.4	1.90	0.75
12	2.4	70	20	24	10	114	4.2	2.20	0.86
13	6.0	35	90	24	30	122	3.9	1.90	0.75
14	2.4	35	90	24	10	83	3.3	2.35	0.92
15	6.0	70	90	24	10	145	4.2	1.75	0.69
16	2.4	70	90	24	30	82	3.0	2.19	0.86
17	3.4	52.5	55	18	20	206	5.2	1.52	0.80
18	3.4	52.5	55	18	20	204	5.3	1.56	0.82
19	3.4	52.5	55	18	20	205	5.4	1.59	0.83

A two way analysis of variance (ANOVA) test was performed with *Statistica 11.0* software, with the data from Table 6-2, where total production time and permeate production rate were the independent variables. A two way ANOVA tests the effect of multiple independent factors on one dependent variable, testing the main effect of each factor and also if there is any significant interaction between two independent factors (Montgomery et al., 1998).

The factorial design experiments and the ANOVA results were used to determine which factors affect membrane scaling the most. Therefore, the *p-values* from each ANOVA were used to compare the statistical significance of each factor. The p-value indicates the probability that a factor or an interaction of two factors has a significant influence on the dependant variable. The null hypothesis is rejected if the p-value is larger than a certain value which is based on a certain confidence level (Montgomery et al., 1998). In this study the null hypothesis indicated that a factor or an interaction of factors had no effect on the dependant variable. The typical confidence interval of 95% was chosen, thus any p-value lower than 0.05 resulted in the rejection of the null hypothesis i.e. the factor had no significant influence on membrane scaling. However, it is very important to notice that this was only true within the studied range of values for each factor. If a factor had a p-value larger than 0.05, it did not automatically mean that a certain factor had no effect on the dependant variable. This could imply the following: the factor had no effect on the dependent variable because other factors had a larger influence on the dependent variable, thus masking the influence of the factor insignificant. Alternatively, it simply meant that a factor had an insignificant statistical influence on the dependent variable within the studied range of conditions.

The p-values are presented in Figure 6-4, showing which factors had a significant effect on membrane scaling within the experimental range of conditions, whereas the complete ANOVA results are given in Appendix D. The statistical analysis indicated that flushing frequency, permeate flux and instantaneous recovery have a significant effect on the total production time (i.e. membrane scaling prevention: the longer the total production time, the more effective the membrane scaling was prevented), whereas soaking time and flushing volume had an insignificant effect. Further, the statistical analysis showed that only instantaneous recovery had no effect on the permeate production rate, whereas all the other factors were significant.

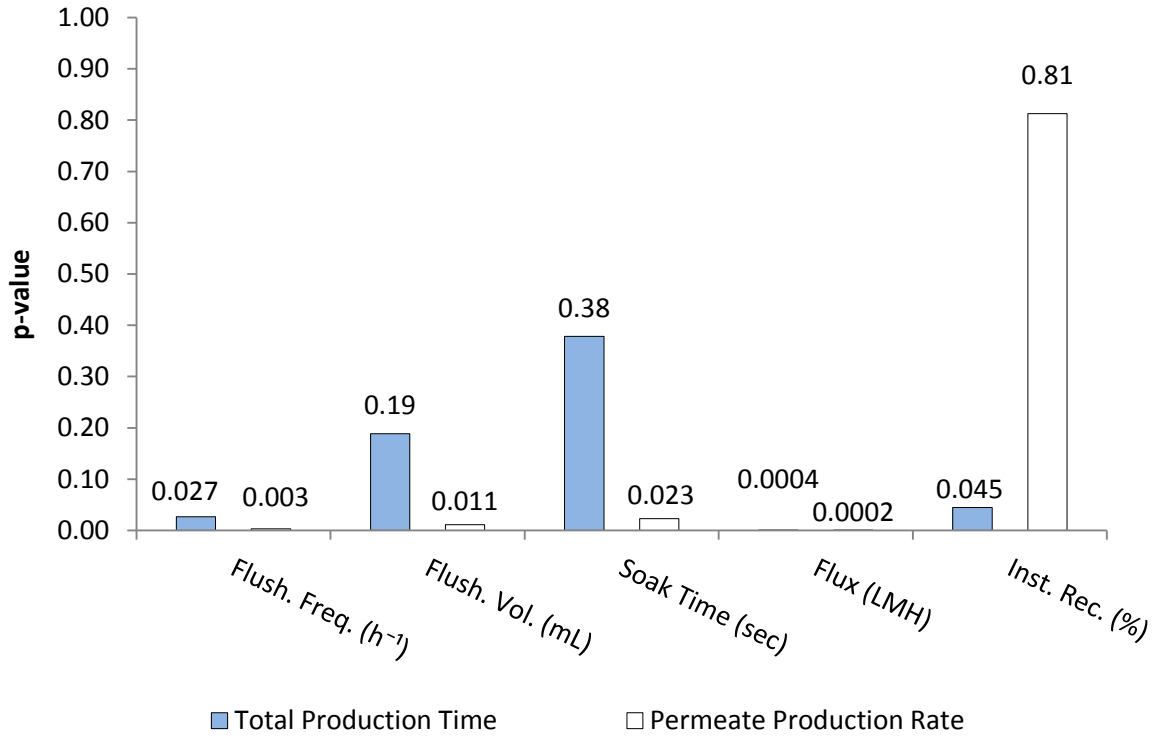

Figure 6-4 *Comparison of p-values with total production time and permeate production rate as dependent variables.*

Permeate flux had the most profound effect on membrane scaling, as indicated by the very low p-values in Figure 6-4, with values of 0.0004 and 0.0002 for total production time and permeate production rate respectively. In other words, the chance that the effect was caused randomly was only 0.04 or 0.02 % respectively, which is highly unlikely.

It is very important to note that these statistical results are only applicable to the specific factorial design, within the respective low and high values for each factor. Changing the limits of the factorial design could result in completely different statistical results. However, for the purpose of this study the factorial design experiment was very useful to identify which factors have a significant effect on membrane scaling and clear trends were identified.

In this section only the main results from the statistical analysis are presented. A more detailed discussion of how each factor influences calcium sulphate membrane scaling is given in the subsequent sections.

6.3. Membrane scaling evaluation: total production time

The primary objective of the factorial run experiments was to determine which operating conditions will result in the longest total production time i.e. the longer the total production time, the longer the scale free operation. The total production time was primarily influenced by permeate flux, flushing frequency and instantaneous recovery, as identified in Figure 6-4.

Permeate flux was identified as the most significant factor, as it can be seen in Figure 6-5, indicating that an increased permeate flux resulted in a lower total production time. Further, increasing the flushing frequency increased the total production time. This was especially evident at lower permeate fluxes; however this effect was less significant. The surface plot suggests that further increasing the flushing frequency and permeate flux will result in even higher total production times, implicating longer scale free operation.

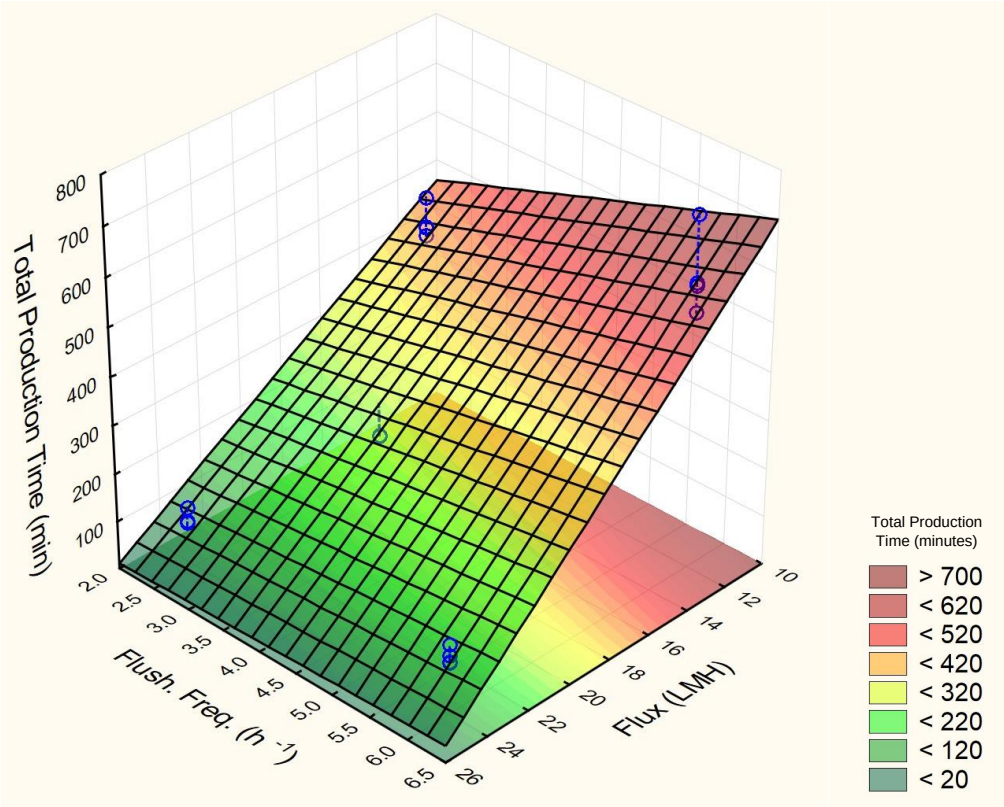

Figure 6-5 *Surface plot showing the effect of permeate flux and flushing frequency on total production time.*

Figure 6-6 shows the effect of permeate flux and instantaneous recovery has on total production time. Again, the strong influence of permeate flux is visible, since a steep increase in total production time occurs if the permeate flux was lowered from 24 LMH to 12 LMH. Furthermore, a

decrease in instantaneous recovery resulted in a slight increase in total production time although this effect was less profound. The effect of the both factors resulted in a linear surface plot, predicting total production times of about 700 minutes if the if the permeate flux and instantaneous recovery were lowered below, 12 LMH and 10 % respectively.

A more detailed discussion of each factor is given in the subsequent sections, where selected experimental results are given and discussed. In each subsection two experimental runs are compared were the specific factor was low and high respectively, while the other factors were constant to isolate the effect of the factor. The experimental data was also compared to the non-flushing, non-seeding baseline data.

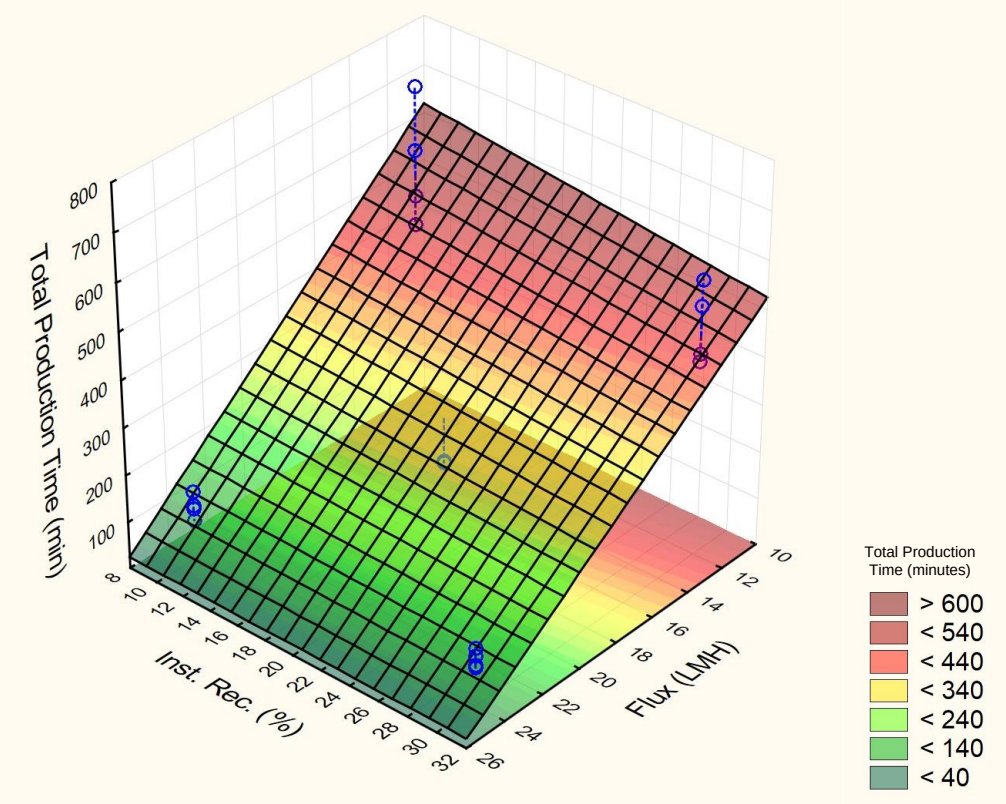

Figure 6-6 *Surface plot showing the effect of permeate flux and instantaneous recovery on total production time.*

6.3.1. The effect of permeate flux

In this section the results for Run 3 and 15 are compared, isolating the effect of permeate flux on total production time, since the other factors were constant in both runs, while the flux was 12 and 24 LMH respectively. Instantaneous recovery directly influences cross flow velocities if the permeate

flux stayed constant, thus the effect of cross flow velocities on membrane scaling are also discussed in this section.

The effective membrane permeability decline (i.e. permeate flux per bar of feed pressure) was useful to compare the rate of scaling for different experimental runs. In Figure 6-7 the effective membrane permeability for Run 3 and 15 is given, comparing it to the baseline data at the same permeate fluxs. Operating the lab-scale unit at 12 LMH permeate flux, significantly increased the total production time until the membrane was completely scaled. At 12 LMH the total production time was 720 minutes, and only 145 minutes at 24 LMH, indicating the strong correlation between permeate flux and total production time. Further, the flushing technique effectively prolonged the total production time. Scaling occurred relatively fast in the baseline experiments, especially at the lower flux where the flushing technique increased the total production time by approximately 480 minutes. In Run 3, 9.7 L of permeate was produced in 720 minutes of operating time, while only 4.23 L was produced in 145 minutes in Run 15. This showed that lower fluxes are beneficial to produce more permeate, at the expense of longer operating times.

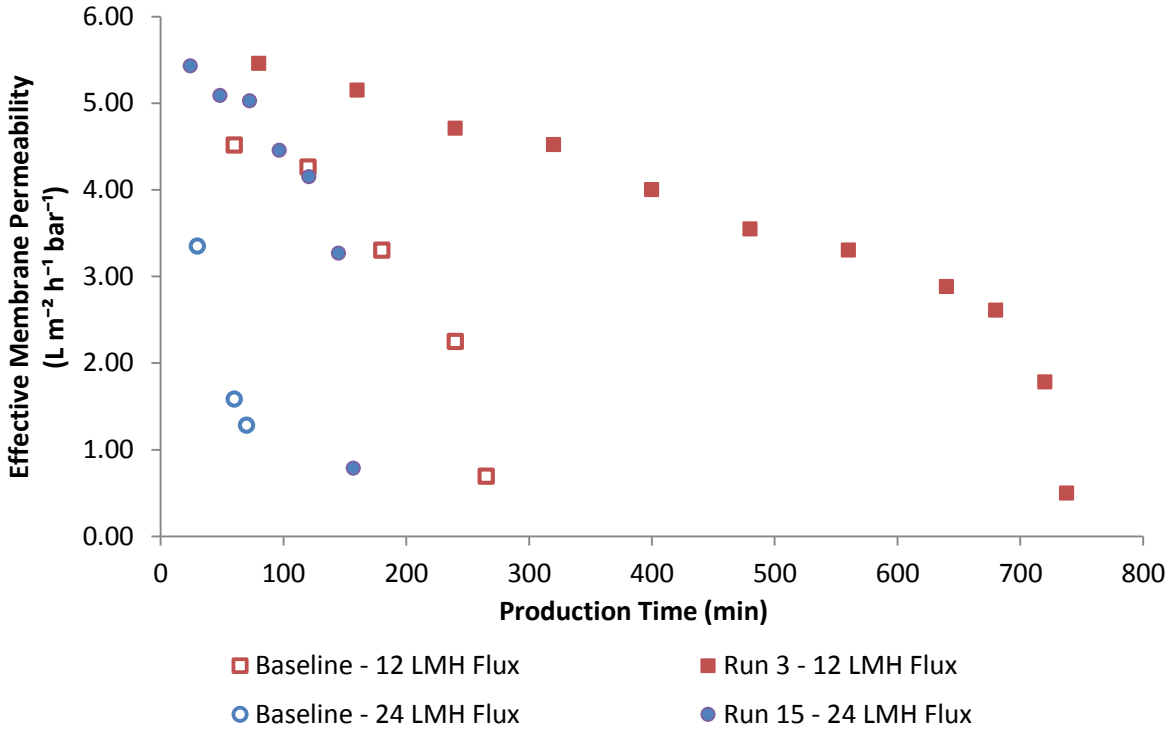

Figure 6-7 *The effect of permeate flux on effective membrane permeability for Run 3 and 15, at 12 and 24 LMH respectively, while the other factors are the same for both runs. The baseline data refer to the non-flushing and non-seeding experiments.*

The effect of permeate flux on conductivity is shown in Figure 6-8. Initially all conductivities increased approximately linearly, until a conductivity drop was observed for the baseline runs and Run 15 within 240 minutes or less. The conductivity in Run 3 continued to rise exponentially until the end of the experiment and no drop in conductivity was observed. At higher recoveries the overall concentration factor increased significantly, hence the drop in calcium and sulphate concentrations due to membrane scaling were negligible and not detectable. Nonetheless, it was evident that 12 LMH permeate flux was beneficial to extend the total production time i.e. to produce more permeate.

Similar trends were observed for the concentrate calcium concentrations, shown in Figure 6-9. In the baseline experiments the calcium concentrations rose steeply and complete membrane scaling occurred within 240 and 60 minutes at permeate fluxes of 24 and 12 LMH respectively. The calcium concentrations exceeded 1000 mg/L very quickly, resulting in gypsum saturation indexes of up to 2.6 in the RO concentrate. With antiscalants, RO plants can operate up to scaling indexes of 4 (Pomerantz et al., 2006), hence the rapid scaling in the baseline experiments was not surprising since no antiscalants were used and the saturation indexes greatly surpassed 1.0. Furthermore, complete membrane scaling occurred at 145 and 720 minutes for the flushing experiments, while the calcium concentration only increased gradually since the saturation index stayed constant due to the intermediate concentrate desupersaturation.

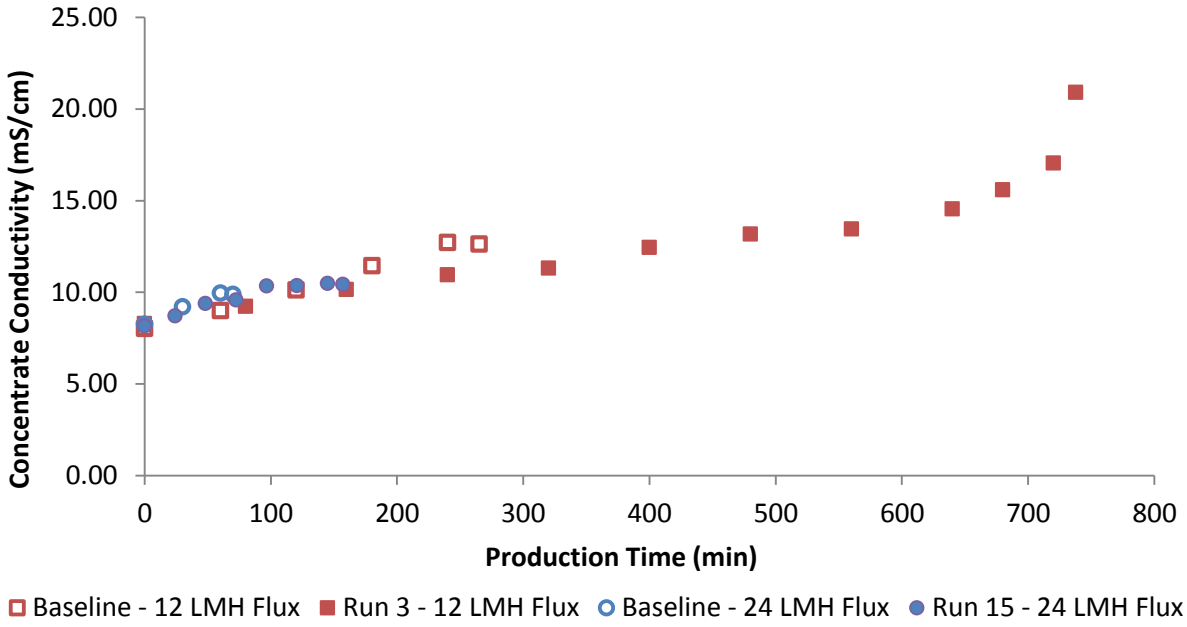

Figure 6-8 *The effect of permeate flux on concentrate specific conductivity for Run 3 and 15, at 12 and 24 LMH respectively, while the other factors are the same for both runs. The baseline data refer to the non-flushing and non-seeding experiments.*

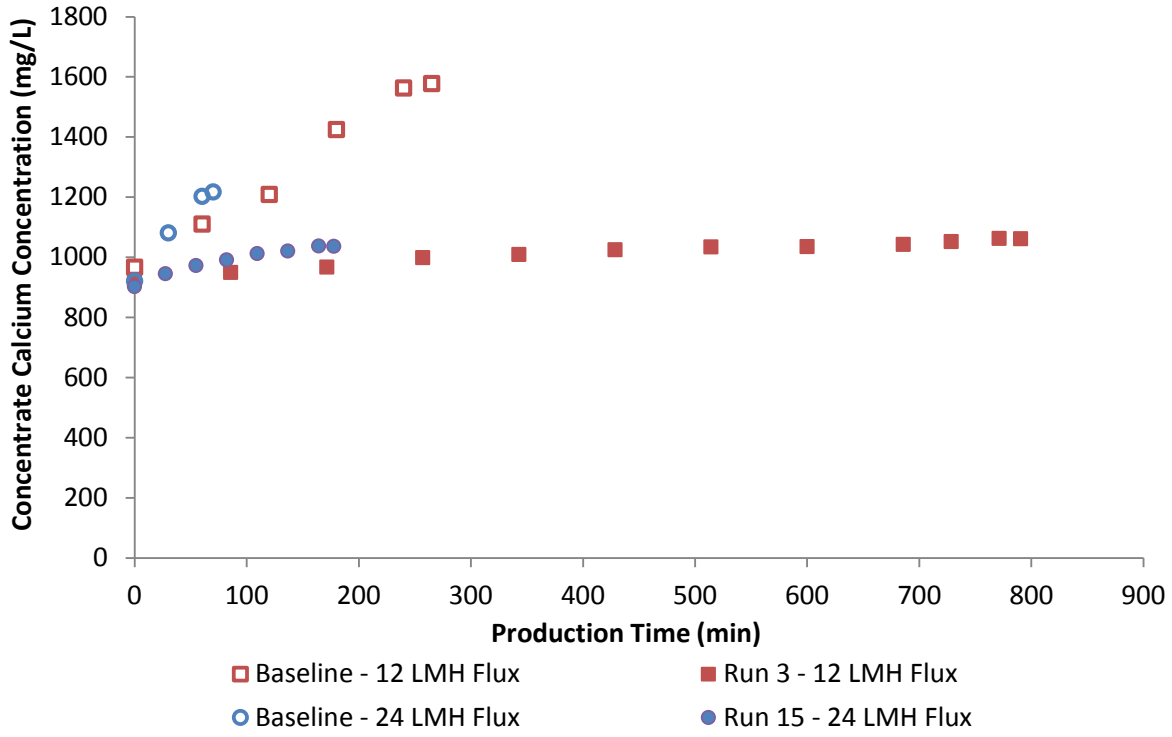

Figure 6-9 *The effect of permeate flux on concentrate calcium concentration for Run 3 and 15, at 12 and 24 LMH respectively, while the other factors are the same for both runs. The baseline data refer to the non-flushing and non-seeding experiments.*

The experiments have shown that permeate flux had a significant influence on membrane scaling, evident in Figure 6-7 to Figure 6-9. A higher permeate flux resulted in higher levels of concentration polarisation at the membrane surface increasing the membrane scaling propensity (Bartman et al., 2011; Gabelich et al., 2007; Oh et al., 2009; Pomerantz et al., 2006; Shih et al., 2004). It is beneficial to operate the lab-scale system at 12 LMH flux, to extend the total production time, although it drastically reduces the permeate production rate. Further permeate flux reduction should theoretically result in longer total production times (i.e. scale free operation), at the expense of further reduced permeate production rates (refer to section 6.4. for more detailed discussions how PPR affects membrane scaling).

6.3.2. The effect of flushing frequency

In this section the results for Run 5 and 2 are compared, isolating the effect of flushing frequency on total production time, since the other factors were constant in both runs while the flushing frequency was 6 and 2.4 h^{-1} respectively.

The effective membrane permeabilities for Run 5 and 2 were shown in Figure 6-10, as well as the permeability for the baseline runs under similar conditions without permeate flushing. Increasing the flushing frequency from 2.4 to 6 h^{-1} prolonged the total production time from about 430 to 590 minutes. Complete membrane scaling occurred within 240 minutes in the baseline experiment. In both cases membrane scaling was not completely prevented, the onset of severe scaling was merely delayed. However, more frequent flushing was beneficial to extend the total operation time until a flux decline was observed, at the expense of a lower permeate production rate. For Run 5 the PPR was 0.86 L/h, while it was 1.07 L/h for Run 2. Correspondingly, the net permeate production was 8.4 L and 7.7 L respectively, indicating that higher flushing frequencies were beneficial to produce slightly more permeate.

The concentrate conductivity measurements showed similar trends. Longer total production times whilst flushing 6 times per hour were observed, as seen in Figure 6-11, compared to flushing 2.4 times per hour. Similar trends were observed for the concentrate calcium concentration, as shown in Figure 6-12, comparing well to the observed conductivity trends. In the baseline run the calcium concentration initially increased steeply, until a drop was observed after 240 minutes. More frequent flushing at 6 h^{-1} resulted in slightly longer total production times, as indicted by the conductivity measurements.

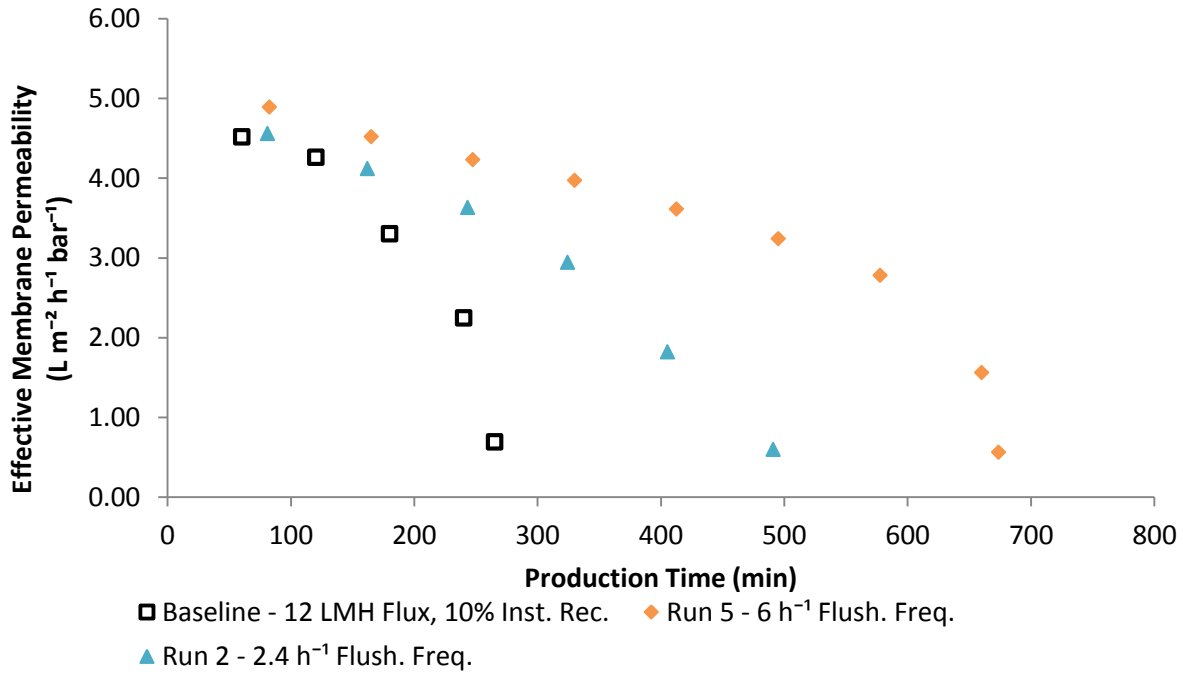

Figure 6-10 *The effect of flushing frequency on effective membrane permeability for Run 5 and 2, at 6 and 2.4 h^{-1} respectively, while the other factors were the same for both runs. The baseline data refer to the non-flushing and non-seeding experiments.*

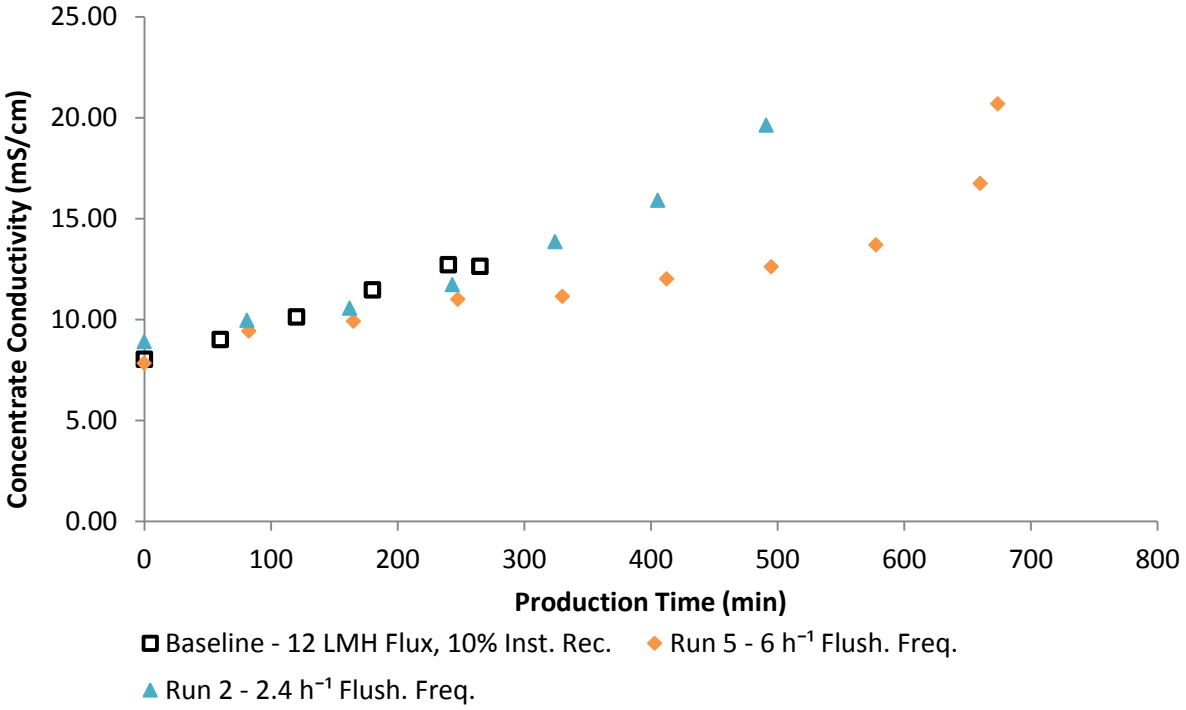

Figure 6-11 *The effect of flushing frequency on concentrate specific conductivity for Run 5 and 2, at 6 and 2.4 h^{-1} respectively, while the other factors were the same for both runs. The baseline data refer to the non-flushing and non-seeding experiments.*

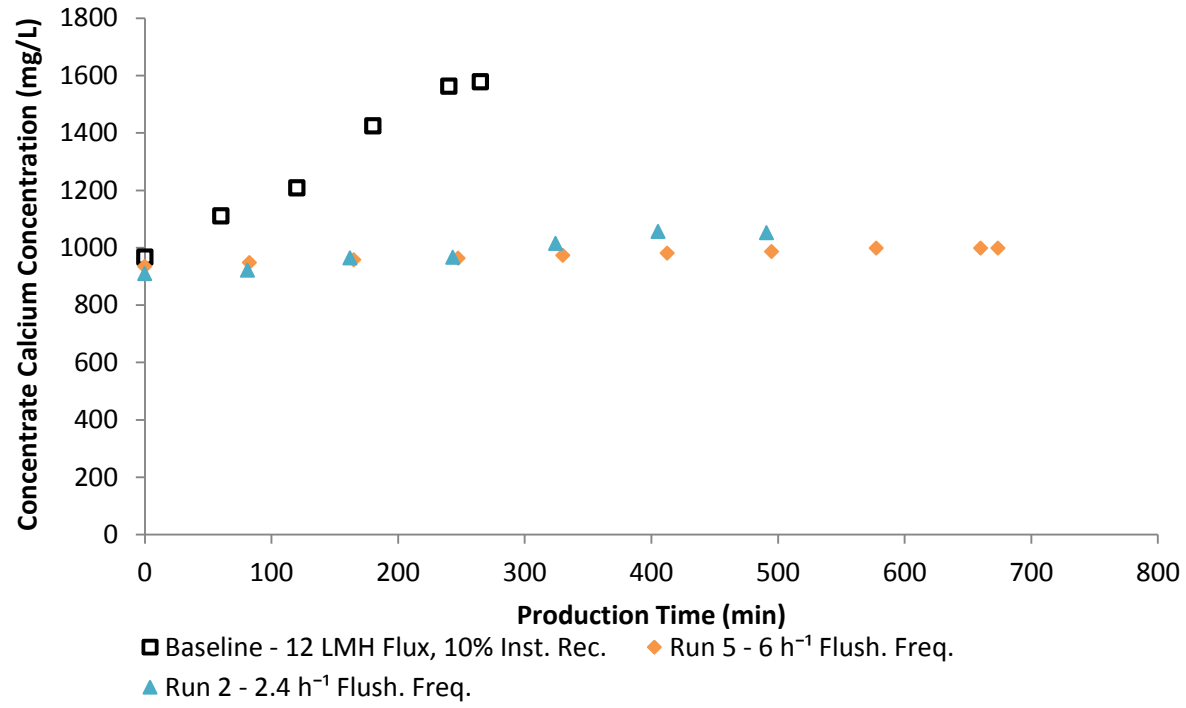

Figure 6-12 *The effect of flushing frequency on concentrate calcium concentration for Run 5 and 2, at 6 and 2.4 h^{-1} respectively, while the other factors were the same for both runs. The baseline data refer to the non-flushing and non-seeding experiments.*

From Figure 6-10 to Figure 6-12, it is evident that more frequent flushing resulted in higher total production times (i.e. a higher net permeate production rate). However, membrane scaling was not prevented completely with the tested flushing frequencies. The factorial design experiments suggested that higher flushing frequencies higher than 6 h^{-1} (refer to Figure 6-5) could improve the membrane scaling prevention significantly, at the expense of reduced permeate production rates. Membrane scaling was caused by concentration polarisation, causing the saturation indexes well above one near the membrane, leading to surface crystallisation (Bartman et al., 2011; Rahardianto et al., 2006). Concentration polarisation is a reversible process (Sablani et al., 2001), explaining why increasing the flushing frequency had a positive effect on scaling prevention. During every flushing cycle, the concentration polarisation layer diffuses back into the bulk fluid, thus a higher flushing frequency was desirable for high recovery operation, however also resulting in reduced permeate production indexes. This agrees with experimental data from Al-Bastaki and Abbas (2003), where recycling permeate into the feed stream effectively reduced the concentration polarisation at the membrane surface. The higher the recycle ratio, the less concentration polarisation occurred, thus lowering the scaling propensity with the disadvantage of lowering the production rate.

In the preliminary evaluation of the flushing technique, flushing 2.4 times per hour effectively prevented scaling from occurring (refer to section 5.3). However, the results in this section suggested otherwise. The unit was operated with an undersaturated feed solution in full recycle mode (concentrate and permeate recycled) in the preliminary test, whereas the RO unit was operated in concentrate recycle mode with supersaturated feed solutions in the factorial design experiments, explaining the different observations.

6.3.3. The effect of instantaneous recovery

In this section the results for Run 3 and 7 are compared. The scaling effect of instantaneous recovery on total production time was isolated, since the other factors were constant in both runs, while the instantaneous recovery was 10 and 30 % respectively.

A rapid drop in membrane permeability was observed for the baseline cases, whereas a gradual drop was observed for Run 3 and 7 in Figure 6-13. The effective membrane permeability dropped rapidly in the baseline experiments, whereas gradual declines were observed for Run 3 and 7 with membrane flushing. Ultimately the membrane permeability approached zero, where constant flux operation was impossible due to severe surface blockage. In the baseline experiments the membrane was completely scaled after 180 and 240 minutes at 30 and 10 % instantaneous recovery

respectively. Periodic flushing effectively extended the scale free operation, resulting in total production times of 580 and 720 minutes at 30 and 10 % instantaneous recovery, indicating that lower instantaneous recoveries are beneficial to reduce membrane scaling.

Correspondingly, similar trends were observed for the conductivity and calcium concentration measurements, as shown in Figure 6-14 and Figure 6-15. As expected, the conductivity initially rises exponentially in the baseline experiments, however dropping rapidly thereafter due to surface crystallisation causing surface blockage. In the baseline experiments the concentrate calcium concentrations rose up to 1800 mg/L, corresponding to saturations indexes well above 2.5, greatly increasing the rate of membrane scaling. Conversely, the saturation index stayed constant at approximately 1.2 during the flushing experiments, indicating an effective concentration demineralisation via the seeded gypsum precipitation.

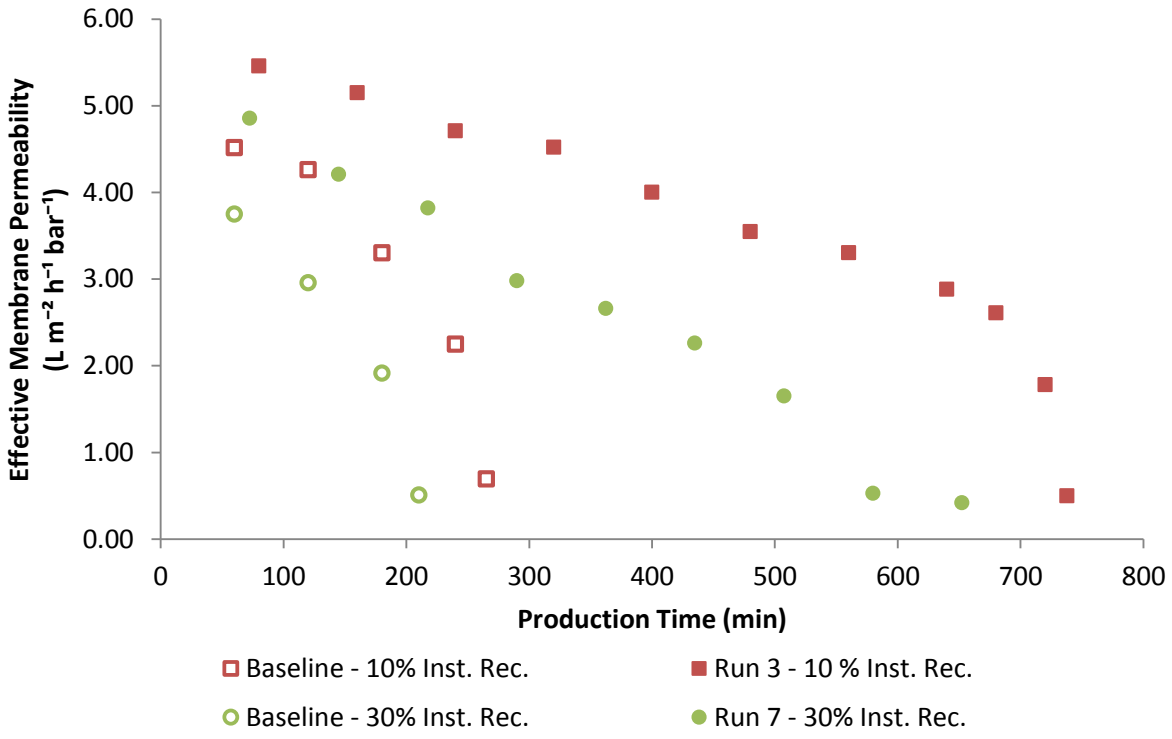

Figure 6-13 *The effect of instantaneous recovery on effective membrane permeability for Run 3 and 7, at 10 and 30 % respectively, while the other factors are the same for both runs. The baseline data refer to the non-flushing and non-seeding experiments.*

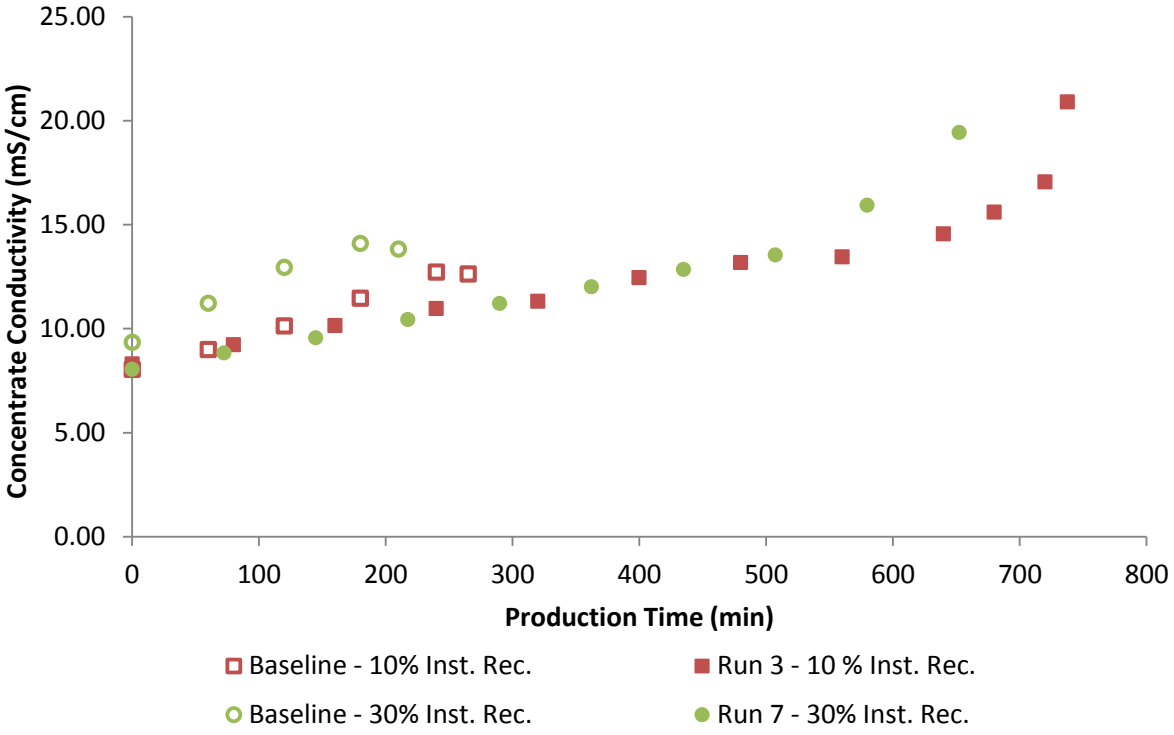

Figure 6-14 *The effect of instantaneous recovery on concentrate specific conductivity for Run 3 and 7, at 10 and 30 % respectively, while the other factors are the same for both runs. The baseline data refer to the non-flushing and non-seeding experiments.*

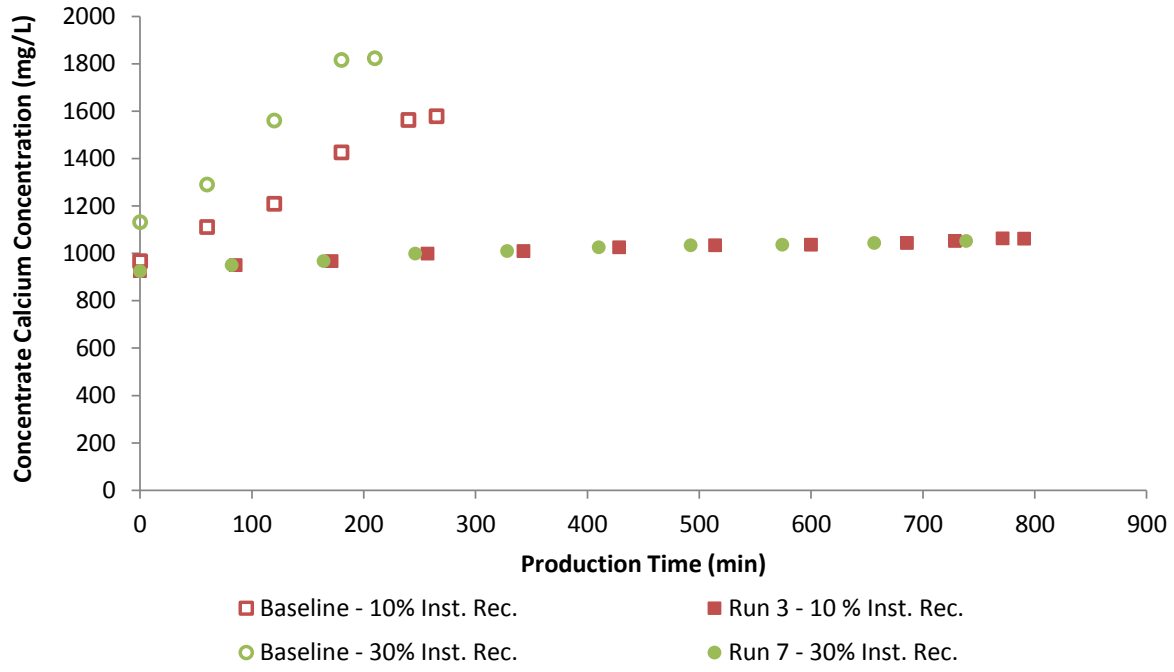

Figure 6-15 *The effect of instantaneous recovery on concentrate calcium concentration for Run 3 and 7, at 10 and 30 % respectively, while the other factors are the same for both runs. The baseline data refer to the non-flushing and non-seeding experiments.*

The results in Figure 6-13 and Figure 6-15 showed that instantaneous recovery had a significant effect on the membrane scaling, generally increasing the total production time by 140 minutes if the instantaneous recovery was decreased from 30 to 10 %. Instantaneous recovery and cross flow velocity are inversely proportional, because higher instantaneous recoveries result in higher cross flow velocities, provided the permeate flux is constant.

In Table 6-3 the entry (channel 1), exit (channel 6) and average feed-brine cross flow velocities are given, calculated with measured flow rates and dimensions of the flow channel. Considering the RO unit operation at 12 LMH and 10% instantaneous recovery, the average CF velocity was 0.075 m/s, approximately three times higher than during 30 % instantaneous recovery operation. This explains why higher total production times were achieved at lower instantaneous recoveries throughout the factorial design experiments. An increase in cross flow velocity reduced the membrane scaling propensity, due to the thinner boundary layer at the membrane surface (Kucera, 2010). A thinner boundary layer reduced the level of concentration polarisation at the membrane surface, thus reducing the risk of membrane scaling (Oh et al., 2009; Sablani et al., 2001; Uchymiak et al., 2008). Conversely, lower cross flow velocities resulted in thicker boundary layers, increasing the scaling propensity due to larger solute residence time within the boundary layer (Kucera, 2010).

Table 6-3 *Experimental cross flow velocities along the RO membrane under various operating conditions*

		Flowrates (L/h)			Cross Flow Velocity (m/s)		
Permeate Flux (LMH)	**Inst. Rec. (%)**	**Feed**	**Conc.**	**Permeate**	**Entry**	**Exit**	**Avg.**
12	10	12.7	11.5	1.3	0.071	0.080	0.075
12	30	4.3	3.0	1.3	0.024	0.021	0.022
24	10	24.6	22.0	2.6	0.14	0.15	0.14
24	30	8.6	6.0	2.6	0.048	0.042	0.045

The cross flow velocities approximately double if the permeate flux increases from 12 to 24 LMH, hence one could expect the total production times to be higher at 24 LMH permeate flux operation, provided the RO feed flow is kept constant. However, the factorial results indicated lower total production times at 24 LMH (refer to section 6.3.1). This further indicated that the effect of permeate flux on membrane scaling was more profound, compared to instantaneous recovery. This was also indicated by the p-values (given in Table 6-2), where the p-value is significantly lower for permeate flux. The lower the p-value the more significant the factor, hence the lower the probability that the result was caused by chance and the null hypothesis can be rejected.

6.3.4. The effect of flushing volume and soak time

The factorial design ANOVA analysis suggested that flushing volume and soak time accept the null hypothesis, indicating that the two factors have a negligible effect on the total production time (i.e. membrane scaling), having p-values of 0.19 and 0.38 respectively. It is very important to understand what these statistical results suggest. Firstly, the statistical findings were only true within the constraints of the specific factorial design with the respective high and low values for each factor. Secondly, it does not necessarily imply that the two factors have absolutely no effect on membrane scaling. It, merely suggests that the other factors (permeate flux, flushing frequency and instantaneous recovery) have a more significant effect on membrane scaling prevention within the chosen factor values of factorial design experiment.

Flushing volume certainly has an effect on calcium sulphate membrane scaling, although the statistical analysis proved otherwise. Theoretically, a higher permeate flushing volume replaces a greater number of feed-brine flow channel volumes. The oversaturated calcium sulphate solution inside the feed-brine flow channel is replaced with an undersaturated solution, thus reducing the scaling propensity significantly. For instance, a flushing volume of 1000 mL per flush should undoubtedly be more beneficial to prevent membrane scaling, compared to 5 mL per flush. In the all experiments the flushing volume was either 35 or 70 mL, approximately replacing 4 and 8 times the total feed-brine flow channel volume respectively, since the total feed-brine flow channel had a total volume of 9 mL. In the objectives of the study it was established to only operate the pilot unit above a permeate production index of 0.5 (refer to section 3.5.5). 70 mL was the maximum value for the flushing volume high value in the factorial design, yielding a PPI just above 0.5, hence no higher values were considered in this study.

The statistical results potentially imply that the magnitudes of the high and low values were too close to each other, thus not having a significant impact on the factorial design statistical results. Surely, if the low and high values would be 5 and 1000 mL respectively, the statistical analysis would be different, however this would result in PPI much lower than 0.5 if the flushing volume would be greater than 70 mL. Operating the lab-scale at PPI's below 0.5 was considered to be impractical.

Similarly, the statistical analysis indicated the low significance of soaking time on calcium sulphate membrane scaling. However, this was only true within the limits of the factorial design. Theoretically, a longer soak time may be more favourable to reduce membrane scaling, since the undersaturated solution spends more time in the feed-brine flow channel. This could enhance the

mass transfer of salt ions away from the membrane surface into the bulk fluid, thus effectively reducing the level of concentration polarisation (Lyster et al., 2009). For instance, a soaking time of 500 seconds would surely enhance the mass transfer drastically, compared to 5 seconds. Throughout the study the soak time was either 20 or 90 seconds, based on initially calculations to ensure a permeate production index above 0.5 in all of the factorial design experiments (refer to section 3.5.5).

6.4. Permeate production rate and index

In the previous section it was shown that the permeate flushing technique effectively prolonged the scale free production time, thus also increasing the net permeate production, however scaling occurred eventually. In all experiments, flushing or non-flushing, severe calcium sulphate scaling ultimately caused surface blockage leading to flux declines. The obvious disadvantage of the flushing technique was the reduction in overall permeate production rate, however, this increased the net permeate production through longer production times. In this section the effect of permeate production rate and index on membrane scaling is discussed.

The ANOVA analysis from the experimental data in Figure 6-4 showed that flushing rate, flushing volume, soaking time and permeate flux had a significant effect on the PPR. Instantaneous recovery was the only factor which had no effect on the PPR, only affecting the cross flow velocity along the membrane.

Figure 6-16 shows the experimental and calculated permeate production rate for each experimental run. The permeate production rate was calculated with Equation 4-3, based on the production efficiency and flushing volume. The experimental data compared well to the calculated data, where the average relative error was less than 3 % between the two values, most likely caused by the random errors from measurement equipment. A strong inverse trend is observed in Figure 6-16, where high PPR's relate to low net permeate produced and vice versa. This is attributed to the strong effect of permeate flux on PPR. The permeate flux was 12 LMH for Run 1-8, while the permeate flux was 24 LMH for Run 9-16.

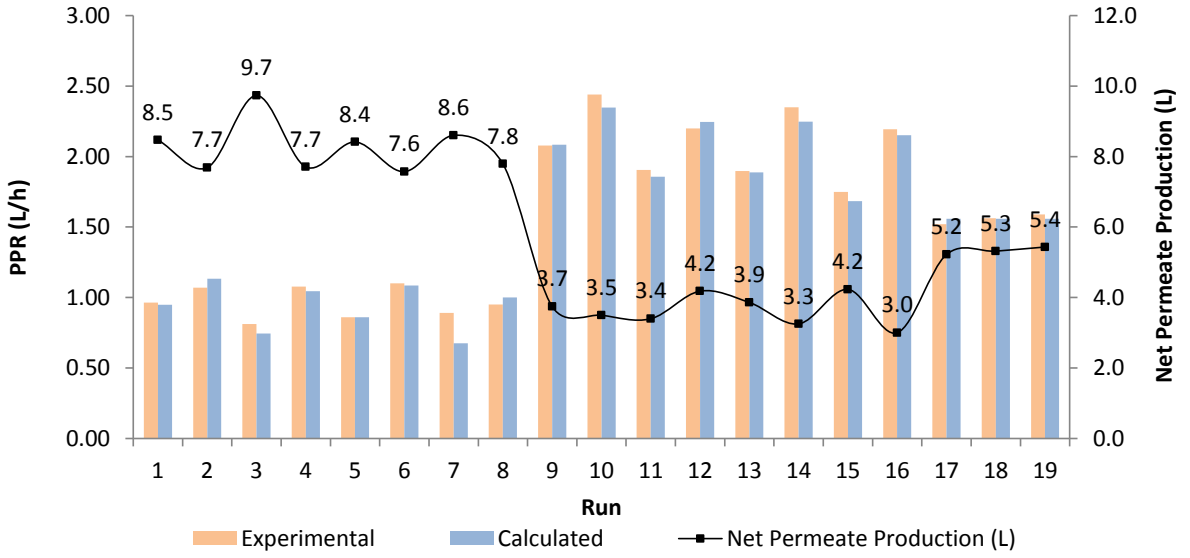

Figure 6-16 *Comparison of experimental and calculated permeate production rate (PPR). The black dots show the experimental net permeate production for each run.*

In Figure 6-17 net permeate production is plotted against PPR for all 19 factorial runs. Again, the strong effect of permeate flux on total production time was evident. The data points are clearly separated into two groups, with no data points between 1.10 and 1.50 L/h. This corresponds to low permeate flux experiments below 1.10 L/h and high permeate flux experiments above 1.75 L/h. A least squares regression model was fitted to the experimental data. A good fit was obtained for the inverse relationship between net permeate produced and PPR, with a R^2 value of 0.937.

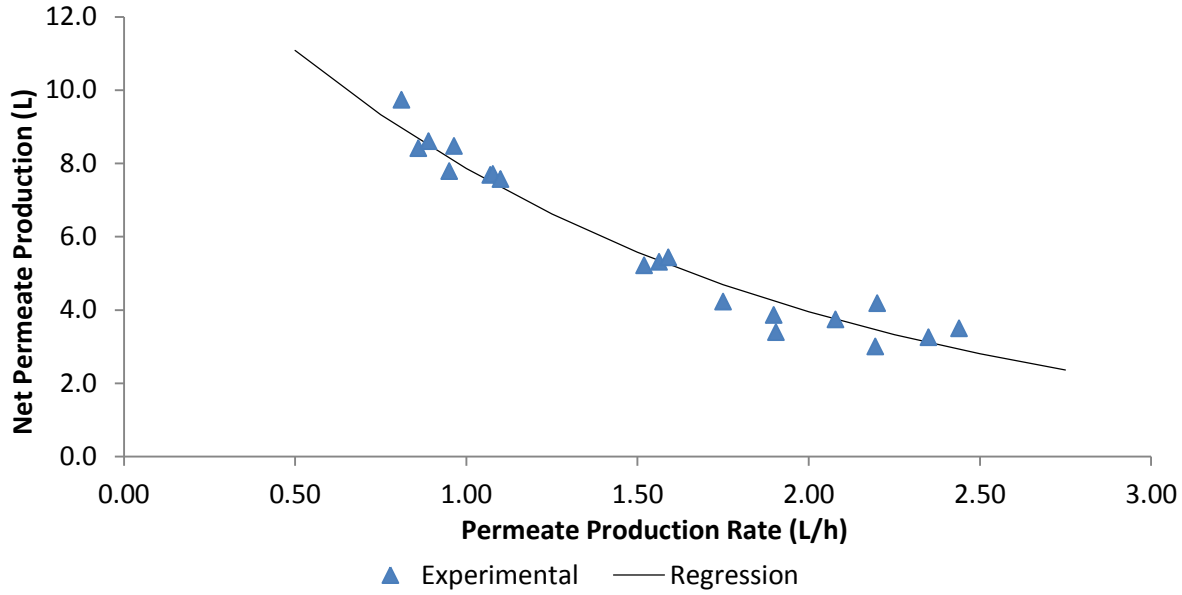

Figure 6-17 *The relationship between PPR and net permeate produced, based on the factorial design experimental data*

The inverse relationship showed that more permeate was recovered while operating the plant at lower PPR's, however this resulted in longer operating times. The opposite was also true, where higher PPR's resulted in more rapid scaling and ultimately lower volumes of net recovered permeate. This shows that the PPR is mainly affected by the actual permeate flux for each experimental run, where lower fluxes automatically resulted in lower PPR's, while the effect of the other factors was less significant.

The regression predicted that a higher net permeate production can be achieved by lowering the permeate production rate, for instance by lowering the permeate flux, flushing volume and/or increasing the flushing frequency. It is important to note that this trend was only observed within the tested factorial design. In theory, there should be an optimum permeate production rate, where the net permeate produced is at its maximum. However, no experimental data for PPR's below 0.8 L/h was collected in this study, hence further experimental work in future studies is necessary.

The PPR quantitatively indicated how much permeate was produced per hour, while the dimensionless PPI indicated how the PPR compared to the non-flushing permeate flow rate at a specific flux. The permeate production index for all 19 factorial design experiments is given in Figure 6-18, comparing it to the net permeate produced. The data are clearly separated into three groups, each showing the PPI at 12, 18 or 24 LMH permeate flux. At 12 LMH the PPI varied between 0.64 and 0.86, while the net permeate produced was always larger or above 7.7 L. For the high flux experiments at 24 LMH, the PPI was generally higher at values between 0.69 and 0.96, however the net permeate produced was never above 4.2 L. The highest permeate production was observed in Run 3, where the lab-scale unit was operated for 720 minutes without a flux decline while producing 9.7 L of permeate. On the other hand, Run 3 had the lowest experimental PPI at 0.64, indicating that the high net permeate production came at a high cost of reduced productivity. This corresponds with the data from Figure 6-17, where the same trend was observed. The three experimental runs at 18 LMH permeate flux indicated the opposite trend, where it appears that an increase in permeate production index results in higher net permeate production. However, this is not true since all three data points where derived from the experimental results from the 3 factorial centre runs at the same operating conditions. Therefore, the data points do not actually indicate any trend, and merely indicate one data point, with small experimental variances within the runs. If more experimental runs were performed at 18 LMH a trend would probably be visible.

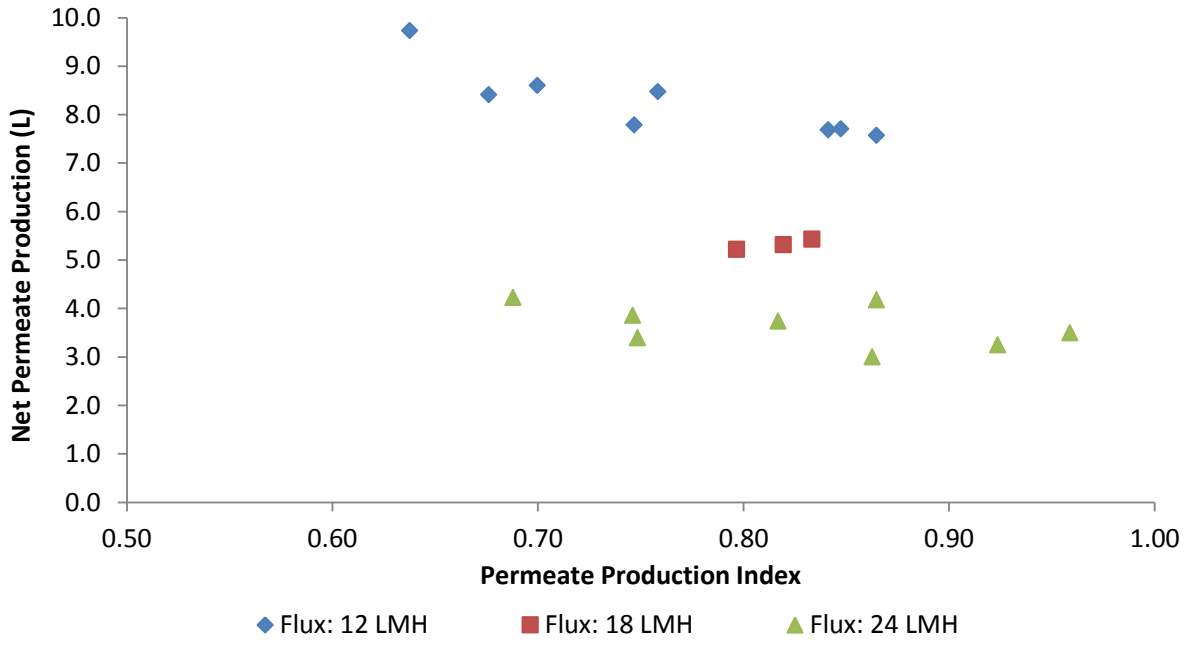

Figure 6-18 *Comparison of experimental permeate production index and net permeate produced, based on the factorial design experimental data*

Ultimately these results confirm that permeate flux had the biggest impact on the operation of the lab-scale RO unit, to prevent membrane scaling. For instance, when one compares Run 8 (12 LMH flux) and 11 (24 LMH), both having an experimental PPI of 0.75, a notable difference in net permeate production was observed. In Run 8 the 7.8 L of net permeate produced was more than double the 3.4 L in Run 11. However, as expected the PPR for Run 11 was almost double at 1.9 L/h, compared to 0.95 L/h in Run 8. This indicated that it was beneficial to operate at lower fluxes in order to achieve higher net permeate production.

Clear trends were identified in Figure 6-18, showing the strong relationship between net permeate production and permeate flux. However, in Figure 6-18 the influence of the other factors was not shown. In Figure 6-19 the same data was plotted again, however the data points were separated by flushing frequency and permeate flux. A very clear trend can be identified, where the higher flushing frequency at 6.0 h^{-1} resulted in a higher net permeate production, if one compares the data to the lower flushing frequency at 2.4 h^{-1}. This was true at both 12 and 24 LMH permeate flux. These results fully agree with the statistical analysis (discussed in section 6.2), where permeate flux and flushing frequency had the lowest P-values in the ANOVA analysis.

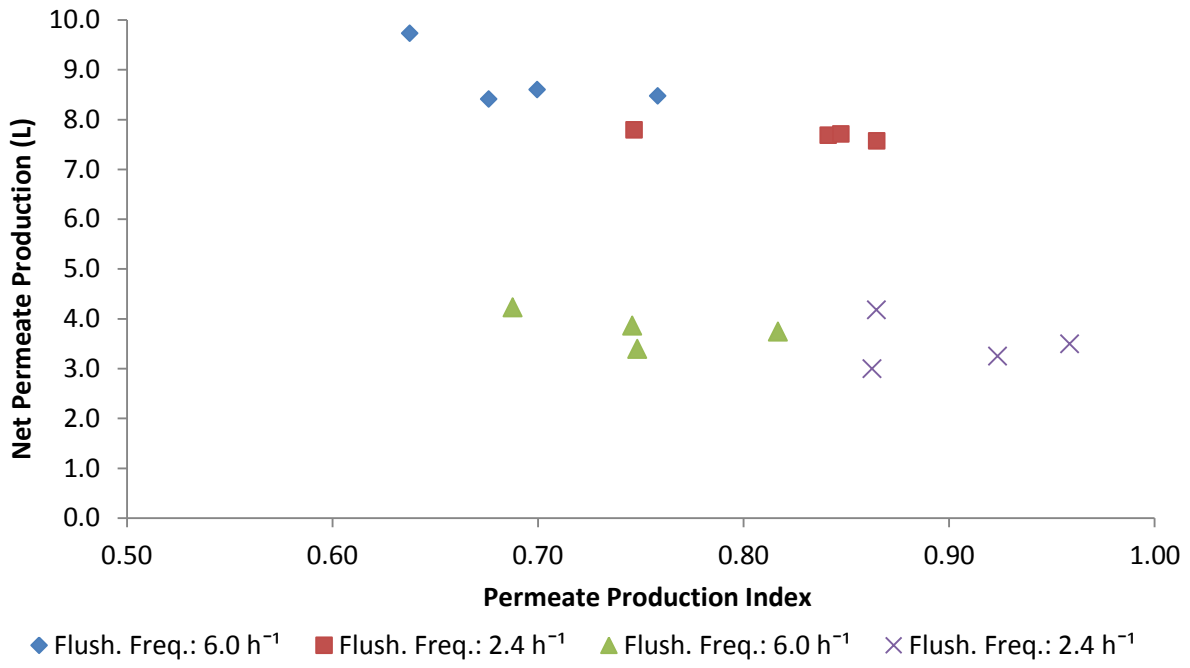

Figure 6-19 *Comparison of experimental permeate production index and net permeate produced, showing the influence of flushing frequency*

The overall optimum flushing operating conditions can be identified in Figure 6-19, if one considers the data points furthest to the left at 12 and 24 LMH flux. For these experimental runs the permeate production was the highest, and clearly 6.0 h^{-1} is the optimum flushing frequency, regardless of the permeate flux. Not surprisingly, the instantaneous recovery was 10 % for both runs, which was identified as the best value within the selected range of experimental recoveries, based on the ANOVA analysis in section 6.2, where instantaneous recovery was identified as a significant factor.

Chapter 7 - Conclusions

The purpose of this study was to assess the feasibility of reducing calcium sulphate scaling on RO membranes, by using periodic permeate flushing when feeding the RO unit with a supersaturated calcium sulphate solution in the absence of anti-scalant. Further, intermediate concentrate desupersaturation via seeded gypsum precipitation and operation in concentrate recycle mode was used to simulate multiple stage high recovery brackish RO desalination. It was tested if periodically replacing the supersaturated solution near the membrane surface, with an undersaturated permeate, was effective to prevent calcium sulphate membrane scaling. The overall recovery was increased by using intermediate concentrate desupersaturation to reduce the scaling propensity of the RO concentrate, thus allowing high recovery operation by concentrate recycling.

Initial experiments confirmed that the permeate flushing technique and intermediate seeded gypsum precipitation worked effectively. Operation in full recycle mode without seeded gypsum precipitation, where concentrate and permeate are recycled, completely prevented gypsum scaling. This was achieved for over 24 hours operation, with a feed solution of 0.9 SI_g, operating at all three flushing frequencies: 12, 6 and 2.4 h^{-1}. After 24 hours the RO unit was switched to non-flushing operation, resulting in membrane scaling within 2-3 hours, detected by a flux decline. Preliminary experiments showed that seeded gypsum precipitation at 2 g/L with a hydraulic residence time of 120-130 minutes effectively reduced the gypsum saturation index from 1.5 to about 1.1 in the RO concentrate. A longer residence time would be required in the precipitation reactors to further reduce the gypsum saturation index to 1.0 where the thermodynamic equilibrium would be reached. On average the calcium and sulphate concentrations dropped by 104 ± 9 mg/L and 201 ± 27 mg/L respectively, which was in stoichiometric proportion, suggesting that only calcium sulphate precipitation occurred.

The size of the surface scale crystals and rate of crystallisation increased along the flow path from the channel entry region to exit region, corresponding to increasing levels of concentration polarisation in the direction of flow. XRD analysis for various experimental runs confirmed that only calcium sulphate dihydrate scaling occurred.

The ANOVA analysis showed that total production time (i.e. operation time until a flux decline indicated membrane scaling) was primarily affected by permeate flux. Operation at 24 LMH resulted in much lower total production times between 82 - 145 min, compared to 413 - 720 min at 12 LMH. Higher permeate fluxes resulted in higher levels of concentration polarisation at the membrane

surface increasing the propensity for membrane scaling. Further, flushing frequency and instantaneous recovery were also identified as significant factors by the ANOVA analysis, where high flushing frequencies and low instantaneous recoveries were beneficial to prolong scale free operation. Concentration polarisation is a reversible process, explaining why the flushing technique is effective to a certain extent. Increasing the flushing frequency and cross flow velocity or lowering the permeate flux, lowers the degree of concentration polarisation and consequently the scaling propensity.

The highest total production time within the factorial experiments was 720 minutes with a net permeate production of 9.7 L, while operating the lab-scale system at 12 LMH permeate flux, 10 % instantaneous recovery and flushing 6 times per hour in concentrate recycle mode. For comparison, the total production time for the same baseline experiment without flushing was only 240 minutes, with a net permeate production of 4.3 L. However, the permeate production rate during flushing experiment was only 0.64 L/h whereas it was 1.27 L/h during the non-flushing baseline experiment. This shows that the prolonged scale free operation came at a high cost due to the significant loss in productivity.

As expected, the permeate production rate was significantly affected by permeate flux, and to a lesser extent by flushing frequency, flushing volume and soak time. Generally, high permeate production rates between 1.75 - 2.44 L/h resulted in low total production times between 82 - 145 min, compared to 413 - 720 min at lower production rates of 0.71-1.25 L/h. In other words, lower permeate production rates ultimately resulted in higher net permeate production. This inverse trend was confirmed by a least squares regression of the experimental data having a relatively good fit, with a R^2 value of 0.898.

The ANOVA analysis of the factorial design experiments suggested that increasing the flushing frequency, while lowering permeate flux and instantaneous recovery below the optimum values used in the factorial design would further increase total production time. In conclusion, it was shown that periodic permeate flushing could delay the membrane scaling process. However, it failed to prevent membrane scaling, while operating the unit with supersaturated calcium sulphate solutions. The flushing technique effectively delayed the onset of precipitation, but scaling eventually occurred if the lab-scale unit was operated in concentrate recycle mode with oversaturated feed solution (SI_g = 1.2). The delay in membrane scaling resulted in significant loss in productivity, suggesting that the use of antiscalants is inevitable to prevent scaling when saturation levels are exceeded notably.

Chapter 8 - Recommendations

Experiments should be repeated with field water with a moderate scaling propensity, to determine if the flushing technique is effective if other ions, suspended particles and/or organic matter are present. Potentially the flushing technique is effective to reduce fouling and/or biofouling, however the presence of other foreign matter can also reduce the effectiveness of the flushing technique.

In this study only calcium sulphate dihydrate scaling was considered, since it is the most common scalant on RO membranes in brackish RO desalination. Further experiments could investigate if the flushing technique is effective to prevent/reduce other common scalants, such as calcium carbonate, silicate, barium sulphate or magnesium sulphate.

A flat sheet laboratory scale RO membrane test cell was used to investigate the permeate flushing technique, however typical spiral wound membranes should be used in a larger pilot plant to determine how the hydrodynamics of the spiral wound membrane influence the permeate flushing.

The current flat sheet RO test cell should be redesigned, to reduce the scaling potential, by improving the hydrodynamics. Firstly, the dead zones between the outer 5mm o-ring and the flow channel should be eradicated. The 180° bends between individual flow channels in the tortuous flow path should have smooth edges and no 90˚ edges, to ensure a constant flow velocity throughout the entire flow channel. Further, a feed channel spacer should be used to induce turbulences and reduce concentration polarisation.

In theory a higher flushing velocity should enhance the flushing technique drastically, compared to the current gravity flushing operation with a head of 11m. This could be achieved by installing an additional pump, only activated during the flushing operation. Alternatively, compressed air could be used to increase the pressure during permeate flushing.

Chapter 9 - References

Ahmed, M., Arakel, A., Hoey, D., Coleman, M., 2001a. Integrated power, water and salt generation: a discussion paper. Desalination 134, 37–45.

Ahmed, M., Shayya, W., Hoey, D., Al-Handaly, J., 2001b. Brine disposal from reverse osmosis desalination plants in Oman and the United Arab Emirates. Desalination 133, 135–147.

Ahmed, M., Shayya, W.H., Hoey, D., Mahendran, A., Morris, R., Al-Handaly, J., 2000. Use of evaporation ponds for brine disposal in desalination plants. Desalination 130, 155–168.

Al-Bastaki, N., Abbas, A., 2003. Permeate recycle to improve the performance of a spiral-wound RO plant. Desalination 158, 119–126.

Alimi, F., Elfil, H., 2003. Kinetics of the precipitation of calcium sulfate dihydrate in a desalination unit. Desalination 157, 9–16.

Amjad, Z., 1985. Applications of antiscalants to control calcium sulfate scaling in reverse osmosis systems. Desalination 54, 263–276.

Amjad, Z., 1988. Kinetics of a crystal growth of calcium sulfate dihydrate:the influence of polymer composition, molecular weight, and solution pH. Can. J. Chem. 66, 1529–1536.

Amjad, Z., Hooley, J., 1986. Influence of polyelectrolytes on the crystal growth of calcium sulfate dihydrate. J. Colloid Interface Sci. 111, 496–503.

Arnal, J.M., Sancho, M., Iborra, I., Gozálvez, J.M., Santafé, a., Lora, J., 2005. Concentration of brines from RO desalination plants by natural evaporation. Desalination 182, 435–439.

Baker, R.W., 2004. Membrane Technology and Applications. John Wiley & Sons, Ltd, Chichester, UK.

Bartman, A.R., Lyster, E., Rallo, R., Christofides, P.D., Cohen, Y., 2011. Mineral scale monitoring for reverse osmosis desalination via real-time membrane surface image analysis. Desalination 273, 64–71.

Ben Ahmed, S., Tlili, M.M., Amor, M. Ben, 2008. Influence of a polyacrylate antiscalant on gypsum nucleation and growth. Cryst. Res. Technol. 43, 935–942.

Bhagwan, J., 2012. Turning Acid Mine Drainage Water into Drinking Water: The eMalahleni Water Recycling Project. Guidel. Water Reuse Water Res. Comm. 102–103.

Borden, J., Gilron, J., Hasson, D., 1987. Analysis of RO flux decline due to membrane surface blockage. Desalination 66, 257–269.

Bowell, R., 2000. Sulphate and salt minerals: the problem of treating mine waste. Min. Environ. Manag. 5, 11–13.

Brandse, W.P., van Rosmalen, G.M., Brouwer, G., 1977. The influence of sodium chloride on the crystallization rate of gypsum. J. Inorg. Nucl. Chem. 39, 2007–2010.

Bremere, I., Kennedy, M., Johnson, A., 1998. Increasing conversion in membrane filtration systems using a desupersaturation unit to prevent scaling. Desalination 119, 199–204.

Bremere, I., Kennedy, M., Michel, P., van Emmerik, R., Witkamp, G.-J., Schippers, J., 1999. Controlling scaling in membrane filtration systems using a desupersaturation unit. Desalination 124, 51–62.

Brusilovsky, M., Borden, J., 1992. Flux decline due to gypsum precipitation on RO membranes. Desalination 86, 187–222.

Chesters, S.P., 2009. Innovations in the inhibition and cleaning of reverse osmosis membrane scaling and fouling. Desalination 238, 22–29.

Christoffersen, M., Christoffersen, J., Weijnen, M., van Rosmalen, G., 1982. Crystal growth of calcium sulphate dihydrate at low supersaturation. J. Cryst. Growth 58, 585–595.

Crittenden, J.C., Trussell, R.R., Hand, D.W., Howe, K.J., Tchobanoglous, G., 2005. Water Treatment - Principles and Design (2nd Edition). John Wiley & Sons, Ltd.

Davies, C.W., 1962. Ion Association. Butterworth & Co, London.

Dickson, J.M., 1998. ”Fundamental Aspects of Reverse Osmosis,” in Reverse Osmosis Technology. Marcel Dekker, Inc., New York.

DOW Filmtec, 2011. Product information Membranes DOW FILMTEC Extra Low Energy (XLE) Elements for Commercial Systems.

DOW Filmtec, 2013. Membrane System Design Guidelines Commercial Elements.

El-Dessouky, H.T., Ettouney, H.., 2002. Fundamentals of salt water desalination. Elsevier, New York.

Freyer, D., Voigt, W., 2003. Crystallization and Phase Stability of CaSO 4 and CaSO 4 - Based Salts. Monatshefte für Chemie / Chem. Mon. 134, 693–719.

Fritzmann, C., Lowenberg, J., Wintgens, T., Melin, T., 2007. State-of-the-art of reverse osmosis desalination. Desalination 216, 1–76.

Gabelich, C.J., Rahardianto, A., Northrup, C.R., Yun, T.I., Cohen, Y., 2011. Process evaluation of intermediate chemical demineralization for water recovery enhancement in production-scale brackish water desalting. Desalination 272, 36–45.

Gabelich, C.J., Williams, M.D., Rahardianto, A., Franklin, J.C., Cohen, Y., 2007. High-recovery reverse osmosis desalination using intermediate chemical demineralization. J. Memb. Sci. 301, 131–141.

Gerber, D.H., 2011. The chemical manipulation of meta-stable brine super- saturated with gypsum: forcing precipitation by overriding the inhibitory effect of antiscalants on crystal formation. University of Stellenbosch.

Gilron, J., Hasson, D., 1987. Calcium sulphate fouling of reverse osmosis membranes: flux decline mechanism. Chem. Eng. Sci. 42, 2351–2360.

Glater, J., Cohen, Y., 2003. Brine disposal from land based membrane desalination plants: a critical assessment. Los Angeles.

Glueckstern, P., 1986. Current and long term considerations for the application of reverse osmosis technology in Israel. Desalination 58, 69–75.

Glueckstern, P., Priel, M., 1997. Optimized brackish water desalination plants with minimum impact on the environment. Desalination 108, 19–26.

Hamann, M.L., 2010. System hydrodynamics to reduce Fouling of air-sparged immersed Flat-sheet microfiltration Membranes. University of Stellenbosch.

Hamdona, S.K., Al Hadad, U. a., 2007. Crystallization of calcium sulfate dihydrate in the presence of some metal ions. J. Cryst. Growth 299, 146–151.

Hasson, D., Drak, A., Semiat, R., 2001. Inception of CaSO4 scaling on RO membranes at various water recovery levels. Desalination 139, 73–81.

Helalizadeh, A., Müller-Steinhagen, H., Jamialahmadi, M., 2000. Mixed salt crystallisation fouling. Chem. Eng. Process. 39, 29–43.

Hoek, E.M.V., Allred, J., Knoell, T., Jeong, B.-H., 2008. Modeling the effects of fouling on full-scale reverse osmosis processes. J. Memb. Sci. 314, 33–49.

Hutton, B., Kahan, I., Naidu, T., Gunther, P., 2009. Operating and maintenance experience at the Emalahleni water reclamation plant. Int. Mine Water ….

Juby, G., 1994. Development of a Novel Membrane Desalination Technique for Treating Calcium Sulphate Scaling Mine Water: The SPARRO Process. University of Pretoria.

Juby, G., Schutte, C., 2000. Membrane life in a seeded-slurry reverse osmosis system. Water SA 26, 239–248.

Kim, S., Hoek, E., 2005. Modeling concentration polarization in reverse osmosis processes. Desalination 186, 111–128.

Klepetsanis, Dalas, E., Koutsoukos, P.G., 1999. Role of temperature in the spontaneous precipitation of calcium sulfate dihydrate. Langmuir 1534–1540.

Klepetsanis, Koutsoukos, P., 1991. Spontaneous precipitation of calcium sulfate at conditions of sustained supersaturation. J. Colloid Interface Sci. 143, 299–308.

Kucera, J., 2010. Reverse Osmosis: Design, Processes, and Applications for Engineers. Scrivener Publishing, Salem, MA.

Le Gouellec, Y.A., Elimelech, M., 2002. Control of calcium sulfate (gypsum) scale in nanofiltration of saline agricultural drainage water. Environmantal Eng. Sci. 19, 387.

Liu, S., 1975. A kinetic and morphological study of the seeded growth of calcium sulfate dihydrate in the presence of additives. J. Colloid Interface Sci. 52, 593.

Liu, S.-T., Nancollas, G.H., 1973. The crystal growth of calcium sulfate dihydrate in the presence of additives. J. Colloid Interface Sci. 44, 422–429.

Lonsdale, H.K., Merten, U., Riley, R.L., 1965. Transport properties of cellulose acetate osmotic membranes. J. Appl. Polym. Sci. 9, 1341–1362.

Lui, S., Nancolass, G.H., 1970. The kinetics of crystal growth of calcium sulfate dihydrate. J. Cryst. Growth 6, 281–289.

Lyster, E., Au, J., Rallo, R., Giralt, F., Cohen, Y., 2009. Coupled 3-D hydrodynamics and mass transfer analysis of mineral scaling-induced flux decline in a laboratory plate-and-frame reverse osmosis membrane module. J. Memb. Sci. 339, 39–48.

Marshall, W.L., Slusher, R., 1966. Thermodynamics of calcium sulfate dihydrate in aqueous sodium chloride solutions , 0-110°C. J. Phys. Chem. 70, 4015.

Matthiasson, E., Sivik, B., 1980. Concentration polarisation and fouling. Desalination 35, 59–103.

McCartney, E.R., Alexander, A.E., 1958. The effect of additives upon the process of crystallization. J. Colloid Sci. 13, 383–396.

McCool, B.C., Rahardianto, A., Cohen, Y., 2012. Antiscalant removal in accelerated desupersaturation of RO concentrate via chemically-enhanced seeded precipitation (CESP). Water Res. 46, 4261–71.

McCool, B.C., Rahardianto, A., Faria, J.I., Cohen, Y., 2013. Evaluation of chemically-enhanced seeded precipitation of RO concentrate for high recovery desalting of high salinity brackish water. Desalination 317, 116–126.

Montgomery, D.C., Runger, G.C., Humbele, N.F., 1998. Engineering Statistics. John Wiley & Sons, Inc, New York.

Najibi, S.H., Müller-Steinhagen, H., Jamialahmadi, M., 1997. Calcium sulphate scale formation during sub-cooled flow boiling. Chem. Eng. Sci. 52, 1265–1284.

Niewersch, C., 2011. Nanofiltration zur Grundwasseraufbereitung und Sulfatabscheidung bei der Trinkwasseraufbereitung am Beispiel von kippenbelastetem Grundwasser in einem Braunkohletagebaurevier. Aachen.

Oh, H.-J., Choung, Y.-K., Lee, S., Choi, J.-S., Hwang, T.-M., Kim, J.H., 2009. Scale formation in reverse osmosis desalination: model development. Desalination 238, 333–346.

OLI Systems, 2011. A Guide to Using OLI ScaleChem Version 4.1.

Oner, M., Dogan, O., Oner, G., 1998. The influence of polyelectrolytes architecture on calcium sulfate dihydrate growth retardation. J. Cryst. Growth 186, 427–437.

Pomerantz, N., Ladizhansky, Y., Korin, E., Waisman, M., Daltrophe, N., Gilron, J., 2006. Prevention of Scaling of Reverse Osmosis Membranes by “Zeroing” the Elapsed Nucleation Time. Part I. Calcium Sulfate. Ind. Eng. Chem. Res. 45, 2008–2016.

Potts, D., Ahlert, R., Wang, S., 1981. A critical review of fouling of reverse osmosis membranes. Desalination 36, 235–264.

Power, W., 1964. Transient Solubilities in the Calcium Sulfate-Water System. J. Chem. Eng. Data 9, 437–442.

Rahardianto, A., Gao, J., Gabelich, C.J., Williams, M.D., Cohen, Y., 2007. High recovery membrane desalting of low-salinity brackish water: Integration of accelerated precipitation softening with membrane RO. J. Memb. Sci. 289, 123–137.

Rahardianto, A., McCool, B.C., Cohen, Y., 2010. Accelerated desupersaturation of reverse osmosis concentrate by chemically-enhanced seeded precipitation. Desalination 264, 256–267.

Rahardianto, A., Shih, W.-Y., Lee, R.-W., Cohen, Y., 2006. Diagnostic characterization of gypsum scale formation and control in RO membrane desalination of brackish water. J. Memb. Sci. 279, 655–668.

Robinson, R.O.D., Ho, G., Mathew, K., 1992. Development of a Reliable Low-Cost Reverse Osmosis Desalination Unit for Remote Communities. Desalination 86, 9–26.

Sablani, S., Goosen, M., Al-Belushi, R., Wilf, M., 2001. Concentration polarization in ultrafiltration and reverse osmosis: a critical review. Desalination 141, 269–289.

Sanciolo, P., Ostarcevic, E., Atherton, P., Leslie, G., Fane, T., Cohen, Y., Payne, M., Gray, S., 2012. Enhancement of reverse osmosis water recovery using interstage calcium precipitation. Desalination 295, 43–52.

Sanciolo, P., Zou, L., Gray, S., Leslie, G., Stevens, D., 2008. Accelerated seeded precipitation pre-treatment of municipal wastewater to reduce scaling. Chemosphere 72, 243–9.

SANS 241, 2011. Drinking Water Part 1: Microbiological, physical, aesthetic and chemical determinands.

Seader, J.D., Henley, E.J., 2006. Seperation Process Principles. John Wiley & Sons, Ltd, Hoboken, NJ.

Seewoo, S., Van Hille, R., Lewis, A., 2004. Aspects of gypsum precipitation in scaling waters. Hydrometallurgy 75, 135–146.

Seidell, A., 1958. Solubilities: Inorganic and Metal-organic Compounds. A-Ir, 4th ed. ed. Van Nostrand- Reinhold, New York.

Shih, W.-Y., Albrecht, K., Glater, J., Cohen, Y., 2004. A dual-probe approach for evaluation of gypsum crystallization in response to antiscalant treatment. Desalination 169, 213–221.

Shih, W.-Y., Rahardianto, A., Lee, R.-W., Cohen, Y., 2005. Morphometric characterization of calcium sulfate dihydrate (gypsum) scale on reverse osmosis membranes. J. Memb. Sci. 252, 253–263.

Söhnel, O., Garside, J., 1992. Precipitation: Basic Principles and Industrial Applications. Butterworth-Heinemann Ltd., Oxford, UK.

Söhnel, O., Mullin, J.W., 1987. Interpretation of crystallization induction periods. J. Colloid Interface Sci. 123, 43–50.

Srinivasan, S., Chi, T., 1970. A simplified method for the prediction of concentration polarization in reverse osmosis operation for multi-component systems. Desalination 7, 133–145.

Uchymiak, M., Lyster, E., Glater, J., Cohen, Y., 2008. Kinetics of gypsum crystal growth on a reverse osmosis membrane. J. Memb. Sci. 314, 163–172.

Van de Lisdonk, C. a. C., Rietman, B.M., Heijman, S.G.J., Sterk, G.R., Schippers, J.C., 2001. Prediction of supersaturation and monitoring of scaling in reverse osmosis and nanofiltration membrane systems. Desalination 138, 259–270.

Varian, 1979. Analytical methods for flame spectroscopy. Springvale, Australia.

Walton, N., 1989. Electrical conductivity and total dissolved solids—what is their precise relationship? Desalination 12, 275–292.

Watson, B., Marksl, G., Gabbrielliz, E., Chapplez, L., 1994. Design and operation of a 5 ml / d RO desalination plant in arid Australia. Desalination 96, 369–377.

WHO/UNICEF, 2012. Progress on Drinking Water and Sanitation - 2012 Update.

Wijmans, J., Baker, R., 1995. The solution-diffusion model: a review. J. Memb. Sci. 107, 1–21.

Yang, Q.F., Liu, Y., David, H., Semiat, R., 2008. Scaling salt removal by addition of inorganic particles. J. Chem. Eng. Japan 41, 6–12.

Appendix A – Design, diagrams and photos

A.1. Overall design specifications

The primary aim of this study was to determine if calcium sulphate scaling on RO membranes can be prevented, using a permeate flushing technique together with intermediate concentrate desupersaturation via seeded gypsum precipitation, without the use of any antiscalants. After the literature review, the unit was designed according the following specifications:

- The desalination unit must use a flat sheet RO membrane test cell, and not the typical spiral wound membrane. The smallest commercially available brackish ultra-low pressure 2.5" DOW *Filmtec XLE – 2540* spiral RO membrane is designed for an average permeate flow of 58 L/h (DOW Filmtec, 2011), which is well beyond a lab-scale plant size. Plate and frame flat sheet RO membrane test cells have been extensively in laboratory calcium sulphate scaling studies (Chesters, 2009; Gabelich et al., 2007; Shih et al., 2005; Uchymiak et al., 2008), thus it was decided to design a unit capable to produce permeate at 1.0 - 2.5 L/h at a constant cross flow velocity.
- The cross flow velocity in the flow fee-brine flow channel is constant at velocities that minimise scaling, based on literature findings. The recommended maximum recovery per 2.5" spiral element is 15 % (DOW Filmtec, 2011), thus the unit should operate at recoveries between 10-30 % to investigate different cross flow velocities.
- The literature review suggested that high recovery brackish desalination is only possible by using multiple RO stages, with intermediate concentrate desupersaturation (Gabelich et al., 2007; McCool et al., 2013; Rahardianto et al., 2007; Sanciolo et al., 2012). In the lab-scale system a secondary desalination step was not possible; hence the treated concentrate is recycled to the feed tank to increase the overall recovery by mimicking a secondary RO desalination step.
- The RO unit will be operated in a semi-batch manner, initially filling the feed tank with saline solution. Operation is either in full or concentrate recycle mode, where permeate and concentrate or just concentrate is recycled to the feed tank respectively.
- The maximum operating pressure is based on a the osmotic pressure of the feed solution corresponding to a concentration factor of 20 at the maximum recovery of 95 %.

A.2. Mass balances

A.2.1. Method and assumptions

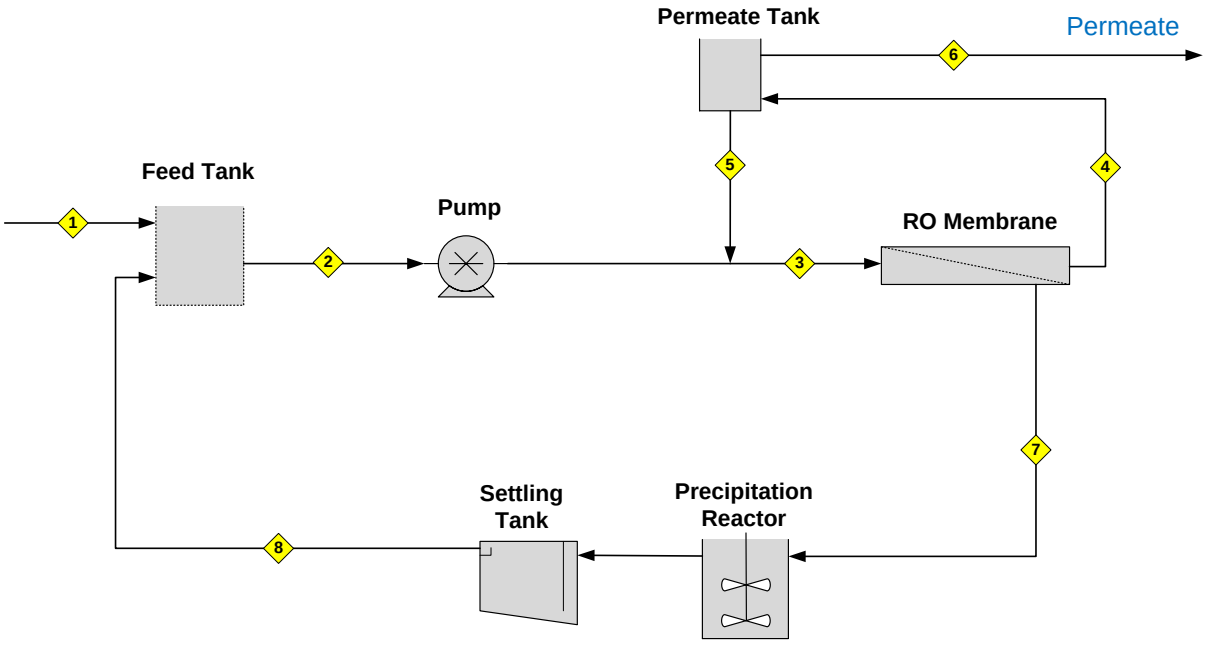

Figure A-1 *Basic flow diagram used in for the mass balance calculation, showing the stream numbers used in the mass balances.*

A detailed mass balance calculation was performed based on the basic flow diagram in Figure A-1.All the calculations were done in *Microsoft Excel*, setting up a spread sheet where various parameters could be changed, to determine the flow rates and operating conditions at certain recoveries. The method and various assumptions are discussed below:

- The desalination unit will operate in a semi-batch mode, hence a steady state mass balance was not possible due to the concentrate recycling. In other words, the process is time or recovery dependent since the concentrations change with time. In the mass balance a theoretical steady state stream of fresh saline solution is fed to the feed tank, where the stream is mixed with the concentrate. This simulates the batch fed saline solution at the start of an experiment, where the fresh solution is dosed continuously; mixing with the recycled concentrate to make up the membrane feed solution in the feed tank. It is important to notice that the classical overall mass balance where mass in equals mass out is not true for this system, due to the accumulation of sodium and chloride in the system.

- The feed solution is made up by mixing calcium chloride dihydrate and sodium sulphate and demineralised water, hence only Ca^{2+}, Na^{+}, SO_4^{2-} and Cl^{-} are considered in the mass balances.
- The effluent from the precipitation reactor (stream 8) and the fresh feed (stream 1) have a constant gypsum saturation index of 1.2, based on findings in literature where the saturation index was reduced to 1.1 after seeded gypsum precipitation (McCool et al., 2013; Rahardianto et al., 2010). The sodium and chloride concentration are not affected by the seeded calcium sulphate precipitation, thus the concentration are the same in stream 7 and 8.
- The sodium and chloride ion concentrations are accumulating in the system, increasing according to the concentration factor based on overall recovery. Therefore, the mass balances are time dependent due to the changing concentrations with increasing recovery.
- In all mass balance calculations the PPI is constant at 0.8 (PPI is explained in section 4.2), implicating that 20 % of the produced permeate in stream 4 is recycled back during flushing in stream 5.
- In the mass balances constant salt rejection of 95 % is assumed since a flat sheet membrane test cell is used, which is below the 99.0% specified by the manufacturer (DOW Filmtec, 2011). The permeate concentrations in stream 4 is calculated with the salt rejection, based on the feed stream 3.
- The instantaneous recovery varied between 10-30%, determining the RO concentrate concentrations in stream 7.

A.2.2. Data

The data from the mass balances was used to design the lab-scale desalination unit. The data for the mass balances at 12 LMH permeate flux at 10 and 30 % instantaneous recovery is given in Table A-1 and Table A-2 respectively. Additionally, the mass balances at 24 LMH permeate flux at 10 and 30 % instantaneous recovery is given in Table A-3 and Table A-4 respectively. As expected the TDS, osmotic pressure and conductivity are increasing as the recovery increased.

Table A-1 *Mass balance data from Microsoft Excel at various recoveries for operation 12 LMH permeate flux and 10 % instantaneous recovery.*

Recovery: 25 %									
	Stream Number	**1**	**2**	**3**	**4**	**5**	**6**	**7**	**8**
	Flow Rate (L/h)	1.00	12.25	12.50	1.25	0.25	1.00	11.25	11.25
	Temperature (°C)	15	15	15	15	15	15	15	15
	Pressure (bar)	1	1	7	1.1	1.1	1.1	1	1
	TDS (mg/L)	5345	6101	5985	308	308	308	6677	6168
	Conductivity (mS/cm)	8.35	9.53	9.35	0.48	0.48	0.48	10.43	9.64
	Osmotic Pressure (bar)	3.09	3.72	3.65	0.19	0.19	0.19	4.07	3.78
	Species Conc. (mg/L)								
	Na^+	971	1268	1244	65	65	65	1295	1295
	Ca^+	847	847	831	42	42	42	928	847
	Cl^-	1498	1957	1919	100	100	100	1997	1997
	SO_4^{-2}	2029	2029	1990	101	101	101	2223	2029

Recovery: 50 %									
	Stream Number	**1**	**2**	**3**	**4**	**5**	**6**	**7**	**8**
	Flow Rate (L/h)	1.00	12.25	12.50	1.25	0.25	1.00	11.25	11.25
	Temperature (°C)	15	15	15	15	15	15	15	15
	Pressure (bar)	1	1	8	1.1	1.1	1.1	1	1
	TDS (mg/L)	5345	7612	7468	391	391	391	8330	7814
	Conductivity (mS/cm)	8.35	11.89	11.67	0.61	0.61	0.61	13.02	12.21
	Osmotic Pressure (bar)	3.09	4.99	4.89	0.26	0.26	0.26	5.45	5.16
	Species Conc. (mg/L)								
	Na^+	971	1863	1827	97	97	97	1942	1942
	Ca^+	847	847	831	42	42	42	928	847
	Cl^-	1498	2874	2819	150	150	150	2996	2996
	SO_4^{-2}	2029	2029	1990	101	101	101	2223	2029

Recovery: 75 %									
	Stream Number	**1**	**2**	**3**	**4**	**5**	**6**	**7**	**8**
	Flow Rate (L/h)	1.00	12.25	12.50	1.25	0.25	1.00	11.25	11.25
	Temperature (°C)	15	15	15	15	15	15	15	15
	Pressure (bar)	1	1	12	1.1	1.1	1.1	1	1
	TDS (mg/L)	5345	12147	11917	638	638	638	13291	12752
	Conductivity (mS/cm)	8.35	18.98	18.62	1.00	1.00	1.00	20.77	19.93
	Osmotic Pressure (bar)	3.09	8.78	8.61	0.46	0.46	0.46	9.60	9.28
	Species Conc. (mg/L)								
	Na^+	971	3646	3577	194	194	194	3884	3884
	Ca^+	847	847	831	42	42	42	928	847
	Cl^-	1498	5625	5519	300	300	300	5992	5992
	SO_4^{-2}	2029	2029	1990	101	101	101	2223	2029

Recovery: 85 %									
	Stream Number	**1**	**2**	**3**	**4**	**5**	**6**	**7**	**8**
	Flow Rate (L/h)	1.00	12.25	12.50	1.25	0.25	1.00	11.25	11.25
	Temperature (°C)	15	15	15	15	15	15	15	15
	Pressure (bar)	1	1	17	1.1	1.1	1.1	1	1
	TDS (mg/L)	5345	18194	17849	967	967	967	19904	19336
	Conductivity (mS/cm)	8.35	28.43	27.89	1.51	1.51	1.51	31.10	30.21
	Osmotic Pressure (bar)	3.09	13.83	13.57	0.74	0.74	0.74	15.12	14.79
	Species Conc. (mg/L)								
	Na^+	971	6024	5910	324	324	324	6473	6473
	Ca^+	847	847	831	42	42	42	928	847
	Cl^-	1498	9294	9118	499	499	499	9987	9987
	SO_4^{-2}	2029	2029	1990	101	101	101	2223	2029

Recovery: 95 %									
	Stream Number	**1**	**2**	**3**	**4**	**5**	**6**	**7**	**8**
	Flow Rate (L/h)	1.00	12.25	12.50	1.25	0.25	1.00	11.25	11.25
	Temperature (°C)	15	15	15	15	15	15	15	15
	Pressure (bar)	1	1	42	1.1	1.1	1.1	1	1
	TDS (mg/L)	5345	48427	47510	2613	2613	2613	52972	52256
	Conductivity (mS/cm)	8.35	75.67	74.23	4.08	4.08	4.08	82.77	81.65
	Osmotic Pressure (bar)	3.09	39.10	38.36	2.11	2.11	2.11	42.74	42.30
	Species Conc. (mg/L)								
	Na^+	971	17914	17575	971	971	971	19420	19420
	Ca^+	847	847	831	42	42	42	928	847
	Cl^-	1498	27637	27114	1498	1498	1498	29960	29960
	SO_4^{-2}	2029	2029	1990	101	101	101	2223	2029

Table A-2 *Mass balance data from Microsoft Excel at various recoveries for operation 12 LMH permeate flux and 30 % instantaneous recovery.*

	Stream Number	1	2	3	4	5	6	7	8
Recovery: 25 %	Flow Rate (L/h)	1.00	3.92	4.17	1.25	0.25	1.00	2.92	2.92
	Temperature (°C)	15	15	15	15	15	15	15	15
	Pressure (bar)	1	1	7	1.1	1.1	1.1	1	1
	TDS (mg/L)	5345	5958	5619	308	308	308	8131	6168
	Conductivity (mS/cm)	8.35	9.31	8.78	0.48	0.48	0.48	12.71	9.64
	Osmotic Pressure (bar)	3.09	3.61	3.40	0.19	0.19	0.19	4.91	3.78
	Species Conc. (mg/L)								
	Na^+	971	1212	1143	65	65	65	1295	1295
	Ca^+	847	847	799	42	42	42	1159	847
	Cl^-	1498	1870	1764	100	100	100	1997	1997
	SO_4^{-2}	2029	2029	1913	101	101	101	2777	2029
Recovery: 50 %	Stream Number	1	2	3	4	5	6	7	8
	Flow Rate (L/h)	1.00	3.92	4.17	1.25	0.25	1.00	2.92	2.92
	Temperature (°C)	15	15	15	15	15	15	15	15
	Pressure (bar)	1	1	8	1.1	1.1	1.1	1	1
	TDS (mg/L)	5345	7184	6776	391	391	391	9806	7814
	Conductivity (mS/cm)	8.35	11.22	10.59	0.61	0.61	0.61	15.32	12.21
	Osmotic Pressure (bar)	3.09	4.63	4.37	0.26	0.26	0.26	6.31	5.16
	Species Conc. (mg/L)								
	Na^+	971	1694	1598	97	97	97	1942	1942
	Ca^+	847	847	799	42	42	42	1159	847
	Cl^-	1498	2614	2466	150	150	150	2996	2996
	SO_4^{-2}	2029	2029	1913	101	101	101	2777	2029
Recovery: 75 %	Stream Number	1	2	3	4	5	6	7	8
	Flow Rate (L/h)	1.00	3.92	4.17	1.25	0.25	1.00	2.92	2.92
	Temperature (°C)	15	15	15	15	15	15	15	15
	Pressure (bar)	1	1	11	1.1	1.1	1.1	1	1
	TDS (mg/L)	5345	10861	10247	638	638	638	14829	12752
	Conductivity (mS/cm)	8.35	16.97	16.01	1.00	1.00	1.00	23.17	19.93
	Osmotic Pressure (bar)	3.09	7.70	7.27	0.46	0.46	0.46	10.49	9.28
	Species Conc. (mg/L)								
	Na^+	971	3140	2963	194	194	194	3884	3884
	Ca^+	847	847	799	42	42	42	1159	847
	Cl^-	1498	4845	4572	300	300	300	5992	5992
	SO_4^{-2}	2029	2029	1913	101	101	101	2777	2029
Recovery: 85 %	Stream Number	1	2	3	4	5	6	7	8
	Flow Rate (L/h)	1.00	3.92	4.17	1.25	0.25	1.00	2.92	2.92
	Temperature (°C)	15	15	15	15	15	15	15	15
	Pressure (bar)	1	1	15	1.1	1.1	1.1	1	1
	TDS (mg/L)	5345	15764	14876	967	967	967	21527	19336
	Conductivity (mS/cm)	8.35	24.63	23.24	1.51	1.51	1.51	33.64	30.21
	Osmotic Pressure (bar)	3.09	11.80	11.14	0.74	0.74	0.74	16.08	14.79
	Species Conc. (mg/L)								
	Na^+	971	5068	4784	324	324	324	6473	6473
	Ca^+	847	847	799	42	42	42	1159	847
	Cl^-	1498	7819	7380	499	499	499	9987	9987
	SO_4^{-2}	2029	2029	1913	101	101	101	2777	2029
Recovery: 95 %	Stream Number	1	2	3	4	5	6	7	8
	Flow Rate (L/h)	1.00	3.92	4.17	1.25	0.25	1.00	2.92	2.92
	Temperature (°C)	15	15	15	15	15	15	15	15
	Pressure (bar)	1	1	34	1.1	1.1	1.1	1	1
	TDS (mg/L)	5345	40279	38019	2613	2613	2613	55016	52256
	Conductivity (mS/cm)	8.35	62.94	59.40	4.08	4.08	4.08	85.96	81.65
	Osmotic Pressure (bar)	3.09	32.29	30.48	2.11	2.11	2.11	44.00	42.30
	Species Conc. (mg/L)								
	Na^+	971	14710	13885	971	971	971	19420	19420
	Ca^+	847	847	799	42	42	42	1159	847
	Cl^-	1498	22693	21421	1498	1498	1498	29960	29960
	SO_4^{-2}	2029	2029	1913	101	101	101	2777	2029

Table A-3 *Mass balance data from Microsoft Excel at various recoveries for operation 24 LMH permeate flux and 10 % instantaneous recovery.*

Recovery: 25 %	Stream Number	1	2	3	4	5	6	7	8
	Flow Rate (L/h)	2.03	24.89	25.40	2.54	0.51	2.03	22.86	22.86
	Temperature (°C)	15	15	15	15	15	15	15	15
	Pressure (bar)	1	1	7	1.1	1.1	1.1	1	1
	TDS (mg/L)	5345	6101	5985	308	308	308	6677	6168
	Conductivity (mS/cm)	8.35	9.53	9.35	0.48	0.48	0.48	10.43	9.64
	Osmotic Pressure (bar)	3.09	3.72	3.65	0.19	0.19	0.19	4.07	3.78
	Species Conc. (mg/L)								
	Na^+	971	1268	1244	65	65	65	1295	1295
	Ca^+	847	847	831	42	42	42	928	847
	Cl^-	1498	1957	1919	100	100	100	1997	1997
	SO_4^{-2}	2029	2029	1990	101	101	101	2223	2029

Recovery: 50 %	Stream Number	1	2	3	4	5	6	7	8
	Flow Rate (L/h)	2.03	24.89	25.40	2.54	0.51	2.03	22.86	22.86
	Temperature (°C)	15	15	15	15	15	15	15	15
	Pressure (bar)	1	1	8	1.1	1.1	1.1	1	1
	TDS (mg/L)	5345	7612	7468	391	391	391	8330	7814
	Conductivity (mS/cm)	8.35	11.89	11.67	0.61	0.61	0.61	13.02	12.21
	Osmotic Pressure (bar)	3.09	4.99	4.89	0.26	0.26	0.26	5.45	5.16
	Species Conc. (mg/L)								
	Na^+	971	1863	1827	97	97	97	1942	1942
	Ca^+	847	847	831	42	42	42	928	847
	Cl^-	1498	2874	2819	150	150	150	2996	2996
	SO_4^{-2}	2029	2029	1990	101	101	101	2223	2029

Recovery: 75 %	Stream Number	1	2	3	4	5	6	7	8
	Flow Rate (L/h)	2.03	24.89	25.40	2.54	0.51	2.03	22.86	22.86
	Temperature (°C)	15	15	15	15	15	15	15	15
	Pressure (bar)	1	1	12	1.1	1.1	1.1	1	1
	TDS (mg/L)	5345	12147	11917	638	638	638	13291	12752
	Conductivity (mS/cm)	8.35	18.98	18.62	1.00	1.00	1.00	20.77	19.93
	Osmotic Pressure (bar)	3.09	8.78	8.61	0.46	0.46	0.46	9.60	9.28
	Species Conc. (mg/L)								
	Na^+	971	3646	3577	194	194	194	3884	3884
	Ca^+	847	847	831	42	42	42	928	847
	Cl^-	1498	5625	5519	300	300	300	5992	5992
	SO_4^{-2}	2029	2029	1990	101	101	101	2223	2029

Recovery: 85 %	Stream Number	1	2	3	4	5	6	7	8
	Flow Rate (L/h)	2.03	24.89	25.40	2.54	0.51	2.03	22.86	22.86
	Temperature (°C)	15	15	15	15	15	15	15	15
	Pressure (bar)	1	1	17	1.1	1.1	1.1	1	1
	TDS (mg/L)	5345	18194	17849	967	967	967	19904	19336
	Conductivity (mS/cm)	8.35	28.43	27.89	1.51	1.51	1.51	31.10	30.21
	Osmotic Pressure (bar)	3.09	13.83	13.57	0.74	0.74	0.74	15.12	14.79
	Species Conc. (mg/L)								
	Na^+	971	6024	5910	324	324	324	6473	6473
	Ca^+	847	847	831	42	42	42	928	847
	Cl^-	1498	9294	9118	499	499	499	9987	9987
	SO_4^{-2}	2029	2029	1990	101	101	101	2223	2029

Recovery: 95 %	Stream Number	1	2	3	4	5	6	7	8
	Flow Rate (L/h)	2.03	24.89	25.40	2.54	0.51	2.03	22.86	22.86
	Temperature (°C)	15	15	15	15	15	15	15	15
	Pressure (bar)	1	1	42	1.1	1.1	1.1	1	1
	TDS (mg/L)	5345	48427	47510	2613	2613	2613	52972	52256
	Conductivity (mS/cm)	8.35	75.67	74.23	4.08	4.08	4.08	82.77	81.65
	Osmotic Pressure (bar)	3.09	39.10	38.36	2.11	2.11	2.11	42.74	42.30
	Species Conc. (mg/L)								
	Na^+	971	17914	17575	971	971	971	19420	19420
	Ca^+	847	847	831	42	42	42	928	847
	Cl^-	1498	27637	27114	1498	1498	1498	29960	29960
	SO_4^{-2}	2029	2029	1990	101	101	101	2223	2029

Table A-4 *Mass balance data from Microsoft Excel at various recoveries for operation 24 LMH permeate flux and 30 % instantaneous recovery.*

Recovery: 25 %	Stream Number	1	2	3	4	5	6	7	8
	Flow Rate (L/h)	2.03	7.96	8.47	2.54	0.51	2.03	5.93	5.93
	Temperature (°C)	15	15	15	15	15	15	15	15
	Pressure (bar)	1	1	7	1.1	1.1	1.1	1	1
	TDS (mg/L)	5345	5958	5619	308	308	308	8131	6168
	Conductivity (mS/cm)	8.35	9.31	8.78	0.48	0.48	0.48	12.71	9.64
	Osmotic Pressure (bar)	3.09	3.61	3.40	0.19	0.19	0.19	4.91	3.78
	Species Conc. (mg/L)								
	Na^+	971	1212	1143	65	65	65	1295	1295
	Ca^+	847	847	799	42	42	42	1159	847
	Cl^-	1498	1870	1764	100	100	100	1997	1997
	SO_4^{-2}	2029	2029	1913	101	101	101	2777	2029

Recovery: 50 %	Stream Number	1	2	3	4	5	6	7	8
	Flow Rate (L/h)	2.03	7.96	8.47	2.54	0.51	2.03	5.93	5.93
	Temperature (°C)	15	15	15	15	15	15	15	15
	Pressure (bar)	1	1	8	1.1	1.1	1.1	1	1
	TDS (mg/L)	5345	7184	6776	391	391	391	9806	7814
	Conductivity (mS/cm)	8.35	11.22	10.59	0.61	0.61	0.61	15.32	12.21
	Osmotic Pressure (bar)	3.09	4.63	4.37	0.26	0.26	0.26	6.31	5.16
	Species Conc. (mg/L)								
	Na^+	971	1694	1598	97	97	97	1942	1942
	Ca^+	847	847	799	42	42	42	1159	847
	Cl^-	1498	2614	2466	150	150	150	2996	2996
	SO_4^{-2}	2029	2029	1913	101	101	101	2777	2029

Recovery: 75 %	Stream Number	1	2	3	4	5	6	7	8
	Flow Rate (L/h)	2.03	7.96	8.47	2.54	0.51	2.03	5.93	5.93
	Temperature (°C)	15	15	15	15	15	15	15	15
	Pressure (bar)	1	1	11	1.1	1.1	1.1	1	1
	TDS (mg/L)	5345	10861	10247	638	638	638	14829	12752
	Conductivity (mS/cm)	8.35	16.97	16.01	1.00	1.00	1.00	23.17	19.93
	Osmotic Pressure (bar)	3.09	7.70	7.27	0.46	0.46	0.46	10.49	9.28
	Species Conc. (mg/L)								
	Na^+	971	3140	2963	194	194	194	3884	3884
	Ca^+	847	847	799	42	42	42	1159	847
	Cl^-	1498	4845	4572	300	300	300	5992	5992
	SO_4^{-2}	2029	2029	1913	101	101	101	2777	2029

Recovery: 85 %	Stream Number	1	2	3	4	5	6	7	8
	Flow Rate (L/h)	2.03	7.96	8.47	2.54	0.51	2.03	5.93	5.93
	Temperature (°C)	15	15	15	15	15	15	15	15
	Pressure (bar)	1	1	15	1.1	1.1	1.1	1	1
	TDS (mg/L)	5345	15764	14876	967	967	967	21527	19336
	Conductivity (mS/cm)	8.35	24.63	23.24	1.51	1.51	1.51	33.64	30.21
	Osmotic Pressure (bar)	3.09	11.80	11.14	0.74	0.74	0.74	16.08	14.79
	Species Conc. (mg/L)								
	Na^+	971	5068	4784	324	324	324	6473	6473
	Ca^+	847	847	799	42	42	42	1159	847
	Cl^-	1498	7819	7380	499	499	499	9987	9987
	SO_4^{-2}	2029	2029	1913	101	101	101	2777	2029

Recovery: 95 %	Stream Number	1	2	3	4	5	6	7	8
	Flow Rate (L/h)	2.03	7.96	8.47	2.54	0.51	2.03	5.93	5.93
	Temperature (°C)	15	15	15	15	15	15	15	15
	Pressure (bar)	1	1	34	1.1	1.1	1.1	1	1
	TDS (mg/L)	5345	40279	38019	2613	2613	2613	55016	52256
	Conductivity (mS/cm)	8.35	62.94	59.40	4.08	4.08	4.08	85.96	81.65
	Osmotic Pressure (bar)	3.09	32.29	30.48	2.11	2.11	2.11	44.00	42.30
	Species Conc. (mg/L)								
	Na^+	971	14710	13885	971	971	971	19420	19420
	Ca^+	847	847	799	42	42	42	1159	847
	Cl^-	1498	22693	21421	1498	1498	1498	29960	29960
	SO_4^{-2}	2029	2029	1913	101	101	101	2777	2029

A.3. RO unit diagrams and photos

A.3.1. Process Flow Diagram (PFD)

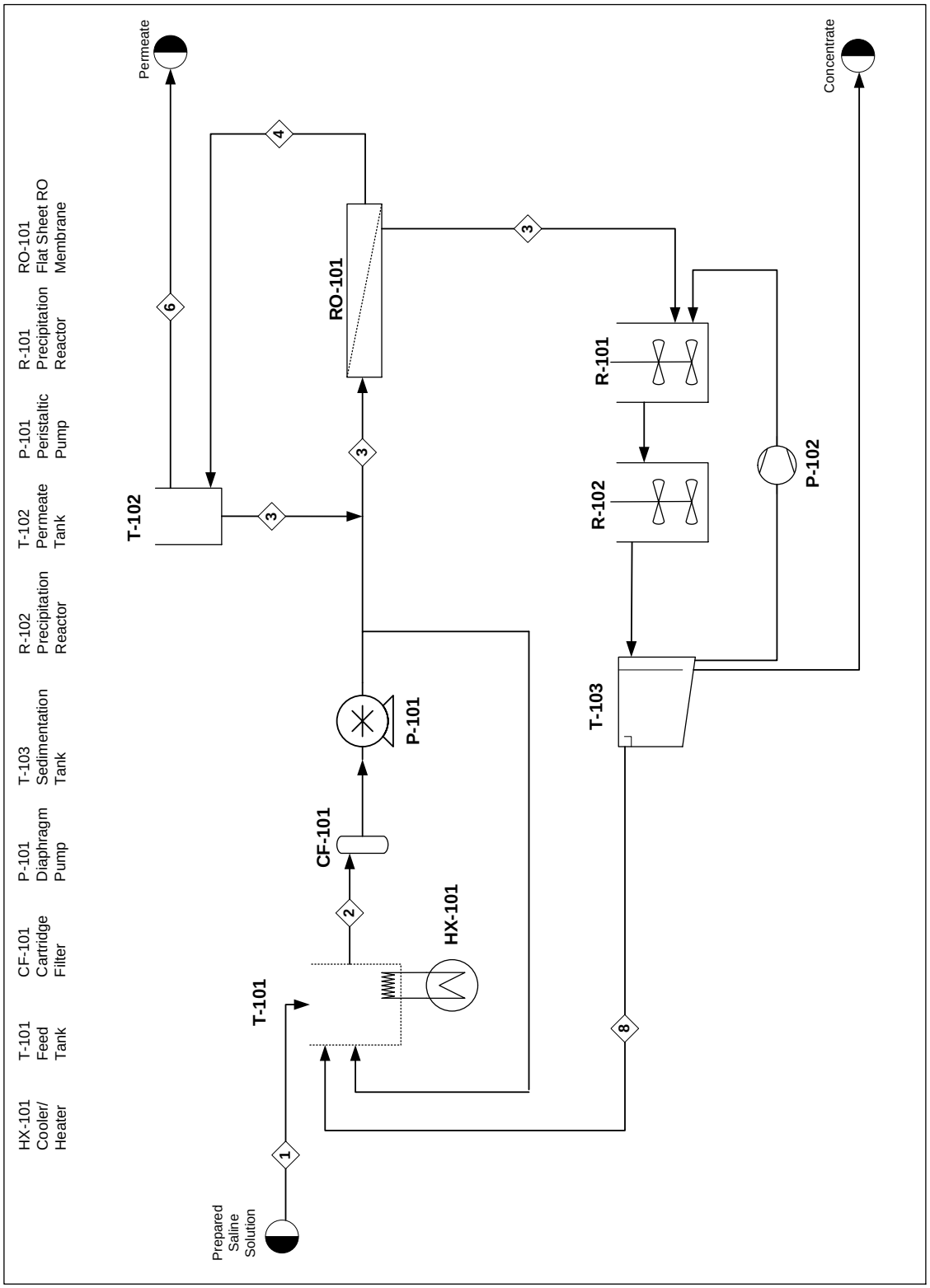

Figure A-2 *Process Flow Diagram (PFD)*

A.3.2. Piping and Instrumentation Diagram (P&ID)

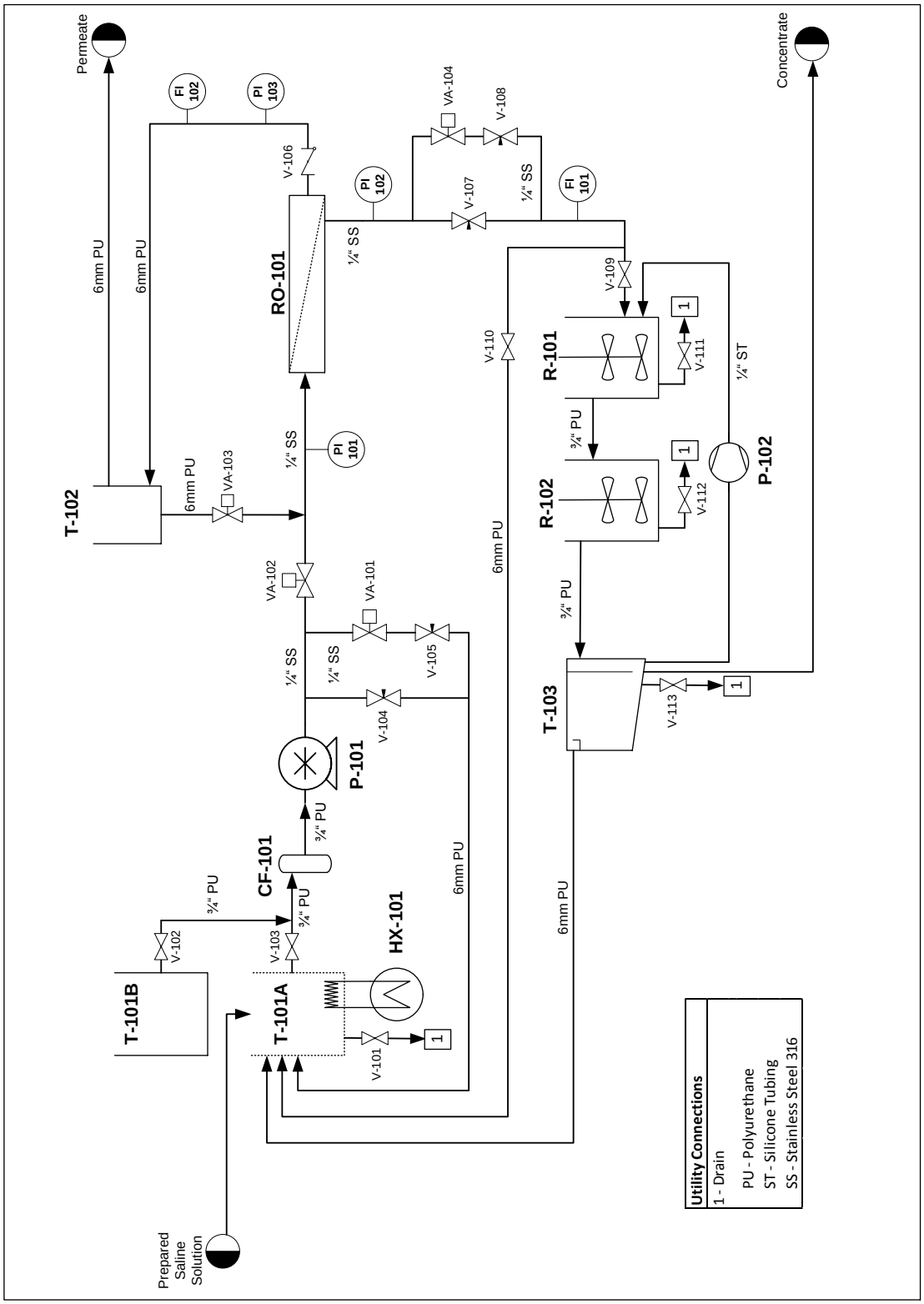

Figure A-3 *Piping and Instrumentation Diagram (P&ID)*

A.3.3.Photograph

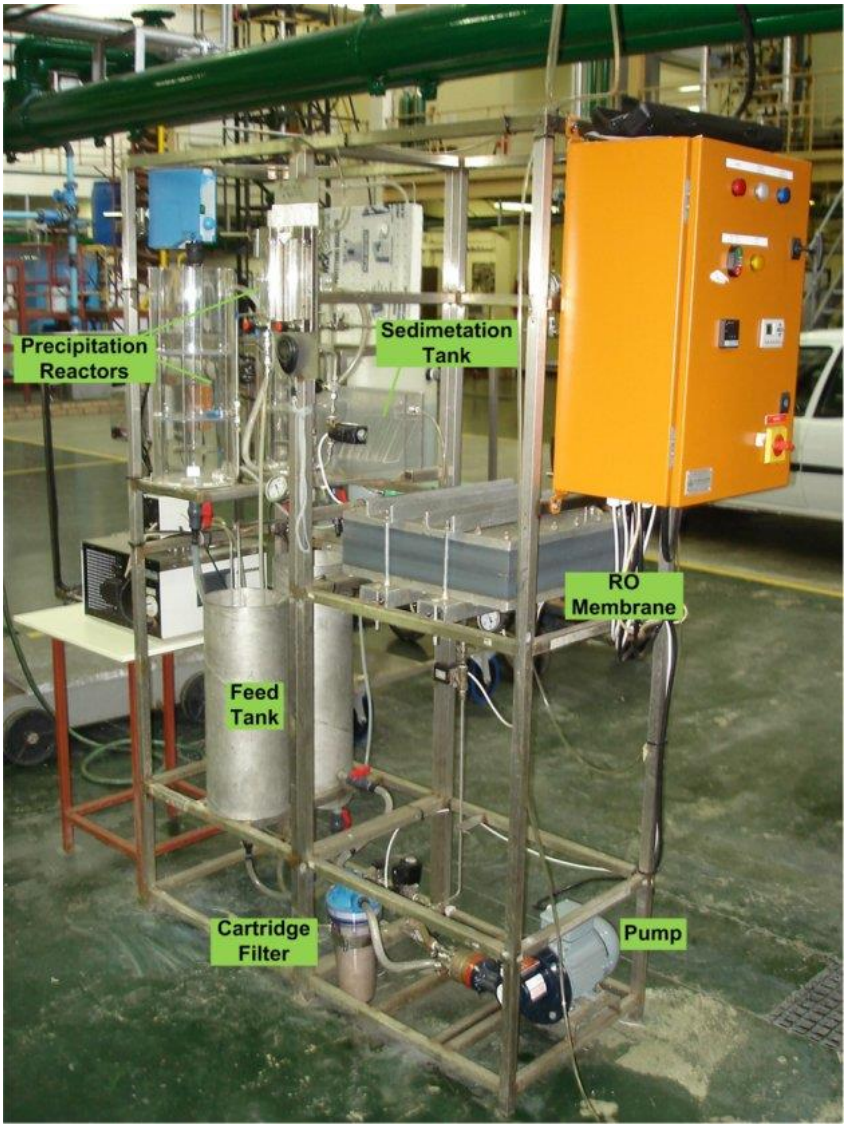

Figure A-4 *Photograph of lab-scale desalination unit*

A.4. Plate and frame RO membrane test cell

Plate and frame flat sheet RO membranes test cells (a typical design is shown in Figure 3-4) are commonly used for calcium sulphate scaling laboratory studies, since the smallest commercially available brackish ultra-low pressure 2.5" DOW *Filmtec XLE - 2540* spiral RO membrane is designed for an average permeate flow of 58 L/h (DOW Filmtec, 2011), which is well beyond a lab-scale plant size. In Table A-5the cross flow velocities, membrane areas and channel depth for each plate and frame flat sheet membrane test cell are given.

Table A-5 *Comparison of previous studies investigating calcium sulphate scaling using a flat sheet plate and frame RO laboratory systems.*

Reference	Cross Flow Velocity (m/s)	Membrane Area (cm^2)	Channel Depth (mm)
Li et al. (2006)	0.011	144.5	1.00
Bartman et al. (2011)	0.043	26.0	2.66
Lyster et al. (2009)	0.043	26.0	2.54
Rahardianto et al. (2008)	0.048 or 0.091	19.8	2.66
Uchymiak et al. (2008)	0.092	20.0	2.50
Rahardianto et al. (2007)	0.11	19.8	2.66
Shih et al. (2005)	0.11	19.8	2.66
Rahardianto et al. (2006)	0.1 - 0.3	19.8	2.66
Oh et al. (2009)	0.4	27.4	3.00

The design of the flat sheet plate and frame RO membrane test cell was critical for the success of the study, with a design specification of 1.0 -2.5 L/h of permeate. Initial design estimates showed that the required active RO membrane area is about 1000 cm^2 for fluxes varying between 12 and 24 LMH as shown in Table A-5. Generally only a single flow channel was considered in previous studies (refer to Table A-5), however the membrane area was much smaller than 1000 cm^2. In order to maintain a constant cross flow velocity over the entire membrane area, a tortuous tapered flow channel design was considered. As the feed water moves along the membrane the flow rate decreases since a certain portion of water permeates through the membrane (Al-Bastaki and Abbas, 2003), thus the tortuous flow should consist of parallel flow channels decreasing in width from feed entry to brine exit.

Table A-6 *Initial calulations to determine the active RO membrane area, based on the intial design specifcations.*

Flux (LMH)	Membrane Area (m^2)	Membrane Area (cm^2)	Permeate Flow (L/h)
12	0.0001	1	0.0012
12	0.001	10	0.012
12	0.01	100	0.12
12	0.1	1000	1.2
12	1	10000	12
18	0.0001	1	0.0018
18	0.001	10	0.018
18	0.01	100	0.18
18	0.1	1000	1.8
18	1	10000	18
24	0.0001	1	0.0024
24	0.001	10	0.024
24	0.01	100	0.24
24	0.1	1000	2.4
24	1	10000	24

The final design of the membrane test cell is given in Figure A-5 and Figure A-8, showing the feed-brine and permeate parts respectively. Actual photographs are shown in Figure A-6 and Figure A-7. In Figure A-5 the o-ring grooves are visible, firstly the two 4mm grooves for the 5mm oring around the entire flow channel to prevent any fluid from leaking out of the membrane block and then the 3 mm o-ring groves separating the individual flow channels. Further, the tapered flow path is shown with a decreasing channel width from 50 to 40 mm, resulting in a total active membrane area of 0.106 m^2. The design calculation showed that a decrease in channel depth greatly increases the instantaneous recovery. A final channel depth of 1mm was chosen, due to limitation during the milling process, with the main design data shown in Table A-7.. The permeate PVC block has a 344 x 307 x 1 mm groove as shown in Figure A-8, fitted with an stainless steel perforated plate (0.4 mm holes at 1.5mm triangular pitch) as the permeate spacer. Underneath 2 x 1 mm deep grooves allow evenly distributed distribution of permeate, eventually flowing towards the exit. 20mm steel plates are placed on either side of the membrane test cell to provide a rigid support. The entire membrane test cell is bolted together with 22 M8 high tensile galvanised iron bolts. High operating pressure result in large forces acting on the entire block, 75mm channel irons were used provide additional support by pressing the two blocks firmly together.

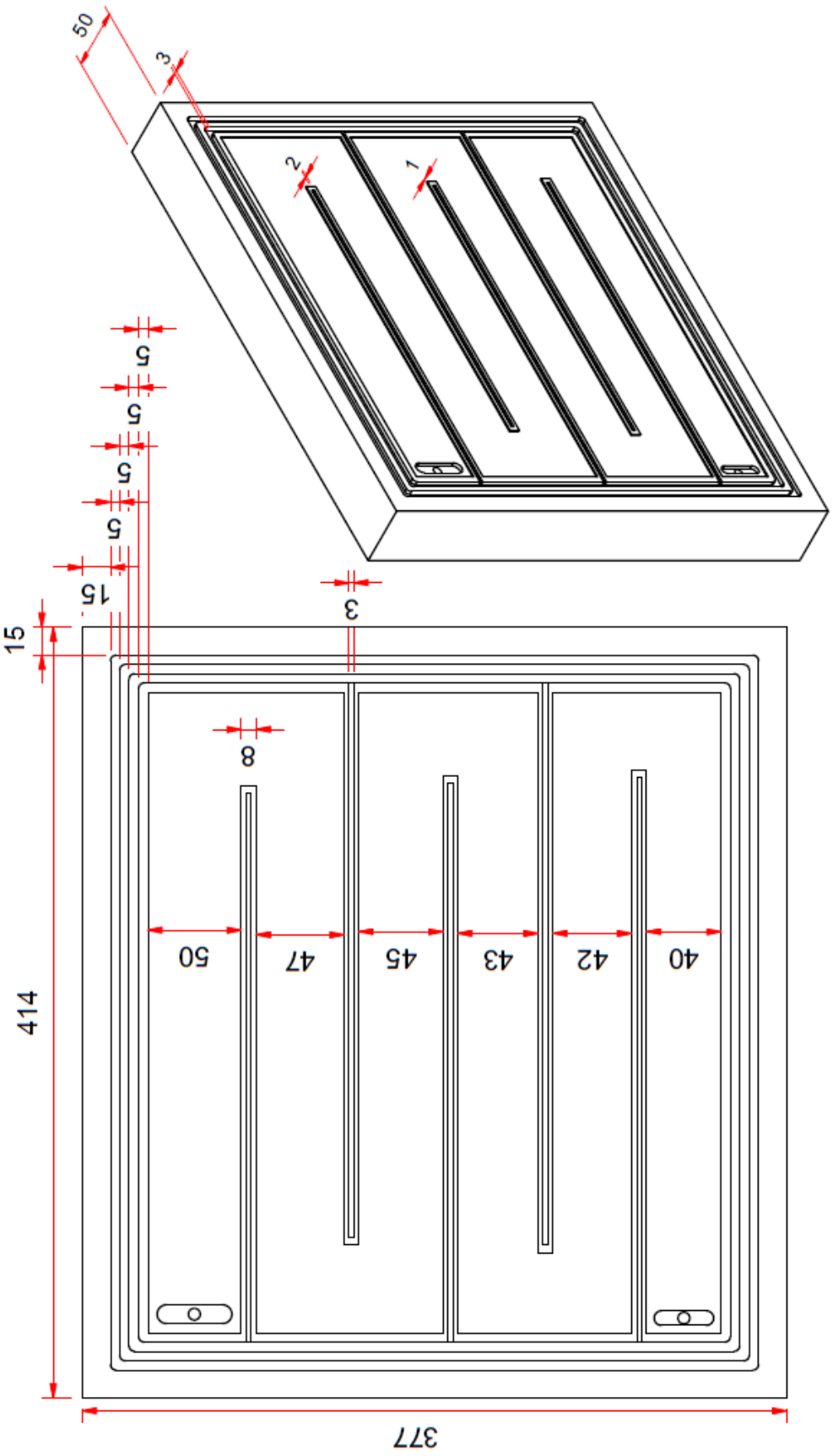

Figure A-5 *CAD drawing of the actual PVC feed part, showing the tapered feed-brine flow channel and oring groves.*

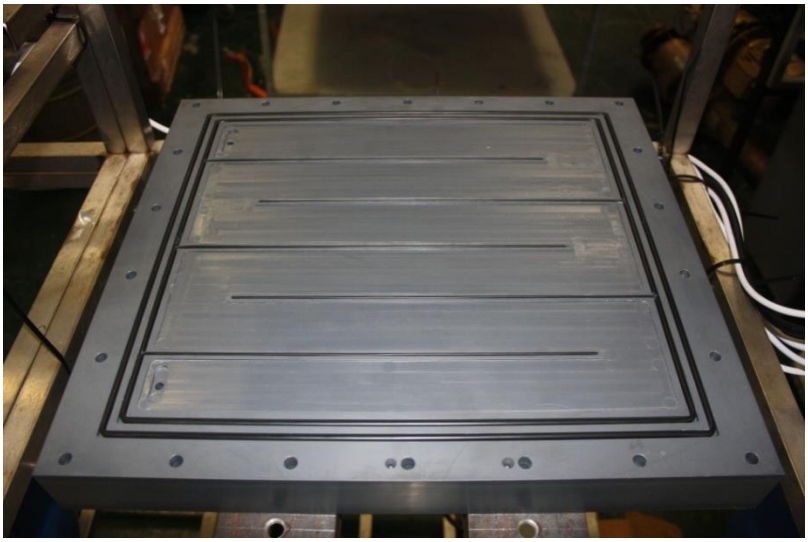

Figure A-6 *Photograph of feed-brine PVC part in the flat sheet RO membrane test cell.*

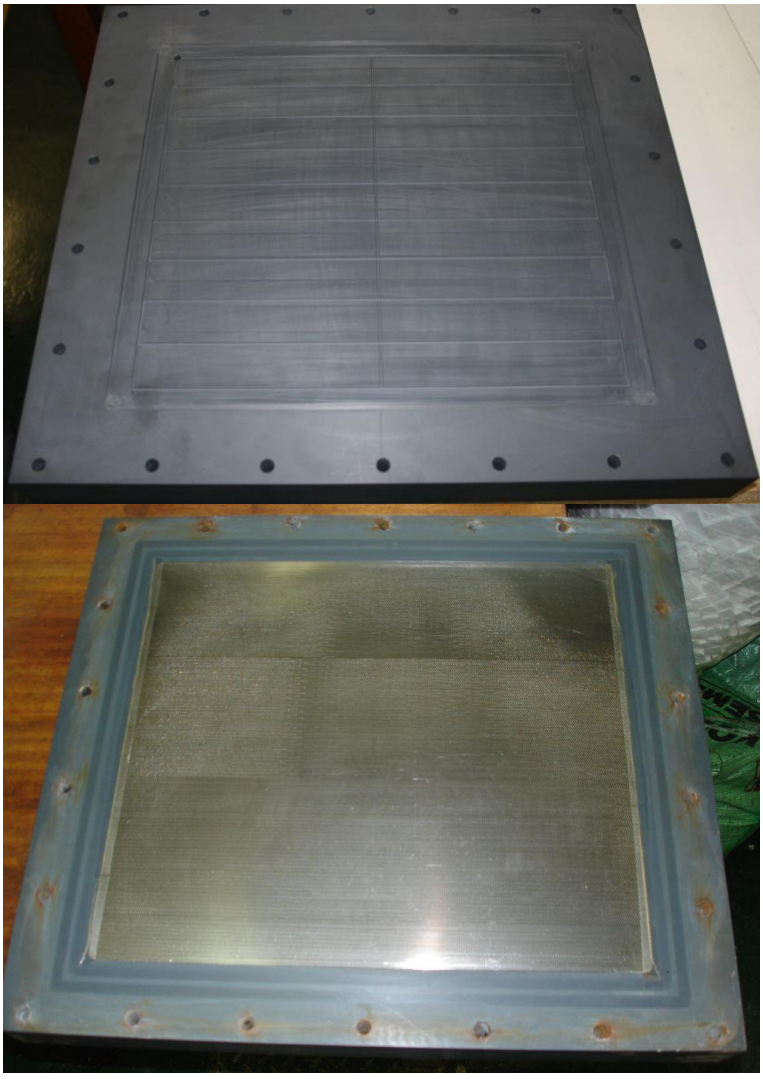

Figure A-7 *Photographs of PVC permeate part in the flat sheet RO membrane test cell, without and with perforated stainless steel permeate spacer.*

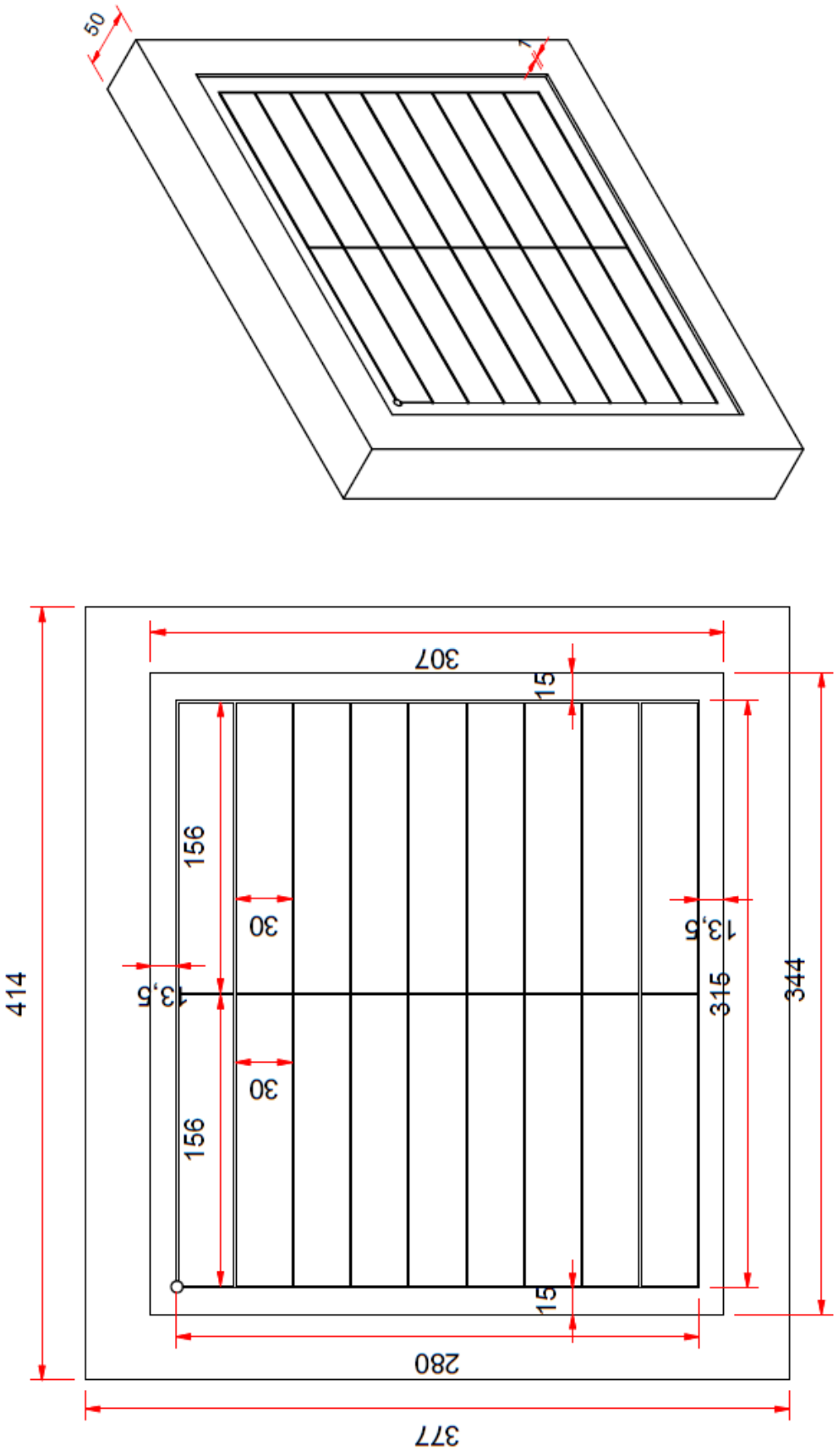

Figure A-8 *CAD drawing of the actual PVC permeate part in the flat sheet RO membrane test cell, showing groves that allow permeate to collect and flow towards the exit.*

Table A-7 *Detailed RO membrane test cell feed-concentrate flow channel design, showing the flowrates, recoveries and cross-flow velocities for each pass.*

Permeate Flux: 12 LMH Inst. Rec.: 10 %	Pass	Channel Depth (m)	Channel Width (m)	Mem. Area (m²)	CS Area (m²)	Flow In (L/h)	Permeate Produced (L/h)	Flow Out (L/h)	Recovery per pass (%)	Overall Rec. (%)	CF Velocity In (m/s)	CF Velocity Out (m/s)
	1	0.001	0.050	0.017	0.000050	11.51	0.206	11.30	1.79	1.79	0.064	0.063
	2	0.001	0.048	0.016	0.000048	11.30	0.196	11.11	1.73	3.53	0.066	0.065
	3	0.001	0.045	0.015	0.000045	11.11	0.186	10.92	1.67	5.20	0.069	0.067
	4	0.001	0.043	0.015	0.000043	10.92	0.178	10.75	1.63	6.82	0.071	0.069
	5	0.001	0.042	0.014	0.000042	10.75	0.173	10.57	1.61	8.44	0.071	0.070
	6	0.001	0.040	0.014	0.000040	10.57	0.165	10.41	1.56	10.00	0.073	0.072

Permeate Flux: 12 LMH Inst. Rec.: 30 %	Pass	Channel Depth (m)	Channel Width (m)	Mem. Area (m²)	CS Area (m²)	Flow In (L/h)	Permeate Produced (L/h)	Flow Out (L/h)	Recovery per pass (%)	Overall Rec (%)	Velocity In (m/s)	Velocity Out (m/s)
	1	0.001	0.050	0.017	0.000050	4.17	0.206	3.96	4.95	4.95	0.023	0.022
	2	0.001	0.048	0.016	0.000048	3.96	0.196	3.77	4.95	9.90	0.023	0.022
	3	0.001	0.045	0.015	0.000045	3.77	0.186	3.58	4.93	14.83	0.023	0.022
	4	0.001	0.043	0.015	0.000043	3.58	0.178	3.40	4.96	19.79	0.023	0.022
	5	0.001	0.042	0.014	0.000042	3.40	0.173	3.23	5.10	24.89	0.023	0.021
	6	0.001	0.040	0.014	0.000040	3.23	0.165	3.06	5.11	30.00	0.022	0.021

Permeate Flux: 24 LMH Inst. Rec.: 10 %	Pass	Channel Depth (m)	Channel Width (m)	Mem. Area (m²)	CS Area (m²)	Flow In (L/h)	Permeate Produced (L/h)	Flow Out (L/h)	Recovery per pass (%)	Overall Rec (%)	Velocity In (m/s)	Velocity Out (m/s)
	1	0.001	0.050	0.017	0.000050	23.02	0.413	22.61	1.79	1.79	0.128	0.126
	2	0.001	0.048	0.016	0.000048	22.61	0.392	22.22	1.73	3.53	0.132	0.130
	3	0.001	0.045	0.015	0.000045	22.22	0.372	21.85	1.67	5.20	0.137	0.135
	4	0.001	0.043	0.015	0.000043	21.85	0.355	21.49	1.63	6.82	0.141	0.139
	5	0.001	0.042	0.014	0.000042	21.49	0.347	21.14	1.61	8.44	0.142	0.140
	6	0.001	0.040	0.014	0.000040	21.14	0.330	20.81	1.56	10.00	0.147	0.145

Permeate Flux: 24 LMH Inst. Rec.: 30 %	Pass	Channel Depth (m)	Channel Width (m)	Mem. Area (m²)	CS Area (m²)	Flow In (L/h)	Permeate Produced (L/h)	Flow Out (L/h)	Recovery per pass (%)	Overall Rec (%)	Velocity In (m/s)	Velocity Out (m/s)
	1	0.001	0.050	0.017	0.000050	8.34	0.413	7.92	4.95	4.95	0.046	0.044
	2	0.001	0.048	0.016	0.000048	7.92	0.392	7.53	4.95	9.90	0.046	0.044
	3	0.001	0.045	0.015	0.000045	7.53	0.372	7.16	4.93	14.83	0.046	0.044
	4	0.001	0.043	0.015	0.000043	7.16	0.355	6.81	4.96	19.79	0.046	0.044
	5	0.001	0.042	0.014	0.000042	6.81	0.347	6.46	5.10	24.89	0.045	0.043
	6	0.001	0.040	0.014	0.000040	6.46	0.330	6.13	5.11	30.00	0.045	0.043

The effect of instantaneous recovery on flow rate and CF velocity is shown in Figure A-9andFigure A-10, with the corresponding data in Table A-8. It is evident that with decreasing recovery feed-brine flow rate increasing and the CF velocity increases accordingly. This effect is more pronounced at higher permeate fluxes.

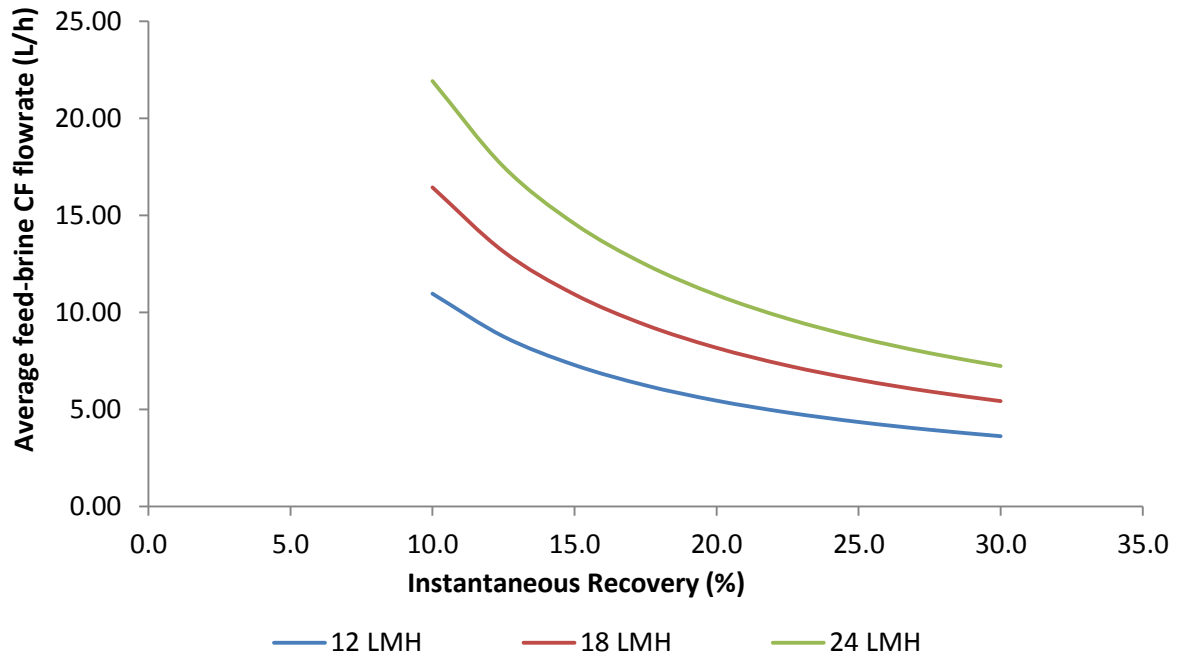

Figure A-9 *The average feed-brine CF flow rate in the membrane flow channel at various instantaneous recoveries, based on calculation with the actual flow channel dimensions.*

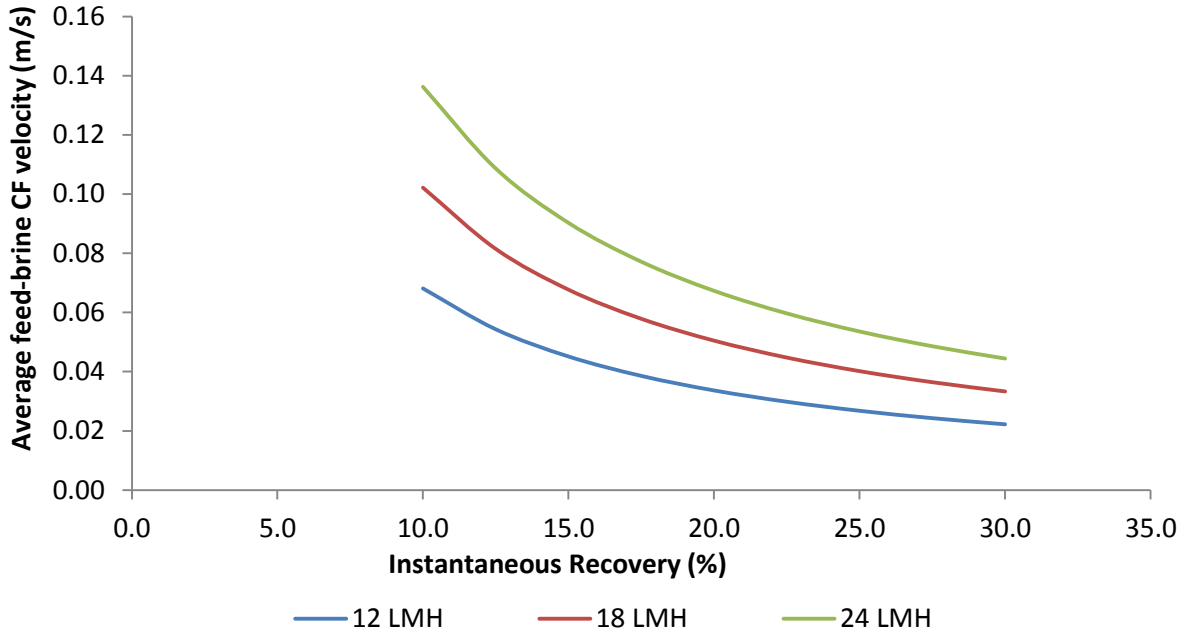

Figure A-10 *The average feed-brine CF velocity in the membrane flow channel at various instantaneous recoveries, based on calculation with the actual flow channel dimensions.*

Table A-8 *The effect of instantanous recovery on flowrates and velocities at the RO test cell channel entry and exit respectively.*

	Flux (12 LMH)				Flux (18 LMH)				Flux (24 LMH)			
	Flowrate (L/h)		CF Velocity (m/s)		Flowrate (L/h)		CF Velocity (m/s)		Flowrate (L/h)		CF Velocity (m/s)	
Inst. Rec. (%)	Feed	Conc.	Channel Entry	Channel Exit	Feed	Conc.	Channel Entry	Channel Exit	Feed	Conc.	Channel Entry	Channel Exit
10.0	11.51	10.41	0.06	0.07	17.27	15.61	0.10	0.11	23.02	20.81	0.13	0.14
12.5	9.31	8.20	0.05	0.06	13.96	12.30	0.08	0.09	18.61	16.40	0.10	0.11
15.0	7.84	6.73	0.04	0.05	11.75	10.10	0.07	0.07	15.67	13.46	0.09	0.09
17.5	6.79	5.68	0.04	0.04	10.18	8.52	0.06	0.06	13.57	11.36	0.08	0.08
20.0	6.00	4.90	0.03	0.03	9.00	7.34	0.05	0.05	12.00	9.79	0.07	0.07
22.5	5.39	4.28	0.03	0.03	8.08	6.43	0.04	0.04	10.78	8.57	0.06	0.06
25.0	4.90	3.80	0.03	0.03	7.35	5.69	0.04	0.04	9.80	7.59	0.05	0.05
27.5	4.50	3.40	0.03	0.02	6.75	5.09	0.04	0.04	9.00	6.79	0.05	0.05
30.0	4.17	3.06	0.02	0.02	6.25	4.60	0.03	0.03	8.34	6.13	0.05	0.04

A.5. Reactor and settling tank

A.5.1.Seeded gypsum precipitation reactor

The batch experiments suggested that a hydraulic residence time of 120 min to effectively reduce the gypsum saturation index from roughly 1.5 to 1.1 at 15 ˚C (refer to Figure 5-1 and Figure 5-2). Therefore the precipitation reactor in the unit was sized accordingly, to provide a hydraulic residence time of over 120 minutes for an average concentrate flow rate of 12 L/h as shown in Table A-9. The exact reactor design is given Figure A-11, where the red arrows indicate the slurry flow through the reactor. The reactor was manufactured from 5mm think transparent 192 mm ID Perspex tubing, with ½" hose connectors as inlet and outlet. Each reactor was fitted with two horizontal 5mm Perspex baffles, positioned inside the reactor with four 6mm threaded stainless steel rods. The reactors were each agitated with a stirrer *(Camlab, R50D and VelpScientifica, F20100151),* where two 4 blade (dimensions of each blade 18x55mm, 45˚ pitch) stainless steel impellers were fitted to the 6mm stainless steel shaft to create axial flow. Actual photographs of the reactors are shown in Figure A-12.

Table A-9 *Design specifications and main dimensions for precipitation reactors*

	R-101	R-102
Reactor Diameter (m)	0.192	0.192
Total Height (m)	0.5	0.5
Liquid Height (m)	0.45	0.45
Liquid Volume (m^3)	0.013	0.013
Liquid Volume (L)	13	13
Flowrate Avg (L/h)	12	12
Retention time (m)	65	65

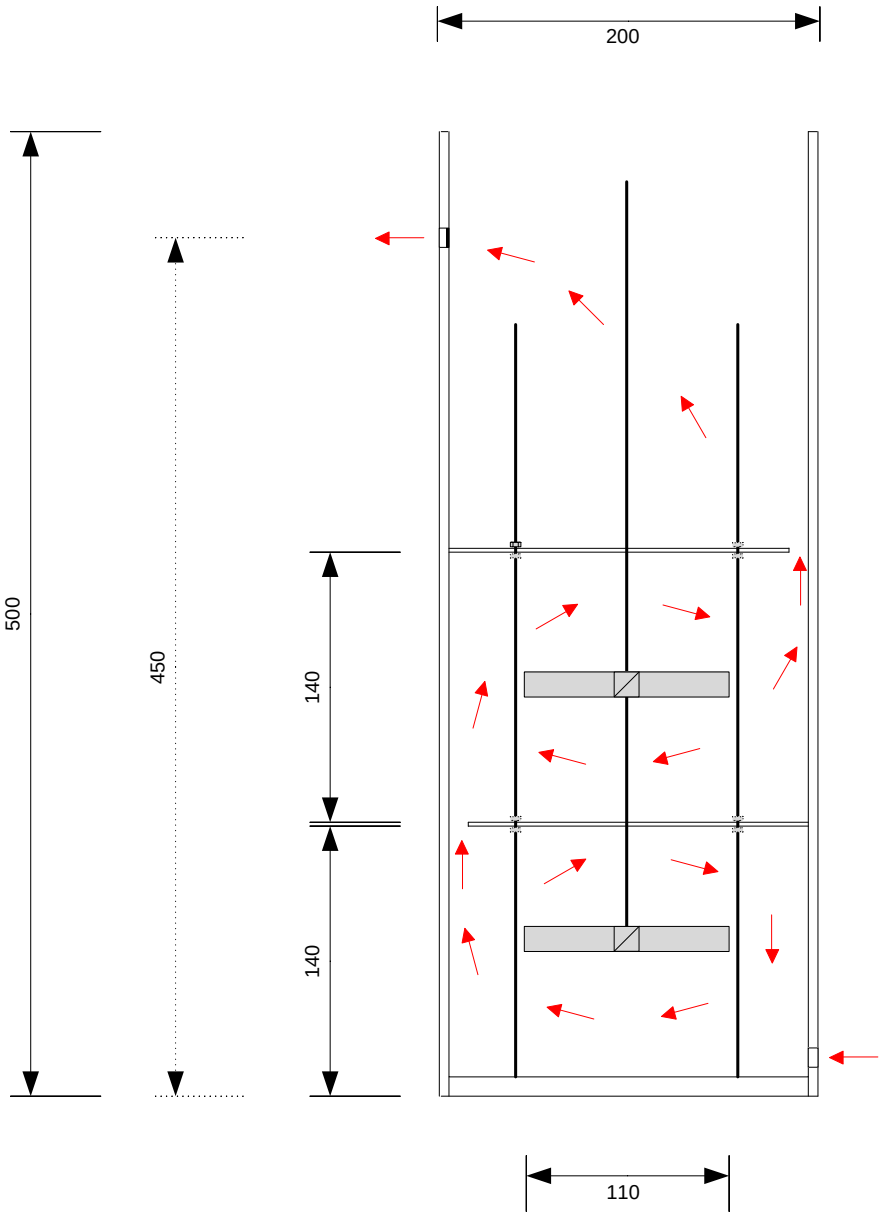

Figure A-11 *Cross sectional diagram showing all the major dimensions of the identical precipitation reactors R-101 and R-102. The red arrows indicate the flow path of the fluid through the reactor.*

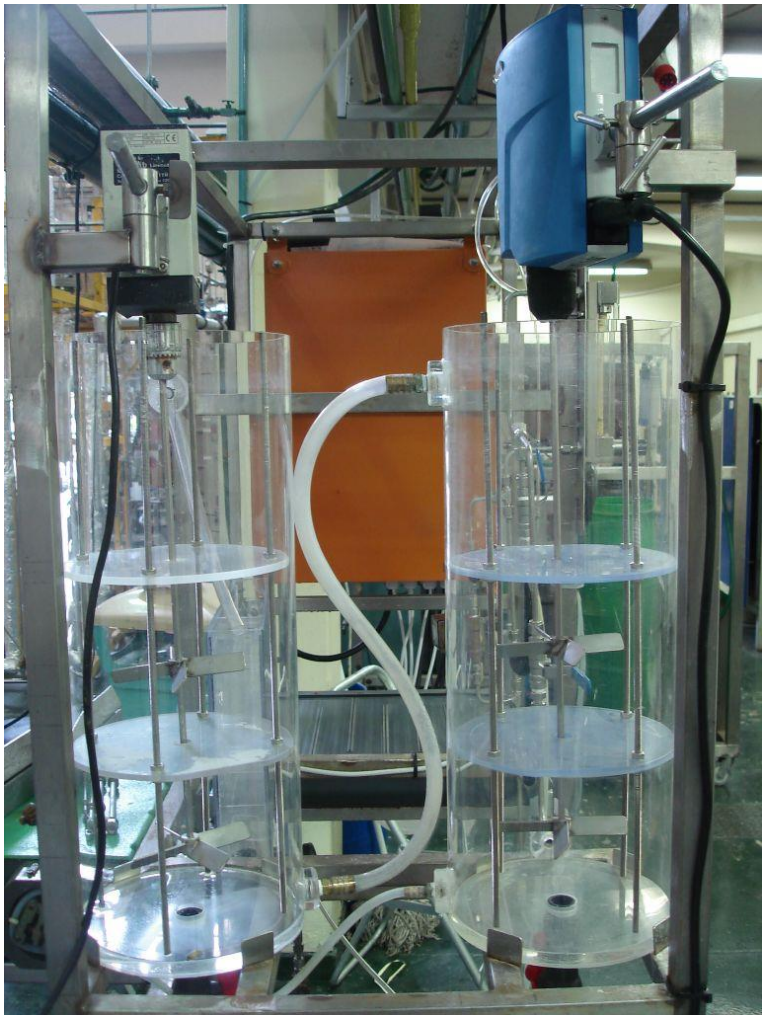

Figure A-12 *Photograph of seeded gypsum precipitation reactors, R-101 (right) and R-102 (left).*

A.5.2. Settling tank

A small scale settling tank was designed and constructed for an average slurry flow rate of 12 L/h. The fresh gypsum seed crystals ranged between 1 - 100 µm, with over 50 % of the particles within 10 - 40µm, as shown in Figure A-13. The particle size distribution was determined with a *Micromeritics Saturn DigiSizer 520*, using isopropanol as a background fluid. Previous studies with seeded gypsum precipitation suggested settling velocities between 0.24 - 6 mm/s (Niewersch, 2011), for particles with similar size. The settling tank was designed with an average settling velocity of 0.24 m/s, since the smallest particles ultimately determine the size.

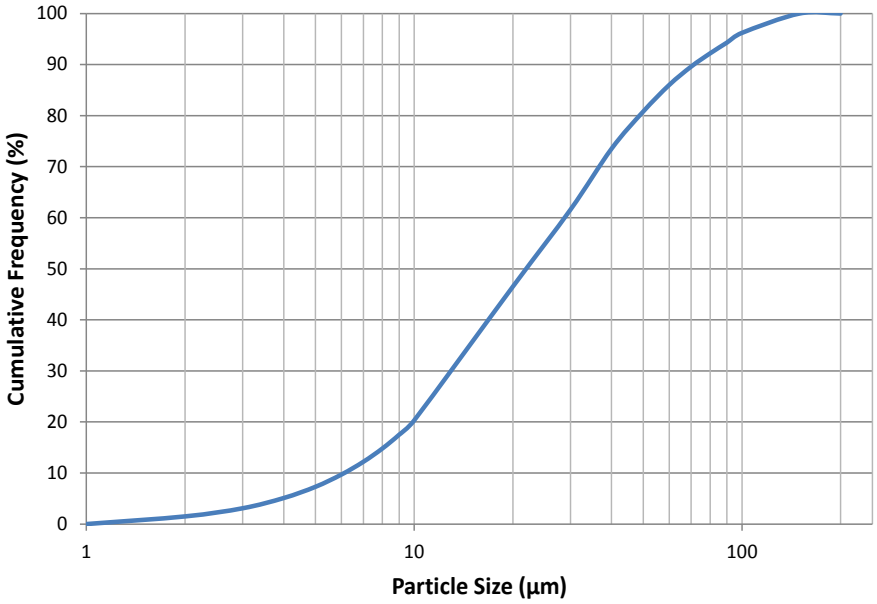

Particle Size (µm)	Frequency (%)
200 - 100	0
150 - 100	3.8
100 - 90	1.9
90 - 80	2.1
80 - 70	2.6
70 - 60	3.6
60 - 50	5.2
50 - 40	7.3
40 - 30	11.9
30 - 20	15.1
20 - 10	26.2
10 - 9	2.8
9 - 8	2.7
8 - 7	2.6
7 - 6	2.5
6 - 5	2.4
5 - 4	2.2
4 - 3	2
3 - 2	1.6
2 - 1	1.5
1 - 0.9	0

Figure A-13 *Cumulative particle size distribution (PSD) of gypsum seed crystals*

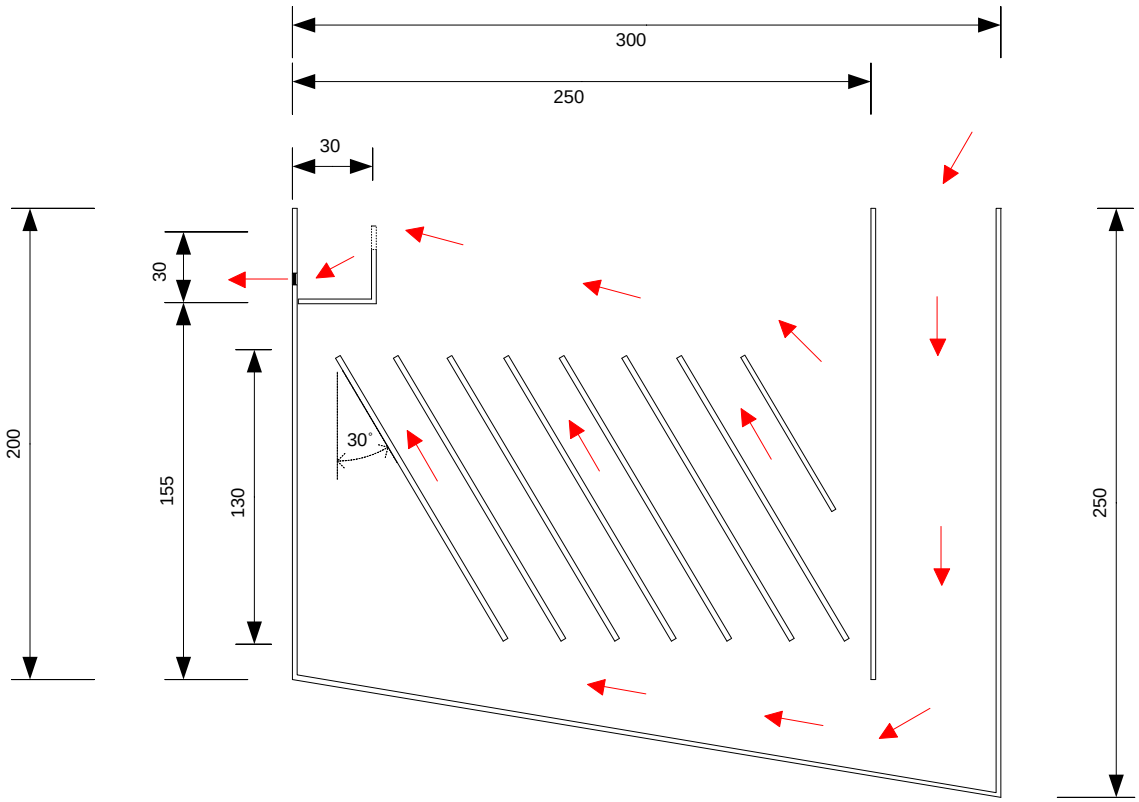

Figure A-14 *Cross sectional diagram showing all the major dimensions of settling tank T-103, with a width of 50 mm. The red arrows indicate the flow path of the fluid through the settling tank.*

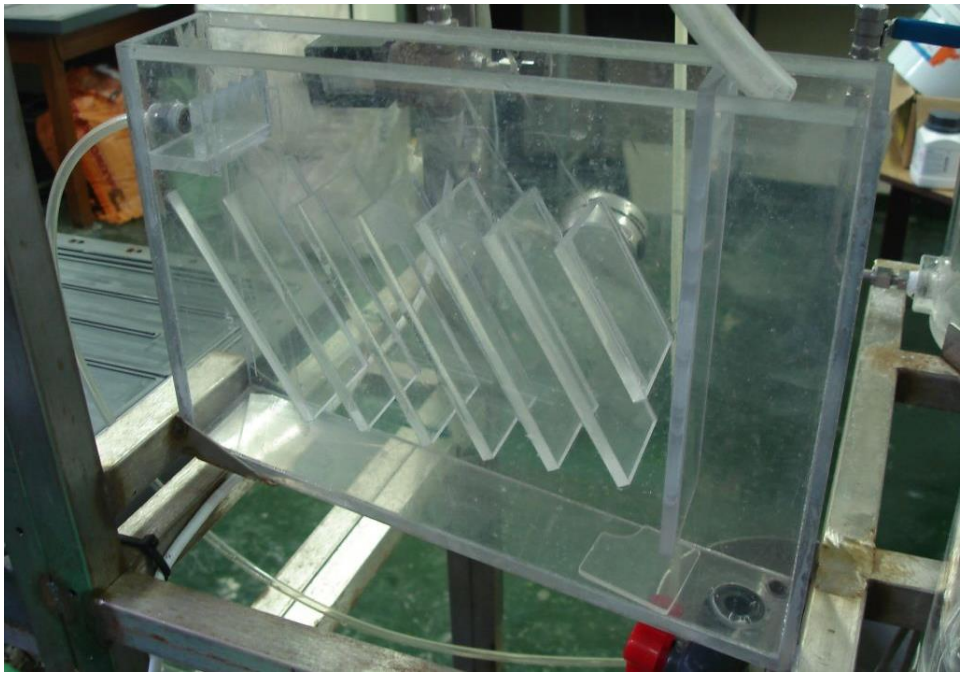

Figure A-15 *Photographs of rectangular settling tank*

A.6. Photographs - additional equipment

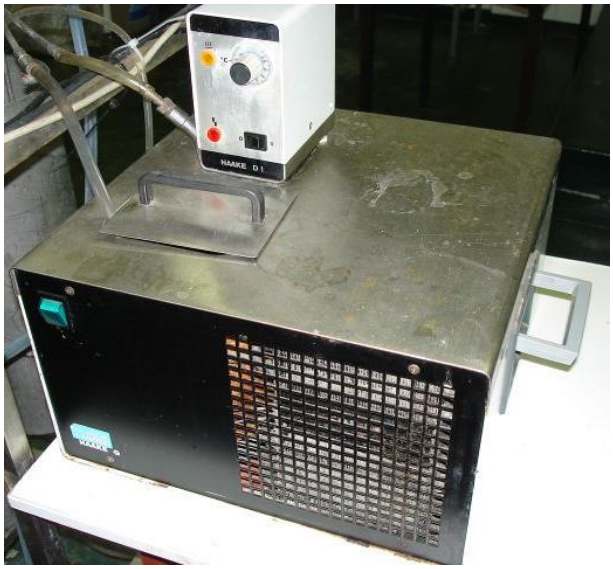

Figure A-16 *Heater/cooler used to maintain a constant process temperature of 15 ˚C by circulating water through a stainless steel coil placed inside the feed tank*

Figure A-17 *Left: RO feed Hydracell F-20 diaphragm pump. Right: Watson Marlow 504U slurry recycle pump.*

Figure A-18 *Filter housing with polypropylene 1 µm filter cartridge*

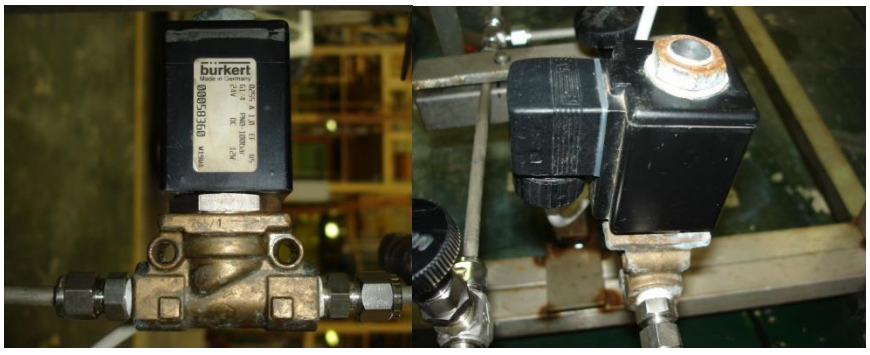

Figure A-19 *Burkert solenoid valves used for periodic permeate flushing*

Appendix B – Initial Tests with NaCl solutions

Initial tests with 4.4 g/L sodium chloride solution, under flushing conditions, showed that high recoveries are possible with non-scaling solutions and continuous operation at high pressures is possible. The effective membrane permeability gradually decreases with increasing overall recovery, as shown in Figure B-1 ; due to the effect of concentrate recycling. The measured conductivities compare well to the predicted *OLI Analyser* values, as shown in Figure B-2 .

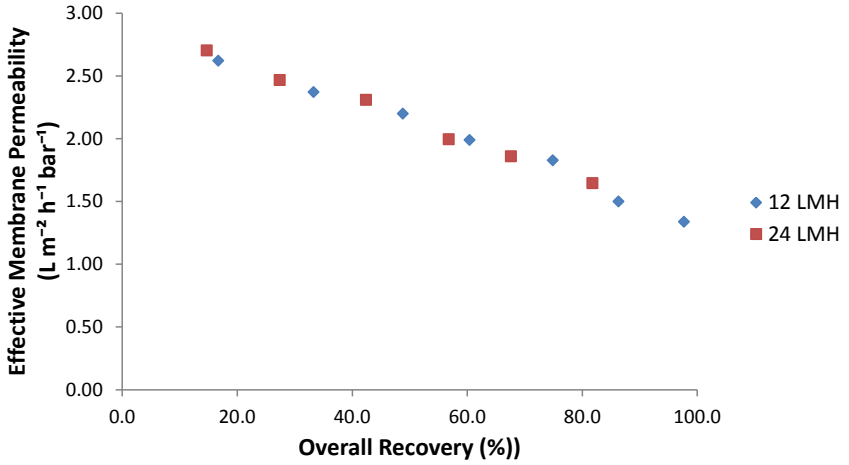

Figure B-1 *Effective membrane permeability for a non-scaling sodium chloride solution, 4.4 g/L NaCl, equivalent to the initial sodium and chloride concentration used in all the calcium sulphate experimental runs.*

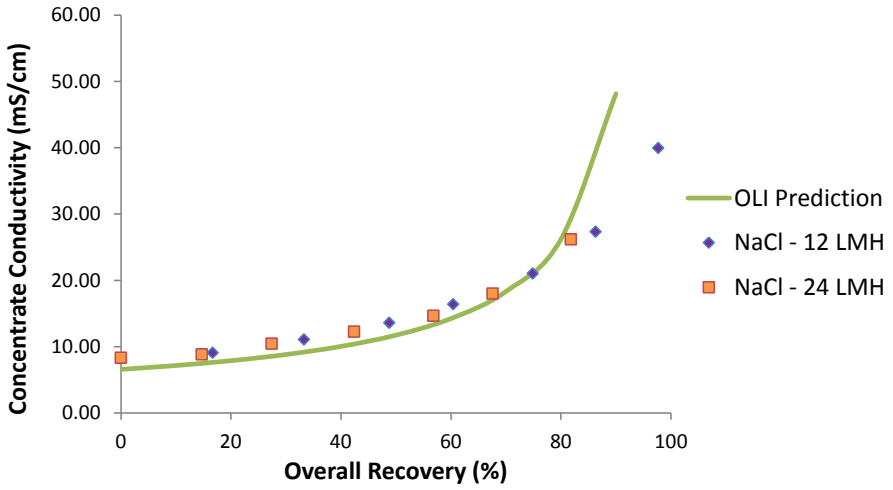

Figure B-2 *RO feed conductivity for sodium chloride solution experimental runs, prepared from 4.4 g/L NaCl, equivalent to the initial sodium and chloride concentration used in all the calcium sulphate experimental runs.*

Appendix C – Raw and processed data

C.1. OLI Analyser ScaleChem 9.0

Table C-1 *OLI data for theoretical non-scaling non-seeding concentrate recycle mode operation at 10 and 30 % instantaneous recovery respectively.*

Overall		Instantaneous		Feed Conc. (mg/L)				Concentrate Conc. (mg/L)				Feed			Concentrate		
Rec (%)	CF	Rec (%)	CF	Na^+	Ca^{+2}	Cl^-	SO_4^{-2}	Na^+	Ca^{+2}	Cl^-	SO_4^{-2}	SI	Cond (mS/cm)	π (bar)	SI	Cond (mS/cm)	π (bar)
0		10	1.09	971	847	1498	2029	1063	927	1639	2221	1.22	5.71	3.25	1.35	6.16	3.54
10	1.09	10	1.09	1063	927	1639	2221	1163	1015	1794	2430	1.35	6.16	3.54	1.50	6.64	3.85
20	1.21	10	1.09	1177	1027	1816	2460	1289	1124	1988	2693	1.52	6.70	3.89	1.68	7.22	4.24
30	1.36	10	1.09	1325	1156	2044	2768	1450	1265	2237	3030	1.73	7.38	4.35	1.91	7.94	4.74
40	1.57	10	1.09	1521	1327	2347	3179	1665	1452	2569	3479	2.01	8.25	4.96	2.22	8.87	5.40
50	1.85	10	1.09	1796	1567	2771	3754	1966	1715	3033	4108	2.41	9.41	5.80	2.65	10.10	6.32
60	2.28	10	1.09	2209	1927	3408	4616	2418	2109	3730	5052	3.00	11.04	7.06	3.29	11.82	7.69
70	2.98	10	1.09	2897	2527	4469	6053	3170	2766	4891	6625	3.96	13.48	9.14	4.34	14.58	9.96
80	4.40	10	1.09	4272	3727	6591	8928	4676	4079	7214	9771	5.82	19.61	13.27	6.35	21.12	14.48
90	8.65	10	1.09	8399	7327	12958	17551	9192	8019	14181	19208	10.89	33.95	25.72	11.80	36.46	28.14

Overall		Instantaneous		Feed Conc. (mg/L)				Concentrate Conc. (mg/L)				Feed			Concentrate		
Rec (%)	CF	Rec (%)	CF	Na^+	Ca^{+2}	Cl^-	SO_4^{-2}	Na^+	Ca^{+2}	Cl^-	SO_4^{-2}	SI	Cond (mS/cm)	π (bar)	SI	Cond (mS/cm)	π (bar)
0		30	1.36	971	847	1498	2029	1325	1156	2044	2768	1.22	5.71	3.25	1.73	7.38	4.35
10	1.09	30	1.36	1063	927	1639	2221	1450	1265	2237	3030	1.35	6.16	3.54	1.91	7.94	4.74
20	1.21	30	1.36	1177	1027	1816	2460	1606	1401	2478	3356	1.52	6.70	3.89	2.14	8.62	5.22
30	1.36	30	1.36	1325	1156	2044	2768	1807	1577	2788	3777	1.73	7.38	4.35	2.43	9.46	5.84
40	1.57	30	1.36	1521	1327	2347	3179	2075	1810	3202	4337	2.01	8.25	4.96	2.81	10.53	6.65
50	1.85	30	1.36	1796	1567	2771	3754	2451	2138	3781	5121	2.41	9.41	5.80	3.34	11.94	7.79
60	2.28	30	1.36	2209	1927	3408	4616	3014	2629	4649	6298	3.00	11.04	7.06	4.13	13.95	9.49
70	2.98	30	1.36	2897	2527	4469	6053	3952	3447	6097	8258	3.96	13.48	9.14	5.40	18.39	12.31
80	4.40	30	1.36	4272	3727	6591	8928	5829	5084	8992	12180	5.82	19.61	13.27	7.81	25.29	17.94
90	8.65	30	1.36	8399	7327	12958	17551	11459	9996	17678	23944	10.89	33.95	25.72	14.33	43.29	35.19

Table C-2 *OLI data for theoretical seeding concentrate recycle mode operation at 10 % instantaneous recovery with a constant feed saturation index of 1.2.*

Overall		Instantaneous		Feed Conc. (mg/L)				Concentrate Conc. (mg/L)				Reactor Overflow Conc. (mg/L)			
Rec (%)	CF	Rec (%)	CF	Na^+	Ca^{+2}	Cl^-	SO_4^{-2}	Na^+	Ca^{+2}	Cl^-	SO_4^{-2}	Na^+	Ca^{+2}	Cl^-	SO_4^{-2}
0		10	1.09	971	847	1498	2029	1063	927	1639	2221	1063	803	1639	1925
10	1.09	10	1.09	1063	852	1639	2042	1163	932	1794	2235	1163	816	1794	1956
20	1.21	10	1.09	1177	869	1816	2083	1289	951	1988	2279	1289	833	1988	1996
30	1.36	10	1.09	1325	891	2044	2135	1450	975	2237	2337	1450	856	2237	2052
40	1.57	10	1.09	1521	918	2347	2200	1665	1005	2569	2408	1665	881	2569	2112
50	1.85	10	1.09	1796	948	2771	2272	1966	1038	3033	2487	1966	916	3033	2195
60	2.28	10	1.09	2209	995	3408	2385	2418	1089	3730	2610	2418	964	3730	2310
70	2.98	10	1.09	2897	1069	4469	2562	3170	1170	4891	2804	3170	1035	4891	2481
80	4.40	10	1.09	4272	1189	6591	2850	4676	1301	7214	3119	4676	1156	7214	2771
90	8.65	10	1.09	8399	1460	12958	3499	9192	1598	14181	3830	9192	1426	14181	3418

Overall		Instantaneous		Feed			Concentrate			Reactor Overflow		
Rec (%)	CF	Rec (%)	CF	SI	Cond (mS/cm)	π (bar)	SI	Cond (mS/cm)	π (bar)	SI	Cond (mS/cm)	π (bar)
0		10	1.09	1.22	5.71	3.34	1.35	6.16	3.54	1.10	5.99	3.43
10	1.09	10	1.09	1.20	6.06	3.47	1.33	6.53	3.78	1.10	6.37	3.68
20	1.21	10	1.09	1.20	6.50	3.76	1.33	7.01	4.09	1.10	6.85	3.99
30	1.36	10	1.09	1.21	7.06	4.13	1.34	7.62	4.49	1.11	7.46	4.38
40	1.57	10	1.09	1.21	7.80	4.60	1.34	8.42	5.02	1.11	8.25	4.89
50	1.85	10	1.09	1.20	8.80	5.26	1.33	9.51	5.73	1.11	9.35	5.60
60	2.28	10	1.09	1.20	10.30	6.23	1.33	11.13	6.79	1.11	10.97	6.64
70	2.98	10	1.09	1.21	12.72	7.81	1.34	13.76	8.52	1.11	13.59	8.35
80	4.40	10	1.09	1.21	17.40	10.89	1.34	18.82	11.90	1.11	18.66	11.68
90	8.65	10	1.09	1.20	30.74	19.90	1.33	33.28	21.79	1.10	33.08	21.48

Table C-3 *OLI data for theoretical seeding concentrate recycle mode operation at 30 % instantaneous recovery with a constant feed saturation index of 1.2.*

Overall		Instantaneous		Feed Conc. (mg/L)				Concentrate Conc. (mg/L)				Reactor Overflow Conc. (mg/L)			
Rec (%)	CF	Rec (%)	CF	Na^{+}	Ca^{+2}	Cl^{-}	SO_4^{-2}	Na^{+}	Ca^{+2}	Cl^{-}	SO_4^{-2}	Na^{+}	Ca^{+2}	Cl^{-}	SO_4^{-2}
0		30	1.36	971	847	1498	2029	1325	1156	2044	2768	1325	838	2044	2008
10	1.09	30	1.36	1063	852	1639	2042	1450	1162	2237	2786	1450	853	2237	2044
20	1.21	30	1.36	1177	869	1816	2083	1606	1186	2478	2841	1606	871	2478	2088
30	1.36	30	1.36	1325	891	2044	2135	1807	1216	2788	2913	1807	896	2788	2147
40	1.57	30	1.36	1521	918	2347	2200	2075	1252	3202	3002	2075	925	3202	2217
50	1.85	30	1.36	1796	948	2771	2272	2451	1293	3781	3100	2451	967	3781	2318
60	2.28	30	1.36	2209	995	3408	2385	3014	1357	4649	3253	3014	1018	4649	2440
70	2.98	30	1.36	2897	1069	4469	2562	3952	1458	6097	3495	3952	1097	6097	2629
80	4.40	30	1.36	4272	1189	6591	2850	5829	1622	8992	3888	5829	1234	8992	2958
90	8.65	30	1.36	8399	1460	12958	3499	11459	1992	17678	4774	11459	1545	17678	3703

Overall		Instantaneous		Feed			Concentrate			Reactor Overflow		
Rec (%)	CF	Rec (%)	CF	SI	Cond (mS/cm)	π (bar)	SI	Cond (mS/cm)	π (bar)	SI	Cond (mS/cm)	π (bar)
0		30	1.36	1.22	5.71	3.34	1.73	7.38	4.35	1.10	6.98	4.07
10	1.09	30	1.36	1.20	6.06	3.47	1.71	7.84	4.66	1.10	7.45	4.38
20	1.21	30	1.36	1.20	6.50	3.76	1.71	8.42	5.04	1.10	8.03	4.75
30	1.36	30	1.36	1.21	7.06	4.13	1.71	9.16	5.54	1.10	8.77	5.23
40	1.57	30	1.36	1.21	7.80	4.60	1.71	10.14	6.19	1.10	9.74	5.85
50	1.85	30	1.36	1.20	8.80	5.26	1.70	11.47	7.08	1.11	11.08	6.72
60	2.28	30	1.36	1.20	10.30	6.23	1.70	13.44	8.40	1.10	13.05	7.99
70	2.98	30	1.36	1.21	12.72	7.81	1.71	16.63	10.56	1.10	16.25	10.08
80	4.40	30	1.36	1.21	17.40	10.89	1.70	22.85	14.79	1.11	22.42	14.19
90	8.65	30	1.36	1.20	30.74	19.90	1.69	40.31	27.26	1.11	39.87	26.42

C.2. Factorial experiments

Table C-4 *Raw and processed data for Run 1*

Run 1	Flush Freq (h^{-1})	Flush Vol (mL)	Soak time (sec)	Flux (LMH)	Inst. Rec. (%)
	2.4	35	20	12	30

Operating Time (min)		0	90	180	270	360	450	540	585	630
Production Time (min)		0	86	172	259	345	431	517	560	603
Gauge Pressure (bar)	Feed	8.2	8.4	8.8	9.2	9.8	10.6	12.4	15.4	25.6
	Concentrate	7.4	7.6	8.0	8.4	9.0	9.8	11.6	14.6	24.8
	Permeate	1.1	1.1	1.1	1.1	1.1	1.1	1.1	1.1	1.1
Spcific Conductivity (mS/cm)	Feed	7.36	8.11	8.95	9.04	9.28	10.02	11.05	14.20	20.45
	Concentrate	8.65	9.26	10.15	10.34	10.28	11.22	11.95	15.40	21.99
	Permeate	-	0.823	0.864	0.884	0.896	0.902	0.924	0.942	0.956
Temperature (˚C)	Feed	13.1	15.0	14.5	14.4	14.8	14.8	14.8	15.1	15.4
	Concentrate	13.0	14.5	15.2	15.6	16.0	15.8	16.0	15.7	15.6
	Permeate	-	13.2	14.3	14.3	14.8	15.0	14.9	14.9	14.7
Flow rate (L/h)	Concentrate	3.00	3.00	2.95	3.00	3.00	2.95	3.05	3.00	3.00
	Permeate	1.25	1.25	1.25	1.25	1.25	1.25	1.25	1.25	1.05
	Feed	4.25	4.25	4.20	4.25	4.25	4.20	4.30	4.25	4.05
Salt Rejection (%)		NA	89.9	90.3	90.2	90.3	91.0	91.6	93.4	95.3
Inst. Recovery (%)		29.4	29.4	29.8	29.4	29.4	29.8	29.1	29.4	25.9
Permeate Flux (LMH)		11.8	11.8	11.8	11.8	11.8	11.8	11.8	11.8	9.9
Osmotic Pressure (bar)	Feed	3.58	3.94	4.35	4.40	4.51	4.87	5.37	6.90	9.94
	Concentrate	4.21	4.50	4.93	5.03	5.00	5.46	5.81	7.49	10.69
	Permeate	-	0.40	0.42	0.43	0.44	0.44	0.45	0.46	0.46
TMP (bar)		-	3.76	3.77	4.13	4.63	5.07	6.38	7.85	15.02
Lp (L/m².h.bar)		-	3.14	3.13	2.85	2.55	2.33	1.85	1.50	0.66
Lp (25°C) (L/m².h.bar)		-	4.47	4.44	4.02	3.55	3.25	2.57	2.09	0.91
Permeate Recovered (mL)		-	1340	1100	1330	1490	1400	1380	770	250
Overall Recovery (%)		0	13	24	38	53	67	80	88	91
Concentration Factor		-	1.1	1.3	1.5	2.0	2.8	4.8	7.9	10.2
Ca+ Conc. (mg/L)	Concentrate	909	934	936	953	959	979	1013	1023	1021
	Overflow Sed. Tank	872	852	845	855	870	882	882	885	889
	Feed	841	842	838	867	851	858	862	872	874

Pemeate Flushing	Total time	630	min
	Time / Flush Cycle	1566	sec
	Total Flushes	24	
	Flushing Time	9	sec
	Flushing Flowrate	14	L/h
	Total Flushing Volume	0.84	L
	Total Feed	10.0	L
	Total Permeate	9.1	L
PPR (L/h)	Calculated	1.14	L/h
	Measured	0.86	L/h

Table C-5 *Raw and processed data for Run 2*

Run 2	Flush Freq (h^{-1})	Flush Vol (mL)	Soak time (sec)	Flux (LMH)	Inst. Rec. (%)
	6	35	20	12	10

Operating Time (min)		0	90	180	270	360	450	545
Production Time (min)		0	81	162	243	324	405	491
Gauge Pressure (bar)	Feed	7.2	8.2	9.4	10.2	12.2	16.6	26.8
	Concentrate	6.2	7.5	10.2	11.0	13.0	17.4	27.6
	Permeate	1.1	1.1	1.1	1.1	1.1	1.1	1.1
Spcific Conductivity (mS/cm)	Feed	7.59	8.56	9.56	10.52	12.56	14.50	18.12
	Concentrate	8.89	9.96	10.56	11.72	13.86	15.90	19.62
	Permeate	-	0.823	0.856	0.887	0.912	0.956	0.986
Temperature (˚C)	Feed	13.4	14.2	15.2	15.1	15.4	15.3	15.6
	Concentrate	14.2	14.9	15.4	15.6	15.9	15.7	15.6
	Permeate	-	14.2	15.1	15.4	15.6	15.6	15.7
Flow rate (L/h)	Concentrate	11.50	11.50	11.50	11.50	11.50	11.40	11.00
	Permeate	1.25	1.25	1.25	1.25	1.25	1.25	0.80
	Feed	12.75	12.75	12.75	12.75	12.75	12.65	11.80
Salt Rejection (%)		NA	90.4	91.0	91.6	92.7	93.4	94.6
Inst. Recovery (%)		9.8	9.8	9.8	9.8	9.8	9.9	6.8
Permeate Flux (LMH)		11.8	11.8	11.8	11.8	11.8	11.8	7.5
Osmotic Pressure (bar)	Feed	3.69	4.16	4.65	5.11	6.11	7.05	8.81
	Concentrate	4.32	4.84	5.13	5.70	6.74	7.73	9.54
	Permeate	-	0.40	0.42	0.43	0.44	0.46	0.48
TMP (bar)		-	2.61	4.23	4.53	5.52	8.98	17.41
Lp (L/m².h.bar)		-	4.52	2.79	2.61	2.14	1.31	0.43
Lp (25°C) (L/m².h.bar)		-	4.56	4.12	3.63	2.95	1.82	0.60
Permeate Recovered (mL)		-	1750	1650	1620	1660	1480	590
Overall Recovery (%)		0	18	34	50	67	82	88
Concentration Factor		-	1.2	1.5	1.9	2.9	5.1	7.6
Ca+ Conc. (mg/L)	Concentrate	910	922	965	966	1015	1056	1052
	Overflow Sed. Tank	840	848	860	861	900	897	923
	Feed	867	872	854	884	885	911	936

Pemeate Flushing	Total time	545	min
	Time / Flush Cylce	666	sec
	Total Flushes	49	
	Flushing Time	9	sec
	Flushing Flowrate	14	L/h
	Total Flushing Volume	1.72	L
	Total Feed	10.0	L
	Total Permeate	8.8	L
PPR (L/h)	Calculated	0.96	L/h
	Measured	1.25	L/h

Table C-6 *Raw and processed data for Run 3*

Run 3	Flush Freq (h^{-1})	Flush Vol (mL)	Soak time (sec)	Flux (LMH)	Inst. Rec. (%)
	2.4	70	20	12	10

Operating Time (min)		0	90	180	270	360	450	540	630	720	765	810	830
Production Time (min)		0	86	171	257	343	429	514	600	686	729	771	790
Gauge Pressure (bar)	Feed	7.4	8.4	9.8	10.2	11.6	12.2	12.8	14.0	16.8	20.0	26.4	28.8
	Concentrate	6.6	7.6	9.0	9.4	10.8	11.4	12.0	13.2	16.0	19.2	25.6	28.0
	Permeate	1.1	1.1	1.1	1.1	1.1	1.1	1.1	1.1	1.1	1.1	1.1	1.1
Spcific Conductivity (mS/cm)	Feed	7.54	8.56	9.23	9.65	10.02	10.68	11.26	11.78	12.46	13.56	15.23	18.50
	Concentrate	8.30	9.23	10.15	10.96	11.32	12.45	13.17	13.45	14.56	15.60	17.06	20.91
	Permeate	-	0.802	0.812	0.832	0.835	0.812	0.887	0.890	0.902	0.924	0.936	0.947
Temperature (˚C)	Feed	14.9	14.5	15.0	15.0	14.9	15.0	15.0	15.1	15.1	15.0	15.2	15.2
	Concentrate	15.6	16.0	15.6	16.5	16.0	16.3	16.6	16.5	16.2	16.0	15.9	15.8
	Permeate	-	14.6	15.3	15.6	15.8	16.2	15.9	15.7	15.5	15.5	15.5	15.5
Flow rate (L/h)	Concentrate	11.40	11.40	11.60	11.60	11.60	11.60	11.50	11.50	11.50	11.50	11.50	11.50
	Permeate	1.25	1.25	1.25	1.25	1.25	1.25	1.25	1.25	1.25	1.25	1.25	1.05
	Feed	12.65	12.65	12.85	12.85	12.85	12.85	12.75	12.75	12.75	12.75	12.75	12.55
Salt Rejection (%)		NA	90.6	91.2	91.4	91.7	92.4	92.1	92.4	92.8	93.2	93.9	94.9
Inst. Recovery (%)		9.9	9.9	9.7	9.7	9.7	9.7	9.8	9.8	9.8	9.8	9.8	8.4
Permeate Flux (LMH)		11.8	11.8	11.8	11.8	11.8	11.8	11.8	11.8	11.8	11.8	11.8	9.9
Osmotic Pressure (bar)	Feed	3.67	4.16	4.49	4.69	4.87	5.19	5.47	5.73	6.06	6.59	7.40	8.99
	Concentrate	4.03	4.49	4.94	5.33	5.50	6.05	6.40	6.54	7.08	7.58	8.29	10.16
	Permeate	-	0.39	0.39	0.40	0.41	0.39	0.43	0.43	0.44	0.45	0.46	0.46
TMP (bar)		-	3.53	4.61	4.81	6.03	6.30	6.66	7.61	10.08	12.76	18.35	19.17
Lp (L/m².h.bar)		-	3.34	2.56	2.45	1.95	1.87	1.77	1.55	1.17	0.92	0.64	0.52
Lp (25°C) (L/m².h.bar)		-	5.46	5.15	4.71	4.52	4.00	3.55	3.30	2.88	2.61	1.78	0.50
Permeate Recovered (mL)		-	1000	1000	1010	900	960	960	940	920	820	520	210
Overall Recovery (%)		0	10	20	30	39	49	58	68	77	85	90	92
Concentration Factor		-	1.1	1.2	1.4	1.6	1.9	2.3	2.9	4.1	6.3	9.7	12.5
Ca+ Conc. (mg/L)	Concentrate	924	950	967	999	1009	1025	1034	1035	1043	1052	1063	1061
	Overflow Sed. Tank	866	878	890	907	926	949	941	951	962	974	977	985
	Feed	851	878	885	901	903	914	948	959	976	974	982	981

Pemeate Flushing	Total time	830	min
	Time / Flush Cycle	1575	sec
	Total Flushes	32	
	Flushing Time	18	sec
	Flushing Flowrate	14	L/h
	Total Flushing Volume	2.21	L
	Total Feed	10.0	L
	Total Permeate	9.2	L
PPR (L/h)	Calculated	1.05	L/h
	Measured	0.81	L/h

Table C-7 *Raw and processed data for Run 4*

Run 4	Flush Freq (h^{-1})	Flush Vol (mL)	Soak time (sec)	Flux (LMH)	Inst. Rec. (%)
	6	70	20	12	30

Operating Time (min)		0	90	180	270	360	450	470
Production Time (min)		0	80	160	240	320	400	418
Gauge Pressure (bar)	Feed	8.2	9.0	10.6	11.8	14.8	16.6	28.2
	Concentrate	7.4	8.2	9.8	11.0	14.0	15.8	27.4
	Permeate	1.1	1.1	1.1	1.1	1.1	1.1	1.1
Spcific Conductivity (mS/cm)	Feed	7.38	8.56	9.63	10.32	11.45	13.56	16.23
	Concentrate	9.71	10.52	11.56	12.56	13.32	15.89	18.56
	Permeate	-	0.789	0.823	0.865	0.915	0.945	0.956
Temperature (˚C)	Feed	13.7	14.3	14.5	14.6	14.7	15.1	15.1
	Concentrate	13.8	14.9	15.9	16.0	16.5	16.5	16.5
	Permeate	-	13.9	14.4	14.7	14.9	15.3	15.3
Flow rate (L/h)	Concentrate	3.00	3.00	3.00	3.00	3.00	3.00	3.00
	Permeate	1.25	1.25	1.25	1.25	1.25	1.25	1.05
	Feed	4.25	4.25	4.25	4.25	4.25	4.25	4.05
Salt Rejection (%)		NA	90.8	91.5	91.6	92.0	93.0	94.1
Inst. Recovery (%)		29.4	29.4	29.4	29.4	29.4	29.4	25.9
Permeate Flux (LMH)		11.8	11.8	11.8	11.8	11.8	11.8	9.9
Osmotic Pressure (bar)	Feed	3.59	4.16	4.68	5.02	5.57	6.59	7.89
	Concentrate	4.72	5.12	5.62	6.11	6.48	7.72	9.02
	Permeate	-	0.38	0.40	0.42	0.44	0.46	0.46
TMP (bar)		-	4.12	5.22	6.10	8.58	12.20	19.67
Lp (L/m².h.bar)		-	2.86	2.26	1.93	1.37	0.97	0.50
Lp (25°C) (L/m².h.bar)		-	4.09	3.17	2.70	1.90	1.33	0.69
Permeate Recovered (mL)		-	1560	1530	1580	1520	1560	350
Overall Recovery (%)		0	16	31	47	62	78	81
Concentration Factor		-	1.2	1.4	1.8	2.5	4.2	5.0
Ca+ Conc. (mg/L)	Concentrate	939	958	974	1007	1021	1033	1033
	Overflow Sed. Tank	852	883	889	897	906	923	924
	Feed	845	861	870	885	879	891	896

Pemeate Flushing	Total time	470	min
	Time / Flush Cycle	675	sec
	Total Flushes	42	
	Flushing Time	18	sec
	Flushing Flowrate	14	L/h
	Total Flushing Volume	2.92	L
	Total Feed	10.0	L
	Total Permeate	8.1	L
PPR (L/h)	Calculated	0.76	L/h
	Measured	1.08	L/h

Table C-8 *Raw and processed data for Run 5*

Run 5	Flush Freq (h^{-1})	Flush Vol (mL)	Soak time (sec)	Flux (LMH)	Inst. Rec. (%)
	2.4	35	90	12	10

Operating Time (min)		0	90	180	270	360	450	540	630	720	735
Production Time (min)		0	83	165	248	330	413	495	578	660	674
Gauge Pressure (bar)	Feed	7.0	9.2	10.4	11.8	12.4	13.0	14.6	17.6	25.0	29.2
	Concentrate	6.2	8.4	9.6	11.0	11.6	12.2	13.8	16.8	24.2	28.4
	Permeate	1.1	1.1	1.1	1.1	1.1	1.1	1.1	1.1	1.1	1.1
Spcific Conductivity (mS/cm)	Feed	7.54	8.32	8.78	9.89	10.02	10.89	11.52	12.60	15.63	19.56
	Concentrate	7.83	9.42	9.91	10.99	11.14	12.01	12.60	13.69	16.74	20.68
	Permeate	-	0.789	0.802	0.816	0.887	0.875	0.915	0.965	0.986	0.998
Temperature (˚C)	Feed	13.5	14.1	14.5	14.7	15.3	15.1	15.3	15.8	15.6	15.6
	Concentrate	14.3	15.2	15.6	15.8	16.9	17.1	16.9	17.1	17.3	17.3
	Permeate	-	14.6	15.2	15.8	16.0	16.3	16.0	16.5	16.2	16.2
Flow rate (L/h)	Concentrate	11.50	11.40	11.50	11.60	11.50	11.70	11.30	11.50	11.50	11.50
	Permeate	1.25	1.25	1.25	1.25	1.25	1.25	1.25	1.25	1.25	0.85
	Feed	12.75	12.65	12.75	12.85	12.75	12.95	12.55	12.75	12.75	12.35
Salt Rejection (%)		NA	90.5	90.9	91.7	91.1	92.0	92.1	92.3	93.7	94.9
Inst. Recovery (%)		9.8	9.9	9.8	9.7	9.8	9.7	10.0	9.8	9.8	6.9
Permeate Flux (LMH)		11.8	11.8	11.8	11.8	11.8	11.8	11.8	11.8	11.8	8.0
Osmotic Pressure (bar)	Feed	3.67	4.04	4.27	4.81	4.87	5.29	5.60	6.13	7.60	9.51
	Concentrate	3.81	4.58	4.82	5.34	5.42	5.84	6.13	6.66	8.14	10.05
	Permeate	-	0.38	0.39	0.40	0.43	0.43	0.44	0.47	0.48	0.49
TMP (bar)		-	4.44	5.42	6.29	6.86	7.03	8.34	10.84	16.78	19.08
Lp (L/m².h.bar)		-	2.66	2.18	1.88	1.72	1.68	1.41	1.09	0.70	0.42
Lp (25°C) (L/m².h.bar)		-	4.89	4.52	4.23	3.97	3.61	3.24	2.78	1.56	0.56
Permeate Recovered (mL)		-	1220	1180	1120	1120	1060	1120	1110	1111	250
Overall Recovery (%)		0	12	24	35	46	57	68	79	90	93
Concentration Factor		-	1.1	1.3	1.5	1.8	2.2	3.0	4.5	9.8	13.4
Ca+ Conc. (mg/L)	Concentrate	934	947	958	963	973	981	987	998	998	998
	Overflow Sed. Tank	858	878	889	902	918	918	920	921	923	926
	Feed	855	878	894	894	894	899	903	921	919	911

Pemeate Flushing	Total time	735	min
	Time / Flush Cycle	1636	sec
	Total Flushes	27	
	Flushing Time	9	sec
	Flushing Flowrate	14	L/h
	Total Flushing Volume	0.94	L
	Total Feed	10.0	L
	Total Permeate	9.3	L
PPR (L/h)	Calculated	1.09	L/h
	Measured	0.86	L/h

Table C-9 *Raw and processed data for Run 6*

Run 6	Flush Freq (h^{-1})	Flush Vol (mL)	Soak time (sec)	Flux (LMH)	Inst. Rec. (%)
	6	35	90	12	30

Operating Time (min)		0	90	180	270	360	450	540
Production Time (min)		0	73	147	220	293	367	440
Gauge Pressure (bar)	Feed	7.3	8.8	10.2	11.0	12.6	14.6	24.6
	Concentrate	6.5	8.0	9.4	10.2	11.8	13.8	23.8
	Permeate	1.1	1.1	1.1	1.1	1.1	1.1	1.1
Spcific Conductivity (mS/cm)	Feed	7.16	8.56	9.89	11.23	12.03	13.89	17.45
	Concentrate	8.60	10.44	12.16	13.93	14.44	17.36	21.29
	Permeate	-	0.793	0.814	0.837	0.832	0.912	0.948
Temperature (˚C)	Feed	12.9	13.5	14.3	14.4	14.3	14.8	14.9
	Concentrate	13.0	14.5	14.9	15.4	16.2	16.9	16.7
	Permeate	-	13.2	14.1	14.4	14.7	14.7	15.2
Flow rate (L/h)	Concentrate	3.00	3.00	2.95	3.00	3.00	2.95	3.05
	Permeate	1.25	1.25	1.25	1.25	1.25	1.25	0.70
	Feed	4.25	4.25	4.20	4.25	4.25	4.20	3.75
Salt Rejection (%)		NA	90.7	91.8	92.5	93.1	93.4	94.6
Inst. Recovery (%)		29.4	29.4	29.8	29.4	29.4	29.8	18.7
Permeate Flux (LMH)		11.8	11.8	11.8	11.8	11.8	11.8	6.6
Osmotic Pressure (bar)	Feed	3.48	4.16	4.81	5.46	5.85	6.75	8.48
	Concentrate	4.18	5.08	5.91	6.77	7.02	8.44	10.35
	Permeate	-	0.39	0.40	0.41	0.40	0.44	0.46
TMP (bar)		-	3.92	4.69	4.85	6.06	7.19	15.48
Lp (L/m².h.bar)		-	3.01	2.52	2.43	1.95	1.64	0.43
Lp (25°C) (L/m².h.bar)		-	4.39	3.60	3.44	2.72	2.25	0.59
Permeate Recovered (mL)		-	1500	1510	1520	1620	1600	1000
Overall Recovery (%)		0	15	30	45	62	78	88
Concentration Factor		-	1.2	1.4	1.8	2.5	4.2	7.6
Ca+ Conc. (mg/L)	Concentrate	951	977	995	997	1012	1043	1043
	Overflow Sed. Tank	848	849	856	876	886	909	924
	Feed	850	885	908	917	916	946	958

Pemeate Flushing	Total time	540	min
	Time / Flush Cycle	736	sec
	Total Flushes	44	
	Flushing Time	9	sec
	Flushing Flowrate	14	L/h
	Total Flushing Volume	1.54	L
	Total Feed	10.0	L
	Total Permeate	8.8	L
PPR (L/h)	Calculated	0.87	L/h
	Measured	1.10	L/h

Table C-10 *Raw and processed data for Run 7*

Run 7	Flush Freq (h^{-1})	Flush Vol (mL)	Soak time (sec)	Flux (LMH)	Inst. Rec. (%)
	2.4	70	90	12	30

Operating Time (min)		0	90	180	270	360	450	540	630	720	810
Production Time (min)		0	82	164	246	328	410	492	574	657	739
Gauge Pressure (bar)	Feed	7.8	8.0	9.2	10.2	11.4	12.0	14.8	16.4	22.4	30.4
	Concentrate	7.0	7.2	8.4	9.4	10.6	11.2	14.0	15.6	21.6	29.6
	Permeate	1.1	1.1	1.1	1.1	1.1	1.1	1.1	1.1	1.1	1.1
Spcific Conductivity (mS/cm)	Feed	7.25	7.89	8.23	9.23	10.23	11.02	11.65	12.20	14.23	17.20
	Concentrate	8.04	8.84	9.56	10.43	11.21	12.01	12.84	13.54	15.94	19.44
	Permeate	-	0.794	0.812	0.832	0.851	0.847	0.889	0.921	0.946	0.986
Temperature (˚C)	Feed	13.1	14.3	15.9	15.1	14.9	15.2	15.1	15.3	15.6	15.4
	Concentrate	13.7	15.3	16.4	17.1	17.6	17.6	16.7	16.5	16.9	16.8
	Permeate	-	14.3	14.7	15.3	15.6	15.6	15.8	15.6	15.4	15.3
Flow rate (L/h)	Concentrate	3.00	3.00	2.95	3.00	3.00	2.95	3.05	3.00	3.00	3.00
	Permeate	1.25	1.25	1.25	1.25	1.25	1.25	1.25	1.25	1.25	1.05
	Feed	4.25	4.25	4.20	4.25	4.25	4.20	4.30	4.25	4.25	4.05
Salt Rejection (%)		NA	89.9	90.1	91.0	91.7	92.3	92.4	92.5	93.4	94.3
Inst. Recovery (%)		29.4	29.4	29.8	29.4	29.4	29.8	29.1	29.4	29.4	25.9
Permeate Flux (LMH)		11.8	11.8	11.8	11.8	11.8	11.8	11.8	11.8	11.8	9.9
Osmotic Pressure (bar)	Feed	3.52	3.84	4.00	4.49	4.97	5.36	5.66	5.93	6.92	8.36
	Concentrate	3.91	4.30	4.65	5.07	5.45	5.84	6.24	6.58	7.75	9.45
	Permeate	-	0.39	0.39	0.40	0.41	0.41	0.43	0.45	0.46	0.48
TMP (bar)		-	3.45	4.49	5.02	5.74	5.95	8.47	9.82	14.84	21.42
Lp (L/m².h.bar)		-	3.42	2.62	2.35	2.05	1.98	1.39	1.20	0.79	0.46
Lp (25°C) (L/m².h.bar)		-	4.85	4.21	3.82	2.98	2.66	2.26	1.65	0.53	0.42
Permeate Recovered (mL)		-	1030	1210	1140	950	960	1120	1120	1100	210
Overall Recovery (%)		0	10	22	34	43	53	64	75	86	88
Concentration Factor		-	1.1	1.3	1.5	1.7	2.0	2.6	3.8	6.9	8.2
Ca+ Conc. (mg/L)	Concentrate	924	950	967	999	1009	1025	1034	1035	1043	1052
	Overflow Sed. Tank	841	860	872	865	861	880	889	902	911	918
	Feed	842	879	860	866	902	882	884	918	903	897

Pemeate Flushing	Total time	810	min
	Time / Flush Cycle	1645	sec
	Total Flushes	30	
	Flushing Time	18	sec
	Flushing Flowrate	14	L/h
	Total Flushing Volume	2.07	L
	Total Feed	10.0	L
	Total Permeate	8.8	L
PPR (L/h)	Calculated	1.01	L/h
	Measured	0.71	L/h

Table C-11 *Raw and processed data for Run 8*

Run 8	Flush Freq (h^{-1})	Flush Vol (mL)	Soak time (sec)	Flux (LMH)	Inst. Rec. (%)
	6	70	90	12	10

Operating Time (min)		0	90	180	270	360	450	540	560
Production Time (min)		0	72	145	217	290	362	435	451
Gauge Pressure (bar)	Feed	7.6	8.6	9.8	12.0	13.2	16.4	20.2	28.2
	Concentrate	6.8	7.8	9.0	11.2	12.4	15.6	19.4	27.4
	Permeate	1.1	1.1	1.1	1.1	1.1	1.1	1.1	1.1
Spcific Conductivity (mS/cm)	Feed	7.30	8.56	9.02	9.56	10.20	11.89	15.56	18.54
	Concentrate	8.03	9.33	10.28	11.09	11.63	13.32	17.74	21.88
	Permeate	-	0.894	0.874	0.856	0.842	0.812	0.802	0.778
Temperature (˚C)	Feed	12.8	13.4	14.1	14.3	14.8	15.2	15.2	15.4
	Concentrate	12.9	14.5	16.5	16.3	17.0	16.9	16.9	13.7
	Permeate	-	13.5	14.8	15.4	15.5	16.1	16.1	16.4
Flow rate (L/h)	Concentrate	11.50	11.50	11.50	11.50	11.50	11.40	11.40	11.00
	Permeate	1.25	1.25	1.25	1.25	1.25	1.25	1.25	1.10
	Feed	12.75	12.75	12.75	12.75	12.75	12.65	12.65	12.10
Salt Rejection (%)		NA	89.6	90.3	91.0	91.7	93.2	94.8	95.8
Inst. Recovery (%)		9.8	9.8	9.8	9.8	9.8	9.9	9.9	9.1
Permeate Flux (LMH)		11.8	11.8	11.8	11.8	11.8	11.8	11.8	10.4
Osmotic Pressure (bar)	Feed	3.55	4.16	4.39	4.65	4.96	5.78	7.56	9.01
	Concentrate	3.91	4.54	5.00	5.39	5.65	6.47	8.62	10.64
	Permeate	-	0.43	0.42	0.42	0.41	0.39	0.39	0.38
TMP (bar)		-	3.77	4.74	6.67	7.55	9.91	11.93	18.46
Lp (L/m².h.bar)		-	3.13	2.49	1.77	1.56	1.19	0.99	0.56
Lp (25°C) (L/m².h.bar)		-	4.57	3.47	2.47	2.14	1.62	1.35	0.81
Permeate Recovered (mL)		-	1500	1560	1520	1330	1350	1370	350
Overall Recovery (%)		0	15	31	46	59	73	86	90
Concentration Factor		-	1.2	1.4	1.8	2.3	3.5	7.0	9.4
Ca+ Conc. (mg/L)	Concentrate	901	920	922	957	1005	1029	1046	1041
	Overflow Sed. Tank	849	826	853	870	873	903	903	903
	Feed	850	854	837	866	902	893	893	885

Pemeate Flushing	Total time	560	min
	Time / Flush Cycle	745	sec
	Total Flushes	45	
	Flushing Time	18	sec
	Flushing Flowrate	14	L/h
	Total Flushing Volume	3.16	L
	Total Feed	10.0	L
	Total Permeate	9.0	L
PPR (L/h)	Calculated	0.69	L/h
	Measured	0.95	L/h

Table C-12 *Raw and processed data for Run 9*

Run 9	Flush Freq (h^{-1})	Flush Vol (mL)	Soak time (sec)	Flux (LMH)	Inst. Rec. (%)
	2.4	35	20	24	10

Operating Time (min)		0	30	60	90	120	130
Production Time (min)		0	29	57	86	115	125
Gauge Pressure (bar)	Feed	11.5	12.0	12.8	13.8	14.8	23.2
	Concentrate	12.4	12.8	13.6	14.6	15.6	24.0
	Permeate	1.1	1.1	1.1	1.1	1.1	1.1
Spcific Conductivity (mS/cm)	Feed	7.32	8.23	8.75	9.23	9.97	10.26
	Concentrate	8.05	9.05	9.98	10.06	11.47	11.49
	Permeate	-	0.823	0.842	0.867	0.871	0.912
Temperature (˚C)	Feed	15.6	15.8	15.8	15.9	16.0	16.2
	Concentrate	15.9	16.1	16.2	16.3	16.3	16.5
	Permeate	-	16.2	16.4	16.2	16.2	16.2
Flow rate (L/h)	Concentrate	22.50	22.00	21.50	22.00	22.00	22.50
	Permeate	2.55	2.55	2.55	2.55	2.55	2.20
	Feed	25.05	24.55	24.05	24.55	24.55	24.70
Salt Rejection (%)		NA	90.0	90.4	90.6	91.3	91.1
Inst. Recovery (%)		10.2	10.4	10.6	10.4	10.4	8.9
Permeate Flux (LMH)		24.1	24.1	24.1	24.1	24.1	20.8
Osmotic Pressure (bar)	Feed	3.56	4.00	4.25	4.49	4.85	4.99
	Concentrate	3.91	4.40	4.85	4.89	5.57	5.59
	Permeate	-	0.40	0.41	0.42	0.42	0.44
TMP (bar)		-	7.30	7.86	8.63	9.28	17.56
Lp (L/m².h.bar)		-	3.30	3.06	2.79	2.59	1.18
Lp (25°C) (L/m².h.bar)		-	4.50	4.17	3.78	3.52	1.59
Permeate Recovered (mL)		-	1260	1220	1230	1250	250
Overall Recovery (%)		0	13	25	37	50	52
Concentration Factor		-	1.1	1.3	1.5	1.9	2.0
Ca+ Conc. (mg/L)	Concentrate	974	1023	1089	1120	1120	1109
	Overflow Sed. Tank	809	832	845	854	854	856
	Feed	841	854	867	876	876	865

Pemeate Flushing	Total time	130	min
	Time / Flush Cycle	1566	sec
	Total Flushes	5	
	Flushing Time	9	sec
	Flushing Flowrate	14	L/h
	Total Flushing Volume	0.17	L
	Total Feed	10.0	L
	Total Permeate	5.2	L
PPR (L/h)	Calculated	2.36	L/h
	Measured	2.08	L/h

Table C-13 *Raw and processed data for Run 10*

Run 10	Flush Freq (h^{-1})	Flush Vol (mL)	Soak time (sec)	Flux (LMH)	Inst. Rec. (%)
	6	35	20	24	30

Operating Time (min)		0	30	60	90	100
Production Time (min)		0	27	54	81	90
Gauge Pressure (bar)	Feed	11.0	11.8	12.4	13.0	23.0
	Concentrate	10.2	11.0	11.6	12.2	22.2
	Permeate	1.1	1.1	1.1	1.1	1.1
Spcific Conductivity (mS/cm)	Feed	7.23	7.74	8.33	8.98	8.99
	Concentrate	7.95	8.67	9.41	9.79	9.87
	Permeate	-	0.875	0.881	0.912	0.923
Temperature (˚C)	Feed	14.2	15.2	15.4	15.4	15.6
	Concentrate	14.5	15.2	15.5	15.6	15.6
	Permeate	-	15.3	15.5	15.6	15.8
Flow rate (L/h)	Concentrate	6.00	6.00	6.00	6.00	6.00
	Permeate	2.55	2.55	2.55	2.55	2.00
	Feed	8.55	8.55	8.55	8.55	8.00
Salt Rejection (%)		NA	88.7	89.4	89.8	89.7
Inst. Recovery (%)		29.8	29.8	29.8	29.8	25.0
Permeate Flux (LMH)		24.1	24.1	24.1	24.1	18.9
Osmotic Pressure (bar)	Feed	3.51	3.76	4.05	4.37	4.37
	Concentrate	3.87	4.21	4.58	4.76	4.80
	Permeate	-	0.43	0.43	0.44	0.45
TMP (bar)		-	7.36	7.68	7.98	17.98
Lp (L/m².h.bar)		-	3.27	3.13	3.02	1.05
Lp (25°C) (L/m².h.bar)		-	4.58	4.35	4.18	1.45
Permeate Recovered (mL)		-	1160	1170	1100	420
Overall Recovery (%)		0	12	23	34	39
Concentration Factor		-	1.1	1.3	1.5	1.6
Ca+ Conc. (mg/L)	Concentrate	965	1069	1117	1139	1130
	Overflow Sed. Tank	820	830	850	864	872
	Feed	844	850	884	880	900

Pemeate Flushing	Total time	100	min
	Time / Flush Cycle	666	sec
	Total Flushes	9	
	Flushing Time	9	sec
	Flushing Flowrate	14	L/h
	Total Flushing Volume	0.32	L
	Total Feed	10.0	L
	Total Permeate	3.9	L
PPR (L/h)	Calculated	2.10	L/h
	Measured	2.44	L/h

Table C-14 *Raw and processed data for Run 11*

Run 11	Flush Freq (h^{-1})	Flush Vol (mL)	Soak time (sec)	Flux (LMH)	Inst. Rec. (%)
	2.4	70	20	24	30

Operating Time (min)		0	30	60	90	120	150
Production Time (min)		0	29	57	86	114	143
Gauge Pressure (bar)	Feed	11.0	11.5	12.2	14.6	16.9	22.0
	Concentrate	10.2	10.8	11.4	13.7	15.7	21.0
	Permeate	1.1	1.1	1.1	1.1	1.1	1.1
Spcific Conductivity (mS/cm)	Feed	7.54	8.12	8.33	8.97	9.23	9.24
	Concentrate	8.30	9.09	9.41	9.96	10.34	10.16
	Permeate	-	0.896	0.893	0.841	0.823	0.956
Temperature (˚C)	Feed	14.6	14.6	14.6	14.9	15.1	15.1
	Concentrate	15.2	15.9	16.3	16.0	15.8	15.6
	Permeate	-	15.4	15.6	15.8	16.0	16.2
Flow rate (L/h)	Concentrate	5.95	5.95	6.00	6.00	6.00	6.00
	Permeate	2.54	2.55	2.50	2.55	2.55	2.25
	Feed	8.49	8.50	8.50	8.55	8.55	8.25
Salt Rejection (%)		NA	89.0	89.3	90.6	91.1	89.7
Inst. Recovery (%)		30.0	30.0	29.4	29.8	29.8	27.3
Permeate Flux (LMH)		24.0	24.1	23.6	24.1	24.1	21.2
Osmotic Pressure (bar)	Feed	3.67	3.95	4.05	4.36	4.49	4.49
	Concentrate	4.03	4.42	4.58	4.84	5.03	4.94
	Permeate	-	0.44	0.43	0.41	0.40	0.46
TMP (bar)		-	6.89	7.48	9.55	11.71	16.87
Lp (L/m².h.bar)		-	3.49	3.15	2.52	2.05	1.26
Lp (25°C) (L/m².h.bar)		-	4.88	4.38	3.50	2.85	1.75
Permeate Recovered (mL)		-	1120	1130	1180	1190	130
Overall Recovery (%)		0	11	23	34	46	48
Concentration Factor		-	1.1	1.3	1.5	1.8	1.8
Ca+ Conc. (mg/L)	Concentrate	978	1036	1068	1105	1123	1089
	Overflow Sed. Tank	889	902	879	881	894	910
	Feed	838	844	850	860	877	897

Pemeate Flushing	Total time	150	min
	Time / Flush Cycle	1575	sec
	Total Flushes	6	
	Flushing Time	18	sec
	Flushing Flowrate	14	L/h
	Total Flushing Volume	0.40	L
	Total Feed	10.0	L
	Total Permeate	4.8	L
PPR (L/h)	Calculated	2.26	L/h
	Measured	1.90	L/h

Table C-15 *Raw and processed data for Run 12*

Run 12	Flush Freq (h^{-1})	Flush Vol (mL)	Soak time (sec)	Flux (LMH)	Inst. Rec. (%)
	6	70	20	24	10

Operating Time (min)		0	30	60	90	120	125
Production Time (min)		0	27	53	80	107	111
Gauge Pressure (bar)	Feed	9.8	10.2	11.0	12.2	13.0	24.2
	Concentrate	9.0	9.4	10.2	11.4	12.2	23.4
	Permeate	1.1	1.1	1.1	1.1	1.1	1.1
Spcific Conductivity (mS/cm)	Feed	7.44	7.77	8.19	8.75	9.68	9.70
	Concentrate	8.18	8.85	9.26	9.89	10.74	10.77
	Permeate	-	0.814	0.852	0.854	0.872	0.907
Temperature (˚C)	Feed	15.3	15.5	16.0	16.0	15.9	16.5
	Concentrate	15.9	15.8	16.1	16.4	16.6	16.4
	Permeate	-	16.3	16.5	16.2	16.2	16.2
Flow rate (L/h)	Concentrate	22.00	23.00	22.50	22.50	23.00	22.50
	Permeate	2.55	2.55	2.55	2.55	2.55	2.10
	Feed	24.55	25.55	25.05	25.05	25.55	24.60
Salt Rejection (%)		NA	89.5	89.6	90.2	91.0	90.6
Inst. Recovery (%)		10.4	10.0	10.2	10.2	10.0	8.5
Permeate Flux (LMH)		24.1	24.1	24.1	24.1	24.1	19.8
Osmotic Pressure (bar)	Feed	3.62	3.78	3.98	4.25	4.71	4.72
	Concentrate	3.98	4.30	4.50	4.81	5.22	5.23
	Permeate	-	0.40	0.41	0.42	0.42	0.44
TMP (bar)		-	5.72	6.33	7.26	7.62	18.83
Lp (L/m².h.bar)		-	4.21	3.80	3.31	3.16	1.05
Lp (25°C) (L/m².h.bar)		-	5.80	5.17	4.48	4.27	1.41
Permeate Recovered (mL)		-	1040	1060	1050	1080	160
Overall Recovery (%)		0	10	21	32	42	44
Concentration Factor		-	1.1	1.2	1.4	1.7	1.7
Ca+ Conc. (mg/L)	Concentrate	912	955	974	1006	1010	1000
	Overflow Sed. Tank	833	834	838	857	852	857
	Feed	823	832	839	857	867	868

Pemeate Flushing	Total time	125	min
	Time / Flush Cycle	675	sec
	Total Flushes	11	
	Flushing Time	18	sec
	Flushing Flowrate	14	L/h
	Total Flushing Volume	0.78	L
	Total Feed	10.0	L
	Total Permeate	4.4	L
PPR (L/h)	Calculated	1.89	L/h
	Measured	2.20	L/h

Table C-16 *Raw and processed data for Run 13*

Run 13	Flush Freq (h^{-1})	Flush Vol (mL)	Soak time (sec)	Flux (LMH)	Inst. Rec. (%)
	2.4	35	90	24	30

Operating Time (min)		0	30	60	90	120	150	180
Production Time (min)		0	28	55	83	110	138	165
Gauge Pressure (bar)	Feed	11.5	11.5	11.6	11.8	12.3	14.5	21.4
	Concentrate	10.7	10.8	10.8	11.0	11.5	13.7	20.5
	Permeate	1.1	1.1	1.1	1.1	1.1	1.1	1.1
Spcific Conductivity (mS/cm)	Feed	7.58	8.47	8.87	9.06	9.54	10.27	10.23
	Concentrate	8.34	9.49	9.76	10.33	10.68	11.40	11.76
	Permeate	-	0.845	0.896	0.902	0.921	0.954	0.965
Temperature (˚C)	Feed	13.6	13.9	14.3	14.7	14.4	14.9	14.7
	Concentrate	14.4	14.9	15.2	15.2	15.6	15.8	16.0
	Permeate	-	14.3	14.5	14.8	14.9	14.9	14.8
Flow rate (L/h)	Concentrate	6.00	5.95	6.00	6.00	6.00	6.05	6.00
	Permeate	2.55	2.55	2.55	2.55	2.55	2.55	2.15
	Feed	8.55	8.50	8.55	8.55	8.55	8.60	8.15
Salt Rejection (%)		NA	90.0	89.9	90.0	90.3	90.7	90.6
Inst. Recovery (%)		29.8	30.0	29.8	29.8	29.8	29.7	26.4
Permeate Flux (LMH)		24.1	24.1	24.1	24.1	24.1	24.1	20.3
Osmotic Pressure (bar)	Feed	3.69	4.12	4.31	4.40	4.64	4.99	4.97
	Concentrate	4.05	4.61	4.74	5.02	5.19	5.54	5.72
	Permeate	-	0.41	0.44	0.44	0.45	0.46	0.47
TMP (bar)		-	6.69	6.62	6.73	7.01	8.87	15.80
Lp (L/m².h.bar)		-	3.59	3.63	3.57	3.43	2.71	1.28
Lp (25°C) (L/m².h.bar)		-	5.18	5.17	5.05	4.84	3.78	1.79
Permeate Recovered (mL)		-	990	910	870	860	880	520
Overall Recovery (%)		0	10	19	28	36	45	50
Concentration Factor		-	1.1	1.2	1.3	1.5	1.7	1.9
Ca+ Conc. (mg/L)	Concentrate	941	965	979	1008	1030	1043	1044
	Overflow Sed. Tank	857	877	888	902	911	943	969
	Feed	848	864	869	892	920	938	958

Pemeate Flushing	Total time	180	min
	Time / Flush Cycle	1636	sec
	Total Flushes	7	
	Flushing Time	9	sec
	Flushing Flowrate	14	L/h
	Total Flushing Volume	0.23	L
	Total Feed	10.0	L
	Total Permeate	5.0	L
PPR (L/h)	Calculated	1.85	L/h
	Measured	1.90	L/h

Table C-17 *Raw and processed data for Run 14*

Run 14	Flush Freq (h^{-1})	Flush Vol (mL)	Soak time (sec)	Flux (LMH)	Inst. Rec. (%)
	6	35	90	24	10

Operating Time (min)		0	30	60	90	105
Production Time (min)		0	0	0	1	1
Gauge Pressure (bar)	Feed	9.4	10.0	11.2	12.0	24.6
	Concentrate	8.6	9.2	10.4	11.2	23.8
	Permeate	1.1	1.1	1.1	1.1	1.1
Spcific Conductivity (mS/cm)	Feed	7.41	7.89	8.23	9.27	9.26
	Concentrate	8.15	8.99	9.30	10.10	10.37
	Permeate	-	0.981	0.702	0.785	0.723
Temperature (˚C)	Feed	15.1	15.5	16.1	15.8	16.2
	Concentrate	15.7	16.1	16.3	16.4	16.3
	Permeate	-	16.4	16.4	16.2	16.1
Flow rate (L/h)	Concentrate	22.50	22.00	23.00	23.00	22.50
	Permeate	2.55	2.55	2.55	2.55	1.90
	Feed	25.05	24.55	25.55	25.55	24.40
Salt Rejection (%)		NA	87.6	91.5	91.5	92.2
Inst. Recovery (%)		10.2	10.4	10.0	10.0	7.8
Permeate Flux (LMH)		24.1	24.1	24.1	24.1	17.9
Osmotic Pressure (bar)	Feed	3.60	3.84	4.00	4.51	4.50
	Concentrate	3.96	4.37	4.52	4.91	5.04
	Permeate	-	0.48	0.34	0.38	0.35
TMP (bar)		-	5.54	6.44	6.78	19.35
Lp (L/m².h.bar)		-	4.34	3.74	3.55	0.93
Lp (25°C) (L/m².h.bar)		-	5.96	5.06	4.83	1.25
Permeate Recovered (mL)		-	1340	1420	1430	490
Overall Recovery (%)		0	13	28	42	47
Concentration Factor		-	1.1	1.3	1.7	1.8
Ca+ Conc. (mg/L)	Concentrate	986	1028	1070	1105	1100
	Overflow Sed. Tank	851	854	877	881	865
	Feed	0	24	49	73	86

Pemeate Flushing	Total time	105	min
	Time / Flush Cycle	736	sec
	Total Flushes	9	
	Flushing Time	9	sec
	Flushing Flowrate	14	L/h
	Total Flushing Volume	0.30	L
	Total Feed	10.0	L
	Total Permeate	4.7	L
PPR (L/h)	Calculated	1.90	L/h
	Measured	2.35	L/h

Table C-18 *Raw and processed data for Run 15*

Run 15	Flush Freq (h^{-1})	Flush Vol (mL)	Soak time (sec)	Flux (LMH)	Inst. Rec. (%)
	2.4	70	90	24	10

Operating Time (min)		0	30	60	90	120	150	180	195
Production Time (min)		0	27	55	82	109	137	164	178
Gauge Pressure (bar)	Feed	10.2	10.6	11.2	11.4	12.4	13.0	15.2	31.0
	Concentrate	9.4	9.8	10.4	10.6	11.6	12.2	14.4	30.2
	Permeate	1.1	1.1	1.1	1.1	1.1	1.1	1.1	1.1
Spcific Conductivity (mS/cm)	Feed	7.42	7.78	8.23	8.56	9.00	9.26	9.45	9.23
	Concentrate	8.16	8.71	9.38	9.59	10.35	10.37	10.49	10.43
	Permeate	-	0.789	0.797	0.812	0.869	0.921	0.947	0.978
Temperature (˚C)	Feed	15.5	15.2	15.2	15.3	15.4	15.6	15.6	15.6
	Concentrate	16.1	16.2	16.4	16.6	16.7	16.8	16.8	17.0
	Permeate	-	16.3	16.4	16.8	16.8	16.9	17.0	17.2
Flow rate (L/h)	Concentrate	22.00	23.00	22.00	22.50	23.00	23.50	22.00	22.50
	Permeate	2.55	2.55	2.55	2.55	2.55	2.55	2.55	1.60
	Feed	24.55	25.55	24.55	25.05	25.55	26.05	24.55	24.10
Salt Rejection (%)		NA	89.9	90.3	90.5	90.3	90.1	90.0	89.4
Inst. Recovery (%)		10.4	10.0	10.4	10.2	10.0	9.8	10.4	6.6
Permeate Flux (LMH)		24.1	24.1	24.1	24.1	24.1	24.1	24.1	15.1
Osmotic Pressure (bar)	Feed	3.61	3.78	4.00	4.16	4.38	4.50	4.59	4.49
	Concentrate	3.97	4.24	4.56	4.66	5.03	5.04	5.10	5.07
	Permeate	-	0.38	0.39	0.39	0.42	0.45	0.46	0.48
TMP (bar)		-	6.10	6.49	6.53	7.35	7.85	9.97	25.89
Lp (L/m².h.bar)		-	3.94	3.71	3.68	3.27	3.07	2.41	0.58
Lp (25°C) (L/m².h.bar)		-	5.43	5.09	5.03	4.45	4.15	3.27	0.79
Permeate Recovered (mL)		-	880	890	900	870	860	820	230
Overall Recovery (%)		0	9	18	27	35	44	52	55
Concentration Factor		-	1.1	1.2	1.3	1.5	1.7	2.0	2.1
Ca+ Conc. (mg/L)	Concentrate	903	945	973	991	1012	1021	1038	1037
	Overflow Sed. Tank	802	834	867	853	857	872	885	898
	Feed	834	855	876	881	886	903	928	939

Pemeate Flushing	Total time	195	min
	Time / Flush Cycle	1645	sec
	Total Flushes	7	
	Flushing Time	18	sec
	Flushing Flowrate	14	L/h
	Total Flushing Volume	0.50	L
	Total Feed	10.0	L
	Total Permeate	5.5	L
PPR (L/h)	Calculated	2.17	L/h
	Measured	1.75	L/h

Table C-19 *Raw and processed data for Run 16*

Run 16	Flush Freq (h^{-1})	Flush Vol (mL)	Soak time (sec)	Flux (LMH)	Inst. Rec. (%)
	6	70	90	24	30

Operating Time (min)		0	30	60	90	100
Production Time (min)		0	24	48	72	81
Gauge Pressure (bar)	Feed	11.6	12.3	12.8	13.6	19.8
	Concentrate	10.8	11.5	12.0	12.8	19.0
	Permeate	1.1	1.1	1.1	1.1	1.1
Spcific Conductivity (mS/cm)	Feed	7.34	8.02	8.23	8.87	8.89
	Concentrate	8.45	9.68	10.04	10.56	10.53
	Permeate	-	0.814	0.865	0.894	0.918
Temperature (˚C)	Feed	15.2	14.7	14.7	14.9	14.9
	Concentrate	15.9	16.2	16.2	16.4	16.4
	Permeate	-	15.9	16.0	15.8	15.8
Flow rate (L/h)	Concentrate	5.95	6.00	6.00	6.00	6.00
	Permeate	2.55	2.55	2.55	2.55	2.55
	Feed	8.50	8.55	8.55	8.55	8.55
Salt Rejection (%)		NA	89.9	89.5	89.9	89.7
Inst. Recovery (%)		30.0	29.8	29.8	29.8	29.8
Permeate Flux (LMH)		24.1	24.1	24.1	24.1	24.1
Osmotic Pressure (bar)	Feed	3.57	3.90	4.00	4.31	4.32
	Concentrate	4.11	4.71	4.88	5.13	5.12
	Permeate	-	0.40	0.42	0.43	0.45
TMP (bar)		-	7.70	8.12	8.62	14.82
Lp (L/m².h.bar)		-	3.13	2.96	2.79	1.62
Lp (25°C) (L/m².h.bar)		-	4.34	4.12	3.85	2.24
Permeate Recovered (mL)		-	1230	1220	1170	150
Overall Recovery (%)		0	12	25	36	38
Concentration Factor		-	1.1	1.3	1.5	1.5
Ca+ Conc. (mg/L)	Concentrate	918	945	962	967	967
	Overflow Sed. Tank	809	832	846	860	870
	Feed	841	883	893	893	872

Pemeate Flushing	Total time	100	min
	Time / Flush Cycle	745	sec
	Total Flushes	8	
	Flushing Time	18	sec
	Flushing Flowrate	14	L/h
	Total Flushing Volume	0.56	L
	Total Feed	10.0	L
	Total Permeate	3.8	L
PPR (L/h)	Calculated	1.71	L/h
	Measured	2.19	L/h

Table C-20 *Raw and processed data for Run 17*

Run 17	Flush Freq (h^{-1})	Flush Vol (mL)	Soak time (sec)	Flux (LMH)	Inst. Rec. (%)
	3.4	52.5	55	18	20

Operating Time (min)		0	45	90	135	180	225	250
Production Time (min)		0	41	82	123	164	204	227
Gauge Pressure (bar)	Feed	9.8	10.6	10.8	11.6	14.6	19.0	29.8
	Concentrate	9.0	9.8	10.0	10.8	13.8	18.2	29.0
	Permeate	1.1	1.1	1.1	1.1	1.1	1.1	1.1
Spcific Conductivity (mS/cm)	Feed	7.38	7.85	8.21	8.65	9.04	9.45	9.62
	Concentrate	8.86	9.42	9.85	10.38	10.85	11.34	11.54
	Permeate	-	0.880	0.892	0.896	0.915	0.966	0.994
Temperature (˚C)	Feed	14.3	14.5	14.5	14.6	14.8	14.9	14.8
	Concentrate	14.4	14.4	14.7	14.8	15.6	15.6	15.4
	Permeate	-	14.2	14.5	14.5	14.7	14.8	14.5
Flow rate (L/h)	Concentrate	7.50	7.60	7.50	7.50	7.60	7.50	7.50
	Permeate	1.90	1.90	1.90	1.90	1.90	1.90	1.10
	Feed	9.40	9.50	9.40	9.40	9.50	9.40	8.60
Salt Rejection (%)		NA	88.8	89.1	89.6	89.9	89.8	89.7
Inst. Recovery (%)		20.2	20.0	20.2	20.2	20.0	20.2	12.8
Permeate Flux (LMH)		17.9	17.9	17.9	17.9	17.9	17.9	10.4
Osmotic Pressure (bar)	Feed	3.59	3.82	3.99	4.21	4.39	4.59	4.68
	Concentrate	4.31	4.58	4.79	5.05	5.27	5.51	5.61
	Permeate	-	0.43	0.43	0.44	0.44	0.47	0.48
TMP (bar)		-	6.11	6.14	6.73	9.55	13.78	24.51
Lp (L/m².h.bar)		-	2.93	2.92	2.66	1.88	1.30	0.42
Lp (25°C) (L/m².h.bar)		-	4.22	4.17	3.80	2.63	1.82	0.60
Permeate Recovered (mL)		-	1240	1310	1260	1300	1310	470
Overall Recovery (%)		0	12	26	38	51	64	69
Concentration Factor		-	1.1	1.3	1.6	1.9	2.6	3.0
Ca+ Conc. (mg/L)	Concentrate	1022	1037	1053	1058	1079	1092	1091
	Overflow Sed. Tank	866	871	879	893	897	903	907
	Feed	869	880	898	916	928	923	930

Pemeate Flushing	Total time	250	min
	Time / Flush Cylce	1156	sec
	Total Flushes	13	
	Flushing Time	14	sec
	Flushing Flowrate	14	L/h
	Total Flushing Volume	0.68	L
	Total Feed	10.0	L
	Total Permeate	6.9	L
PPR (L/h)	Calculated	1.57	L/h
	Measured	1.52	L/h

Table C-21 *Raw and processed data for Run 18*

Run 18	Flush Freq (h^{-1})	Flush Vol (mL)	Soak time (sec)	Flux (LMH)	Inst. Rec. (%)
	3.4	52.5	55	18	20

Operating Time (min)		0	45	90	135	180	225	255
Production Time (min)		0	41	82	123	164	204	232
Gauge Pressure (bar)	Feed	9.0	10.8	11.0	11.6	13.1	16.8	26.6
	Concentrate	8.2	10.0	10.2	10.8	12.3	17.9	25.8
	Permeate	1.1	1.1	1.1	1.1	1.1	1.1	1.1
Spcific Conductivity (mS/cm)	Feed	7.67	7.72	8.50	8.43	9.16	9.51	9.81
	Concentrate	9.16	9.66	9.99	10.32	10.68	11.46	11.49
	Permeate	-	0.608	0.667	0.789	0.700	1.126	1.230
Temperature (˚C)	Feed	15.4	15.4	15.6	15.8	15.7	15.9	15.5
	Concentrate	15.7	15.8	16.3	16.6	17.0	17.1	16.4
	Permeate	-	16.0	16.5	16.8	17.1	16.9	17.3
Flow rate (L/h)	Concentrate	7.60	7.50	7.55	7.60	7.60	7.50	7.50
	Permeate	1.90	1.90	1.90	1.90	1.90	1.90	1.60
	Feed	9.50	9.40	9.45	9.50	9.50	9.40	9.10
Salt Rejection (%)		NA	92.1	92.2	90.6	92.4	88.2	87.5
Inst. Recovery (%)		20.0	20.2	20.1	20.0	20.0	20.2	17.6
Permeate Flux (LMH)		17.9	17.9	17.9	17.9	17.9	17.9	15.1
Osmotic Pressure (bar)	Feed	3.73	3.75	4.13	4.10	4.45	4.63	4.77
	Concentrate	4.46	4.70	4.86	5.02	5.19	5.57	5.59
	Permeate	-	0.30	0.32	0.38	0.34	0.55	0.60
TMP (bar)		-	6.21	6.04	6.79	7.86	11.66	21.31
Lp (L/m².h.bar)		-	2.88	2.97	2.64	2.28	1.54	0.71
Lp (25°C) (L/m².h.bar)		-	3.99	4.05	3.57	3.07	2.06	0.97
Permeate Recovered (mL)		-	1210	1240	1280	1180	1280	590
Overall Recovery (%)		0	12	25	37	49	62	68
Concentration Factor		-	1.1	1.3	1.5	1.9	2.4	2.8
Ca+ Conc. (mg/L)	Concentrate	1002	1018	1042	1062	1074	1117	1119
	Overflow Sed. Tank	854	853	881	871	878	887	921
	Feed	875	858	923	903	941	928	926

Pemeate Flushing	Total time	255	min
	Time / Flush Cylce	1156	sec
	Total Flushes	13	
	Flushing Time	14	sec
	Flushing Flowrate	14	L/h
	Total Flushing Volume	0.70	L
	Total Feed	10.0	L
	Total Permeate	6.8	L
PPR (L/h)	Calculated	1.57	L/h
	Measured	1.52	L/h

Table C-22 *Raw and processed data for Run 19*

Run 19	Flush Freq (h^{-1})	Flush Vol (mL)	Soak time (sec)	Flux (LMH)	Inst. Rec. (%)
	3.4	52.5	55	18	20

Operating Time (min)		0	45	90	135	180	225	240
Production Time (min)		0	41	82	123	164	204	218
Gauge Pressure (bar)	Feed	8.8	9.6	10.6	11.8	13.6	17.4	27.3
	Concentrate	8.0	8.8	9.8	11.0	12.8	16.6	26.5
	Permeate	1.1	1.1	1.1	1.1	1.1	1.1	1.1
Spcific Conductivity (mS/cm)	Feed	7.68	8.19	8.28	8.48	8.96	9.80	9.39
	Concentrate	8.87	9.40	9.80	10.08	11.15	11.22	11.27
	Permeate	-	0.796	0.812	0.985	1.002	1.056	1.370
Temperature (˚C)	Feed	16.3	16.1	15.8	15.4	15.6	15.7	15.6
	Concentrate	17.1	17.1	17.2	17.8	18.0	18.3	17.7
	Permeate	-	17.3	17.7	17.5	18.2	18.0	18.5
Flow rate (L/h)	Concentrate	7.60	7.50	7.55	7.60	7.60	7.50	7.50
	Permeate	1.90	1.90	1.90	1.90	1.90	1.90	1.60
	Feed	9.50	9.40	9.45	9.50	9.50	9.40	9.10
Salt Rejection (%)		NA	90.3	90.2	88.4	88.8	89.2	85.4
Inst. Recovery (%)		20.0	20.2	20.1	20.0	20.0	20.2	17.6
Permeate Flux (LMH)		17.9	17.9	17.9	17.9	17.9	17.9	15.1
Osmotic Pressure (bar)	Feed	3.74	3.98	4.03	4.12	4.36	4.76	4.57
	Concentrate	4.31	4.57	4.76	4.90	5.42	5.46	5.48
	Permeate	-	0.39	0.39	0.48	0.49	0.51	0.67
TMP (bar)		-	4.90	5.91	7.06	8.63	12.09	22.32
Lp (L/m².h.bar)		-	3.66	3.03	2.54	2.08	1.48	0.68
Lp (25°C) (L/m².h.bar)		-	4.88	4.07	3.39	2.75	1.95	0.90
Permeate Recovered (mL)		-	1280	1260	1200	1180	1300	590
Overall Recovery (%)		0	13	25	37	49	62	68
Concentration Factor		-	1.1	1.3	1.5	1.9	2.5	2.8
Ca+ Conc. (mg/L)	Concentrate	1015	1031	1060	1072	1098	1107	1107
	Overflow Sed. Tank	865	866	886	894	915	938	930
	Feed	854	879	886	894	907	923	947

Pemeate Flushing	Total time	240	min
	Time / Flush Cylce	1156	sec
	Total Flushes	12	
	Flushing Time	14	sec
	Flushing Flowrate	14	L/h
	Total Flushing Volume	0.65	L
	Total Feed	10.0	L
	Total Permeate	6.8	L
PPR (L/h)	Calculated	1.57	L/h
	Measured	1.59	L/h

Appendix D – ANOVA Results

Table D-1 *ANOVA table for the linear and quadratic model with main effect interactions, showing the variance of each factor with respect to total production time.*

Factor	SS	df	MS	F	p
(1) Flush. Freq.	22494.7	1	22494.7	16.62	0.0267
(2) Flush. Vol.	3890.9	1	3890.9	2.87	0.1886
(3) Soak Time	1436.7	1	1436.7	1.06	0.3787
(4) Flux	393508.1	1	393508.1	290.70	0.0004
(5) Inst. Rec.	15026.6	1	15026.6	11.10	0.0447
1L by 2L	2716.4	1	2716.4	2.01	0.2516
1L by 3L	964.4	1	964.4	0.71	0.4606
1L by 4L	1057.6	1	1057.6	0.78	0.4418
1L by 5L	399.4	1	399.4	0.30	0.6247
2L by 3L	1580.5	1	1580.5	1.17	0.3590
2L by 4L	3100.8	1	3100.8	2.29	0.2274
2L by 5L	1344.8	1	1344.8	0.99	0.3924
3L by 4L	2444.5	1	2444.5	1.81	0.2716
3L by 5L	1031.6	1	1031.6	0.76	0.4469
4L by 5L	1133.0	1	1133.0	0.84	0.4277
Error	4060.9	3	1353.6		
Total SS	456190.8	18			

Table D-2 *ANOVA table for the linear and quadratic model with main effect interactions, showing the variance of each factor with respect to permeate production rate.*

Factor	SS	df	MS	F	p
(1) Flush. Freq.	0.4	1	0.4	335.14	0.0030
(2) Flush. Vol.	0.1	1	0.1	90.41	0.0109
(3) Soak Time	0.1	1	0.1	41.82	0.0231
(4) Flux	5.2	1	5.2	4144.13	0.0002
(5) Inst. Rec.	0.0	1	0.0	0.07	0.8125
1L by 2L	0.0	1	0.0	0.37	0.6047
1L by 3L	0.0	1	0.0	1.50	0.3460
1L by 4L	0.0	1	0.0	13.54	0.0666
1L by 5L	0.0	1	0.0	0.40	0.5916
2L by 3L	0.0	1	0.0	0.85	0.4543
2L by 4L	0.0	1	0.0	0.40	0.5899
2L by 5L	0.0	1	0.0	4.71	0.1621
3L by 4L	0.0	1	0.0	0.16	0.7322
3L by 5L	0.0	1	0.0	0.18	0.7154
4L by 5L	0.0	1	0.0	0.30	0.6372
Error	0.0	2	0.0		
Total SS	5.8	18			